Measurements and finite element modelling of transformer flux with dc and power frequency current

Thesis by:

Hilary Kudzai Chisepo

Supervisors:

Emeritus Professor C T Gaunt

Professor K A Folly

Department of Electrical Engineering

University of Cape Town

October 2019

A Thesis Submitted to the Faculty of Engineering and the Built Environment in fulfilment of the requirements for the degree of Doctor of Philosophy in Engineering

DECLARATION

I declare that this thesis is my own original work. Where collaborations with other researchers are involved, or materials generated by other researchers are included, the parties and/or materials are acknowledged or are explicitly referenced as appropriate.

This work is being submitted for the degree of Doctor of Philosophy in Engineering of the University of Cape Town, South Africa. The work contained herein has not been submitted to any other university or institution for any other degree or examination.

Signed by candidate

Hilary Kudzai Chisepo **Date:** 16 OCTOBER 2019

Dedicated in loving memory of my Grandparents

Bernard Harris Terayi and Dorcas Chisepo

Thank you for your passion for education and excellence …it lives on

ABSTRACT

Measurements and finite element modelling of transformer flux with dc and power frequency current

Thesis by

Hilary Kudzai Chisepo

October 2019

Geomagnetically induced currents (GIC's) caused by solar storms or other sources of dc excitation in the presence of ac energization can disturb the normal operation of power transformers. If large enough, they cause half-cycle saturation of a power transformer's core which could lead to overheating due to excessive stray flux.

Finite element matrix (FEM) modelling software is of considerable use in transformer engineering as it is able to solve electromagnetic fields in transformers. For many problems, typically involving only specific parts of a transformer, fairly accurate solutions can be reached quickly. Modelling the effects of GIC or leakage currents from dc systems, however, is more complex because dc components are superimposed on ac in transformers with nonlinear electrical core steel parameters.

At the beginning of the investigation, FEM models of different bench-scale laboratory transformers and a 40 MVA three-phase three limb power transformer were investigated, but the results did not sufficiently represent the measurement data due to the application of widely used modelling assumptions regarding the transformer joints. Following the preliminary analyses, practical measurements and FEM simulations were carried out using three industrially made model single-phase four limb transformers (1p4L) without tanks. These test transformers resemble a real power transformer because they have high-quality grain oriented electrical core steel and parallel winding assemblies. Practical laboratory measurements recorded during ac testing were used to calibrate 2D FEM models by adding "equivalent air gaps" at the joints. The implementation of this joint detail helped to overcome the shortcomings of the preliminary FEM simulation. Analyses of the electrical and magnetic responses of the FEM models using simultaneous ac and dc then followed. A refined 3D FEM simulation with more detailed modelling of the core joints of 1p4L model transformers agreed more closely with the practical measurements of ac only no-load conditions. Further, the depiction of stray flux leaving the transformer's saturated core under simultaneous ac and dc excitation showed an improvement in the approach as measured in the physical model.

Saturation inductance (L_{sat}) is an important parameter for input into mid- to low-frequency lumped parameter transformer models that are used in electromagnetic transients software such as PSCAD/EMTDC, but it is not easily measured and is seldom provided by manufacturers. Some L_{sat} measurements on the 1p4L test transformers are presented in this thesis, along with some 3D FEM analyses. The measurements and FEM analyses investigated "air core inductance" which represents a transformer without a core, and "terminal saturation inductance" which represents deep saturation due to dc excitation. An important finding in this thesis is that "terminal saturation inductance" is the more useful of the two for topological transformer models investigating realistic GIC excitation. Further to this, a new composite depiction of half-cycle saturation with a multi-parametric relationships supported by measurement and simulation is presented.

The main contribution of this thesis is that it gives more accurately the electrical response and distribution of the leakage flux under conditions such as those caused by GIC or other sources of leakage dc excitation, as well as including of joint details in the FEM models through calibration with physical models. This calibration can aid transformer modelling and design in industry for mitigation of the effects of GICs, contributing to improved transformer survival during significant geomagnetic disturbances.

ACKNOWLEDGEMENTS

The research in this thesis was undertaken under the close supervision of Em. Prof. C T Gaunt of the department of electrical engineering of the University of Cape Town. I would like to thank Prof. Gaunt for the enormous amount of time he invested in me, imparting his wealth of knowledge freely, challenging me to do better if when I thought I had reached my limits, and his unwavering support in every aspect of my academic career. It is an absolute privilege working with him. I could not have possibly achieved the work presented in this thesis without his resolute belief in my potential.

I would like to thank my entire family for their patience and support, especially my Mum and Dad, for always believing in me my whole life through the 'ups' and the 'downs'.

To my fiancé, Nicole Justine White, thank you for enduring this journey with me. I can categorically say that I did not achieve this alone but that we did it together. I appreciate all the support your family, and especially from you for putting up with all my 'academic weirdness' during the PhD.

My esteemed colleague Leslie David Borrill… we have proven the statement 'two is better than one' by working closely together during the PhD journey. I have learnt a lot from you, but unfortunately, we both still have a lot more to learn! I look forward to learning more with you in the future.

A special thanks to all my friends and colleagues for all your support throughout the journey.

In addition, I would like to thank:

the department of electrical engineering for the postgraduate bursary funding;

SGB-Smit Power Matla (formerly known as Powertech Transformers) for providing practical training, simulation facilities and power transformer data, and collaboration during the research;

Mentor, a Siemens Business for providing the Simcenter MAGNET™ academic license used for FEM simulation in this research;

Eskom Holdings Brackenfell and Royal Smit Transformatoren Netherlands for providing the laboratory testing facilities and model tests transformers, respectively;

a support grant from the Open Philanthropy Project to carry out the research, and last but not least;

a sincere thank you to Carol Hartley for her diligent proofreading of this thesis.

Tot facienda parum factum

TABLE OF CONTENTS

NOMENCLATURE

1p2L	single-phase two limb transformer
1p3L	single-phase three limb transformer
1p4L	single-phase four limb transformer
3p3L	three-phase three limb transformer
3p5L	three-phase five limb transformer
2D/3D	two dimensional/three dimensional
ac	alternating current
ac-dc	simultaneous ac and dc excitation in a transformer
dc	direct current
EMS/EMT/EMTP	electromagnetic transients software
FAT	Factory Acceptance Test
FEM	finite element method/modelling
FEM software	commercial finite element matrix simulation software
GIC	geomagnetically induced current(s)
GMD	geomagnetic disturbance
GOES	high-quality grain oriented electrical core steel
HVDC/HVAC	high voltage dc/high voltage ac
meas.	measured
per unit	pu
P_{loss}	core power loss at no load
Q	reactive power or non-active power unless otherwise specified
SC	search coil
sim.	simulated
T1, T2, T3	1p4L laboratory transformers 1, 2, and 3
V_{knee}	knee point voltage (explained in the text)
YPM	Yokogawa Power Meter (WT1600 or WT1800)

LIST OF TABLES

LIST OF FIGURES

1 INTRODUCTION

The sun freely and continuously provides us with a gift of light, warmth and energy critical for our survival. Occasionally, though, this enormous ball of energy ejects huge streams of high velocity, magnetically charged particles towards Earth and disturbs the Earth's magnetic field. This event is called a geomagnetic disturbance (GMD) or solar storm (Albertson, *et al*., 1993). GMDs negatively affects our electricity transmission networks. The Sun's Gift imposes responsibilities.

In 1989, a severe GMD caused a day-long blackout in Quebec, Canada. It started in the network's power transformers and cost billions of dollars (CENTRA Techonology Inc., 2011). In 2003, the Halloween GMD initiated transformer damage which led to equipment failures in South Africa, and also to a blackout in Sweden affecting 50 000 customers (Gaunt & Coetzee, 2007, Wik *et al*., 2009). Considering these and other past events, extreme GMDs might deprive us of electricity supplies for a day or a week, affecting personal lives, the community and the economy (Schrijver & Mitchell, 2013).

The main negative influence of GMDs is transformer dc bias, which can also originate from high voltage direct current (HVDC) transmission systems and power electronics, and other sources of dc leakage currents (Gong *et al.*, 2017, Wang *et al.*, 2017). And the power transformer's response affects other components of the power system. The other sources of dc leakage currents also affect the comparably smaller distribution transformers, though this has neither been widely reported nor investigated.

Power transformers are essential and vulnerable components in power systems. This thesis, therefore, is aimed at gaining a better understanding of their complex responses during GMDs in order to improve the modelling and design for dc bias.

This research is one part of a broader interdisciplinary study which extends to power transmission and distribution systems' security under various threats from environmental disturbances caused by abnormal space weather.

1.1 Motivation for the research

The immediate concern during a GMD is power transformers drawing Mvars of reactive power, generating even and odd harmonics, overheating and power system voltage instability (Albertson *et al.*, 1993; NERC, 2012). The draw of Mvars affects system stability while the generation of harmonics interferes with other components and affects the power networks' security. Overheating caused by stray magnetic flux can contribute to immediate failure or degradation of the insulation of a transformer, especially when a generator step-up (GSU) transformer is operating at full load with very little capacity for added heat stress (Zhang *et al*., 2011; Babaeiyazdi *et al*., 2019). The vulnerability of transformers to damage (and distortion) by GICs is dependent on the assessed magnitude of the GIC

in the transformer, which depends on both the prospective GIC magnitude and the transformer core structure (NERC 2012, Oyedokun, 2015; Adhikari *et al*., 2017).

Research efforts to prevent or mitigate GIC effects in power systems were spurred by the severe 1989 GMD which resulted in the collapse of a whole power system in Quebec, Canada (Kappenman *et al*., 1991, Berge *et al*., 2011, Hutchins & Overbye, 2011). This research has resulted in the development of some methods to maintain the integrity of power systems and protect 'critical' transformers through GIC blocking/bypassing, and *ad hoc* removal of some parts of the transmission lines to minimize overall impact on the system (Etemadi & Rezaei-Zare, 2014). In their ruling "Reliability standards for transmission system planned performance for geomagnetic disturbance events," the USA's Federal Energy Regulatory Commission (FERC) highlighted that better modelling was required in GMD-related research, which includes transformer modelling (FERC, 2015). The North American Electric Reliability Corporation (NERC) petitioned FERC regarding mandatory periodical thermal assessments of power transformers which would experience a GIC of 75 A/phase (NERC, 2017). Some studies report that GIC levels greater than or equal to 75 A/phase are not likely to reach a thermally critical level resulting in transformer damage (Picher *et al*., 1997, Girgis & Vedante, 2012). Other studies in the literature, however, report that power transformers are vulnerable to significantly lower levels of GIC (Gaunt & Coetzee, 2007; Rezaei-Zare, 2015a; Rezaei-Zare, 2015b). In their transformer study of windfarms operating with GIC, Babaeiyazdi *et al*. (2019) show that a 230/34.5 kV 50 MVA transformer's hot temperature exceeds the permissible limit of 180°C with a GIC of 70 A/phase (which is less than the problematic 75 A/GIC identified by NERC's standard).

South Africa had not been considered to be significantly affected by GMDs until evidence of transformer degradation and failure was reported in the literature (Koen & Gaunt, 2002; Gaunt & Coetzee, 2007; Moodley, 2013; Moodley & Gaunt, 2017). As a result, there is now a renewed awareness of the GIC effect in power networks in Southern Africa. This is evident from the investigations like those of South Africa's Eskom and Namibia's NamPower of the exposure of their networks to GIC, and the work towards possible mitigation strategies through research (Simon, 2013; Gaunt, 2014). Gaunt's study (2014) highlights the transdisciplinary systems approach required to study GMD's in power systems. This involves research in space physics, network analysis, transformer engineering, network reliability and cost assessment, and decision support for network planners and system controllers' models.

In industry, leading power transformer manufacturers such ABB Transformers, Siemens, and SGB-SMIT Royal Smit Transformers (Netherlands) and SGB-SMIT POWER MATLA (Pretoria) have started to consider the GIC effect in their research and development (R&D) and customer specifications (Mulasalihović *et al.*, 2008, Raith & Ausserhofer, 2014, Chisepo, 2015; Chisepo *et al*; 2019).

Transformer response of all core constructions in power transmission networks, however, is still not fully understood and requires further rigorous investigation from various electromagnetics and physical aspects. Previous work limited only to laboratory bench-scale transformers (Chisepo, 2014) showed that a better understanding of the complexities of transformer response through test protocols is needed before any representative model can be realized.

The testing of large power transformers with GIC/dc is impractical due to commercial implications, lack of Mvar capacity and possible damage to equipment. Therefore, such testing is not widely practised (nor is factory verification testing for GIC when specified in procurement contracts), leaving available few practical results such as the study by Raith and Ausserhofer (2015).

Modelling of power transformers to show the effects of GIC offers several ways to characterize the response. In this context, numerical methods can be used in finite element modelling (FEM) environments to investigate different aspects of transformer response. FEM analyses are computationally intensive, depending on the amount of detail used in the modelling, but are fairly accurate for modelling individual components intended for bigger systems.

Currently, the main challenge in FEM analyses of GIC in power transformers is the availability of adeqaute measurement data for validation (Bíró *et al.*, 2014).

The validation and calibration of FEM analysis to improve the understanding of the transformer response requires exhaustive physical testing of transformers that are as closely as possible representative of power transformers with different levels of GIC/dc. The results from such tests to calibrate FEM models could inform the transformer manufacturing industry, which would, in turn, contribute to the interdisciplinary systems approach to the GIC problem depicted in Figure 1.

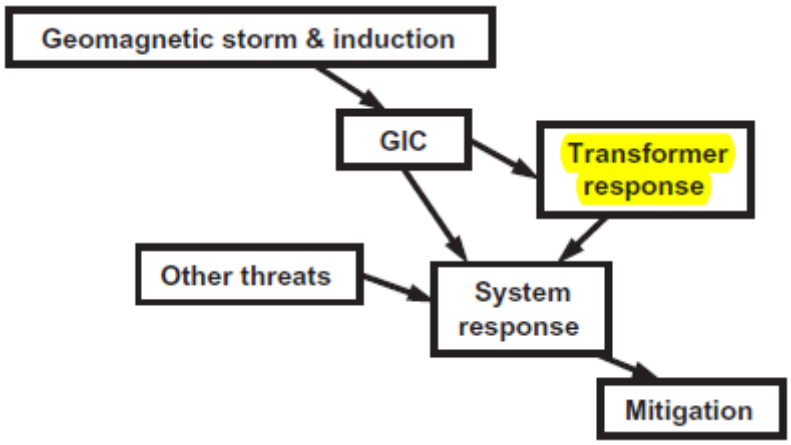

Figure 1: The systems approach to the GIC problem formulated by Gaunt (2014)

1.2 Proposal and Scope

Power transformers play a significant role in power systems by stepping up voltages to much higher levels for transmission with very high efficiencies, and stepping down voltages to the different system levels required. GICs cause these transformers to operate under conditions of simultaneous ac power and quasi-dc GIC excitation, well beyond their usual operating conditions, which drastically reduces the transformers' efficiency to transfer energy and may also result in damage.

The purpose of this study is to improve the understanding of transformer flux distributions in order to improve modelling with simultaneous ac and dc excitation, based on measurement data acquired from rigorous laboratory testing in both previous studies and this research. The nature of this research therefore necessitates the coupling of electrical circuits with the FEM domain in which the spatial distributions can be analysed. This suggests the formulation of an hypothesis that:

"Test results from model transformers can augment the data from testing large power transformers in calibrating simulation models, particularly FEM models, to characterize the responses to quasi-dc currents of large power transformers energised at power frequency."

This study focuses on the interpretation of the transformers' flux due to combined ac-dc excitation, different from the (negligible) leakage flux under normal operating conditions with ac energization only, and also the core saturation associated with over-excitation. Measurements are used in conjunction with FEM analyses to characterize transformer response in a manner that is representative of actual conditions. An approach in the modelling of transformers under GIC conditions is proposed in this study to highlight the important modelling details that need to be considered.

This study is limited to studying the response of transformers using available data from the manufacturers and laboratory measurements. As a result, the FEM analyses of a power transformer do not include the effects of other metallic structural parts with GIC except the tank. The scaled-down laboratory single-phase four limb (1p4L) transformers were deliberately fabricated without any other metallic parts to primarily investigate the response of the core. In the absence of actual power transformer ac-dc measurements, this research is limited to developing the modelling techniques using only 1p4L rigorously measured data.

1.3 Research Questions

In order to test the validity of the hypothesis, the following research questions need to be answered:

- What existing models of power transformers are useful in the modelling of their response to dc and power frequency ac voltages?
- How does the GIC phenomenon influence transformers in power systems, such that its effects, including overheating and reactive/non-active power absorption during ac-dc excitation, can be studied?
- Which transformer core structures have already been sufficiently studied in the context of GIC?
- How can a previous bench-scale protocol (Chisepo *et al.*, 2013) be adapted to investigate the testing in a laboratory or factory environment of larger test transformers representative of power transformers?
- What are the minimum modelling details needed to carry out FEM and related modelling of transformers subjected to GIC (and how does simplification affect the accuracy)?

1.4 Methodology

Figure 2 is a condensed depiction of the research methodology followed in this study. In previous work (Chisepo, 2014) leading to this research, some measurement data on laboratory bench-scale transformers are collected through the development of a transformer-GIC testing protocol. These data are only explored using electromagnetic transients software (EMS).

Not all the transformer core structures are successfully modelled with ac and dc due to the limitations in the software's inherent saturable transformer models. This early work indicates that an extended literature review and further transformer modelling and testing are necessary.

An important part of this research is to investigate the responses of real power transformers thus avoiding drawing inferences from small models which are not sufficiently representative of the underlying mechanisms of the phenomena. Therefore, to grasp the necessary concepts involved in transformer engineering, a secondment to Powertech Transformers Pty. Ltd (PTT) (now known as SGB-SMIT MATLA), a large power transformer manufacturer in Pretoria, was arranged by the University of Cape Town.

The activities of this secondment specific to this research were to assist, under direction, in any aspect of transformer engineering, including design, manufacture and testing of power transformers.

.

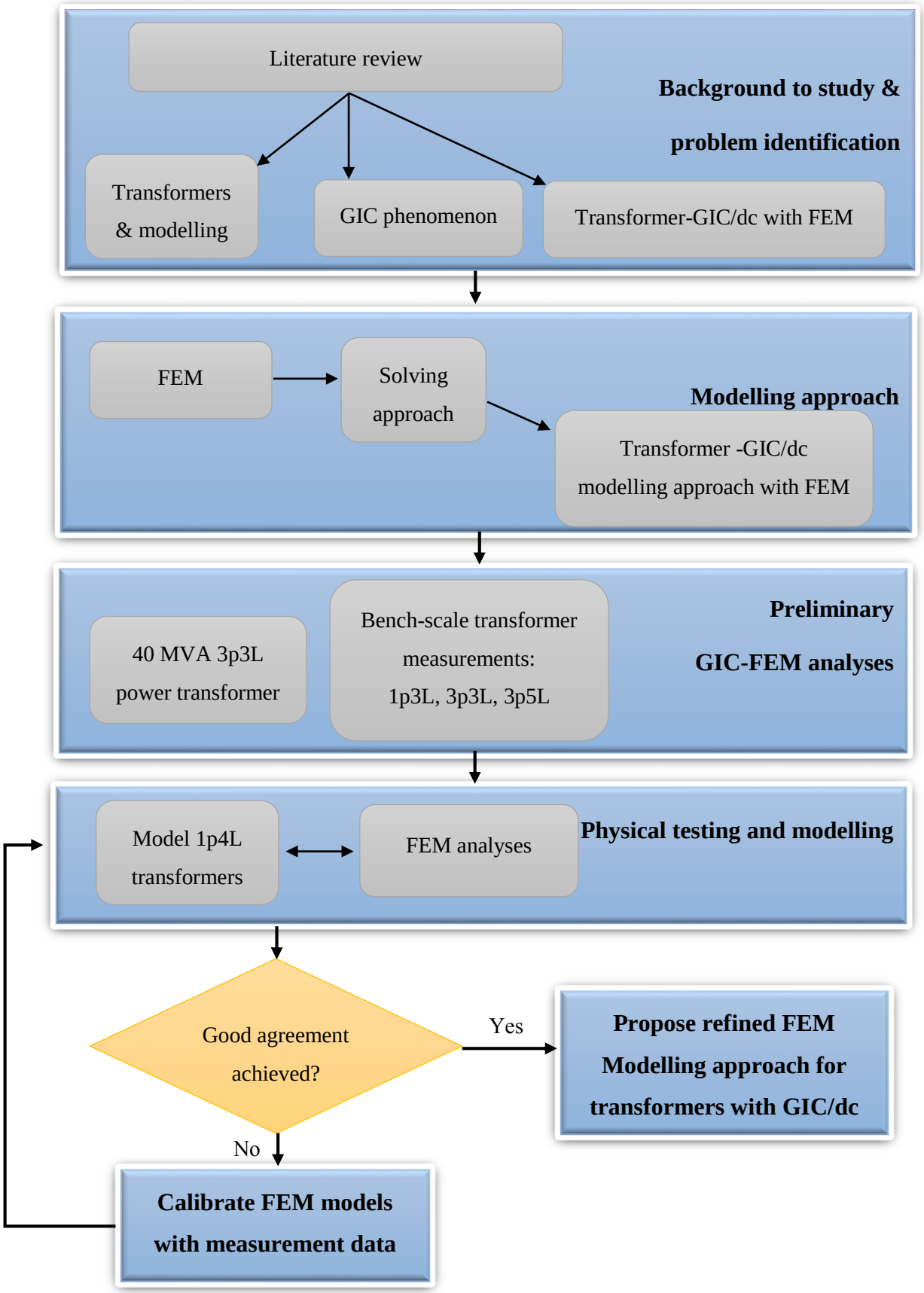

Figure 2: Approach to the study

Unlike the earlier research in EMS, the modelling approach implemented in this study is FEM, which is known to be computationally intensive, involving long iterative calculations. The main motivation for this choice is that while EMS is fast-acting, it is more suitable for modelling power systems and the accuracy needed in GIC studies is limited by the detail of the transformer models (which are deliberately not made easy to modify). FEM overcomes this limitation because virtually any device can be modelled by using parametric analyses, provided the requisite physical properties are available and correct. The transformer bench-scale measurements already carried out (Chisepo, 2014) can be used for comparison with preliminary FEM analyses. Further, some available factory acceptance test (FAT) data of a power transformer can be contrasted with FEM analyses. Results from these tasks are useful for bringing to light any discrepancies that will need to be addressed in the main part of the study.

In order to continue with a more detailed investigation, exhaustive experiments are be performed on three industrially made distribution scale single-phase four limb transformers (1p4L). The focus of the experiments on the 1p4L core structure is due to their availability from a transformer manufacturer during this research. However, the simulation method developed to extend to other core structures will be applicable as well to other stacked core configurations in terms of physical tests and simulation. Therefore, the experimental protocol used in this thesis is applicable to test any type of transformer, provided the supply conditions are adequate. These test transformers resemble a power transformer as they have high-quality electrical core steel and parallel winding configurations. The models are constructed in such a way as to make it possible to perform flux measurements in and around many parts of the core.

Approximations arise in both the accuracy of a 1p4L model transformer to represent a power transformer in every respect, and in the details of the FEM models which are likely to be appropriate for both model and power transformers.

The 1p4L experimental stage of the study leads to the process needed to derive a FEM modelling approach which can address possible discrepancies observed from the preliminary approximate models. It is important that the final FEM model is able to calculate the flux distribution in a transformer (and related electrical parameters e.g. the magnetising current) in the presence of ac-dc excitation caused GIC/dc to represent actual conditions.

1.5 Thesis outline

Chapter 2 undertakes a literature review, guided by the research questions, on models for transformers, the GIC phenomenon and perceived transformer behaviour, and transformer FEM modelling. The closing summary of the findings from the review provides the context for the work described in Chapters 3, 4 and 5.

Chapter 3 provides a background to FEM leading to the approach that will be implemented in this study.

Chapter 4 presents a preliminary FEM modelling approach applied to a real power transformer that has only factory acceptance test measurement data.

Chapter 5 is an FEM investigation based on bench-scale transformers tested in a previous study (Chisepo, 2014)

Chapter 6 identifies the need for further physical tests with transformers more representative of power transformers before describing the physical testing of three industrially made laboratory single-phase four limb transformers to collect useful data. A rigorous experimental procedure is outlined arriving at a carefully considered single-phase test circuit for simultaneous ac and dc energization.

This chapter also contains a discussion of how the core joint configuration of laboratory transformers could negatively influence the core performance at the transformer nameplate ratings.

Chapter 7 presents a 2D FEM simulation protocol which involves calibration with ac excitation using results from the 1p4L transformers tested in Chapter 6. Additional simulations are performed in 3D and with more detail in the core joints to investigate how accurately they can match actual measurements.

Chapter 8 presents the measured results from the physical testing in Chapter 6 and results from the FEM simulation in Chapter 7.

Chapter 9 discusses the results presented in Chapters 4 and 5. First, the challenges encountered in the preliminary modelling approach are analysed. This is followed by a breakdown of the steps implemented in Chapter 6 and Chapter 7 to extend and refine the modelling that yielded the results presented in Chapter 8.

Chapter 10 addresses the research questions posed in Chapter 1 before commenting on the implications of the research. The contributions derived from the research are assessed. In conclusion, the validity of the hypothesis is reviewed.

1.6 Publications

Some of the results in this thesis have been presented at conferences and in a journal (Chisepo, 2015, Chisepo *et al.*, 2016, Chisepo *et al.*, 2017, Chisepo *et al.*, 2018, Chisepo *et al.*, 2019).

2 LITERATURE REVIEW

2.1 Introduction

Chapter 1 contextualized this study, presenting the current challenges faced by power utilities, transformer manufacturers, and researchers in investigating transformer-GIC response. In the absence of measurement data for model validation, some manufacturers in industry and researchers use FEM and other topological modelling techniques (EMS) as a first approximation of the expected response. In most simple or normal operation conditions, this is adequate. Since transformer behaviour under ac-dc conditions is very complex, involving multiple low frequencies, more confidence is still needed in the modelling in research in general.

This chapter is aligned to the five research questions, and it identifies what is already known about transformer behaviour in those extreme conditions which can then can be used as the foundation for the remainder of the research. FEM transformer-GIC modelling in existing literature is then discussed before a concluding summary of this chapter is given. The following abbreviations are be used in several parts of this chapter (and throughout the thesis) to differentiate transformer core constructions into their several configurations:

- single-phase shell two limb – 1p2L,
- single-phase shell type – 1p3L,
- single-phase four limb – 1p4L,
- three-phase three limb – 3p3L,
- three-phase five limb – 3p5L, and
- three-phase seven limb – 3p7L.

2.2 Transformers in power systems and modelling

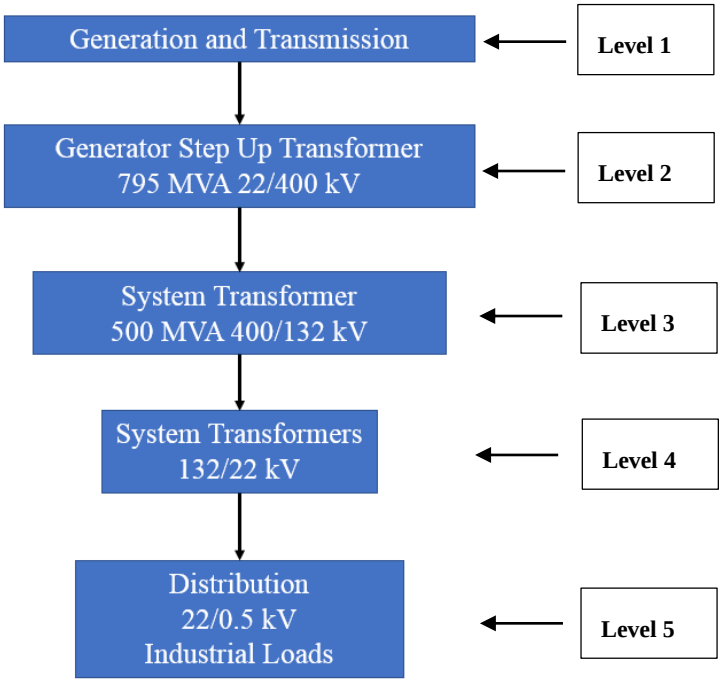

Figure 3: Typical hierarchal arrangement of typical power systems

A transformer basically consists of a lower voltage winding, abbreviated LV, and a higher voltage winding, abbreviated HV. Some power transformers have tertiary, medium voltage (MV) windings. The two windings are magnetically coupled by the transformer core.

A typical power system consists of the components illustrated in Figure 3. The main components of interest to this study in relation to dc bias caused by GIC are generator step up transformers and system transmission transformers indicated by Levels 2 and 3 in Figure 3 .

The two laws which govern the operation of transformers are Faraday's law of electromagnetic induction and Ampère's Law which stipulates that an electric current produces a magnetic field (Griffiths, 1999). The fundamentals of transformers and governing equations of ideal and practical transformers are given in great detail in the textbooks by Sen (1997) and Griffiths (1999), focusing on the electrical equivalent T-model proposed by Steinmetz in 1892. This transformer model is mostly accurate for sinusoidal steady-state studies at power frequencies (50/60 Hz) without harmonics. Kulkarni and Khapharde (2013), in their work more specific to transformers in power systems (often involving complex transient analyses such as inrush current phenomenon, or low-frequency transients caused by ferroresonance and GIC), describe the use a lumped π-model preferred for better accuracy.

The main difference between the T and π equivalent circuits is the representation of the series leakage inductances and the parallel magnetizing branches. The T-model's leakage inductances are shared by both primary and secondary windings belonging to partly the primary windings and partly the

secondary winding as in the T model (Sen, 1997; Griffiths, 1999), the π model uses the principle of duality between magnetic circuits and arrives at a circuit with only one leakage inductance branch in series with two magnetizing branches – see Figure 4.

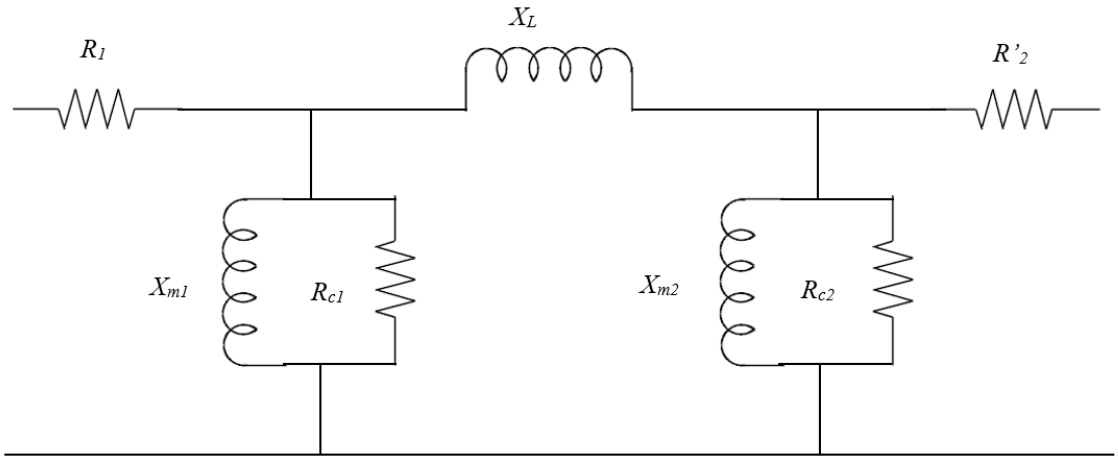

Figure 4: π equivalent circuit diagram adapted from de León *et al.'s* study (2012)

In their comparative study, de León *et al.* (2012) investigated the performance of a T- and π-model in an EMTP software environment. The study focused on the calculation of inrush currents in three toroidal transformers, a standard unit, and two other with a reduced leakage inductance and a higher leakage inductance. (The saturation which arises from inrush current is similar, because it generates even and odd harmonics, to the half-cycle saturation brought about by GIC/dc.) The EMTP software employed requires an air core inductance parameter (also known as saturation inductance) in order to increase the accuracy of calculations in the saturation region of the BH curve. Saturation inductance is difficult to measure practically due to the excessive amount of dc required to push the core into deep saturation, and so 3D FEM software was used to calculate it as the 'air core inductance' with core-less windings. Comparing measured results from the two models, it was found that the π-model gives more accurate responses throughout, and that the T-model produced large underestimation errors of the inrush currents, particularly when the leakage reactance was large.

In another study (Corea-Araujo *et al*., 2017), a single-phase π-model is compared with ferroresonance measurements to demonstrate an imporvement in the response when hysteresis is taken into account.

These examples of the implementation of the π-model show that in cases where a transformer is experiencing a degree of saturation, conventional approaches result in discrepancies. Even though duality derived topological models (Rezaei-Zare, 2015a; Rezaei-Zare, 2015b) show an improvement in modelling slow transients and GIC conditions, there still seems to be a question about whether transformer "saturation inductance" and "air core inductance" in deep or complete saturation are the same or different (Jazebi *et al.*, 2016). The FEM domain offers an alternative approach to investigate several related parameters in the virtual domain for analytical deductions of the saturation inductances

but there is a paucity of such studies in the literature. This shows the need for further investigation to increase model accuracy by better understanding different types of transfomer (saturation) inductance.

Topological modelling relies on resistors, inductors, and capacitors lumped together to represent *physical relationships* in transformers. On the other hand, the accuracy of any FEM model depends on the amount of necessary detail in the *physical properties* of the transformer components to be modelled, especially the components with electromagnetic significance such as the core (Lu & Liu, 1993a). Further, there is a need to investigate the extent to which acceptable accuracy can be achieved with detailed physical properties in the FEM.

Permeability μ in magnetic circuits is analogous to conductivity in electrical circuits. Simply put, it is the ability of the core material to conduct magnetic flux (McLyman, 2004). Analytically, it is defined as the ratio of the flux density B to the magnetizing force H and is expressed in the form $B=\mu H$. (μ is the product of the permeability in free space μ_0 and the relative permeability of the core material μ_r.)

Hysteresis loss in a ferromagnetic material is represented by the area of the B-H curve when there is an applied changing magnetic field (MIT Press, 1944). When the flux density in a region is increased from a value B_1 to B_2 energy w is absorbed by the same region and it is given in per unit volume by

$$w = \int_{B_1}^{B_2} \boldsymbol{H} \bullet \boldsymbol{dB},$$

(2.1)

as derived from Poynting's theorem (Cheng, 1989).

When the flux density is decreased from one value to another, w in Equation 2.1 is reversed and energy is given up by the material for transformation to occur. Using a rigorous derivation in MIT Press (1944), it follows that the energy absorbed when the flux density is increased from B_1 to B_2 is larger than the energy returned when the flux density is reduced B_2 to B_1. The magnitude of the hysteresis loss is, therefore, the difference between these two energies.

The analytical calculation for hysteresis loss P_h is given in Equation 2.2 (MIT Press, 1944):

$$P_h = k_h f B_{max}^n$$

(2.2)

where k_h is the material dependent hysteresis coefficient, B_{max} is the peak flux density and n is the Steinmetz constant with values between 1.6-2.0 for hot rolled laminations and 2.0 for cold-rolled laminations due to their higher operating flux densities (MIT Press, 1944; Kulkarni & Khaparde, 2013). Each full cycle has the same value of loss making P_h directly proportional to frequency f. This means that the higher the frequency, the higher the loss, and this is due to the skin effect.

When magnetic flux flows in the core, electric fields appear within it resulting in circulatory currents known as eddy currents. These currents are responsible for the i^2R heat loss called *eddy current loss*. The electrical resistance of the core material becomes important to reduce this loss because the higher the resistance, the lower the losses. Also, the thinner the laminations, the lower the eddy current losses (McLyman, 2004).

The analytical calculation of eddy current loss P_e is given in Equation 2.3:

$$P_e = k_e f^2 t^2 B_{peak}^2 \tag{2.3}$$

where k_e is the material dependent eddy current coefficient, t is the thickness of the core laminations, and B_{peak} is the peak flux density corresponding to the rated voltage (MIT Press, 1944).

In most literature, anomalous loss or excess loss in transformer core steel with a varying magnetic field is not clearly defined. The anomalous loss has, therefore, often been simplified to the component of total core loss remaining after accounting for P_h and P_e. Specifically, in power transformers, the difference between the measured core loss in kW and the calculated hysteresis loss is the *apparent* eddy current loss (Kulkarni & Khaparde, 2013). The difference between the apparent and classical eddy losses is the anomalous loss and it can constitute up to 50% of the total core loss according to experimental measurements on GOES (Brailsford & Fogg, 1964). Brailsford and Fogg (1964) in their study also state that, though it is proven by experiment that anomalous loss can be quite high in GOES, its origin is still unclear.

Pry and Bean (1958) noting the anomalous loss in their model, proposed that it is the result of microscopic eddy currents due to domain wall motion. As a result, a physical source that is widely associated with anomalous loss is *magnetostriction*. This is the rotating of the magnetic dipoles which results in the change in dimensions of the crystal lattice in the presence of an applied changing field (Hastenrath, 2014).

Several efforts have been made toward the inclusion of anomalous loss in the total core loss calculation (Pry & Bean, 1958, Bertotti, 1988, Cheng & Pillay, 2002, Ionel *et al*., 2007) resulting in the general expression for total core loss P_T:

$$P_T = k_h f B_{peak}^n + k_e f^2 B_{peak}^2 + k_a f^{1.5} B_{peak}^{1.5} \tag{2.4}$$

where, at frequency f, B_{peak} is the peak flux density k_h and n are the coefficients associated with hysteresis loss, k_e is the coefficient associated with eddy currents and k_a is the coefficient associated with anomalous loss.

In practice, however, the numerical separation of eddy current loss from anomalous loss is questionable and some published models do not include the third term in Equation 2.4 with f and B raised to the power of 1.5 (thus assuming that $k_a = 0$) (Ionel *et al*., 2007).

A typical core loss profile that core steel manufacturers provide for various forms of transformer modelling is given in Figure 5.

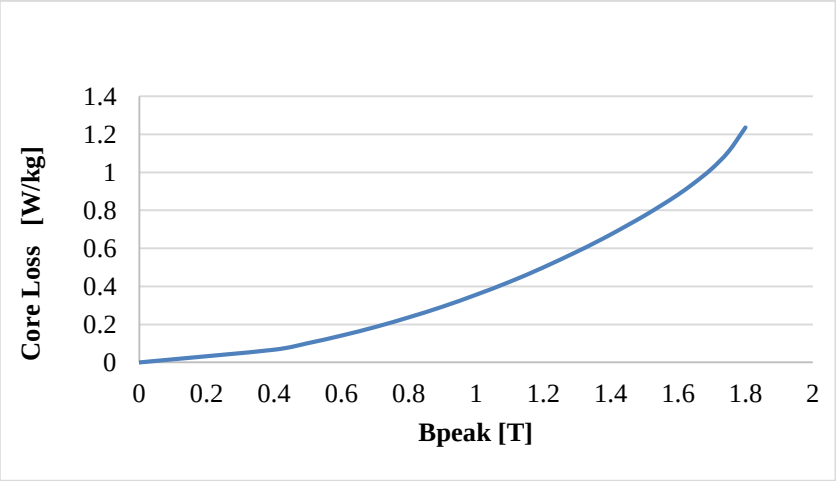

Figure 5: Core loss for an HGO 0.3 mm grade core steel at 50 Hz

When a core loss profile is used as input into FEM software, the necessary coefficients are derived from the curve and incorporated into forms of Equation 2.4 for the core loss calculation. In studies involving GIC where partially saturated transformer could have peak flux densities up to 2.05 T the curves like the one in Figure 5 will need to be extended beyond 1.8 T using curve fitting tool.

With reference to Figure 6, the 3p3L (d) is a more economically viable transformer than a bank of three single-phase transformers made of either 1p3L (a), 1p2L (b) or 1p4L(c). In order to increase reliability of transmission, a spare transformer is often required to be on stand-by, but it becomes too costly to have two 3p3L power transformers.

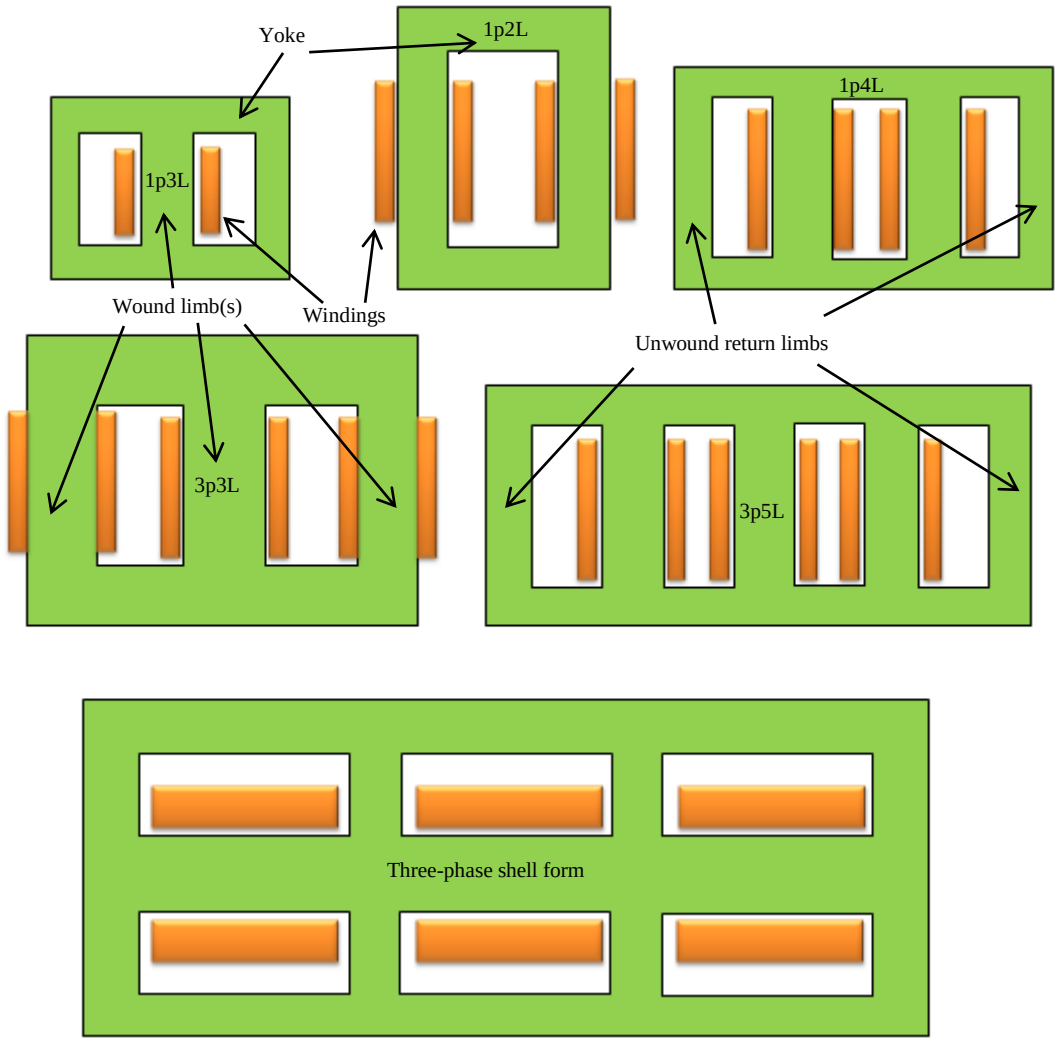

Figure 6: Different core constructions of transformers adapted from Berge (2011) and Kulkarni and Khaparde (2013). A 3p7L (not shown here) could be described as a combination of three 1p3L's with a common magnetic circuit

It is, therefore, often cheaper to have a three-phase bank of three single-phase transformers with only one spare unit on stand-by. When high capacity power transformers are required (>500 MVA), 3p5L's (e) may be preferred to 3p3L's because their reduced height makes transportation easier. When even higher capacities are needed (>1000 MVA), then single-phase banks with three limbs or four limbs are preferred for similar reasons. The way that the flux is distributed from the wound limb(s) to the yoke(s) and return limb(s) varies with each core construction, and so, when testing or modelling it is important to have a good understanding of the different flux responses under certain excitation conditions.

The core serves two purposes, namely to offer a low reluctance path for magnetic flux, and to provide support for the windings. The purpose of laminating the core is to reduce eddy current loss as discussed earlier. The core assembly is either a 90° butt-type configuration (butt joints) or a mitred configuration with overlapping joints as described in early literature (Jones & Moses, 1974), or a combination of both in some distribution units. The mitred configurations are generally preferred, to reduce iron losses. The 3D illustration in Figure 7 shows the difference between butt joints and mitred overlap joints as

described in their patents and in the literature (Jones & Moses, 1974; Mechler & Girgis, 2000). When modelling the core in FEM, it is not unusual practice to simplify the core to have solid core joints, whereas in reality, air gaps exist at the joints due to joint dimension stacking error (Nakata & Kawase, 1986).

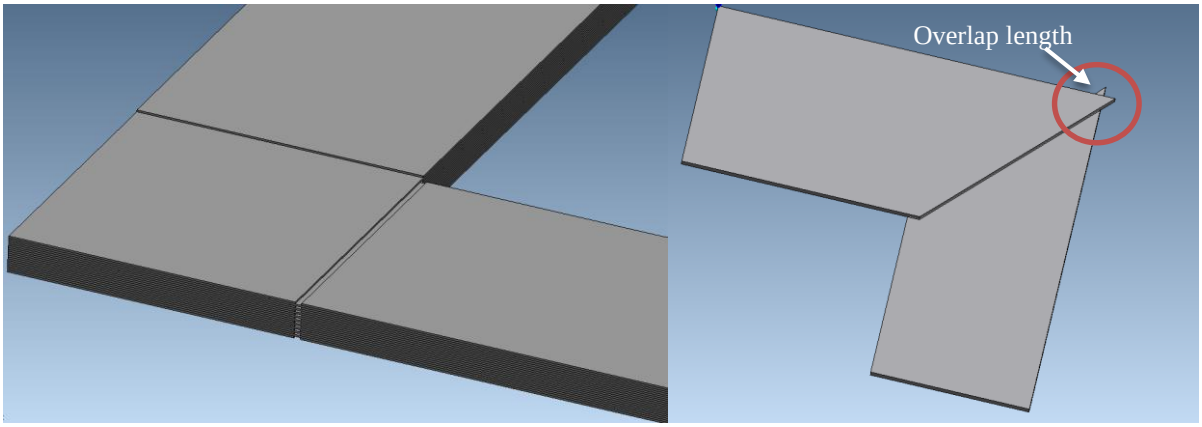

Figure 7: Illustration of a butt joint (left) and mitred joint (right) with the overlap region circled in red

Reduction in losses can be achieved by using single-step lap joints (SSL), also known as conventional joints or non-step lap joints, and multi-step lap joints (MSL). The latter consists of a set of laminations called a packet (5 to 7 sheets of core steel) stacked with a staggered joint and it is favoured above the SSL because studies show that it yields lower core loss, noise, and excitation current (Mechler & Girgis, 2000). In their study, Mechler & Girgis showed that with a nomimal operating flux density *B* of 1.7 T, the *B* can rise to 2.7 T for conventional SSL, which is far beyond the saturation point, with an air gap flux density of 0.7 T. On the other hand, the MSL has a *B* varying from 2.028-2.035 T at the joints, showing effective flux loading or a more uniform distribution. The *B* in the air gaps is as small as 0.04 T, meaning that it virtually avoids the air gaps.

Transformer windings, the current carrying conductors wound around the limbs of the core, are typically made of copper. Aluminium windings may also be used as a cheaper alternative to copper. In their parametric analysis of the selection of copper over aluminium, Olivares-Galván *et al.* (2010) concluded that for transformers with a capacity of 190 kVA or less, aluminium is the better choice for transformer windings. For 190 kVA units and higher, copper becomes better than aluminium because the total owning cost (TOC) becomes lower. Comparing the electrical conductivity of copper and aluminium at 20°C ($5.77*10^7$ Siemens/m and $3.8*10^7$ S/m, respectively as per the Infolytica MagNet software's library of common materials), their study observed that when aluminium is substituted for copper to carry the same current, a larger cross section is required. Apart from this consideration, Olivares-Galván *et al.* also stated that the TOC with copper for larger transformers is further reduced because it allows for less use of core material, insulation, structural steel and oil.

Different types of windings are used for the LV and HV sides. For instance, transformer manufacturers typically use helical windings for LV, disk windings for HV and loop layer windings for the regulator winding operated by the tap changer. Rectangular continuously transposed cables (CTC) are normally

used as transformer windings to avoid circulating currents, thus reducing losses while providing extra mechanical strength than other windings (Kulkarni & Khaparde, 2013).

2.2.1 Summary

Section 2.2 has presented, first, a background on transformers in power systems, then a brief description of conventional modelling applied in research and in the industry, and lastly, a discussion of some important aspects regarding different core structures, core stacking, and some components. The remaining sections of this chapter open the discussion of the extent to which the GIC/dc phenomenon has been investigated in the literature, and compares the findings.

2.3 GIC phenomenon and reports on its effect

Geo-effective coronal mass ejections (CMEs) launched from the sun have complex interactions with the Earth's magnetosphere, resulting in the flow of ionospheric currents (Pinto *et al*., 2005). As these currents flow, there is an induced magnetic field, as set out in Faraday's law of electromagnetic induction (Boteler & Pirjola, 1997). When grounded power transformers at the ends of high voltage transmission lines are separated by hundreds of kilometres, they form a loop within which the magnetic field induced by the ionospheric currents causes induced currents to flow in their neutrals. Such currents are known as geomagnetically induced currents (GIC).

These major disturbances occur approximately every 11 years due to the sun's magnetic activity cycle but are not limited to just this period. GIC typically have very low frequencies (in the milliHertz range), making them quasi-dc currents at power frequency (50/60 Hz) (Price, 2002).The resultant dc excitation drives transformers into half cycle core saturation, causing incipient and cumulative damage (Heindl *et al.*, 2011, Moodley, 2013). A partially saturated transformer is characterized by a significantly increased asymmetrical magnetizing current, the generation of unwanted harmonics, noise and overheating, large reactive/non-active power (Mvar) consumption, and voltage depressions (Kappenman & Albertson, 1990). Many other studies (Molinski, 2002, Lahtinen & Jarmo, 2002, Marti *et al*., 2013, Chisepo *et al.*, 2013, Raith & Ausserhofer, 2014, Ramírez-Niño *et al*., 2016, Borrill *et al*., 2016) which report on field measurements with GIC and laboratory tests with dc confirm these responses.

In their experimental analysis, Takasu *et al.* (1994) declare three-phase three limb transformers (3p3L's) to be practically insusceptible to GIC effects based on a small-scale test system, prompting a widespread belief in the transformer research community. Against this, Kappenman in the discussion of the same study reports that significant harmonic distortion and draw of reactive power was observed in a real 3p3L power transformer, indicating that a 3p3L actually has a response to GIC, though not as high as a single-phase shell type (1p3L). Later, Koen and Gaunt (2002) reported a correlation between 'saturating harmonics' (the presence of even current harmonics) and GIC flow in a South African 3p3L transmission transformer, and stated that these recordings appear to contradict the theory that a 3p3L

is ‘GIC-immune’. More recently, the derivation of an enhanced transformer model (Rezaei-Zare, 2015a; Rezaei-Zare, 2015b) found that a GIC even as low as 10 A/phase can saturate 3p3L power transformers due to *the influence* of the transformer tank, the air inside (or oil) and structural parts. The influence being referred to in this study is the individual reluctances of components inside a transformer not commonly accounted for in most transformer electrical equivalent circuits. Figure 8 is an illustration of the stray flux paths (white arrows) of a partially saturated 3p3L power transformer with GIC at full load at a time instant *t*. This response of a 3p3L transformer was also reported by Mulasalihović *et al*. (2008) in planar eddy loss study. Their research highlighted the importance of the proximity of the tank to the core, the magnitude of the GIC/dc, and the degree of GIC/dc unbalance in a 3p3L when incremental dc injection levels up to 10 A/phase are applied.

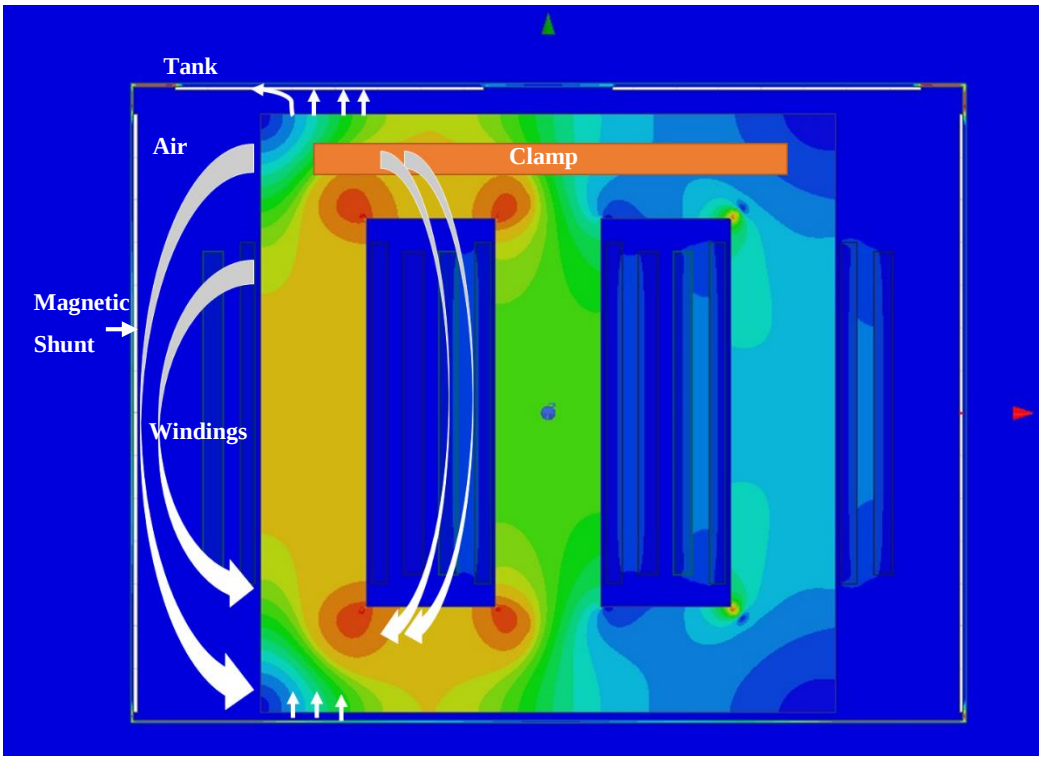

Figure 8: Stray flux paths in a partially saturated 3p3L power transformer to illustrate the descriptions in Rezaei-Zare’s study (2015a)

Because of the high number of turns in the transmission side of a power transformer, there are several dc Ampère-turns (dc current × number of HV winding turns) which induce considerable dc flux. This leads to core saturation resulting in flux leaving the core relying on air (or transformer oil), structural parts and the tank for return paths due to the combined ac-dc magnetization. No wonder the earlier study (Takasu *et al*., 1994) with model transformers using only an 18-turn winding for (balanced) dc injection deemed 3p3L’s to be immune to GIC.

The GIC phenomenon is not the only power system security threat that injects quasi-dc components into power networks. A very early report (Maruvada & Drogi, 1988) forsaw the possibility of ac and dc circuits running in parallel and sharing the same right of way due to the increased use of HVDC in existing HVAC networks.

Corona-generated space charge from dc line conductors may inject direct current components into the ac conductors for adjacent-tower and same-tower configurations. Also, multiple interactions that take place in HVDC equipment add to this dc effect. The equipment includes converters, wind farm inverters and other rectifier interfaces. This sharing of the same right of way between ac and dc in the transmission lines could, therefore, result in quasi-dc currents leaking into transformer windings, and have the same effect as that brought about by GIC. Only recently has transformer modelling and research in this area started to investigate this phenomenon. Several studies (Tenbohlen *et al.*, 2013, Gong *et al*., 2017, Wang *et al*., 2017) show that this is especially the case in countries with considerable use of dc transmission, and there is a possibility of ac systems interacting with monopolar or unbalanced bipolar HVDC systems.

During a significant GIC event, power transformers introduce multiple undesirable conditions into power systems (Kappenman & Albertson, 1990). The response to GIC depends on the transformer core structure and its magnetization characteristics (Mulasalihović *et al*., 2008, Berge, 2011). Because of the distortion of the *B-H* characteristics, the peak magnetizing current increases significantly in one half-cycle by factors of ten, a hundred or even a thousand (Albertson *et al.*, 1993). Since the magnetizing current lags the system voltage by 90°, the reactive/non-active power absorbed by the transformer increases dramatically. This large asymmetrical magnetizing current also causes the production of increased even and odd harmonics which pose a threat to the function of relay protection systems, Static Var Compensators, and ultimately power system stability (Kappenman & Albertson, 1990). As the reactive/non-active power increases, the efficiency of energy transfer decreases significantly, and this may be accompanied by a voltage collapse.

Reactive power calculated conventionally under the assumption of balanced sinusoidal conditions differs from non-active power under unbalanced, distorted conditions with dc components of current. Because of the generation of several even and odd harmonics in a transformer undergoing half-cycle saturation, imbalance in the transformer neutrals may occur and add to the total losses in the system. The concept of non-active power under these non-ideal conditions is rigorously derived and defined in two companion studies in a general power theory (Malengret & Gaunt, 2011; Malengret & Gaunt, 2012). Further studies validate and contextualize the differences in the calculation of Q through rigorous transformer GIC/dc experiments and EMTP simulation in PSCAD/EMTDC (Gaunt & Malengret, 2012; Chisepo, 2014) and using a proof-of-concept non-active power smart meter (Martindale *et al*., 2014). The important finding from these studies is that the conventional calculation of reactive power consistently underestimates the (actual) Q drawn by transformers with GIC/dc since the non-active power calculated by the general power theory yielded higher losses due to the unbalance, distortion and dc components.

GIC flowing in transformer windings induces dc magnetization which is characterised by a dc component in the ac magnetic flux. The mean magnetic flux in the transformer core is proportional to the integral of this voltage (Faraday's law) and depending on the size of the GIC, the transformer will

go into half-cycle saturation. There are several diagrams in the literature that explain half-cycle saturation and they differ in detail in the context of B, H, I_{mag}, voltage, etc. (Kappenman & Albertson, 1990, Tousignant *et al*., 1996, Bolduc *et al.*, 2000, Lahtinen & Elovaara, 2002, Girgis & Vedante, 2012). It should be noted, however, that the representation of the magnetizing current, flux and BH characteristic in these studies is valid for a single-phase transformer (in a three-phase bank) which only possesses its own self-inductance. The response of a multi-limb three-phase transformer with mutual inductances between the phases may differ from these depictions due to the different reluctances seen by each limb.

It is widely agreed that, among the most common transformer core types in power transmission networks (PTN's), the most vulnerable and problematic core structure is the 1p3L. Experimental tests based on small transformers of the same VA capacity and voltage ratings demonstrated this (Chisepo, 2014), and reported that the three-phase five limb (3p5L) is the next most vulnerable, and the 3p3L is the least responsive (but not invulnerable, because it showed some response regarding increases in reactive power with increasing dc).

The susceptibility is a function of the core structure's ability to offer dc flux return paths. The 1p3L and 3p5L readily provide low reluctance dc flux return paths through their outer limbs. In power transformers, the 3p3L does not readily offer any zero sequence return path for the dc flux (since all three limbs are wound with ac excitation in the windings), but due to the increased stray flux during a GIC event, the dc flux must find its way through the transformer tank via other metallic parts and the air (Price, 2002; Girgis & Vedante, 2012; Rezaei-Zare, 2015a). An illustration of the dc flux paths in different core constructions is given in Figure 9 showing the laboratory transformers described earlier (Chisepo, 2014).

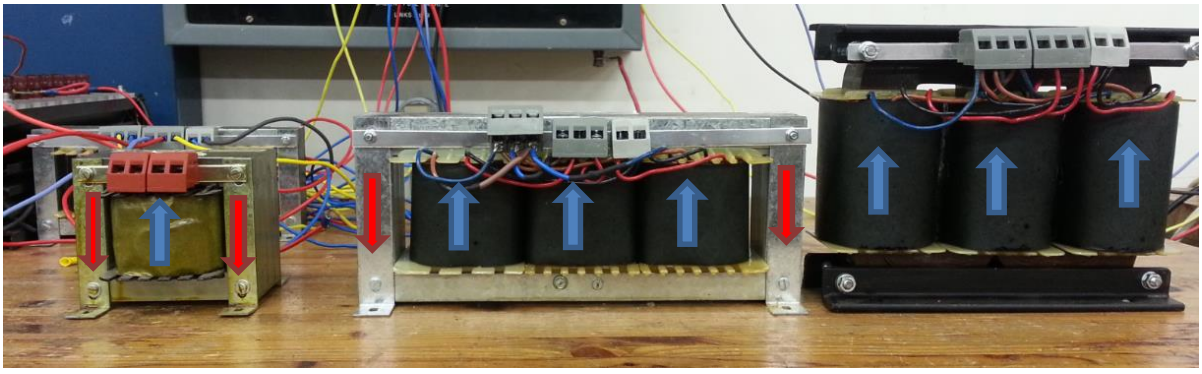

Figure 9: Industrially fabricated laboratory bench-scale transformers: 1p3L (left), 3p5L (centre), and 3p3L (right) (Chisepo, 2014) showing their dc flux paths in the cores, as described in the literature (Girgis & Vedante, 2012)

South Africa's nuclear power station in Koeberg installed a three-phase bank of single-phase four limb transformers (1p4L) fairly recently. This core construction is uncommon in the Eskom networks and the prediction of its response is vital for system operations and studies involving GIC. The 1p4L bank is preferred as a GSU because the nuclear power station is capable of delivering close to 1000 MVA to the grid. The physical dimensions for most of the other core constructions of the same capacity make them impractical to transport due to their height. The most common core constructions of transformers are explored in several studies in the literature resulting in some transformer models for 1p3L, 3p3L and 3p5L in most topological commercial software e.g. PSCAD/EMTDC. Currently there is not much literature in the investigation of 1p4L topological and FEM models, and so investigating its response, especially in the context of GIC would be valuable.

2.4 Transformer modelling for GIC/dc and other non-sinusoidal conditions

Chapter 1 introduced the usefulness of the FEM approach. This section begins with a Transformer-GIC FEM study using commercial software developed as early as 1989 which provided helpful information on the differential flux analyses across several core structures. Related studies since are then discussed while raising important questions.

Lu & Lui (1993)

Identifying that there are very few reports on the flux analysis and overheating in transformers with GIC, Lu and Liu (1993a) investigated the response of five different transformer core structures, namely 1p3L, 3p3L, 3p5L, 3p7L and 3p3L conventional shell-form core structure (a diagram of this particular core structure can be found in the illustrations of dc flux return paths given by Girgis and Vedante (2012)). Lu and Liu used an early version (1989) of Ansoft FEM software (later known as ANSYS) and managed to analyse magnetic field intensity profiles (H) and transformer impedance matrices (Z) under dc excitation.

The simulations focused on 2D small scale models for reduced calculation time with their cores further simplified as solid under dc excitation only. The effect of the laminations were not included because of the small size of the models. It was found that all transformer core structures were susceptible to GIC to a degree that depends on the combined function of the size of the GIC, the core construction and the dimensions of the legs and limbs of the transformer. In addition, this report strongly recommended a transformer tank in future modelling. Lu & Liu's early FEM study (1993a) is important, because, although the models are limited by being subjected only to dc excitation, this research was one of the starting points in the literature in understanding the flux distributions which cause overheating in transformers due to GIC.

Later in the same year, Lu and Liu (1993b) tested a new 1p3L transformer equivalent circuit based on flux distributions from a 3D FEM analysis to investigate transformer response under GIC. This 3D FEM solution appears to have been derived from the earlier study (Lu & Liu, 1993a).

Some conclusions were drawn regarding total harmonic distortion (THD) trends and the negligibility of core loss under GIC, but there is no experimental data for verification.

Picher et al. (1997)

Identifying that the tie plates of 1p3L power transformers are the component most susceptible to temperature under dc excitation and ac over-excitation through measurements, Picher *et al.* (1997) attempted to determine a tolerable dc current limit in power transformers using FEM simulations. The modelling approach excluded the core from the geometry of the FEM model because they considered it to be fully saturated or just an "air core" with high levels of dc up to 75 A/phase. It was observed that 75 A dc resulted in less distortion and a lower temperature rise than 50 A dc. The researchers explained that higher levels of dc increase saturation and limit the eddy currents thus generated, and that they therefore reduced the percentage of distortion. The team further concluded that the heating of the tie plates due to dc was not likely to reach a critical level when exposed to permissible temperature standards (IEC), but that even that much heat could reduce the strength of insulation in the long term, thus causing incipient damage only. This study was limited to structures of 1p2L and 1p4L cores and 2D FEM analyses which assume a "core-less transformer" when very high dc is applied.

Dong et al. 2001

In 2001, Dong *et al*. developed linear empirical models for determining the reactive power (Q) consumption under GIC which needed only the value of GIC in the neutral, the no load reactive power and the core construction (e.g. 1p3L or 3p3L). The motivation for their investigation to develop a simple model is the difficulty in acquiring detailed design information and the complexities which are necessary with FEM. Other studies also support the linear relationship between GIC and reactive power (Molinski, 2002, Berge *et al.*, 2011) until, more recently, it has been shown that Q-GIC characteristic is not strictly linear (Razaei-Zare, 2014; Bergsåker, 2014). Through measurements and an analytical approach on 1p3L's, Rezaei-Zare (2014) reports that with increasing GIC the linear models overestimate the true draw of Q from the power system at higher levels of GIC. This was demonstrated by testing the 'initial slope' approach, which remains linear for increasing dc, against transformer test data and simulation resulting in a change in slope at relatively higher levels of dc. Bergsåker's observations (2014) from EMTP simulations of different sizes of 3p3L and 3p5L transformers (with detailed design and test data) are consistent with those of Rezaei-Zare (2014), and Bergsåker concluded that reactive power consumption is dependent on core size. In contradistinction, the IEEE Guide entitled: "Establishing power transformer capability while under geomagnetic disturbances," still regards the transformer Q-GIC characteristic to be linear (IEEE Std ™ C57.163, 2015) and does not seem to consider that the Q requirements for different transformers are not easily predicted.

Yao et al. 2005

In an effort to analyse the eddy current losses which may result in localised heating of power transformers, Yao *et al.* (2005) explored the possibility of incorporating the FEM approach for online transformers in a power system. They point out that the main difficulty in a power system study is the near impossibility of achieving a FEM solution, due to the very large computational scale needed to consider various system parameters, such as the time duration of saturation. In their approach to tackle the problem, they simulated a power system with the required system condition and constraints, avoiding the 3D non-linear calculation other methods need. Results from this stage were then used to generate some equivalent exciting sources and magnetic parameters for input in a 3D transient FEM analysis. Modelling involving dc bias in 1p3L power transformers up to 50 A dc was carried out, whose results suggested that thermal performance (i.e. overheating and average temperature rise) can be 'easily evaluated' for conventional 1p3L transformers. This conclusion is based on the findings that increasing dc excitation is proportional to overheating. This approach appears to use symmetric 3D transformer models with their cores simplified as solid but there are no measurement data for validation. In a similar study, though, Mulasalihović *et al.* (2008) performed an experimental analysis with some consistent findings of increased losses with increasing dc up to 10 A/phase in model cores.

Mohammed et al. (2006)

This study focused on problems of power quality in transformers, and it showed that modelling transient harmonics for a wide range of frequencies was problematic with conventional approaches (sinusoidal case). To address this difficulty, Mohammed *et al*. proposed a method to couple FEM and the electrical circuit domain together with wavelet packet transform (WPT). The extended capability of wavelets allowed for the quantifying of disturbances by extracting harmonics, disregarding their (short) period of occurrence i.e. local representation. The method developed in this study appears to be more suited for problems with electrical machines and power electronics with unique short duration high frequency signatures that need to be identified during faults. Normal FFT processing of global parameters is, however, adequate for studies of transformers and GIC because of the low-frequency slow transient nature of the problem. This study shows that it might be necessary to couple the FEM domain with the electrical circuit domain when more complex signal inputs e.g. ac-dc excitations need to be modelled.

Zhao et al. 2011

Aiming to improve the accuracy of previous modelling approaches which used time-stepping FEM for eddy current loss evaluation with dc (Yao *et al*., 2005), Zhao *et al.* (2011) incorporated the harmonic balance finite element method (HBFEM). In their approach, they investigated the calculation of the non-linear magnetic field with dc bias. The results were compared with an Epstein frame-like core subjected to ac-dc excitation and the harmonic analyses between the two correlated well.

2D FEM simulation with solid core joints is then used to analyse some flux distributions of different harmonic components.

Mousavi et al. (2011)

Mousavi *et al.* (2011) modelled various versions of single-phase transformers (1p3L, 1p2L and 1p4L) to investigate core loss under dc magnetization using 3D FEM. The core loss calculation was based on Bertotti's model (1988) which includes anomalous loss in addition to hysteresis and eddy loss. Some FAT measurements under normal and ac over-excitation conditions are used to validate the models. Two significant conclusions are that GIC could increase core loss by over 40%, and that the degree of loss was core material dependent, however, there was no measured power transformer-GIC/dc data for comparison. These findings directly contradict the report by Lu and Liu (1993) which states that the influence on core loss with increasing dc is negligible. Neither of the studies has ac-dc experimental data for comparison with the modelling.

Bíró et al. (1999, 2007, 2008,2014)

Using a two-stage finite element method and experimental data for comparison, Bíró *et al*. (2007) managed to predict the magnetizing currents of a single-phase transformer under dc bias. The method involved a 3D static FEM analysis with dc followed by the implementation of edge element formulations, which have been shown to be a robust approach (Bíró, 1999), in a time-harmonic/eddy loss problem. The single-phase (1p3L) study is then extended to predict magnetizing currents for a 3p5L power transformer to demonstrate an iterative numerical technique (Bíró *et al*., 2008). There was no measurement data for comparison. A more detailed approach was then introduced to analyze the response of a 3p3L power transformer (Bíró *et al*., 2014). This method, requiring very high computational power, used parallel algorithms to achieve a steady state solution without having to step through transients. Although the improved numerical technique is soundly presented with plausible results under dc bias, the authors respectfully state in their concluding remarks:

"Unfortunately, no measurement results are available to validate the above analysis."

thus showing the need in the literature for further investigations which provide measurement data for FEM validation.

Jazebi et al. (2013, 2016)

FEM can be used to assist in the derivation of topological equivalent circuit parameters where measurements are difficult to take or cannot provide the required information. Jazebi *et al.* (2013) improved the accuracy of a π equivalent circuit model for the calculation of low-frequency transients i.e. ferroresonance, inrush currents and GIC. 3D FEM was used to study the behaviour of the magnetic fields in the air in order to make analytical adjustments of the air inductances in the improved π model. Earlier FEM studies considered a power transformer in deep saturation (i.e. 75 A/phase) to be virtually

a “core less” transformer in the modelling (Picher *et al*., 1997) thus having only an “air core inductance”. A more recent study (Jazebi *et al*., 2016) provides further insight into the practical saturation parameters of transformers and their models, pointing towards a difference existing between “air core inductance” and “terminal saturation inductance”.

Girgis et al. (2016): Guidelines for Transformer GIC specifications

In response to the increasing attention to transformer-GIC research in the literature, an IEEE standard specifically for transformers and GMDs was made available: IEEE Std™ C57.163-2015, “Establishing Power Transformers Capability while under Geomagnetic Disturbances.” It shall be referred to as “the Guide” in this section. In the summary and discussion put together by Girgis *et al.* (2016), GIC signatures are generally categorized into two stages:

- Base stage – multiples of small to moderate GIC magnitudes lasting from several minutes to several hours. Allowable temperatures for the windings and structural parts are defined as 140° C and 160° C, respectively.
- Peak GIC pulse stage – high levels of GIC pulses which last from less than a minute to several minutes. Allowable temperatures for the windings and structural parts are defined as 180° C and 200° C, respectively.

The Guide puts the onus on the manufacturer to assure a customer specified GIC capability by means of calculation, modelling and analysis. The requirements include:

- The transformer-GIC characteristic and current harmonics for a specified range of GIC
- Hot spot temperature of windings and structural parts (and their locations) based on the typical GIC signatures provided by the customer. This requirement also specifies the placing of temperature sensors at the expected areas of localized heating during a GMD event
- Transformer loading capability under GIC
- Customer’s trends in transmission system voltage variation, tap changer settings and routine exposure to over-excitation.

Factory testing with dc on a power transformer that is not loaded is not comparable with an actual GMD event that has a slow varying low-frequency GIC in a loaded transformer. One of the reasons for this is the difference in the viscosity of the oil under no load and loaded conditions which results in dc off load tests being an overestimation of the response. A factory full load test with the HV windings short circuited to simulate a load is also not adequate because of the very low levels of induction used. At the same time, several limitations are inevitable whenever dc tests are involved and the results using low levels of dc on an unloaded power transformer cannot be extrapolated to large GIC values during a GMD. Other power system related issues addressed in the same Guide include GIC monitoring, assessing susceptibility of existing fleets of power transformers, thermal effects, and noise and vibrations.

Gong et al. (2017)

In most of the previous studies discussed, several researchers attempted to improve previous FEM approaches by focusing on better accuracy while reducing computational burden. Gong *et al.* (2017) reintroduced the use of commercial FEM software in a complex magneto-fluid thermal analysis of a 3p3L power transformer with dc bias. This study is one of the first implementations of electromagnetic-thermal coupling with ac-dc excitation. An oil natural air natural cooled (ONAN) 180 MVA 220/110/35 kV power transformer is investigated for hot spot temperature rise in the core and windings. The FEM approach was first compared with the IEC 60076-7 empirical formula, showing good agreement before suggestions on optimization of cooling for ONAN transformers were proposed. Domain coupling in literature was also demonstrated in the form of field-circuit coupled FEM performed in 2D with the added detail of core hysteresis which is often neglected (Wang *et al*., 2017). Improved accuracy is recommended for future 3D analysis.

Kohli, et al. (2018)

The work done by Kohli *et al.* (2018a, 2018b) models some LV 6.9 kVA 3p3L/5L transformers and used ANSYS 2D FEM to analyse the effect on the magnetizing currents, flux distributions and harmonics. The results for both core structures were as expected, i.e. the 3p3L has less distortion than the 3p5L dc, and the models used have simplified 2D solid core joints. Other studies (Lu & Liu, 1993a, Chen *et al.*, 2018) reported consistent success in using FEM in ANSYS with very simple 2D models. These results, even though mostly being qualitative in the 2D case, lead to the use of ANSYS in transformer-GIC studies in the work reported in this thesis (Chapter 4). Furthermore, the application of ANSYS is extended to the 3D domain, where real power transformer data is used (with a tank).

Chen et al. (2018)

Like the study by Gong *et al.* (2017), Chen *et al.* (2018) proposed a co-simulation approach using Matlab for the development of control system models, Simplorer (an ANSYS multi-domain simulation tool that can be interfaced with FEM), and ANSYS FEM to solve the multi-physics problem. The aim of their study was to mitigate the effects of dc excitation through dc demagnetization. The FEM simulation appeared to be qualitative (2D with simplified solid core joints), but it provided a good picture of the potential redistribution of the flux during dc bias when a compensation scheme is applied. The results from this study showed that for very small currents of dc (0.3 A) applied to a model laboratory 0.22/10 kV 10 kVA 1p3L transformer (with additional dc demagnetization scheme attached to dc flux return limbs), there is an increase in I_{mag} from 4.63 A to 7.8 A, and that it can be reduced to 5.17 A (by 34%) after compensation. The mitigation scheme lost its compensatory effectiveness at 1 A dc when it only managed to reduce increased I_{mag} due to dc by only 19%. Seeing that 0.3 A dc is only 6.5% of the I_{mag}, this technique is not practical for power transformers which can have GIC magnitudes in the order 100-1000% of the normal I_{mag} per phase (assuming an I_{mag} of 1 A RMS).

The approach, therefore, is limited to dc current levels which are very small compared to the $I_{mag,}$ and shows the need to characterize the I_{mag} in the context of dc before any relevant GIC mitigation approach can be realized.

2.5 Summary

Power transformers are designed to operate close to the knee of their BH characteristic, typically 1.7 T. The type of core steel used for the laminations and the way it is stacked at the joints greatly influences the amount of loss that will be produced by the transformer affected by GIC.

In FEM modelling, which requires accurate physical properties as input, the transformer core, winding configuration, structural parts, and air are of the greatest importance. Parameterization of these components needs to be carefully considered and tested against available measurement data where possible.

Generally, transformer-GIC FEM studies from as early as 1993 until now have lacked measurement data for comparison or validation. Only very few cases with only certain (model) transformer types are available in the literature. This is mainly due to the impracticability of testing large transformers with dc and the difficulty in taking flux measurements in and around the core to compare with 2D/3D flux distribution analyses.

It appears to be acceptable in the literature to validate a FEM transformer model for GIC studies with ac normal excitation and ac over-excitation (especially when GIC/dc measurement data is not available), but it is still necessary to test the response with measurement data when it becomes available.

FEM is shown to help with the development of lumped parameter transformer electrical equivalent circuits for low-transients like GIC, particularly when some required model parameters are too difficult to measure. One such parameter is “saturation inductance” also referred to as “air core inductance”, and how it affects practical or realistic parameterization for topological models requires further investigation.

The main cause of transformer over-heating is excessive stray flux flowing in the structural parts of the transformer causing increased ohmic loss and eddy loss. The response of transformers to GIC depends on the core construction, actual core dimensions, and the tank, air and structural parts. The common core structures (i.e. 1p3L, 3p3L, and 3p5L) have been modelled in FEM, EMS/EMTP, and some laboratory experiments with dc have been performed on them. The single-phase four limb (1p4L) transformer does not appear to have been thoroughly explored for its response, either through modelling and simulation or experimental methods.

The lack of agreement in the literature regarding the susceptibility of three-phase three limb transformers to GIC or the linear reactive power-GIC characteristic shows the need for better modelling

of the response. The FEM approach may be advantageous because, given enough modelling detail, the response can be predicted with greater confidence and without the need for empirical factors.

Table 1: Minimum modelling details needed to carry out FEM and related topological transformer-GIC modelling

Parameter	FEM	EMS/EMTP (topological)
Nameplate ratings	Yes	Yes
Core structure	Yes	Yes
Core steel BH properties	Yes	No
v-i curve	No	Yes
Core dimensions	Yes	No (yes in very few)
Winding number of turns	Yes	No
Winding dimensions	Yes	No
Voltage transformation ratio	No	Yes
Material properties of structural parts and surroundings	Yes	No (yes in very few)
Boundary conditions	Yes	No
Air core inductance	No	Yes
Joint stacking configuration	Yes	No

In any reliable transformer modelling technique, all the losses need to be adequately represented, despite some publications having omitted some parameters, e.g. anomalous loss, in their investigations. The literature shows that transformer core is often simplified to have solid joints in 2D and 3D FEM analyses. It is shown that joint dimension stacking errors exist in actual transformers, and that they can affect the no load currents under normal ac excitation. Field-circuit coupling in the FEM domain is required for modelling for the complex GIC/dc so as to represent actual laboratory set ups.

The recent IEEE Guide for transformer capability during GMD events recommends the modelling of power transformers for GIC performance characterization by manufacturers, rather than simply accepting the difficulties of doing physical dc testing in the factory. In this thesis, the GIC testing protocol developed by Chisepo (2014) for very small transformers is extended to a larger scale using model transformers tested at a utility facility. The requirements for such testing include the standard characterization of the test transformers' magnetic response under normal conditions and the addition

of flux measurements in order to understand better the effect of stray flux which leads to localized heating in transformers. It is anticipated that an exhaustive approach to the experimentation will aid in the derivation and development of more accurate modelling for GIC/dc which will cover some of the gaps identified in the literature.

From the literature, the minimum modelling details required to carry out the FEM and related modelling of transformers is summarised in Table 1. It is evident that the FEM requires greater detail in the modelling than topological methods, which explains why it is computationally intensive (performing iterative calculations).

Topological modelling in EMS/EMTP software (with inherent saturable transformer models) requires the air core inductance of the transformer to be modelled, and this is often not easy to measure. In literature, this measurement is derived from 3D FEM as a first approximation, by injecting a current into core-less windings. Jazebi *et al.* (2013) proposed a method to measure the "terminal saturation inductance" for a single-phase three limb (1p3L) transformer, however, there are no reports of testing this method with other core structures and then validating it with the FEM. Also, an assumption is often made in literature that a transformer in deep saturation can be treated as an air core. No FEM simulation in the literature has verified this assumption through laboratory testing with the method proposed by Jazebi *et al.* (2013) and then performing a full 3D FEM simulation with a core and its windings. Also, there are no reports of a transformer being stripped of its core and then measuring the air core inductance of the windings with the windings still in their original positions. This prompts the need to investigate the possible difference between the so-called "terminal saturation inductance" and the "air core inductance" both in the FEM and laboratory tests.

Further, in their extensive survey of over fifty published works focusing on transformer losses, Olivares-Galván *et al.* (2009) report that most studies use simulation and modelling only, that fewer studies use experimental methods only, and only 7% of the surveyed reports use both approaches. Therefore, this thesis aims to investigate a rigorous modelling approach contrasted with numerous measurement data from laboratory testing.

3 BACKGROUND TO MODELLING APPROACH

Chapter 2 gave a baseline for power transformers and GIC from the literature. The key parameters for modelling transformers with GIC were identified. Finite element matrix (FEM) modelling is abundant in literature, and it is almost the obvious choice for transformer modelling. However, before FEM is explored, it is necessary to gain an understanding of its background before developing the theory for ensuing simulation protocols. Also, it is necessary to explore methods other than the finite element method which could also be applicable for the modelling outlined in section 3.2.

The differences between analytical techniques and numerical methods is given in section 3.2 Next, the most common numerical methods are explored discussing their advantages, limitations and applicability for transformer engineering.

Finally, a transformer-GIC modelling approach is proposed.

3.1 Background to Computation of Electromagnetic Fields

In transformer engineering, the fields inside a transformer during various operating conditions need to be known accurately to optimize the design and ensure reliability. Lumped parameter equivalent circuits have their limitations, as discussed in Chapter 2, because they are only as accurate as they are able to represent properly physical components and properties of a transformer e.g. sharp edges, the anisotropy of electrical core steel, nonlinearity, hysteresis, etc. (Kulkarni & Khaparde, 2013).

3.1.1 Analytical techniques

In order to overcome the electrical equivalent circuit limitations, analytical techniques can be applied in transformer engineering. Dowell (1966) derived a one-dimensional analytical method calculating the variation of winding resistance and leakage inductance with frequency in transformer windings. In the same study (before computers could perform several repetitive calculations easily), the author commented in the conclusion that,

"A quick simple method has been derived for obtaining a.c. leakage impedance of a transformer…It is rather unfortunate that calculating the d.c. leakage inductance components accurately is a fairly lengthy process… [consisting] of substituting numbers in the given formulas."

Despite the caveat given in closing in the above study, several high-frequency studies exclusively based their analytical approaches between 1979 and 1989 on Dowell's solution (Ferreira, 1994). Ferreira identified some of the restrictions of these analytical approaches as follows:

- Exclusion of magnetizing current of transformers
- Assuming infinitely long solenoid windings
- Error occurrences when simplifying round conductors with square-shaped ones.

An improved analytical approach for conductive losses in transformers by Ferreira (1994) also has some limitations, which includes possible errors due to increased complexity of the transformer geometry, an assumed magnetizing current and tightly wound windings. Analytical techniques are attractive to manufacturers because they are easy to incorporate into their in-house electrical design software (EDS). However, with such limitations, analytical methods cannot be considered for 3D transformer modelling necessary for design optimization.

3.1.2 Numerical methods

Numerical methods have partly replaced analytical approaches because of their ability to handle the complex parameters that analytical techniques cannot address. They come with some error due to the approximating polynomial expression that is chosen for the variables. However, there are techniques such as mesh refinement which can be used to yield highly accurate solutions and increasing the order of the approximating polynomial. Localized mesh refinement is particularly useful for areas in the domain where the fields are rapidly changing direction and require a more intensive calculation for better accuracy (Kulkarni & Khaparde, 2013).

The most common numerical methods used in research and engineering mentioned in the literature are:

- Finite Difference Method (FDM) - Governing equations are approximated using local variables truncated by a Taylor series. Discretization of the domain is in the form of square or rectangular grids (Sod, 1978; Campbell & Weber, 1992).
- FEM – Discretizes the continuum into a series of triangular (2D) or tetrahedral (3D) elements which can then be associated with physical parts before a set of differential equations are satisfied in an average sense over a region (Brebbia *et al*., 1984)
- Boundary Element Method (BEM) - Unlike FDM and FEM which discretize both the domain and the boundary, BEM is based on the discretization of the exterior boundary only (Brebbia *et al.*, 1984, Costabel, 1986).
- Charge Simulation Method (CSM) – The actual electric field is modelled with a field consisting of several discrete charges placed outside the domain where the field solution is desired. CSM is limited to electrostatic problems e.g. the field analysis for HV insulation (Malik, 1989).
- Method of Moments (MOM) - Linear functional equations are transformed into finite subspaces of functional spaces (linear matrix equations). Thereafter, the electromagnetic problem is classified into either *deterministic* or *eigen value* problems which can be handled by the method of moments. MOM is mostly used in modelling communication systems (Ney, 1985).

3.2 Numerical methods in transformer engineering

From the concise comparisons done on numerical methods in section 3.1.2, it can be seen that CSM and MOM are quite specialized for applications not directly related to the responses inside a transformer. This section focuses on the techniques which are the most useful in transformer engineering as summarized by Kulkarni and Khaparde (2013) and other sources.

3.2.1 Finite Difference Method

FDM is the first widely known numerical method, and it is the simplest method which relies on convenient manipulations of Taylor series expansions (Brebbia *et al.*, 1984). The differential equations are converted to difference equations which operate on a square or rectangular meshed domain. The potential at each grid point is expressed as a function of the potentials nearest to it. With known boundary conditions, solving for all the unknown potentials in the grid can be done. Potential at any point that is not on the grid is determined by interpolation, resulting in irregular boundaries which are difficult to handle compared to BEM and FEM. This generally limits FDM's utility for transformers. An extension of FDM to the finite time difference domain method (FDTD), also known as Yee's method (Yee, 1966) was introduced for high frequency (HF) electromagnetic applications. Because of this direct application to HF propagation of waves, FDTD can be used effectively for modelling partial discharge in transformers (Judd, 2000).

3.2.2 Boundary Element Method

A more detailed derivation of the formulations in BEM is found in the work done by Brebbia *et al.* (1994). BEM is normally used for electric field calculations for insulation design (similar to CSM) but it is not widely available in commercial software. Another disadvantage of BEM is that nonlinearities are not handled easily (Kulkarni & Khaparde, 2013). Also, the method is ideally suited for open boundary problems resulting in a very dense square matrix which is often highly computationally intensive (different from the relatively sparse matrix in FEM easier to perform calculations for simple geometries).

3.2.3 Finite Element Method

FEM is the most used numerical method in the modern engineering disciplines of aeronautics, cooling and mechanics, electromagnetics and computational fluid dynamics (Croegeart, 2017; Prevot, 2018; Holling, 2018; Chien & Chung, 2018). The attributes of the FEM regarding transformer modelling include:

- Handling of nonlinear material properties, anisotropy and non-uniform media
- Handling of complex geometries

- Availability in many software packages/modules and because of this, the best commercial packages are continually upgrading the capabilities of their solvers to handle some problems which were too complex for previous formulations.
- Coupling between different domains to solve complex problems

3.2.4 Conclusion

The preceding sections have discussed the various approaches that can be used in modelling. FEM stands out beyond any doubt to handle a wide array of complex problems in transformers. This study will, therefore, focus on modelling in the FEM. An explanation of the underlying mechanisms in FEM is useful for understanding the modelling described in Chapters 4 and 6.

3.3 Maxwell's Equations in FEM

Electromagnetic effects occur due to the interaction of current carrying conductors and other metallic bodies. These interactions are normally classified into three distinct categories namely, constant with time, time harmonic, or varying with time. Most commercial FEM software classifies these 'problems' according to the appropriate solver applying Maxwell's equations to perform calculations for analyses.

The Magnetostatic solver is used for problems with dc and a constant or static magnetic field. Eddy currents are, therefore, not considered and the solution is in the steady state. Some parameters from the solution, for example, stored magnetic energy *w*, can be used to calculate inductances of a device in post-post processing.

For time varying fields or *harmonically* oscillating functions at *one* frequency, Time-harmonic or Eddy Loss solvers are used and the solution is given in steady state. Time-harmonic solvers operate in the frequency domain using complex phasors with the time convention $e^{j\omega t}$ (ω is the angular frequency) and can only handle linear isotropic material properties.

The Transient solvers operate in the time and frequency domain calculating a solution for each time step. They can normally handle linear and nonlinear magnetic materials and winding excitations with multiple frequencies. The solution is given as a transient profile (reaching steady state if the simulation is allowed to run for long enough). Transient solvers are sensitive to phenomena like inrush currents at sudden start-up of transformers. In order to eliminate the exceedingly long time to calculate inrush currents, techniques such as "soft-start" or "slow-rise" sinusoidal voltage sources can be used. These methods normally involve the manipulation of the sinusoidal voltage equation analytically, with the inclusion of an exponential function, or through scripting in a programming language which is compatible with the software.

The general differential forms of Maxwell's equations derived from Stokes' and Gauss' Laws (Jin, 2002) are categorized according each FEM solver in Table II**.**

The key to Table II is given below:

B = magnetic flux density in webers per square meter (wb/m^2) or Tesla (T)

E = electric field intensity in volts per meter (V/m)

D = electric flux density in Coulombs per square meter (C/m^2)

H = magnetic field intensity in Ampère's per meter (A/m)

J = electric current density in Ampère's per square meter (A/m^2)

$\mathbf{J_s}$ **=** surface electric current density (A/$m^{2)}$

ρ = electric charge density in Coulombs per cubic meter (C/m^3)

ε = permittivity in free space or electric constant in Farads per meter (8.85×10^{-12} F/m)

σ = conductivity in Siemens per meter (S/m)

Table II: Solvers in electromagnetic FEM software

Maxwell's Equations for FEM Solvers			
Solver	Magnetostatic	Time-harmonic/Eddy Loss	Transient Solver
Attribute	Time invariant	Time harmonic	Time varying
Faraday's Law	$\frac{\partial \boldsymbol{B}}{\partial t} = 0$	$\boldsymbol{\nabla} \times \boldsymbol{E} = -j\omega \boldsymbol{B}$	$\boldsymbol{\nabla} \times \boldsymbol{E} = -\frac{\partial \boldsymbol{B}}{\partial t}$
Ampère's Law	$\boldsymbol{\nabla} \times \boldsymbol{H} = \boldsymbol{J}$	$\boldsymbol{\nabla} \times \boldsymbol{H} = j\omega \boldsymbol{D} + \boldsymbol{J}$	$\boldsymbol{\nabla} \times \boldsymbol{H} = -\boldsymbol{J} + \frac{\partial \boldsymbol{D}}{\partial t}$
Gauss' Law	$\boldsymbol{\nabla} \cdot \boldsymbol{B} = 0$ $\boldsymbol{\nabla} \cdot \boldsymbol{E} = 0$	$\boldsymbol{\nabla} \cdot \boldsymbol{B} = 0$ $\boldsymbol{\nabla} \cdot \boldsymbol{E} = 0$	$\boldsymbol{\nabla} \cdot \boldsymbol{B} = 0$ $\boldsymbol{\nabla} \cdot \boldsymbol{E} = \frac{\rho}{\varepsilon}$
Ohm's Law	$\boldsymbol{B} = \mu \boldsymbol{H}$	$\boldsymbol{J} = \sigma \boldsymbol{E} + \boldsymbol{J}_s$ $\boldsymbol{B} = \mu \boldsymbol{H}$	$\boldsymbol{J} = \sigma \boldsymbol{E} + \boldsymbol{J}_s$ $\boldsymbol{B} = \mu \boldsymbol{H}$

3.4 Proposed transformer-GIC FEM approach

Based on the discussion of the various modelling approaches leading up to the FEM and the extent of its capabilities, it is now possible to derive a modelling protocol for a transformer with ac excitation in GIC flowing in its windings. There are several FEM software packages available online or commercially such as COMSOL, CADEMA, FEMM, QFIELD, FLUX, MEGA, Vector-Field, ANSYS, and Infolytica (MagNet).

For this thesis the following requirements for the simulation are identified as:

- 2D and 3D magnetostatic, time-harmonic and transient modelling
- Non-linearity of electrical core steel in the calculations
- Generation of ac voltage and current excitations
- Generation of dc excitations
- Field-circuit coupling capability between the FEM domain and electrical circuit domain for complex excitations (at multiple frequencies) and wiring configurations.
- Application of (mirror) symmetry where possible with the use of appropriate boundary conditions

From the literature review, ANSYS (Maxwell) Electronic Desktop appears to meet the above requirements, and it is used widely for modelling transformers in several studies and in the industry (Liu *et al*., 2013, Gong *et al*., 2017, Kohli *et al*., 2018a, Chen *et al*., 2018). This software was chosen, therefore to be used in the preliminary FEM simulation protocol. Experience in the transformer industry further prompts the use of Infolytica MagNet FEM software as an alternative to ANSYS (because of a wider range of capabilities in the details of the modelling), and so this software is also tested in this thesis.

In order to optimize the time taken to compile the calculations, the Time-harmonic/Eddy Loss solver was used for calculations with ac excitation only in the linear region of the transformer core. The limitation which comes with this solver is the exclusion of the non-linearity of the core (ANSYS and MagNet). This involves the no load test for characterization of the transformation of voltages (RMS), magnetizing current (RMS) and total core loss. To test the models in over-excitation with ac only, where the non-linearity of the core needs to be taken into consideration, the Transient solver will be used because it can handle the nonlinear material properties more accurately. Simulations involving dc only, e.g. "air core inductance" with a "core-less transformer" will be investigated in the magnetostatic time-harmonic domains.

For any investigation involving simultaneous ac and dc excitation to simulate a transient or steady state GIC, only the Transient solver can be used. This is because the formulation of the transient analysis allows for superimposition of excitations at any frequency, and because it can handle nonlinear properties in materials.

Sudden start-up excitations of sinusoidal voltages and currents are not desirable in the FEM because they normally cause the generation of inrush currents resulting in exceedingly long simulation times. "Soft start" or "slow rise" excitations will be used to avoid a sudden start-up generating a slowly increasing excitation. An example of a "slow rise" excitation is given in Figure 10. Mathematical expressions derived from the software's libraries can be applied to the sinusoidal excitation equations to modify them (ANSYS). Alternatively, scripting in Visual Basic (VB) can used to convert the sudden start-up sinusoidal excitation to the desired "slow rise" one (MagNet).

VB scripting can also be used to overcome many other limitations which potentially come with the software, e.g. repetitive stacking configurations of individual core laminations for different joint configurations.

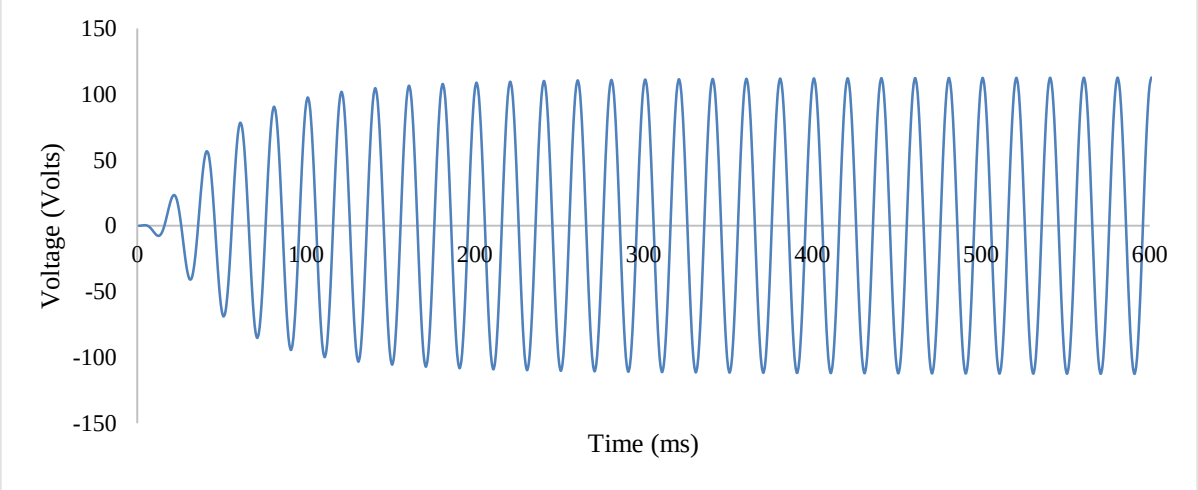

Figure 10: Typical "slow rise" applied voltage excitation reaching steady state after a few cycles

3.5 FEM Modelling (ANSYS) for 40 MVA Power Transformer

Once the geometry of the transformer was created and sufficiently parameterized, the first step in the modelling was the selection of an adequate mesh. A mesh generation of 10 000 elements for each component of the model converged to consistent numerical results for normal open circuit ac excitation. To avoid the sudden start-up transients mentioned in section 3.4, a slow-rise sinusoidal input voltage was applied to each phase using the equations in Table III where V_{pk} is the peak voltage based on the nameplate rating.

Table III: Slow-rise applied voltage

Phase	Applied function
A	V_{pk}*(1-exp(-50*time))*cos(2*pi*50*time)
B	V_{pk}*(1-exp(-50*time))*cos(2*pi*50*time+(2/3*pi))
C	V_{pk}*(1-exp(-50*time))*cos(2*pi*50*time+(4/3*pi))

The total core loss P_T is the sum of the hysteresis loss P_h, eddy current loss P_e, and anomalous loss P_a. In the ANSYS FEM calculation the core loss algorithm is summarized as follows:

$$P_T = P_h + P_e + P_a = K_1 B_m^2 + K_2 B_m^{1.5}. \quad (3.1)$$

Expanding the set in the middle and equating to the right-hand side of equation 3.1 gives

$$k_h f B_m^2 + k_e (f B_m)^2 + k_a (f B_m)^{1.5} = K_1 B_m^2 + K_2 B_m^{1.5}.$$

(3.2)

Therefore $K_1 = k_h f + k_e f^2$ and $K_2 = k_a f^{1.5}$. The classical eddy current loss is calculated directly as

$$k_e = \pi^2 \sigma \frac{d^2}{\delta}$$

(3.3)

where σ is the core steel conductivity and δ is the thickness of each lamination sheet. To obtain K_1 and K_2, the quadratic form can be minimized to

$$err(K_1, K_2) = \sum_i \left[P_{Ti} - \left(K_1 B_{mi}^2 + K_2 B_{mi}^{1.5}\right)\right]^2 = min$$

(3.4)

where P_{Ti}, B_{mi} are the i^{th} point on the loss characteristic on the core loss curve in Figure 12. The hysteresis loss coefficient is obtained as $k_h = \frac{K_1 - k_e f_0^2}{f_0}$ and $k_h = \frac{K_2}{f_0^{1.5}}$ gives the anomalous loss coefficient, where f_0 is the BH curve's testing frequency.

The simulation protocol involved an open circuit test at nominal ratings applied from the LV and HV sides separately. The magnetizing currents, input and induced voltages, core loss, and flux distributions were recorded and compared against the measured and derived factory acceptance test results.

Further simulations were then done with varying levels of GIC solely to test the response of the model to ac-dc excitation, even though there were no practical measurements with dc for comparison. The GIC is modelled by imposing a dc offset to the voltage excitation in each phase of the HV winding to emulate the effect of a transformer in a real power system. The desired level of dc current was derived from the winding resistances given in Appendix A.1. The magnetizing current waveforms were then recorded and the various flux distributions in the core, air, and tank were analysed.

3.6 Solving Approach (MagNet)

The bulk of the FEM simulations in this thesis involved more than one input signal resulting in a saturated transformer with harmonics (up to the 500 Hz), thus the modelling had to be carried out using the MagNetTransient Solver and the governing equations are given in Equations 3.5 – 4.0. These are based on the *T*-Ω method which incorporates the hierarchal method (Webb & Forghani, 1995). This approach allows many polynomial orders to exist in the same mesh in which the magnetic field is represented by the sum of two parts: the gradient of a scalar potential, and an additional vector field

represented with vector edge elements (in the conductor). The *T*-Ω method, which incorporates vector edge elements, is preferred because it is memory efficient (non-conducting regions can be solved with a scalar potential), and it does not exhibit convergence and instability issues that other approaches report to have experienced in the past. For the transformer windings where the fields are time-varying, there is a redistribution of the current density, ***J***, which is unknown before calculating the magnetic field, ***H***, using Equation 3.5. Therefore, there is not a direct representation for ***J***, it is calculated post-process as the curl of ***H*** (Infolytica Corporation, 2017a) .

$$\nabla \times (\sigma^{-1} \cdot \nabla \times \boldsymbol{H}) + \mu \cdot \frac{\partial \boldsymbol{H}}{\partial t} = 0 \tag{3.5}$$

where

$$\boldsymbol{H} = -\nabla\psi + \boldsymbol{T} \tag{3.6}$$

and ψ is a magnetic scalar potential and ***T*** is a current vector potential satisfying

$$\nabla \times \boldsymbol{T} = \boldsymbol{J}. \tag{3.7}$$

The 3D formulation for the transformer core is

$$\nabla \cdot [\mu \cdot (-\nabla\psi + \boldsymbol{H_w})] = 0 \tag{3.8}$$

where

$$H = -\nabla\psi + \boldsymbol{H_w} \tag{3.9}$$

$$\nabla \times \boldsymbol{H_w} = \boldsymbol{J_w} \tag{4.0}$$

$\boldsymbol{H_w}$ is a known field generated by the windings satisfying Equation 4.0 and $\boldsymbol{J_w}$ is the winding current density. The magnetic flux density in a transformer core or windings is computed using the non-linear relationship $\mathbf{B} = \mu(\mathbf{B})\cdot\mathbf{H}$, and the current density is calculated from Ampère's law $\nabla \times \mathbf{H} = \mathbf{J}$. The 2D case simplifies the 3D case in the sense that **B** is only in the x-y plane and **J** is orthogonal to it, producing a simpler and faster calculation.

3.7 Computer requirements for FEM simulation

Electromagnetic transients software and related fast-acting topological modelling are seldom reported take in to account the air gap, tank and other structural components inside a transformer (Zirka *et al.*, 2017)". This disadvantage has resulted in some discrepancies being reported between GIC experimental and simulation results (Chisepo, 2014; Rezaei-Zare, 2015a). 2D and 3D FEM modelling offer an alternative modelling approach to incorporate the air gap, tank and structural parameters under GIC conditions through the virtual construction of real-life geometries with their properties, and the use of rigorous numerical methods based on Maxwell's equations presented in the previous sections of this chapter.

When a transformer has GIC flowing in its windings, it experiences simultaneous ac-dc excitation which causes it to operate under various levels of saturation. This is characterized by a pulsating magnetizing current I_{mag} whose peak in one half cycle is several orders larger than the peak under linear

operation. The large asymmetrical I_{mag} lags the system voltage by 90° which causes the transformer to draw correspondingly larger amounts of non-active power given by a Q-GIC characteristic. At the same time, the distortion in the line currents due to non-linear operation leads to the generation of unwanted even and odd harmonics.

To cope with the unbalance and distortion, the transformer ac-dc modelling was done in the electromagnetic transient domain (refer to Table II), which is computationally intensive. The complexity in the solving is due not only to the extra third dimension in the matrix calculations, but also because of the doubling of the number of edges from a triangular element (3) to a tetrahedron (6). However, the simulation time can be optimized with the use of mirror symmetry and varying mesh densities through the region and device. The limitation of the transient solver is the exclusion of temperature dependency in materials related to specific magnetic field solutions. However, an increase in losses due to stray flux in different parts of the transformer in saturation can be used as a proxy for possible hot spots.

The computational expense of the transient FEM calculations (using of lot of CPU resources) required an adequate computer for the various investigations. Therefore, the computer used for the simulations in this thesis had the following specifications:

- Intel Quad Core i7 processor,
- 16 GB of RAM,
- 1 TB hard drive,
- the operating system is on a 250 GB Solid State drive (which is where the FEM simulations are temporarily stored before being forwarded to the bigger drive),
- and a 2 GB GeForce GT 730 on-board graphics card.

The basic operation of the FEM was providing a virtual laboratory to test the response of devices under various conditions and designs. For the electromagnetic problem, this often involves models with magnetic materials and coils (windings), the analysis or display of graphs and magnetic field plots, etc. For the 2D case, the models are deemed to represent many industrial devices very well, and also offer a considerable saving in the computational requirements i.e. they can be solved quickly with minimal computer resources.

More complex problems often require a 3D solution for better accuracy, and frequently, careful consideration is needed to decide between aiming for faster simulation time or accuracy. Wherever it is appropriate and sufficiently accurate regarding solutions relating to voltages and currents, 2D FEM will be tested against various measurement data. More detailed solutions involving modelling of real-life flux distributions will require 3D modelling, especially under distorted transformer conditions with ac-dc excitation.

The next two chapters will present the Preliminary FEM Protocol, firstly in the modelling of a real 40 MVA power transformer (chapter 4) with ac measurement data only, and then through the modelling of bench-scale models with ac and dc measurement data. Each of these chapters concludes with a discussion of the preliminary findings and leads on to the main experimental and simulation protocols of this thesis.

4 40 MVA POWER TRANSFORMER INVESTIGATION

The first step in the FEM investigation involved the modelling of a real power transformer made with high quality GOES, mitred joints, IEC/SABS standards compliant factory acceptance test data (FAT), and design data. FAT results with only ac excitation are the only available measurement data to compare against the FEM model. Some findings are discussed on the performance of the 2D and 3D models. Even though power transformer-GIC test data is not available to compare with simulations, some conclusions are drawn leading to further analysis on available physical test data (on small model transformers) and FEM simulations.

4.1 Transformer Parameters

The FEM transformer under investigation derived its parameters from a real 40 MVA 132/11 kV 3p3L transformer currently in service as a generator step-up transformer GSU in the Southern African network. The FEM software implemented in this investigation is ANSYS. Table IV shows a summary of the transformer nameplate ratings. The electrical core steel lamination grade is 30H102®, conventional grain oriented (CGO), with a thickness of 0.35 mm, a nominal induction of 1.72 T, and a safe operation upper limit of 1.95 T. Manufacturer data indicated a core loss of 1.01 W/kg at an induction of 1.7 T and a frequency of 50 Hz. These parameters were verified in the laboratory with the historic Epstein frame and the newer single sheet tester (SST) to make sure that the magnetic data for the FEM input is accurate. Appendix A.1 Core, *tank and winding parameterization* shows the onsite laboratory images, IEC standards and a brief description of protocols that were used. The tank is modelled as mild steel with a thickness of 12 mm, which is larger than the magnetic skin depth. Unfortunately, the tank steel samples from the transformer factory's mechanical workshop were too thick for magnetization characterization with the Epstein frame and SST (normally requiring 0.23-0.35 mm sheets), and so a generic mild steel BH curve provided by the transformer manufacturer was used, which can also be found in Appendix A.1. The core was modelled with the inherent TransCore® mitred three limb model with solid joints, and the windings were modelled as stranded cylinders.

Table IV: Three-phase three limb power transformer

Transformer ratings	
Voltage	132/11 kV
Load current LV	2099 A
MVA rating	40 MVA
Vector group	YNd11
Magnetizing current (% of rated full load)	0.056

Table V gives the core dimension and stacking configuration data. Figure 11 and Figure 12 show the magnetic properties of the electrical core steel that were used as input for the FEM. The numerical BH and core loss profiles and further parameterization of the core and windings are given in detail in Appendix A.1. Even though the electrical core steel manufacturer data provided flux only up to 1.92 T for H and 1.8 T for P_{loss} (see Table A:1 in Appendix A.1), the FEM used curve fitting to extrapolate corresponding B values of H and P_{loss} beyond 2 T as shown in Figure 11 and Figure 12 . This is particularly important because a transformer with GIC can easily reach peak flux densities between 1.9 and 2.05 T The transformer design data also specified a lamination stacking factor (sf) of 0.96 to account for the effective areas seen by the flux due to interlaminar insulation and a stacking direction (sd) of V1. Unfortunately, the transient FEM calculation gave significant errors in the core loss and magnetizing currents flowing in the transformer windings when sf and sd were taken into account. Therefore, a solid core composition was used to simplify the model, as a first approximation.

Table V: Core data

Name in ANSYS	Value	Description
DiaLeg	506 mm	Net core diameter
DistLeg	1102 mm	Limb Pitch (Leg centre to centre distance)
DistYoke	2314 mm	Limb height plus core diameter (Yoke centre-to-centre distance)
Stages	18	Total number of packets
ThickCore	10.8 mm	Packet thickness for stage = 1
WidthYoke	0 mm	Yoke width, = 0 for same cross section as leg's
InfoCore	0	Generate whole core (1: legs only, 2: yokes only)

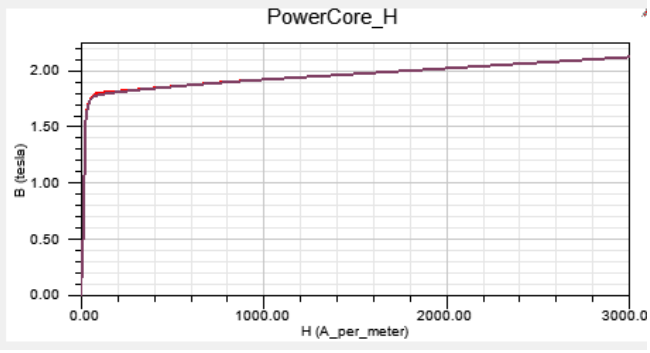

Figure 11: Electrical core steel BH curve at 50 Hz

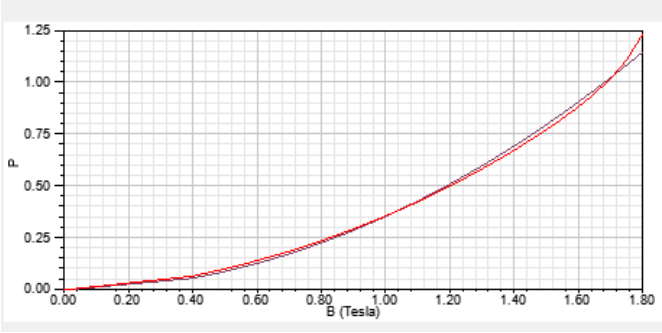

Figure 12: Electrical core steel core loss profile at 50 Hz. P on the horizontal axis is the loss in W/kg

4.1.1 Open circuit results

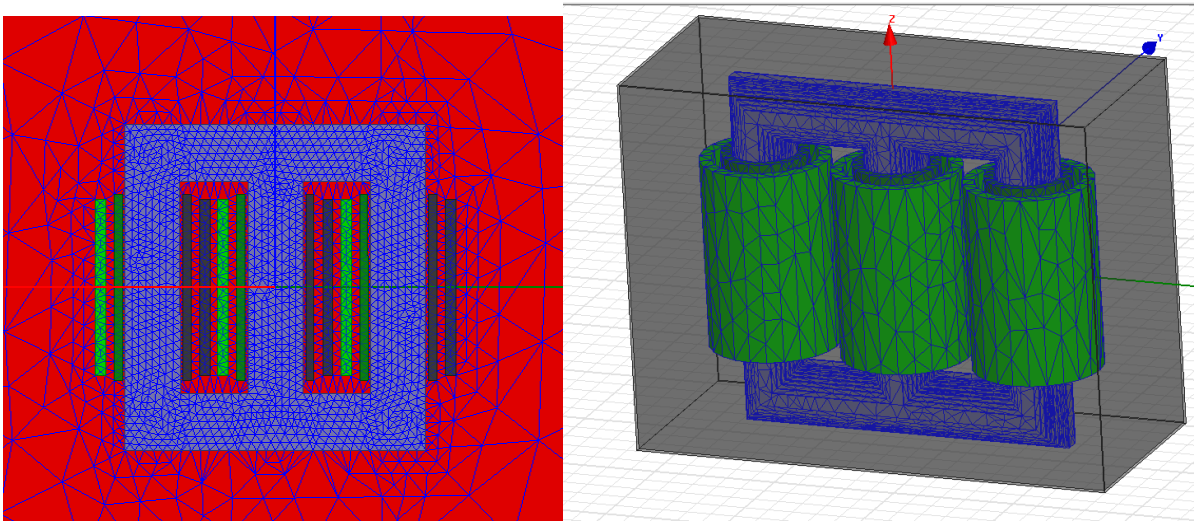

Figure 13: The triangular mesh for the 2D mode (left) and the tetrahedral mesh for 3D transformer model inside tank enclosure (right)

The meshes that were used for the 2D and 3D models are shown in Figure 13. Figure 14 and Figure 15 show the flux distribution of the 3D and 2D FEM models energized on the LV windings at no load at an instant in time in steady state. The slow rise voltage excitations that were used are in accordance with the expressions given in Table II**,** and the transient simulations were run until steady state was reached. After checking for the correct transformation of voltages based on the nameplate rated input, the magnetizing current I_{mag} and core loss in kW were calculated and recorded. The slow rise input and induced voltages are given in Appendix A.2. The use of symmetry for the 3D model in Figure 13 was not considered because it was important to analyse the stray flux for the entire geometry with the inclusion of the tank.

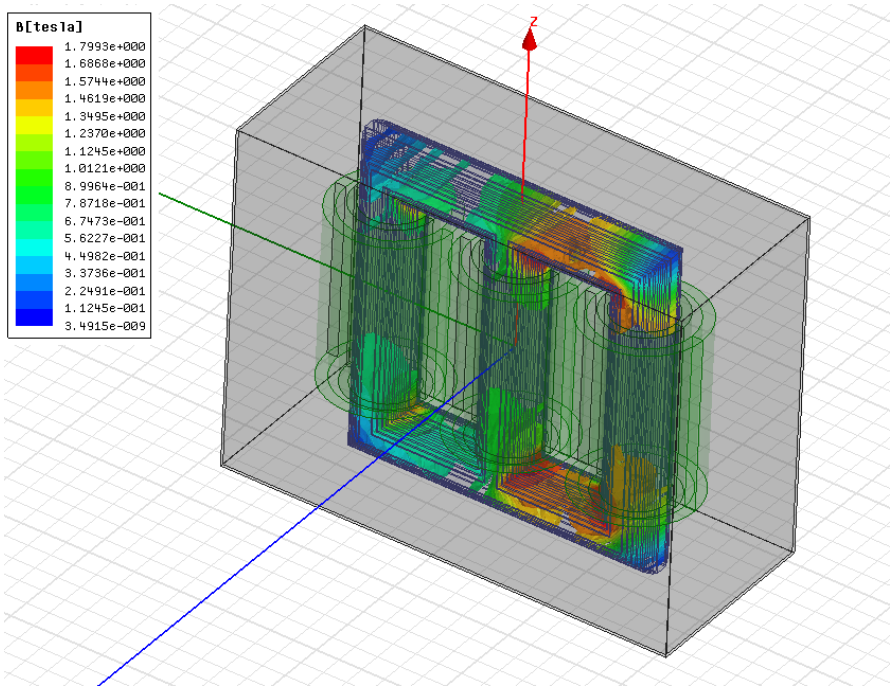

Figure 14: 3D FEM model energized to the nameplate rated voltage at an instant in time (200 ms)

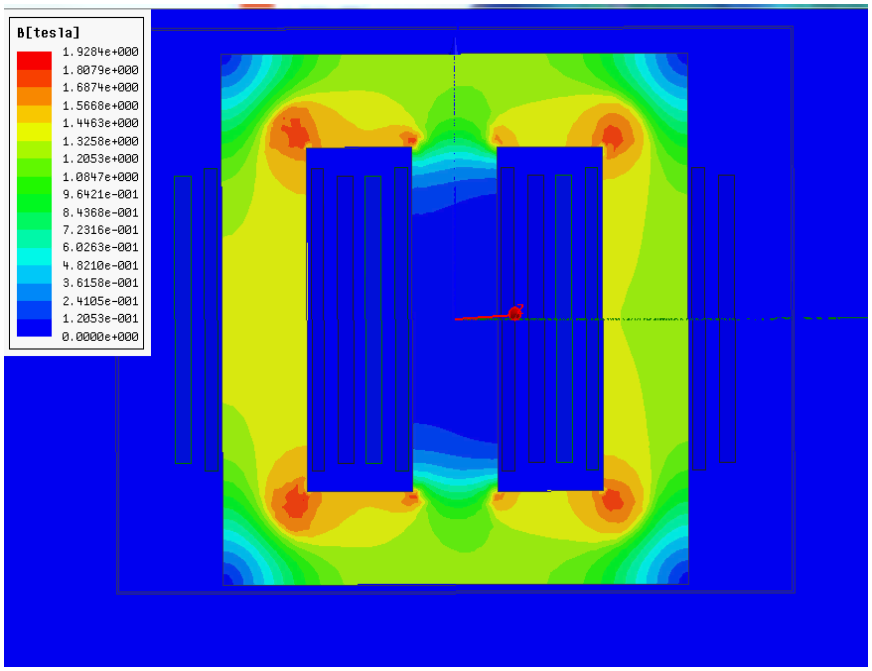

Figure 15: 2D FEM model energized to the nameplate rated voltage at an instant in time (250 ms)

Table VI shows the measurement data contrasted against the simulations from the 2D and 3D FEM models. Only the currents in phase 'a' are shown for comparison with the available measured data. The FAT I_{mag} was derived from the nameplate rating given in Table IV as a percentage of the rated current and the core loss was measured during the FAT. The same table also shows that there were underestimations for the I_{mag} and core loss when the 2D solution is compared with the FAT measured results. (See Appendix A.2 for the time-averaged simulated core loss profiles derived from Equations

3.1 – 3.4.). In the same table, the 3D solution shows a closer correlation in the RMS phase 'a' magnetizing current but with a slight overestimation of 7.2%. The 3D core loss solution also shows a slight improvement in the accuracy increasing the difference compared to the measured value from 22.8% to 22.4%.

Table VI: No load results at nominal voltage 11/132 kV

	I_{mag} (A)	Core loss (kW)	I_{mag} % diff. vs measured	Core loss % diff. vs measured
FAT Derived	1.175	17.14	-	-
2D FEM	0.573	13.24	51.3%	22.8%
3D FEM	1.26	13.3	7.2%	22.4%

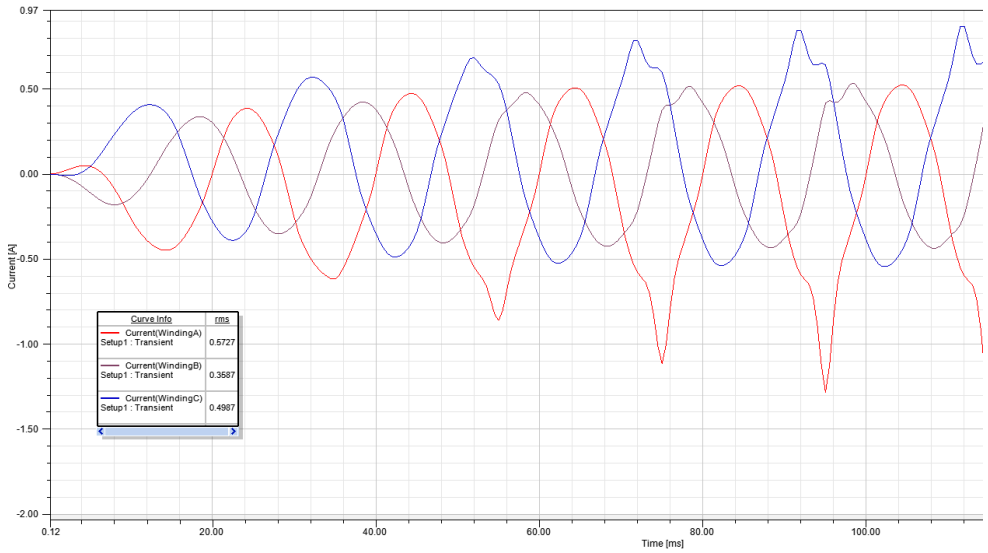

Figure 16: 2D simulated core magnetizing currents after energization. The RMS values shown at the bottom left corner are the final values reached at steady state after 500 ms

Further post-process analysis on the 2D I_{mag} waveforms in Figure 16 indicated that the two outer phases have higher I_{mag} RMS currents than the phase 'b' (which is expected for a 3p3L because the outer phases see a longer magnetic path than the middle phase).

Analysing the 3D model's waveforms given in Figure 17 shows that the phase currents are more representative of three-phase transformer's non-sinusoidal magnetizing currents. The phase currents appear to be unbalanced with phase 'a' having the highest RMS magnitude of 1.284 A, phase 'c' having a lower value of 0.59 A, and the inner phase 'b' having the lowest value of 0.415 A.

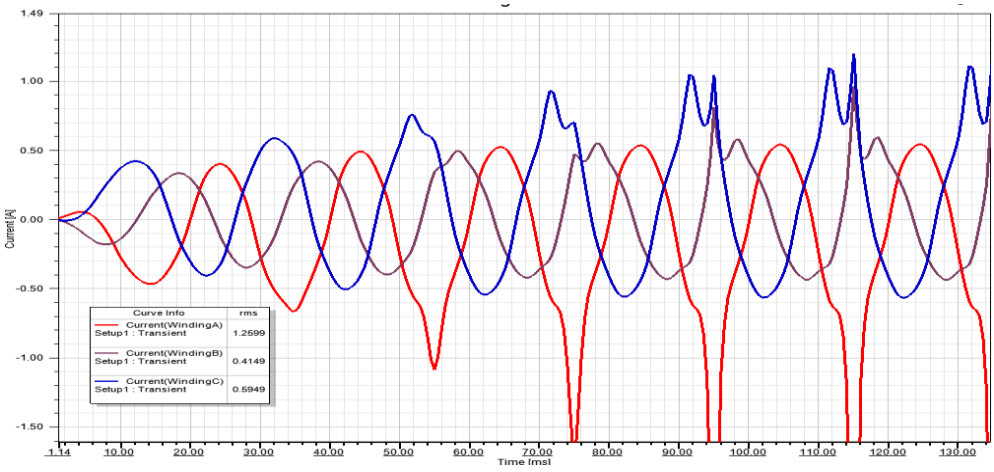

Figure 17: 3D simulated core magnetizing currents after energization. The RMS values shown at the bottom left are the final values reached at steady state after 500 ms

Further modelling was then done with dc to test the flux distribution response of the model for half-cycle saturation.

4.1.2 FEM Transformer-GIC investigation

The model in the previous section was tested for its response to simultaneous ac and dc excitation to simulate transformer operation in the presence of GIC. The dc was injected by superimposing a dc component of voltage on to the existing ac excitation, this then interacted with the winding resistances resulting in the flow of a GIC (simultaneous ac-dc excitation). The injected values of GIC were 0 A, 1 A, 5A, 7.5 A, 10 A, and 30 A per phase. Figure 18 shows that GIC levels as low as 5 A/phase resulted in partial saturation where the flux begins to leave the core and flows through the side walls of the tank.

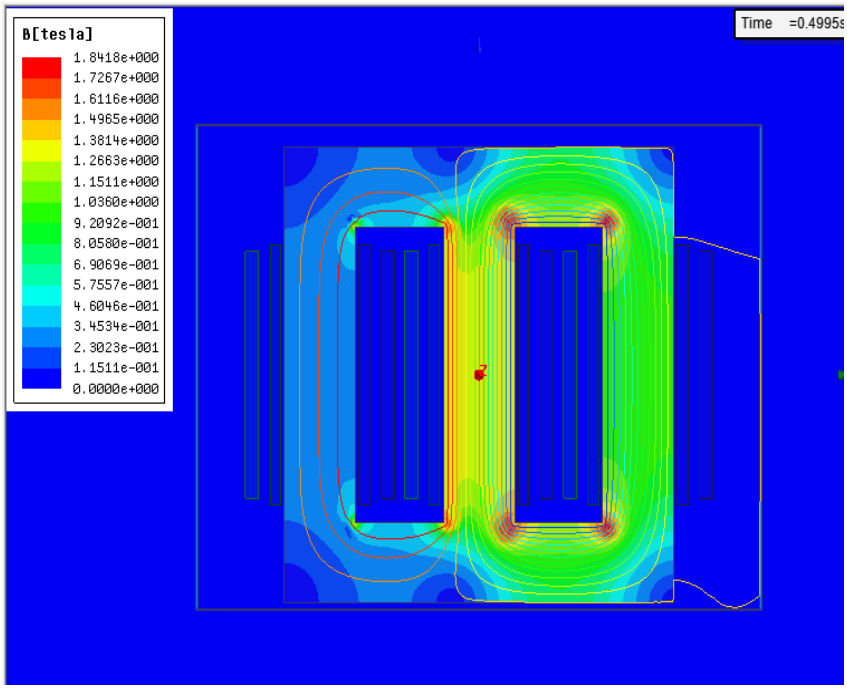

Figure 18: Leakage flux entering side tank walls with 5 A GIC at no load at an instant in time for the 2D solution

Figure 19 is a 3D snapshot of approximately 30 A dc flowing in the windings before reaching steady state (at no load) and the corresponding current waveforms are given in Figure 20 in their transient state.

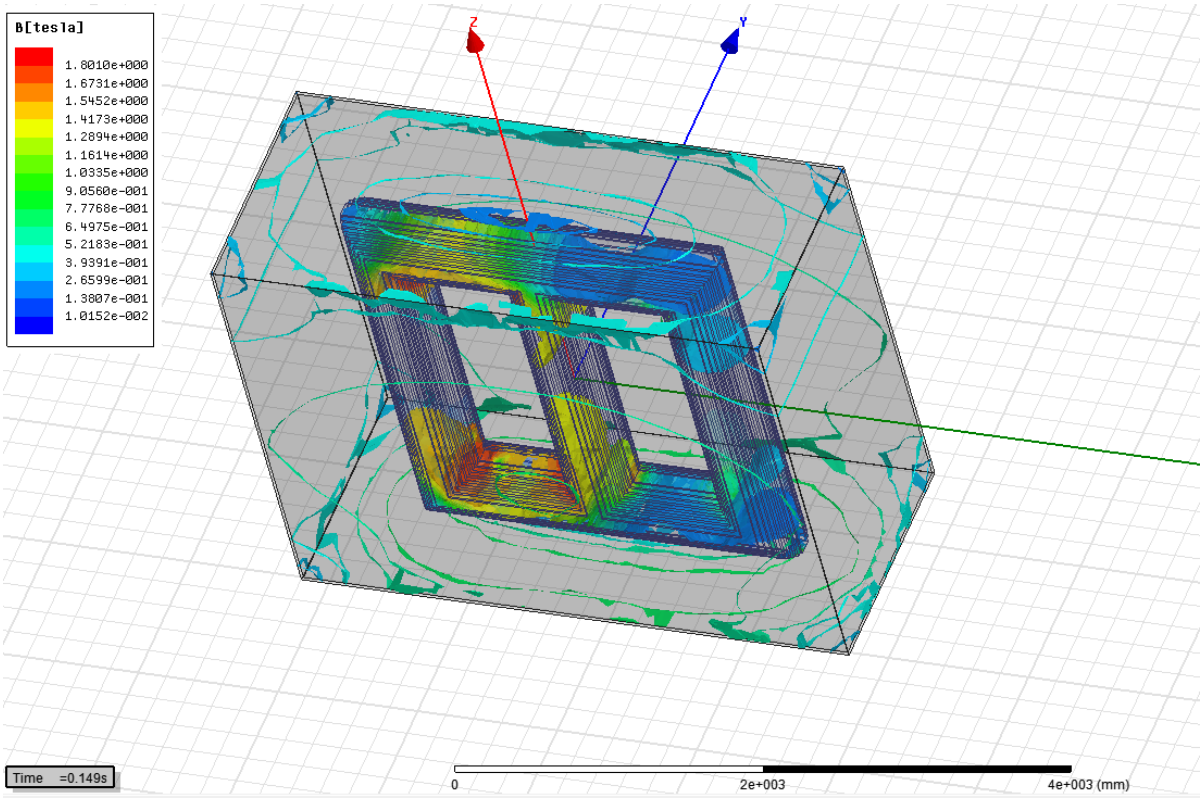

Figure 19: Stray flux in different parts of the transformer tank with 30 A GIC at no load

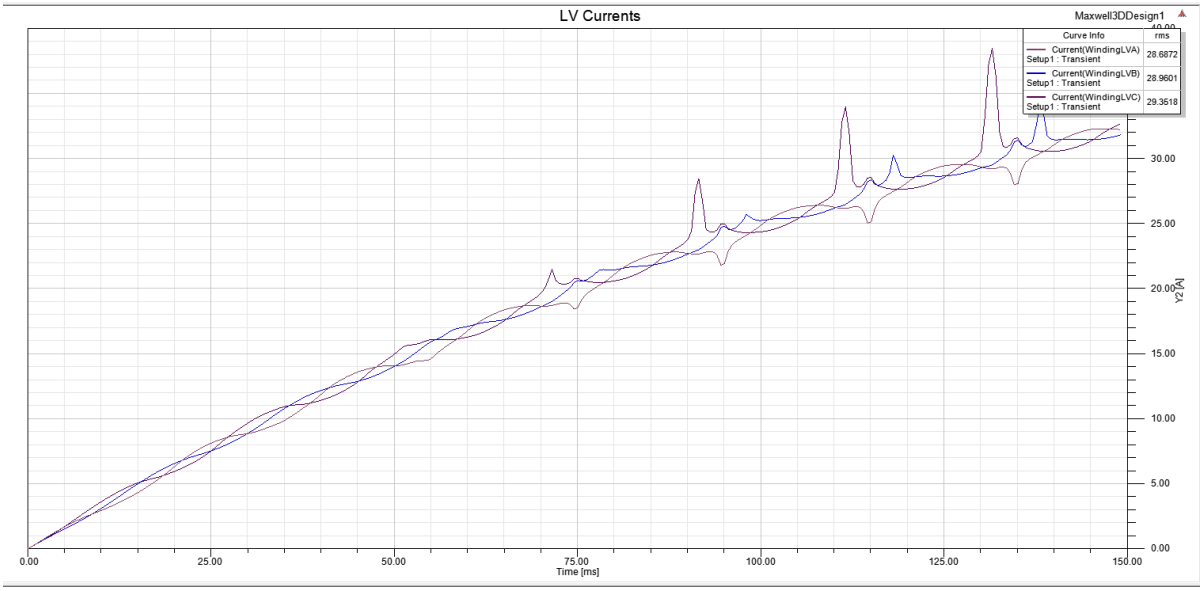

Figure 20: Effect of GIC on transformer magnetiizing currents at no load in transient state

Further simulations were done to investigate the effect of tank shunts made of the same magnetic material as the core, in the presence of GIC related stray flux.

Having identified the areas of the tank which offered stray flux paths (Figure 21), 12 mm shunts were placed along the sides of the tank and area above the top yoke Figure 22.

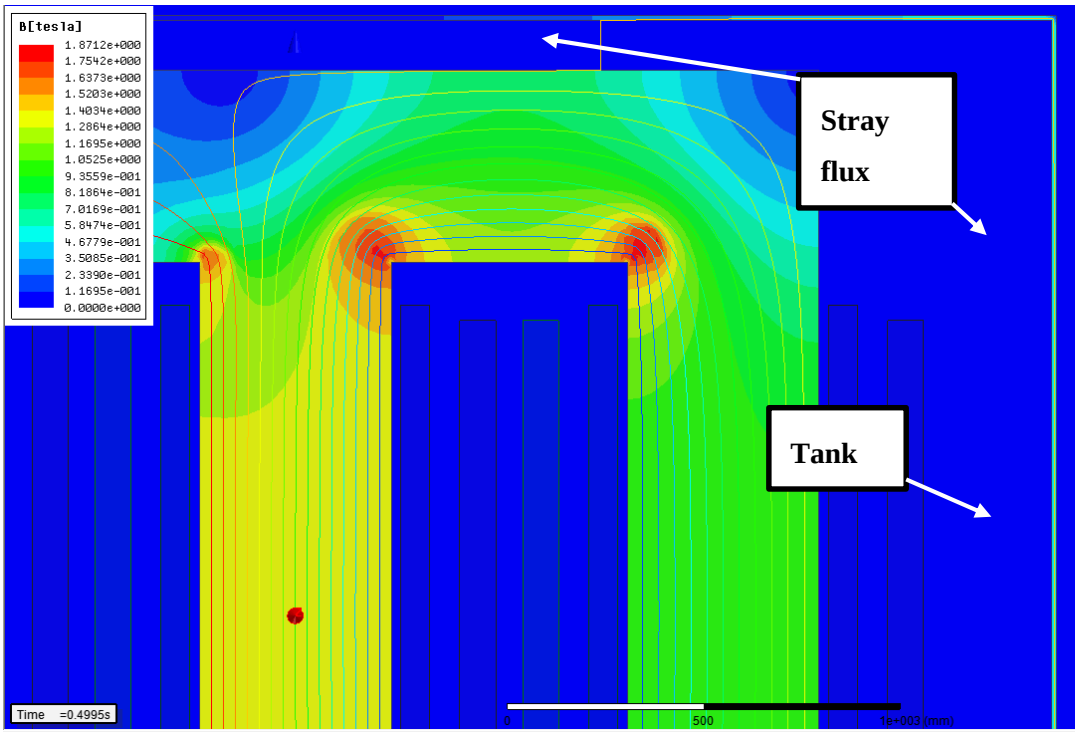

Figure 21: Stray flux entering the top part of the tank and flowing in the tank sides with 10 A GIC at no load

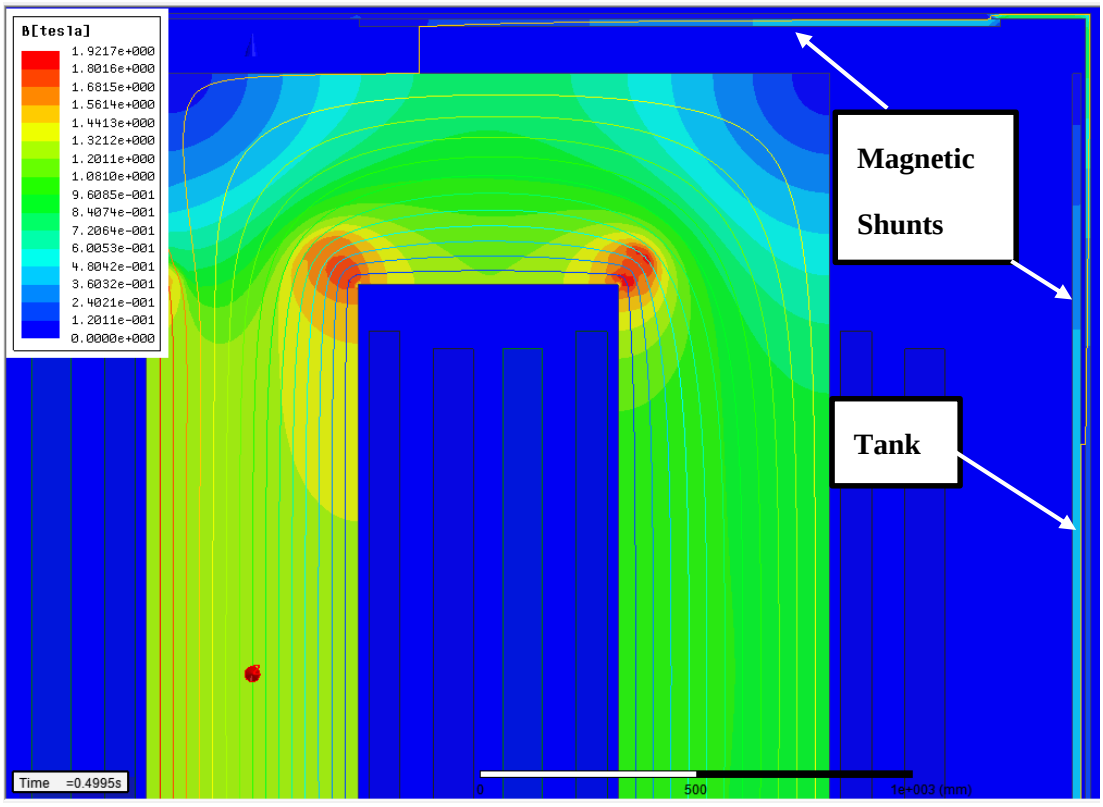

Figure 22: Stray flux mostly flowing through the tank shunts with 10 A GIC at no load

4.1.3 Discussion

The preliminary FEM simulation investigated a real power transformer in the transient analysis domain. It was unclear at this point of the study as to why most of the simulated magnetizing currents and time-averaged core loss profiles were lower than the measured open circuit test data despite the model having an adequate mesh and detailed core loss calculation algorithm. The 3D model, however, showed an improvement in the open circuit investigation, but the solutions were still underestimating the measured data.

Stray flux on the sides of the tank was observed even from as little as 5 A GIC. This could be in agreement with conclusions drawn by Gaunt and Coetzee (2007), and Rezaei-Zare (2015b) regarding the saturation of a 3p3L power transformer with low GIC levels. In addition to this, the stray flux entering different parts of the tank in Figure 19 seems to be in agreement with the depiction of the 3p3L stray flux paths in the study done by Rezaei-Zare (2015a). (See Figure 8 in 2.3.)

When the flux leaves the core and enters the tank it rapidly changes its direction from normal to tangential with respect to the tank. The magnetic orientation of the tank, which is isotropic, was modelled as <110> and it allowed for the flow of flux in the transverse and rolling direction, thus increasing losses and chances of hot spots at the flux penetration points. Though it is not standard practice, the incorporation of anisotropic redirection plates at the top and the bottom tank parts with the ideal <100> GOES orientation, identical to that of the core steel, allowed for flux to flow through them more easily, reducing the previously mentioned adverse effects.

The discrepancies between simulation and measurement data regarding the I_{mag} and core loss, coupled with a lack of transformer-GIC measurement data for comparison, warranted further investigation into the FEM modelling of transformers and their response to GIC/dc. Section 5 presents an investigation in which bench-scale 1p3L, 3p3L, and 3p5L transformers are modelled in FEM and compared with various electrical measurement data with ac excitation only and also with simultaneous ac-dc excitation.

4.1.4 Summary

In this chapter, real power transformer parameters were used to perform FEM analyses with commercial FEM software that is widely used in the transformer design and manufacturing industry. Using Factory Acceptance Test data with ac only, it was found that for complex structures like a power transformer with a mitred and staggered core, a 3D analysis offers more accurate solutions, even though some underestimations in the calculated phase ‘b’ and phase ‘c’ magnetizing currents, and core loss, are observed. There is increasing pressure from international directives to design more eco-friendly, low loss, electrical machines (Hastenrath, 2014; Guillaume & Leconte, 2016). Accordingly, accurate prediction of transformer loss is needed, not only for optimal design, but also for transformers under abnormal conditions during sizeable geomagnetic disturbances.

The transformer-GIC simulations show that 3p3L transformers *can* saturate at low levels of GIC, and that the tank is severely affected in deep saturation. Therefore, manufacturers need to understand better the stray flux paths inside the transformer, under half-cycle saturation. At this point in the study, it was realized that more FEM modelling was necessary, both to understand better the underlying reasons for the discrepancies encountered, and to improve modelling. The next chapter investigates the response of three bench-scale transformers differing in core structure with numerous ac and ac-dc measurement data for comparison with the FEM.

5 BENCH-SCALE FEM INVESTIGATION

The bench-scale transformers under test (TuTs) for comparison with FEM simulation in this section were given in Figure 9 in Chapter 2. In the study referred to (Chisepo, 2014), a method for identifying the knee point of the v-i characteristic was implemented according to McLyman (2004), which led to the definition of the level of dc as a function of the magnetizing current I_{mag} at this knee. In the laboratory experiments, varying levels of dc were injected into the transformer neutrals with a voltage source (dc batteries) to avoid any unwanted harmonics which could arise if a rectified dc source with a small ripple was used instead. Many measurements were recorded, including those of voltages and currents and their harmonics, and reactive power was calculated according to the conventional definition, and non-active power according to the general power theory (Gaunt & Malengret, 2012) which is suitable for three-phase systems under conditions of distortion, unbalance and dc components of current.

The nameplate ratings of the laboratory TuTs are 209/400 V, 300 VA for the 1p3L three-phase bank and 3p5L, and 120/230 V, 300 VA for the 3p3L. However, because of the low-grade lamination steel used in the manufacturing process, the bench-transformers exhibited symmetrical saturation when energized at their nameplate ratings, which signified that they were already over-excited. New nominal values representing under-excitation were then defined as 80/150 V for the 1p3L and 3p5L (line to neutral), and 44/85 V (line to neutral) for the 3p3L, with a new common base of 200 VA. The FEM software that was used for the bench-scale modelling is Infolytica MagNet.

5.1 FEM modelling

The simulation protocol firstly investigated 2D models of all three core structures and various aspects of their solutions are compared with measurements. It is quite well known that the 1p3L is more responsive to GIC than the other core structures. After the 2D models were tested for their individual responses, additional 1p3L 3D simulations were performed to investigate the effect of adding a more detailed third dimension to calculations. In addition, symmetry was applied to test if it would shorten simulation time without causing any loss of accuracy.

5.1.1 Preparation of the geometries and parameterization

The transformer parameters used to prepare the models' geometries are given in Appendix *B.1 Bench-scale Parameters.* Where there was insufficient data from the manufacturer, some physical measurements are done with a Vernier Caliper, and some reasonable assumptions were made where necessary.

5.1.2 Modelling excitations

An external circuit was used to define the excitations in the windings. As mentioned previously, it was necessary to avoid sudden start-up phenomena like inrush currents in transformer windings, since they lead to excessively long computational times with several cycles of fault current magnitudes. A slow-rise start-up excitation was therefore implemented for the applied voltage using the Visual Basic script given in Appendix B.2.

GIC was modelled by putting the ac and dc voltage sources in series in the circuit domain for the 1p3L. The dc was injected with a dc "ramped" pulse after the applied voltage has reached steady state. For the 3p3L and 3p5L models, the dc was injected into the neutral in accordance with Figure 23.

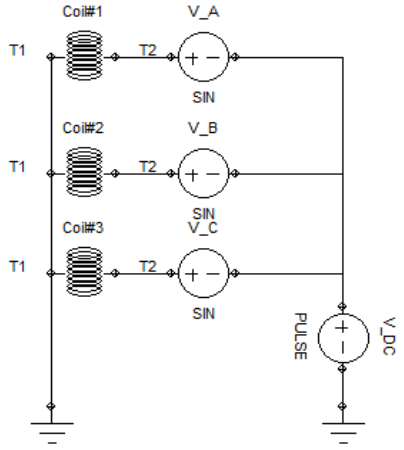

Figure 23: Modelling ac and dc excitation for three-phase multi-limb transformers with an external circuit (primary side only shown)

5.1.3 Material properties

The transformer components of interest to the FEM analysis were the core, and the primary and secondary windings (the bench transformers did not have tank enclosures). Airspaces between the windings, and air windows between windings and core limbs, were also considered where applicable. For each transformer, the BH magnetic data and core loss were derived from the (limited) grade lamination data were provided by the manufacturer. Other important parameters that were considered were the thickness of the windings, conductivity, mass density, thermal conductivity at constant temperature and its classification regarding grain-oriented electrical steel (GOES) or non-grain oriented steel (NOSS).

The 1p3L and 3p5L core types were fabricated using NOSS 50H530, 0.5 mm with core loss of 5.3 W/kg at an induction 1.5 T with a frequency of 50 Hz. The 3p3L core type was fabricated with GOES M6 having a core loss of 1.57 W/kg at 1.7 T induction at 50 Hz. These TuTs have economy grade laminations of low magnetic quality in comparison to power transformer core steel (1.01 W/kg loss at 50 Hz), but this was sufficient for their intended experimental purposes.

5.1.4 Solving

The transient solver was set to use second order differential equations implemented by the Newton Raphson method for 2D. For each time step, instead of using a fixed interval, time step adaptation is preferred here for better and optimal simulation time. After multiple runs were done, an initial step of 0.8 ms and a maximum step size of 1.1 ms were chosen for the simulations to achieve the best accuracy. The solver estimates an appropriate time step length at each solution point by shortening or lengthening the time step so that it does not result in excessive computation and still maintains accuracy. For waveforms that needed to be compared with the recorded waveform data, the discrete fixed interval method was used so that it was possible to trace both measurement and simulation data on the same timescale.

An adaptive mesh was used which resulted in the initial default mesh being refined at the inner corners of the core where the fields were changing direction rapidly, while a less dense mesh is kept along the limbs and yokes where the fields had a constant direction.

Three types of simulations were run for comparison with measured data:

- No load test at the knee point voltage defined as 1 pu This is also referred as the nominal voltage.
- Loaded tests with dc replicating the laboratory test conditions
- Dc injection and recording the time response.

After the performance of each transformer model under normal operating conditions was analysed, varying levels of dc are injected into the neutrals, and the voltage and current data were recorded for post-processing. The time that the dc takes to reach its final value from the point of injection was also recorded for comparison with a separate study which focuses on transformer-GIC investigates transformer time response (Oyedokun, 2015).

5.1.5 Post-processing

Power calculations were performed using the instantaneous voltage and current waveform data from the FEM solutions. The amount of reactive power *Q* drawn at varying levels of GIC was then plotted and compared with the measured data. It was demonstrated in a study by Gaunt and Malengret (2012) that the general power theory gives a result for the amount of *Q* under GIC conditions which implies that the actual conditions in a power system could be worse than when calculated using the conventional power theory. (The general power theory calculates non-active power for systems with any number of phases under non-sinusoidal conditions with dc components, and takes into account the losses in the neutrals which arise from harmonic distortion and unbalance. It, therefore, yields a higher *Q* than the conventional calculation.)

Due to the simplifications in modelling which isolate the investigation to a component level (as opposed to a power transmission system in a network), the conventional calculation was used to

calculate *Q* using Equations 5.1 – 5.3. The real power *P* is given by the average over a few cycles using the instantaneous values expressed in Equation 4.5. The apparent power *S* is calculated using Equation 5.2, where *E* and *I* are the separately derived RMS values of the voltage and current in each phase over the same cycles. The reactive power *Q* is calculated using Equation 5.3.

$$p(t) = e_a(t) \cdot i_a(t) + e_b(t) \cdot i_b(t) + e_c(t) \cdot i_c(t) \tag{5.1}$$

$$S = E_a I_a + E_b I_b + E_b I_b \tag{5.2}$$

$$Q^2 = S^2 - P^2 \tag{5.3}$$

For the 1p3L case, only the first terms of Equations 5.1 and 5.2 are used to determine Q post process, because the simulation is reduced to the response of one phase only of a three-phase transformer bank.

5.1.6 Application of symmetry

2D simulations are very quick to solve, and they are mostly sufficiently accurate for the purposes of this investigation, although the accuracy depends on the geometric complexity of the model. Since a real-life transformer is a 3D object, the most accurate solutions rely on 3D analyses. These simulations require long calculation times and enormous CPU power. One approach to reducing computational time for 3D calculations is to use mirror symmetry once it has been identified. Figure 24 (left) is a representation of the 3D model used to model one single-phase transformer in a bank of three single-phase units (see Figure 9 for the real-life bench transformers). Since there is no mutual coupling between the magnetic circuits of a three-phase transformer bank, the response due to dc excitation is virtually the same in each phase, provided the winding resistances of each unit are also the same. This allows for the FEM modelling of just one single-phase unit, as a first approximation of the three-phase bank's response. These laboratory transformers were stacked with an 'E-I' configuration.

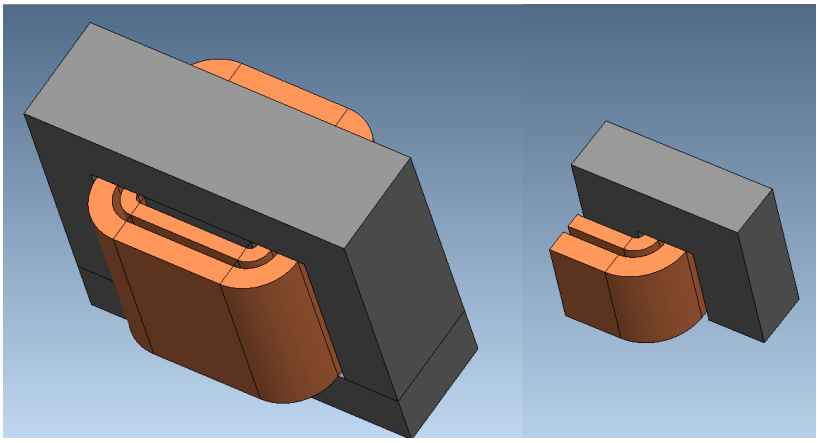

Figure 24: 1p3L Full 3D model (left) and its 1/8 symmetric model (right)

The 1p3L model can be reduced down to 1/8 symmetry depicted in Figure 24 (right). The specific factors are derived from the symmetric modelling Equations 5.4 and 5.5 (Infolytica Corporation, 2015).

For the symmetric model on the right-hand side of Figure 24, the current density J_{sym} should be the same as the current density in the J in the full model on the left. Similarly, for the current in the windings $i = i_{sym}$. For a voltage driven winding of the full model, J is defined as:

$$J = \frac{AV}{NR}.$$

(5.4)

A is the cross-sectional area of the windings as a function of the winding height, V is the applied voltage, N is the number of turns, R is the resistance of the windings given by

$$R = \frac{lN^2}{sA}$$

(5.5)

where l is the circular sweep distance of the windings and s is the conductivity of copper ($5.77*10^7$ Siemens/metre at 20 °C). For the 1/8 symmetric model:

$$l_{sym} = \frac{l}{4}$$

(5.6)

$$A_{sym} = \frac{A}{2}$$

(5.7)

and

$$N_{sym} = \frac{N}{2}$$

(5.8)

because the winding height is now halved.

Therefore, the (new) symmetric resistance R_{sym} can be related to the (old) full model's resistance R by substituting Equations 5.6 – 5.8 into Equation 5.5, yielding

$$R_{sym} = \frac{\left(\frac{l}{4} \cdot \frac{N^2}{4}\right)}{s \cdot \frac{A}{2}} = \frac{R}{8}.$$

(5.9)

Applying Ohm's law then results in the symmetric applied voltage:

$$V_{sym} = \frac{V}{8}.$$

(6.0)

This is also verified by applying symmetric parameters from Equations 5.7 - 5.9 back into Equation 5.4:

$$V_{sym} = \frac{\left(J \cdot \frac{N}{2} \cdot \frac{R}{8}\right)}{\frac{A}{2}} = \frac{JNR}{8A} = \frac{V}{8}.$$

The actual differences in time to compile between the full model and the symmetric were recorded and are discussed in 5.2.

5.1.7 Boundary conditions

Three types of boundary conditions were used for the 1/8 model: 'Field Normal' at the bottom of the windings for the flux entering and exiting the model there, a 'Flux Tangential' boundary at the back of the model for the flux which is tangential to the surface of the core, and another 'Flux Tangential" boundary on the left hand side of the model for the flux which is tangential to the surface of the core.

5.2 Results

5.2.1 Normal operating conditions 2D Models

It can be seen from Table VII that across all the core structures, there is good agreement regarding the measured and simulated transformation of voltages for the no load case. The measured and simulated I_{mag} values are given for phase 'a'. The measured core loss is the per phase open circuit power of each three-phase transformer. The FEM core loss for the three-phase transformers is the time-averaged total

core loss divided by 3 in order to make it comparable with the measured phase values. Under no load, there is very slight underestimation of the core loss, but the magnetizing currents are found once again significantly lower than the measured values. This response is similar to the 2D power transformer response presented in 4.1.1.

Table VII: Measured and 2D simulated results

Parameter	1p3L meas.	1p3L FEM	3p3L meas.	3p3L FEM	3p5L meas.	3p5L FEM
V_{phase} no load (V RMS)	80/152	80/156	44.0/85.0	43.6/84.4	80/153	79.2/154
I mag (A RMS)	0.055	0.024	0.073	0.054	0.070	0.035
Core loss (W)	3.3	2.705	0.696	0.6	4.6	4.3
I load (A RMS)	0.47	0.46 A	0.67	0.67	0.45	0.43

5.2.2 Dc injection – 2D models

Figure 25 shows the measured and simulated Q-dc response of the 3p3L transformer with small dc levels which are a function of I_{mag}. It can be seen that the simulation correlates well with the measured data in terms of the shape of the curve. There is a clear underestimation of the level of Q with each value of dc, possibly due to the initially under-estimated I_{mag} at no load.

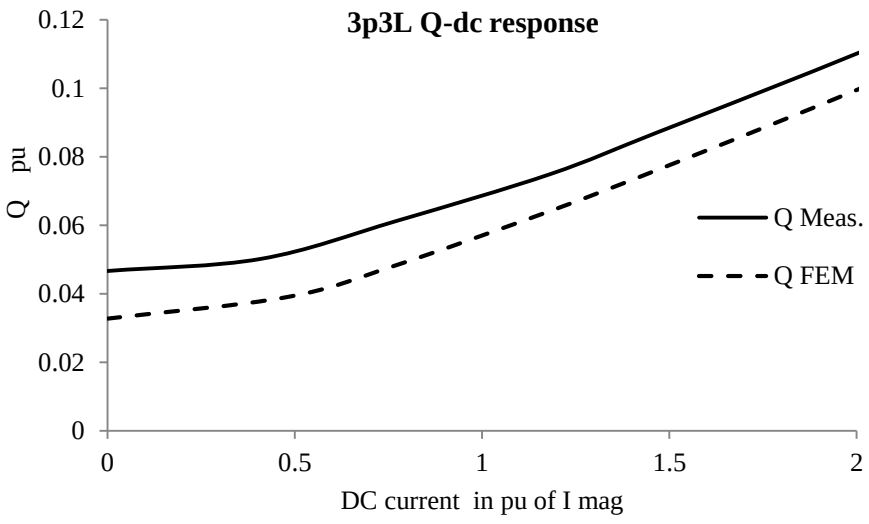

Figure 25: Measured and simulated Q-dc response of 3p3L laboratory transformer with a moderate loading configuration

Figure 26 presents the Q-dc response of one phase of the bank of 1p3L single-phase transformers reaching very high levels of dc which signify 'air-core' operation of transformers (defined by Hock-Chuan and Swift (1984) as 'straight line behaviour' or linear operation of the core in deep saturation). The FEM calculation shown on the same graph underestimates the values of Q for lower levels of dc, possibly for the same reasons as outlined for the 3p3L. For higher levels of dc beyond 10 pu dc (per unitized on the base of the I_{mag}), however, the Q appears as a vertical shift of the measured data. Generally, nonetheless, the conventionally measured linear Q-dc characteristic is followed closely by the FEM (post-processed) result.

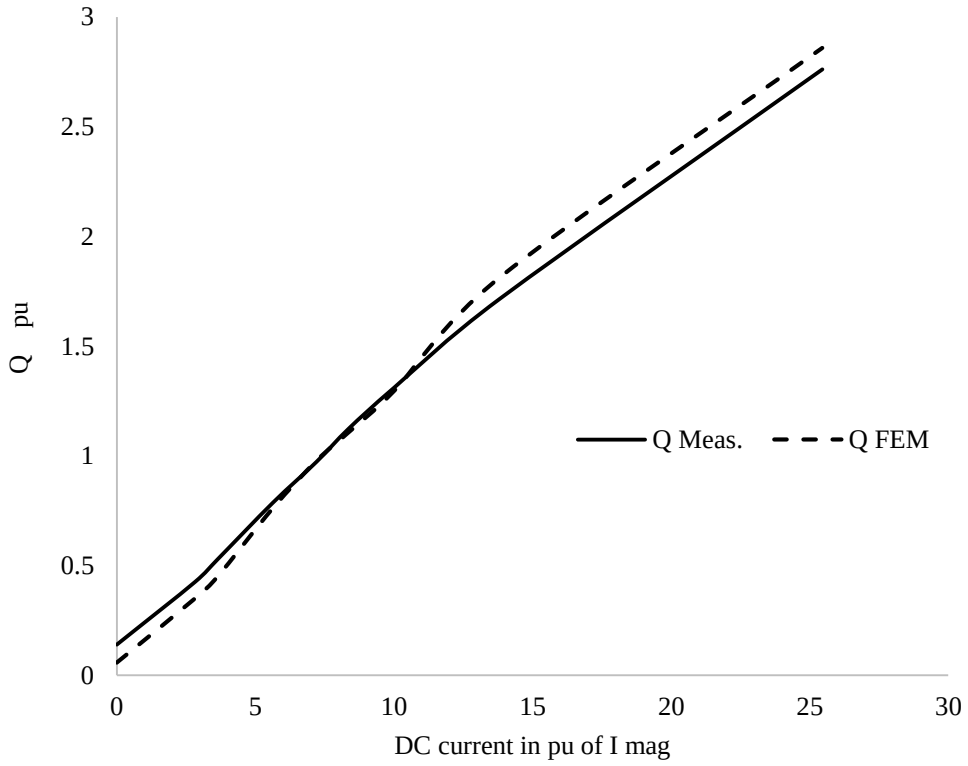

Figure 26: 1p3L measured and simulated Q-dc response with very high levels of dc and at full load

Figure 27 shows the measured and simulated line currents in the 3p3L with a 2.2 pu dc injection. At relatively low level of dc, the line current is shifted vertically upwards (positive dc) and there is virtually no distortion in the wave-shape. This is because a 3p3L transformer with a low number turns outside a tank does not offer the balanced dc flux any return paths back into the core. In the same figure, traces of the distorted line currents in the three-phase bank (made of 1p3L core types) with a full load and a relatively high dc of 10 pu of I_{mag} are also shown. The simulated waveform is compared with the measured data and shows evidence of half-cycle saturation in the positive cycle

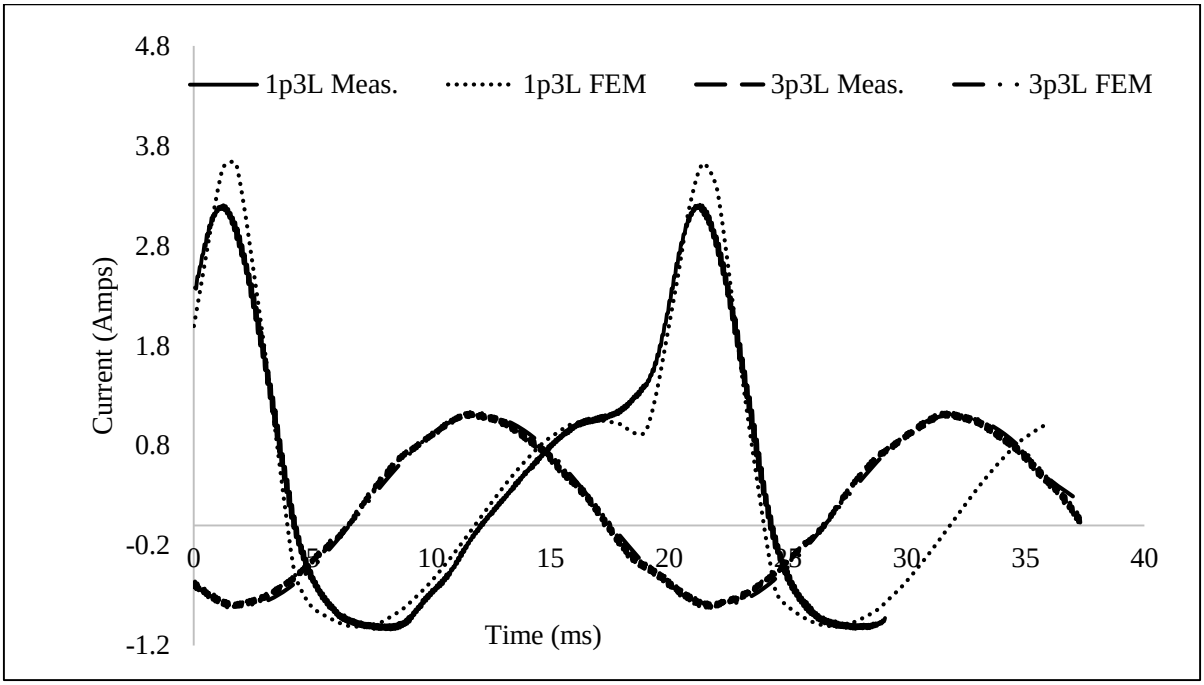

Figure 27: Differences in the responses of 1p3L and 3p3L transformers

In a separate study measuring the time response of the lab transformers to dc injection (Oyedokun, 2015), it is found that the time it takes for the dc to reach its final value varies with each core structure. The three-phase bank has the longest time response, followed by the three-phase five limb, followed by the three-three limb. It was also observed from the laboratory experiments that the bigger the dc value, the shorter the time it took to reach its final value for each core structure. The FEM simulated results were generally consistent with measured response in this regard. The physical turning on of a switch in the laboratory was modelled with a step input from a dc voltage source with a fast rise time. Figure 28 represents the dc current injected in the transformer neutral at t = 0.2 s, with ramp-up time of 0.2 s for the three-phase five limb model. It can be seen that the dc took roughly 10 s to reach steady state and that the values split between the phases are not necessarily balanced during the transient phenomenon period. It was observed from the FEM that calculations with small values of dc take the longest time to solve whereas those with higher values of dc tended to solve much faster.

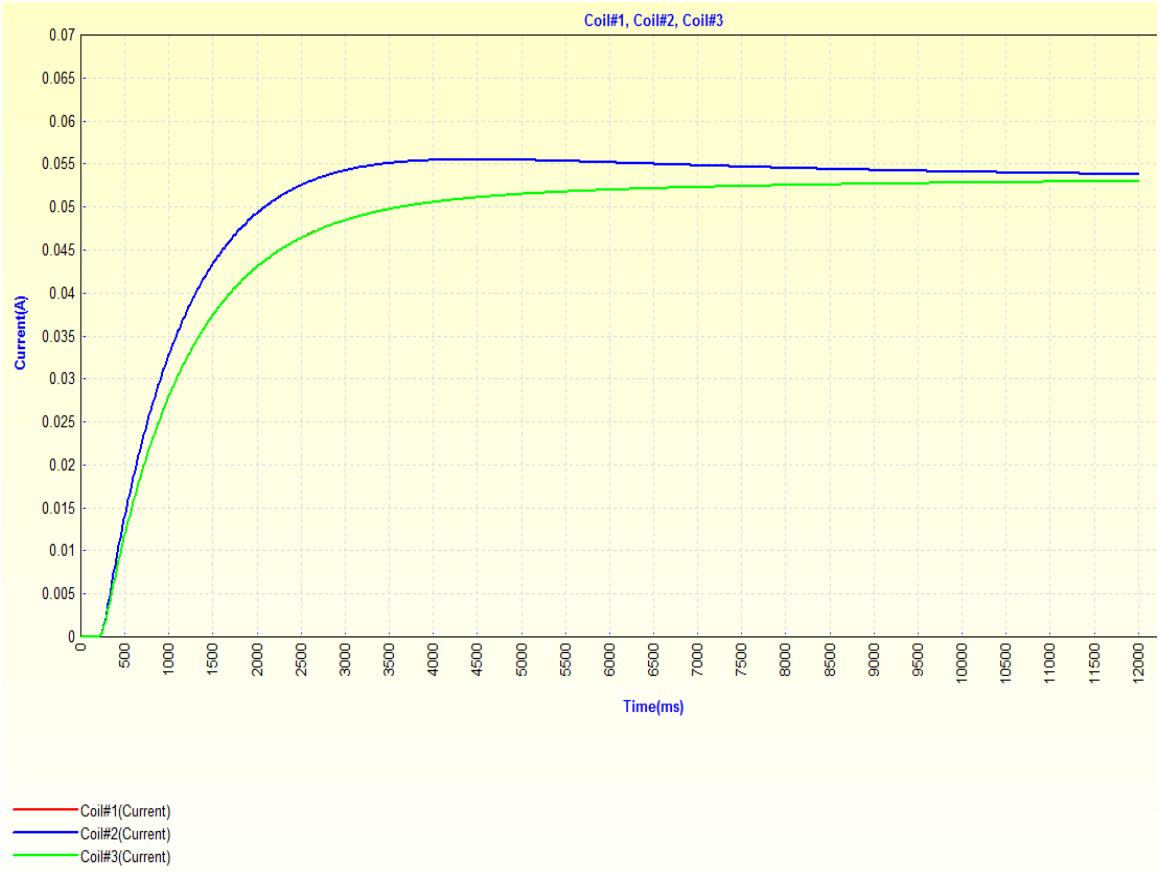

Figure 28: Dc time response of the three-phase five limb - 160 mA in the neutral

5.2.3 Verification of Symmetry: 1p3L

The results presented in the preceding sections were obtained with 2D models for comparison with measured data. This section focuses on the modelling of a 3D 1p3L transformer in order to test the accuracy of its 1/8 symmetric model with ac only. A time-harmonic problem was modelled in the FEM with the nominal voltage applied at no load. The time taken to complete the calculations by the full model was 3 hours 11 minutes and 52 seconds, requiring local disk space of 5.7 GB. The symmetric model converged to a solution within 2 minutes and 4 seconds, taking up only 347 MB of space.

From Table VIII, it can be seen that the 1p3L full 3D model is more accurate than the 2D version as there is a closer correlation with the measured I_{mag} and core loss. Analysing the 1/8 symmetric 3D model after correction in the last column, it is evident that its solved global quantities are virtually the same as those of the full 3D model.

Table VIII: 1p3L response of 3D full and symmetric model to test the application of symmetry

Solved Pparameter	Laboratory measured	Full 3D model	1/8th model	1/8 model correction factor	1/8th model corrected
Stored energy W (Joules)	-	0.00532	0.0006125	*8	0.00499
Primary flux linkage (Webers)	-	0.255	0.0314	*8	0.2512
Secondary flux linkage (Webers)	-	0.489	0.0611	*8	0.4888
Iron loss (W)	3.3	3.374	0.4075	*8	3.26
Primary RMS current (A)	0.055	0.0418	0.0417	*1	0.0417
Primary RMS voltage (V)	80	80	10	*8	80
Secondary RMS voltage (V)	153	154	19.2	*8	153.6

5.3 Discussion

Some of the FEM bench-scale model ac-dc excitation responses closely correlated with the measurements while others differed greatly, the main parameter being the no load magnetizing current. Since the transformers were fabricated by a small-scale manufacturer for the purpose of laboratory experiments, neither requiring industrial standard power quality at nameplate ratings, nor high-quality electrical steel, etc. it is possible that some of the physical properties that were provided by the manufacturer were not specified with the necessary accuracy.

Nevertheless, a preliminary FEM protocol for simulating transformers with ac and dc components has been developed giving results that could be related to measurement data. The use of symmetry in order to reduce time to compile was tested with ac only. It will therefore be implemented and tested in the main simulation protocol involving single-phase four limb transformers, with the aim of achieving a symmetry reduction down to a 1/8th model.

5.4 Summary

Using the Infolytica MagNet FEM environment, the second part of the preliminary protocol involved investigating three different bench-scale core structures with laboratory measured data, this process uncovered some areas where simulation accuracy needs improvement. The analysis led to the verification of how to use symmetry in FEM. When applied correctly, it exponentially reduces calculation time. In addition, the symmetric solutions maintain a good degree of accuracy in relation to the full model solution, which requires both considerable time to compile and CPU usage. Therefore, the use of symmetry for the more complex multi-parameter investigations later in this study is necessary.

Overall, the work presented in Chapter 4 and Chapter 5 forms the basis upon which the rest of the main FEM simulation in this thesis is built. The next chapter presents the main aspects of investigation in which an uncommon power transformer core structure is investigated through physical laboratory tests in conjunction with specific FEM modelling techniques.

6 1P4L LABORATORY TESTING

In the earlier literature survey in Chapter 2, it was established that limited FEM modelling of transformers and GIC had been carried out and that the main challenge was finding/generating power transformer measurement data for comparison with the simulation modelling (Bíró *et al*., 2014). This chapter attempts to address part of this limitation through the ac-dc physical testing of model laboratory transformers.

South Africa's nuclear power station, Eskom – Koeberg, acquired some single-phase four limb (1p4L) power transformers to form a generator step-up three-phase bank about four years ago. This particular core structure was preferred due to transportation limitations (height considerations) which come with three-phase three limb or three-phase five limb transformers in the 400 kV, 1000 MVA. At the same time, it was more economical to have one spare single-phase unit in case of a fault, rather than a whole spare three-phase transformer. Because the 1p4L core structure is uncommon in power transmission systems, very limited modelling and characterization of its response is available in research. Understanding the response under abnormal operating conditions such as those caused by GIC is of considerable value, especially to modellers and utility power system operators.

Since the ac-dc testing of the actual 1p4L power transformers was not possible within the scope of this research, three untanked industrially fabricated distribution scale 1p4L model transformers intended to form a three-phase bank were tested in a rigorous laboratory procedure. These transformers resembled the actual GSU power transformer units in terms of the high-quality core steel and parallel winding assemblies. The purpose of the laboratory testing was, therefore, to generate measurement data, test it with FEM modelling, and improve the modelling of transformers with simultaneous ac-dc excitation. Though the physical tests were exhaustive, being part of a broad study of transformer response to GIC, only the testing protocols relevant to the FEM are presented in this chapter.

6.1 Description of test transformers

The three test transformers were manufactured by Royal SMIT Transformatoren/Transformers Netherlands (RST). RST also manufactured the GSU 1p4L power transformers currently in service at Eskom's nuclear power station. The tests were carried out at an Eskom maintenance facility where there was access to laboratory space and a clean three-phase power supply compliant with IEEE Std. 519-1992 (Blooming & Carnovale, 2006) .

The test 1p4L transformers were stacked with the same PowerCore® H111-30 ThyssenKrupp Electrical Steel that is used in the Eskom – Koeberg GSU units. This grain-oriented electrical steel has a thickness of 0.3 mm, a core loss of 1.06 W/kg at 1.7 T at 50 Hz. Conventional design calculations defined each unit to be an 8.3 kVA, 209/390 V transformer. Due to factory limitations on the core cutting for this size, the test transformers had to be stacked with non-step lap butt joints (90° joints). The dimensions of each 1p4L are illustrated in Figure 29.

There is a relatively larger centre window between the inner limbs because it was envisaged that these transformers could be converted to three-phase five limb models by stacking more core steel for future work in further studies.

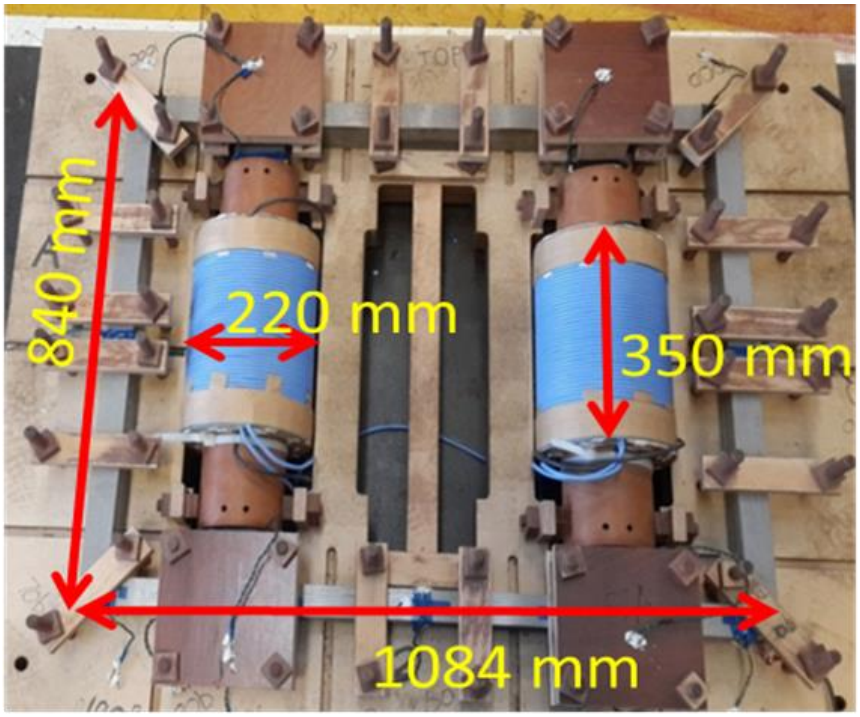

Figure 29: A1p4L 209/390 V laboratory transformer

The transformer has two winding assemblies that are parallel connected as in Figure 30 (left) with opposite polarity to support the flux directions illustrated in Figure 30 (right). Each winding assembly has a 150 turn inner winding and an 80 turn outer winding. This winding configuration and polarities should result in the bulk of flux flowing in the inner wound limbs and interconnecting yokes.

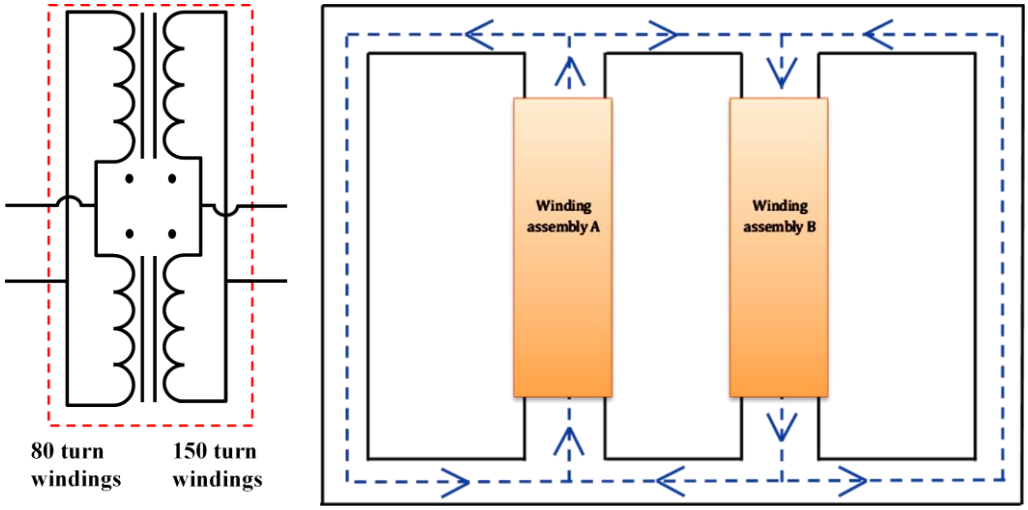

Figure 30: Subtractive parallel winding configuration (left) and expected flux distribution in a 1p4L (right)

6.1.1 Acceptance tests

Upon arrival from the Netherlands (RST), the three model laboratory transformers shown overleaf in Figure 32 (c) were unpacked, visually inspected and labelled T1, T2 and T3. The approach to the acceptance test was in accordance with the test codes in the IEEE Std. C57.12.91-2011 and the general requirements IEEE Std. C57.12.01-2015 for dry-type and power transformers.

A Megger test is first performed to verify that the winding insulation resistances were within the Giga-ohm range. All the tests show that the transformers' winding insulation was satisfactorily between 21.3 GΩ and 26 GΩ at a temperature of 27.2 °C and relative humidity of 43.3%. The winding assemblies were labelled A and B. The next test determined the winding polarities to achieve the flux distribution depicted in Figure 30. A quick 2D FEM analysis using an external circuit to test for the correct response (at no load) was performed. This was done to verify the correct polarity (prescribed by the manufacturer as subtractive) and to explore the effect of the wrong connection (additive) at the same level of induction. From Figure 31 it can be seen that the wrong polarity (right) results in the inefficient use of the core, with virtually no flux flowing in the top and bottom yokes while the side limbs are stressed by the significantly higher levels of flux density.

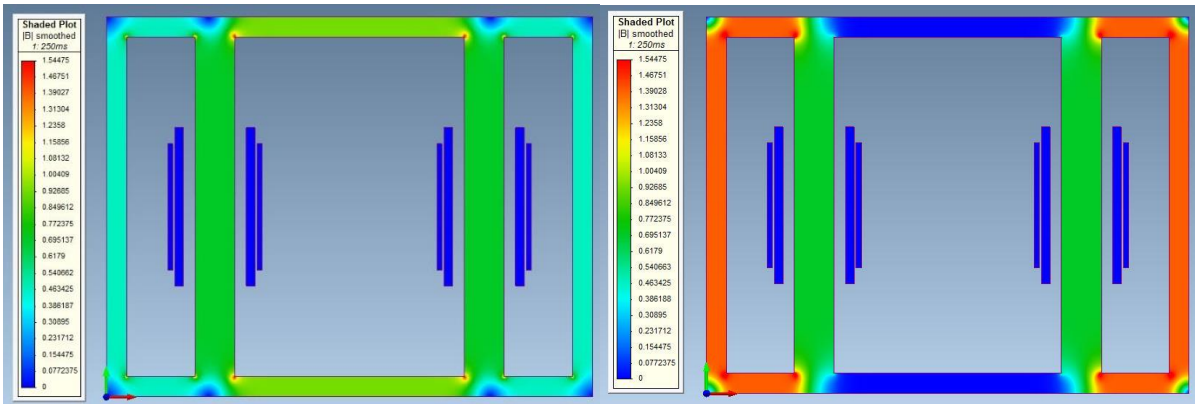

Figure 31: The correct winding polarity (left) and the wrong winding polarity (right) at a 50% voltage excitation generated using 2D FEM

Having verified a subtractive winding polarity, the terminals were labelled accordingly and secured on a DIN rail which is visible in Figure 32 (c). The cold winding resistance of each winding was then measured with a simple circuit involving a 12 V battery, 12 Ω external resistor, ammeter and voltmeter. A table of the measured cold winding resistances (at an ambient temperature fluctuating between 25-26 °C) is given in Appendix C.1 The dc winding resistances corrected to 20 °C are also given in the same appendix. To verify the correct turns ratio, a Vanguard Model ATRT-03A three-phase transformer turns ratio tester was used, resulting in a 1.88:1 transformation ratio with only 0.22% difference against the design ratio of 1.875:1 (see Table C.3 in Appendix C.1).

In summary, the verification of the prescribed subtractive polarity used in parallel connected 1p4L transformers was assisted by preliminary FEM simulation and consequently verified in the laboratory. The Giga-ohm range of the winding insulation shows it was in excellent condition, as expected for the new transformers. The winding resistances for both the 80 turn windings and 150 turn windings differed across the transformers by no more than 1 mΩ, demonstrating consistency in the fabrication process and a good laboratory measurement scheme. Lastly, the ratio test was well within the industrial standard's limit of not more than 0.5%. These series of tests confirm that the test transformers adequately fit the requirements for further tests, and thus formed a stable basis for the work planned.

6.2 Testing protocol and measurements

The preliminary tests that were used to perform a standard acceptance test with industrially compliant instruments have been discussed. The next sections focus on the experimental protocol that was derived to meet some of the main objectives of this thesis by measurement.

6.2.1 Test set up and apparatus

Power from the main supply was controlled with a 0-380 V, 60 A three-phase variac shown in Figure 32 (a). Because of the expected harmonics in the currents drawn by a transformer with simultaneous ac-dc excitation, it was important to isolate the supply ac-dc test circuit from the wall supply. This was done by using two identical 500 kVA, 11 000/415 V Dyn11 3p3L distribution transformers, connected back-to-back to supply the test transformers. See Figure 32 (b). The more detailed nameplate ratings are given in Appendix C.2. The advantage of this set up is that the HV delta side of the back-to-back interface suppressed any triplen harmonics which could have potentially affected the source.

The IEEE Std. 519-1992 (Blooming & Carnovale, 2006), which provides recommendations for maximum allowable voltage and current distortion levels at points of common coupling, was used for verification with Yokogawa WT1600 Digital Power Meter (YPM1). A newer Yokogawa WT1800 (YPM2) with a higher resolution was used to take measurements on the test transformers. Figure 32 (c) is an image of the actual three 1p4L test transformers. A schematic of the entire test set up corresponding to the photo in Figure 32 is given in Figure 33.

The additional measurement apparatus included:

- Digital laser thermometer for winding and ambient temperatures
- DIN rail mounted with terminal connections from 1p4L transformers to Yokogawa Power Meters (shown in Figure 32 (c))
- Several high-resolution multimeters for search coil terminal voltage readings
- 1 mm insulated wires for flux search coil measurements
- Usual mechanical laboratory tools and spare wires

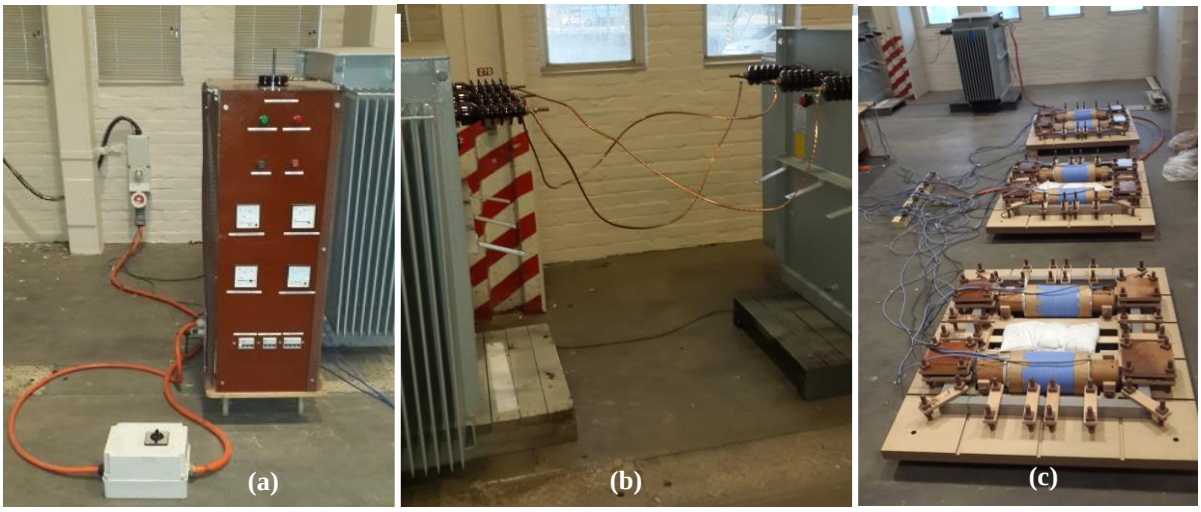

Figure 32: Apparatus for the test set up showing the main supply and robust three-phase variac (a), the back-to-back transformers used for isolation from the source (b) and the 1p4L test transformers (c)

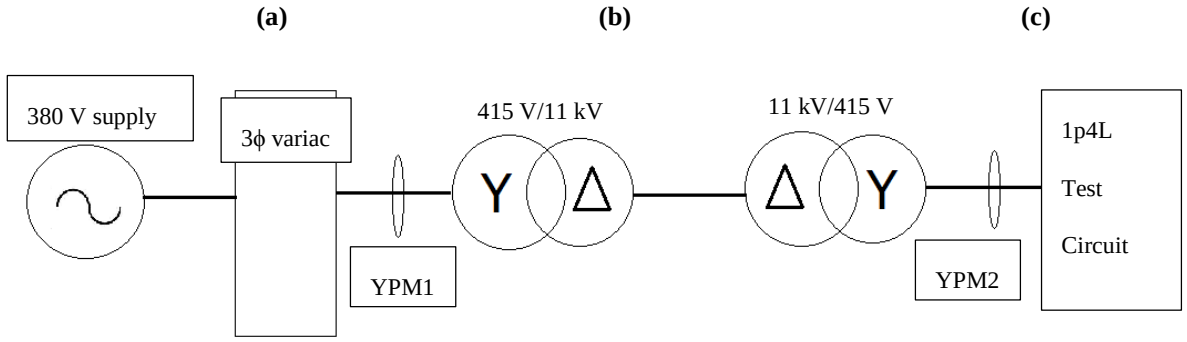

Figure 33: Schematic of the laboratory test set up

6.2.2 Magnetization characteristics

In the context of any simultaneous ac-dc excitation study, it is necessary to predetermine the levels of dc that are to be injected into a test transformer, and also to establish a nominal transformer applied ac voltage under normal (unsaturated) operating conditions. The transformer cores were investigated by generating their individual v-i magnetization curves using a method similar to the protocol tested on

laboratory bench-scale transformers (Chisepo *et al*., 2013). The procedure involved making small increments in the applied voltage at no load and recording several electrical parameters. The final values of the magnetization curves represented over-excitation well beyond the transformer nameplate ratings before this protocol was completed. Results from these tests were used to derive the following important parameters in the following sequence:

1) **McLyman knee point –** This was done using the RMS v and i over a full range of excitation at open circuit. The purpose of this procedure was to distinguish between linear operation and the saturation region of the core as depicted in Figure 35. Correct voltage transformation was also verified. Several electrical parameters were recorded at each step of applied voltage including VA power, real power, reactive power, peak current, mean current, current and voltage THD, wave shapes of voltages and currents, etc.
2) **Reversibility of excitation –** On a nameplate rating per unit base, each transformer was energized from the primary and secondary sides separately to replicate the magnetization curves, to verify consistency of the core performance.
3) **Analytical determination of saturation –** The knee point for each transformer was verified by using a formula to determine the exact point at which saturation commenced under an applied voltage. This point is defined as when the peak exciting current I_{peak} is twice the mean exciting current I_{mean} (McLyman, 2004), and it is expressed as $I_{peak} = 2 \cdot I_{mean}$.
4) **Comparison of saturation characteristics –** The v-i curves of each transformer were superimposed on one graph to see how consistent the manufacturing process had been in making three transformers intended for a three-phase bank using the same design data.
5) **Determination of I_{mag} –** Once the knee point voltages had been identified, the corresponding I_{mag}'s for each transformer could now be determined and later used as a basis for the levels of dc .
6) **The nominal voltage –** Past experience working with model laboratory had transformers revealed that nameplate ratings often represent over-excitation, unlike power transformers. The knee point determined in 1) was applied, and it is found that a new nominal voltage is required, significantly lower than the nameplate ratings. When the voltage was adjusted and the transformers de-rated to an appropriate capacity, open circuit (O.C.) and short circuit (S.C.) tests are performed. The new nominal voltage was applied throughout all the ac-dc experiments.

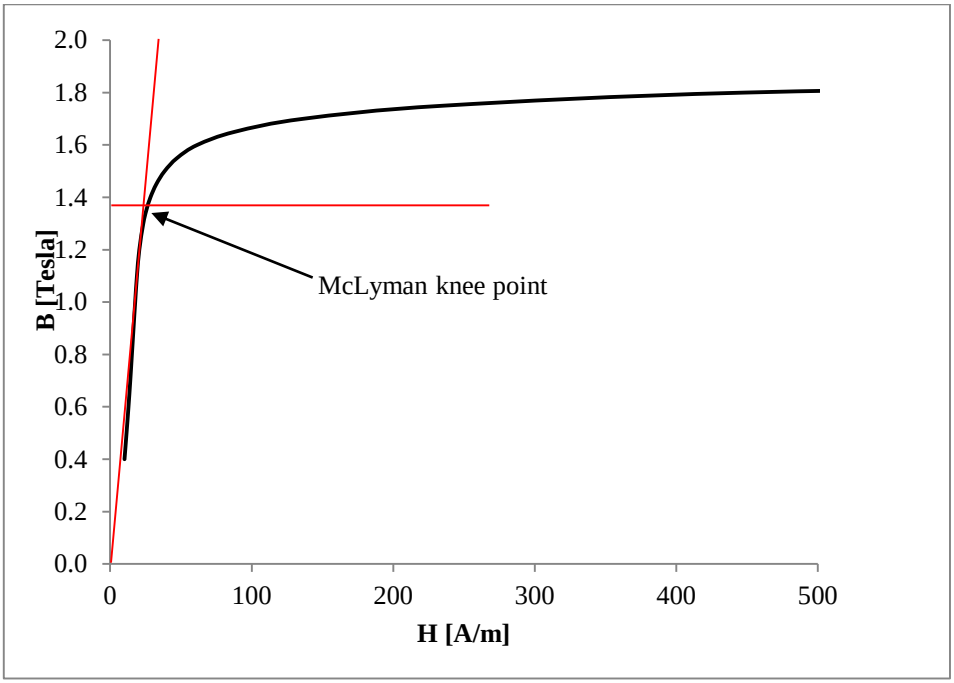

Figure 34: The McLyman knee point for a sample of electrical core steel

6.2.3 Search coil deployment

Based on the prior tests of the magnetization of the test transformer cores, the flux distributions could now be investigated using search coils. Several single turn search coils (SC's) were wound around the core as illustrated with red lines in Figure 35. Further preliminary 2D FEM analyses were done with ac over-excitation to try and verify possible leakage flux paths flowing through the air at the joints. This resulted in the installation of some 20 turn air search coils that were placed in the inner windows against the cores at the joints. These air search coils are illustrated in the same figure with thicker blue lines.

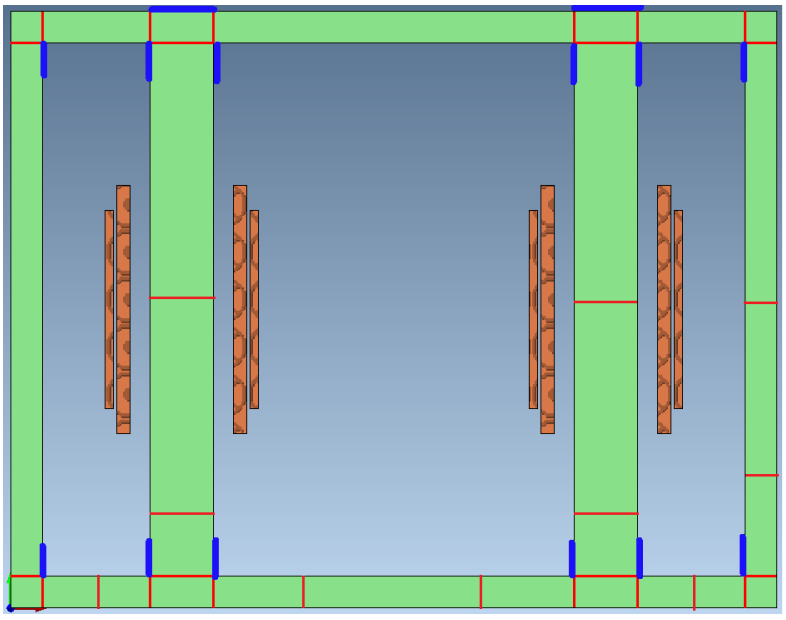

Figure 35: An illustration showing how the search coils were wound around the core (red lines) and how air search coils were placed at the corners of the core (thicker blue lines)

Apart from the expected leakage flux at the joints, the FEM analysis revealed that it was necessary to install two additional air search coils at the T-joints, that is, against the top (or bottom) yokes labelled Y1 and Y2 in Figure 36.

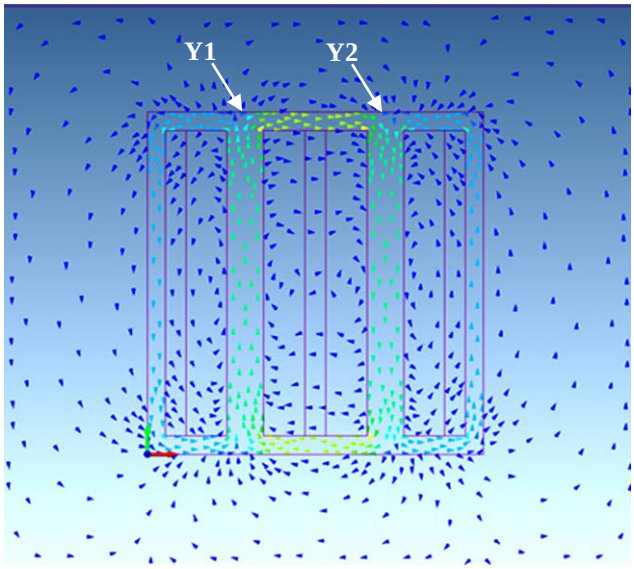

Figure 36: 2D FEM vector plot of an over-excited 1p4L transformer

The search coils were wound in twisted pairs (see Figure 37), and measurements were taken at a distance sufficiently far away from the core to avoid erroneous readings due to leakage flux (as electromagnetic interference from the core interacts with measurement instruments). Each 1p4L transformer was once again tested, and the measurements were recorded. The search coil measurements were used to depict the flux distribution in and around the core. Several high-resolution multimeters were then used to record the induced voltages at the SC outputs corresponding to the flux inside flowing through them.

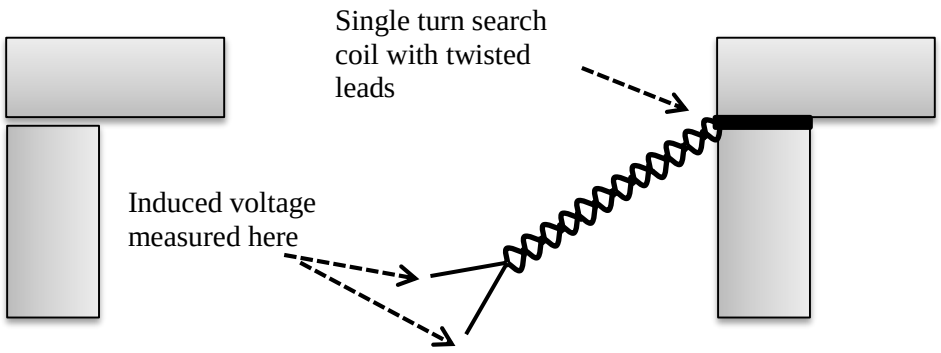

Figure 37: Method of installation of search coils around the core of 1p4L test transformers for core flux distribution measurement (Chisepo *et al.*, 2018)

6.2.4 Dc injection set up

The steps given in sections 6.2.1-6.2.3 provided enough information to set up a dc circuit. Firstly, the magnitude of range of dc to inject in each test transformer was determined from the average of the TuTs I_{mag}'s at the knee point. The air search coils for measuring leakage flux in saturation were verified through measurement and complemented by some 2D FEM analyses. Lastly, the range of the very high peak magnetizing currents to be expected in half-cycle saturation were recorded and used to estimate the peak maxima which would occur during half-cycle saturation due to dc. It is easier to perform tests on a three-phase transformer system because the dc is injected into the transformer neutrals, and then it splits between the phases energized with ac. Minimal out-of-balance ac currents are expected to flow back to the neutral which could potentially harm the dc source. In the single-phase unit, if the dc source is connected in series with the energized windings, the resulting very high ac peak current may cause damage. This is caused by the half-cycle saturation phenomenon explained in section 2.3. In fact, Kappenman and Albertson (1990) reporedt that a peak magnetizing current in the order of 60 times the normal peak I_{mag} may be expected in a power transformer under a moderately high GIC (25 A/phase). A test circuit was, therefore, derived in this thesis together with an adjacent study (Borrill *et al.*, 2016) and it was implemented to inject dc safely while the transformer was energized at its nominal voltage (see Figure 38). In this figure, the purpose of the large inductance was to supply ac current and simulate a no-load condition while allowing dc to pass through. This way, the battery banks were not expected to receive any ac currents more than 500-600 mA for the full range of dc injection in the presence of nominal ac applied voltage across the 80 turn primary windings.

An alternative dc test circuit could be an equivalent single-phase back to back set up adapted from a three-phase power transformer GIC test by Lahtinen and Elovaara (2002). Their circuit involves two test transformers with additional capacitors between the dc generator forming an ac earthing neutral. The ac shunting capacitors also have the purpose of bypassing the dc generator. The circuit is not suitable for this research because not only does it require additional components but it also involves the complex responses of two test transformers making it difficult to characterize the response of only one 1p4L transformer for comparison with the FEM. Therefore, the dc injection scheme in this thesis is set up in accordance with Figure 38.

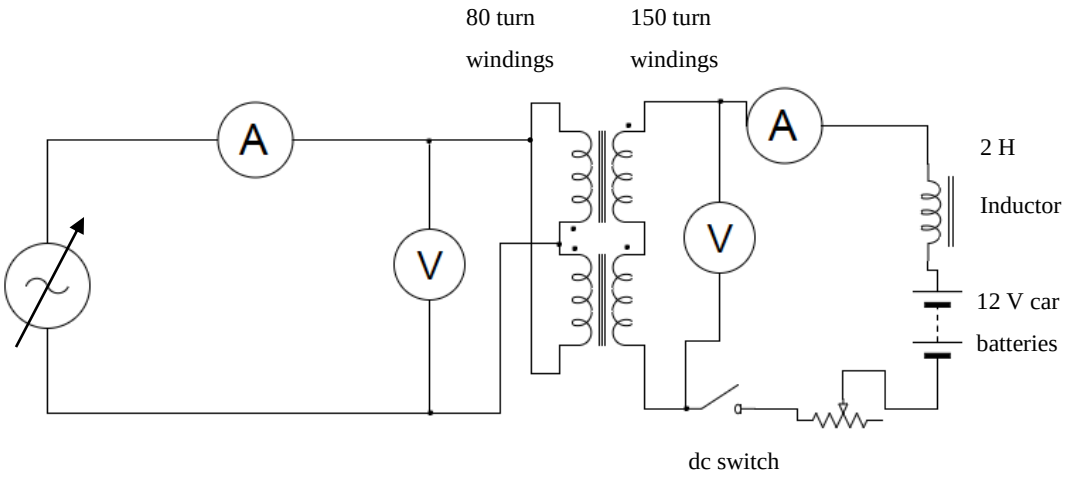

Figure 38: Single-phase test circuit for injecting dc into the 1p4L Transformer under test

In addition to the apparatus described in 6.2.1, the following apparatus was included in the dc test set up:

- Current sensing shunt resistors to deal with very high dc currents
- Heavy duty arc shooting 200 A dc switch
- 12 V 60 Amp-hour automobile battery banks
- Copper strips for very low resistance and high current carrying capacity for dc control
- High current variable resistors for dc control
- Three-phase test transformer with all the windings connected in series to act as a large inductor (this is the "2 H Inductor" in Figure 38)

With the parallel connected 80 turn windings energized at nominal voltage, the secondary side 150 windings were connected in series. On the same side, a three-phase test transformer configured as a 2 H inductor was connected to limit ac current, simulating a no-load condition, while allowing dc to pass through, as explained earlier. The dc flux in the core of the transformer under test offset the ac flux in one half-cycle generated by the voltage applied across the 80 turn windings. The three-phase inductor did not saturate due to dc because of the absence of a zero-sequence dc flux return path, as explained in 2.3, and so the consequent, measured distortion due to dc is solely due to the 1p4L test transformers' response.

6.2.5 Measurements with ac and dc

Varying levels of dc were injected with nominal ac voltage applied. This nominal voltage was determined from the results in section 6.2.2: *Magnetization Curves* where the linear region of operation for each transformer is rigorously determined. Numerous electrical measurements for voltages and currents, harmonics, reactive power, and search coil outputs, etc. were then taken at varying levels of dc injection. For very high levels of dc outside the amperage limit of the power meters, current sensing shunt resistors were used. Similarly, very high dc was controlled using low resistance copper strips in conjunction with variable resistors. A key objective in the dc test protocol is to inject incremental levels of dc from very small magnitudes (<1 A) to very high magnitudes (up to 14 A) to fully characterize the non-linear behaviours of the 1p4L cores. The next tests in the experimental protocol to investigate the saturation inductance needed dc levels over 50 A, to try to achieve deep saturation. This is described in the subsequent sections.

6.3 Saturation inductance

Saturation inductance, the operation of a transformer in deep or 'complete' saturation due to simultaneous ac and dc components of current, in this thesis will be used in two senses:

1. "terminal saturation inductance" ($L_{terminal}$) – defined by de León *et al.* (2014) as the inductance of a transformer determined by measurement at the terminals of the windings, and
2. "air core inductance" (L_{air})– the inductance of transformer windings when its core is removed.

6.3.1 Terminal saturation inductance

Some parameters that are required in EMT software to model the saturation characteristics of transformers with low-frequency transients are not easy to measure or derive from an actual transformer. One of those is the saturation inductance mentioned earlier in the literature review (section 2.2) and often referred to as the 'air core inductance' or 'air core reactance'. $L_{terminal}$ (or L_{air}) is probably the most important parameter for accurate transformer modelling for GIC and other studies involving deep core saturation (de León *et al.*, 2014). It arises from the operation of a non-linear core in deep saturation. Some EMT software recommends that, given the physical limitations in deriving this parameter from measurement, the air core reactance be input as twice the short circuit test derived leakage reactance (as an approximation) (EMTDC/PSCAD, 2005). In their study to overcome such approximations that are not satisfactorily verified anywhere in the literature, de León *et al.* (2014) proposed a method for measuring the 'terminal saturation inductance' of iron-core transformers using a low power non-ideal rectifier.

In the research for this thesis, this method was adapted and implemented to produce sufficient dc to drive the transformer into deep saturation with a small ac ripple to determine the inductance. The de León *et al.* (2014) method involved measuring the current flowing in the energized 80 turn inner

winding and the voltage across the outer 150 turn winding. This captures the incremental flux while removing the winding and source resistances from the calculations, thus removing possible errors caused by fluctuations in resistance. Fast Fourier Transform values from the WT1800 Yokogawa Power meter analyser measured currents and voltages which were then substituted into the following expression (de León *et al*., 2014):

$$L_{terminal} = \frac{V_{out\_k}}{2\pi f_k n I_{in\_k}} \tag{5.1}$$

where $L_{terminal}$ is the "terminal saturation inductance", k is the harmonic order, V_{out_k} is the amplitude of the secondary voltage of the dominant harmonic, f_k is the dominant harmonic frequency, n is the transformer ratio and I_{in_k} is the amplitude of the dominant harmonic of the primary current.

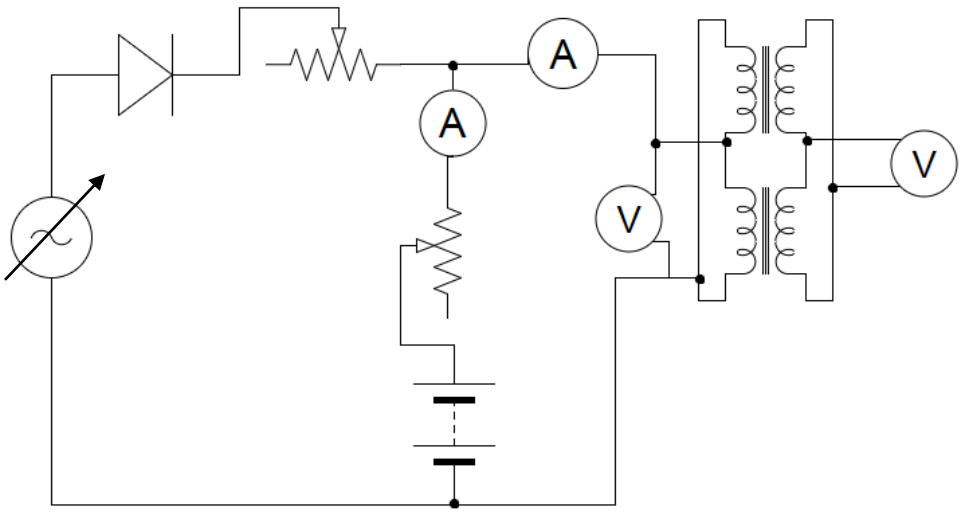

Figure 39: Schematic of the original setup for determining the saturation inductance (de León *et al*., 2014) adapted for a 1p4L transformer by supplementing the dc offset

First, a proof-of-concept simulation was done in PSCAD with a saturable 1p3L transformer (the 1p4L model was not available in the software's library), and the waveforms were analysed. It then followed that the test 1p4L transformers should yield a similar performance since this test is designed for single-phase transformers. The test circuit was set up as shown in Figure 39. Measurements were recorded by the Yokogawa Power Meter (WT 1800). The input was a single-phase variable ac supply whose current was controlled by continuously adjustable resistors. The dc current was controlled by other continuously adjustable resistors connected in parallel with low resistance copper strips for very high dc input. Shunt resistors were used to enable the power meter to measure the total line current values outside its range of 60 A. Calabrò (1986) states that as the transformer gets close to complete saturation, the saturation inductance characteristic is expected to reach a constant value much lower than its

inductance during linear operation. With this information in mind, it was reasoned that a small deviation in the order of <5 μH with a significant step increase in the dc component of current would be regarded as indicating that the "terminal saturation inductance" ($L_{terminal}$) had been reached.

6.3.2 Air core test

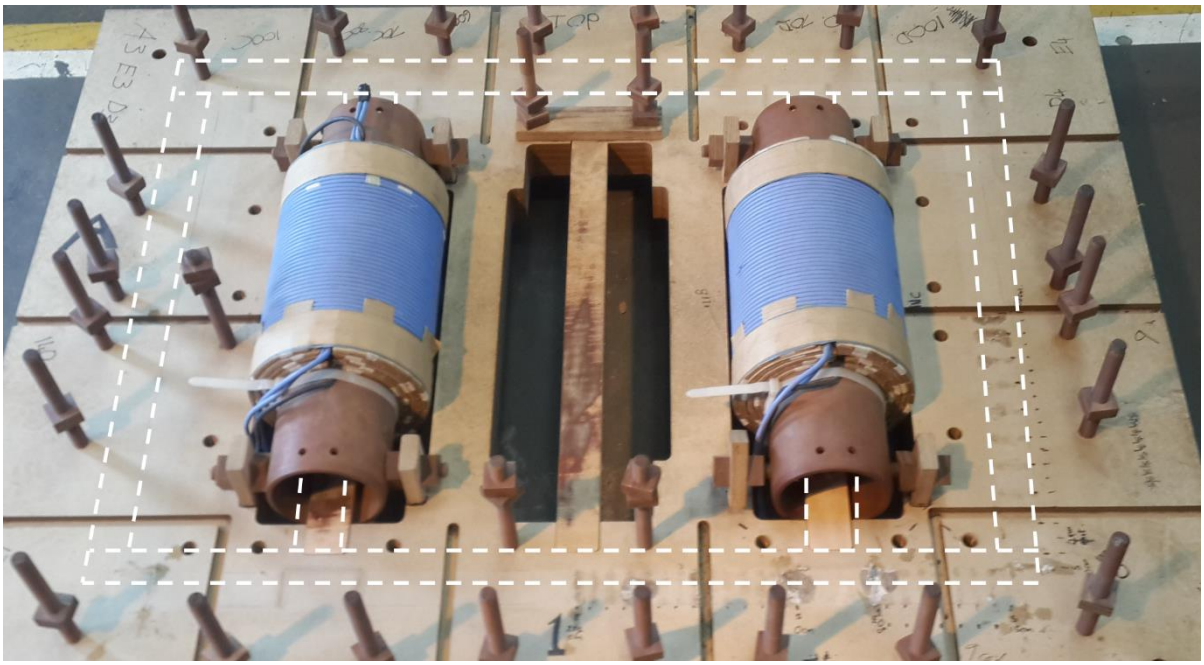

Figure 40: 1p4L test transformer without the core for L_{air} measurements relative to the removed core (indicated by the dotted white lines).

Finally, when all the ac-dc experiments were complete, one of the 1p4L test transformers (T1) was stripped of its core, leaving its windings in their original positions as a stand-alone core-less transformer as shown in Figure 40, and the "air core inductance" (L_{air}) was measured with ac only. The schematic for the setup is shown in Figure 41. A 0-240 V, 20 A single-phase variac powered the circuit, and the current into the windings was controlled with a low resistance variable resistor. Measurements for the 80 turn and 150 turn winding assemblies were taken separately, with the other side open circuited. There are no reports in the literature of measuring L_{air} with which to compare this approach (i.e. stripping the test transformer of its core while carefully maintaining the original positions of the windings).

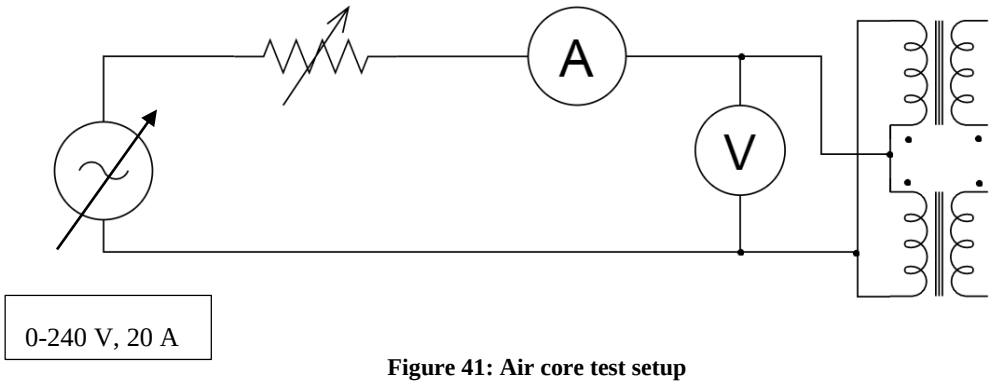

Figure 41: Air core test setup

To verify the linear or constant characteristic of an "air core", current values ranging from 3 to 10 A were used to calculate L_{air} using the expression given in Equation 6.2:

$$L_{air} = \frac{Q}{2\pi f I^2} \tag{6.2}$$

derived from the expression $Q = I^2 X_{air}$, where Q is the reactive power, I is the line current, f is the supply frequency of 50 Hz and X_{air} is the air core reactance.

The two methods of measuring "terminal saturation inductance" and "air core inductance" were then compared against the FEM to analyse their possible differences.

6.4 Summary

In this chapter, the steps taken in the laboratory protocol have been systematically presented. First, the suitability of the test transformers was verified with an acceptance test adapted from widely used industrial standards. After this verification, the individual transformers' magnetization characteristics with ac only were determined with ac measurements at open circuit. The results from this test were important for identifying the linear region, knee point, commencement of saturation, and saturation operation of each transformer. The I_{mag} was used as a guide to derive the range of dc inputs for the ac-dc tests in the later parts of the protocol.

In the industry and the literature, the difficulty in installing search coils and air search coils is often reported (Tang *et al*., 2015). The custom air windows in these 1p4L units made it possible to install search coils at almost any part of the cores and around the cores. The placement of some of these search coils was assisted by some quick 2D FEM analyses to ensure that in the exhaustive experimental procedure, potentially important measurements were not omitted from the protocol. A special dc injection set up was used to impose varying levels of dc bias while ensuring that a negligible ac current flows back to the dc source thus avoiding any damage.

The use of IEC76-1 (1993) compliant WT1600 and WT1800 power meters consolidated the reliability of the measured data for both online and post-experiment processing. The final part of the experimental protocol investigated a key parameter in transformer modelling, i.e. saturation inductance, that seems to be not fully understood in the literature, often resulting in discrepancies in the topological models. The objectives of this part of the protocol are twofold: 1) to adapt and test a method proposed in the literature through physical measurements which are not part of the factory acceptance tests, and 2) to augment the measured results with a FEM approach that will have been developed and improved. Results from this dual approach should provide further insights into the transformer modelling and manufacturing industries.

The next chapter presents the FEM simulation protocol that was further developed and implemented in this research to achieve different corresponding aspects from the measurement protocol.

7 1P4L FEM SIMULATION

Chapter 6 described the laboratory protocol that was used to test 1p4L transformers. The purpose of this chapter is to develop a FEM simulation protocol, based on the actual laboratory experiments, in order to test its validity and improve the accuracy where required.

Various coupled field-circuit models representing the laboratory 1p4L transformers were developed for FEM simulation to investigate the response when a dc component is added to power frequency excitation. The simulation environment in which the modelling took place was Infolytica MagNet, which has three solvers: Magnetostatic/Static Solver, Time-harmonic/Eddy Solver, and Transient Solver.

7.1.1 Parameterization

The transformer material properties of interest to the study were the non-linearity of the core, and the primary and secondary winding data. Air spaces between the windings and air windows between windings and core limbs were also considered. The wooden core clamps and winding bobbins have no electromagnetic significance. For each transformer, the BH magnetic and B-$Core_{loss}$ provided by the manufacturer were used as inputs into the FEM in modelling the core. These curves are shown in Figure 42 and Figure 43, respectively. Table IX shows some more parameters that were used in the transformer models.

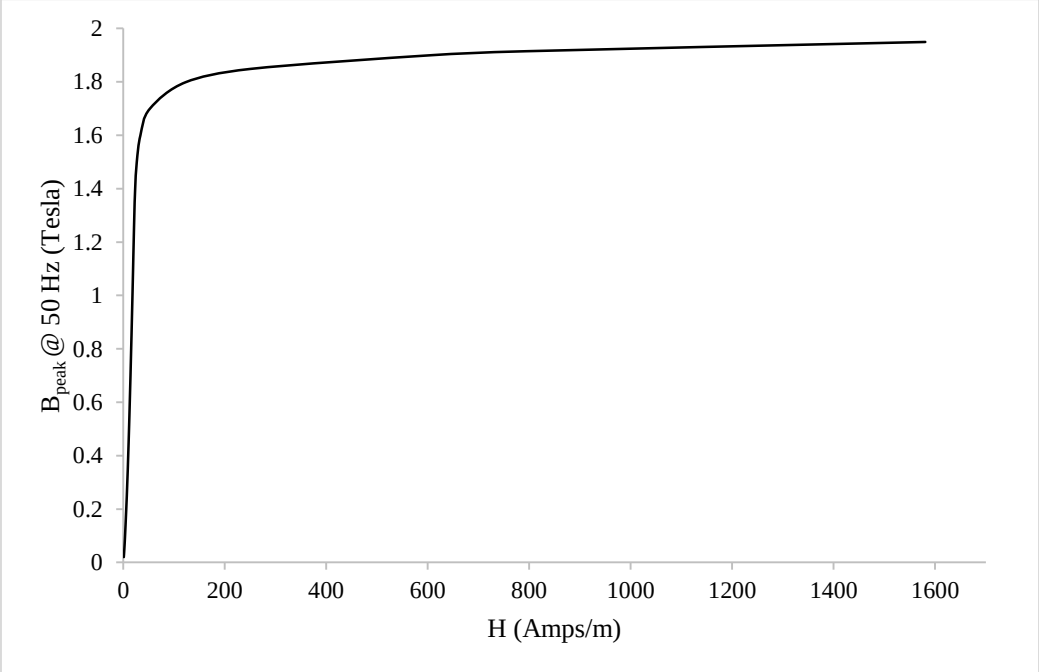

Figure 42: B-H magnetic properties of the electrical core steel in the rolling direction

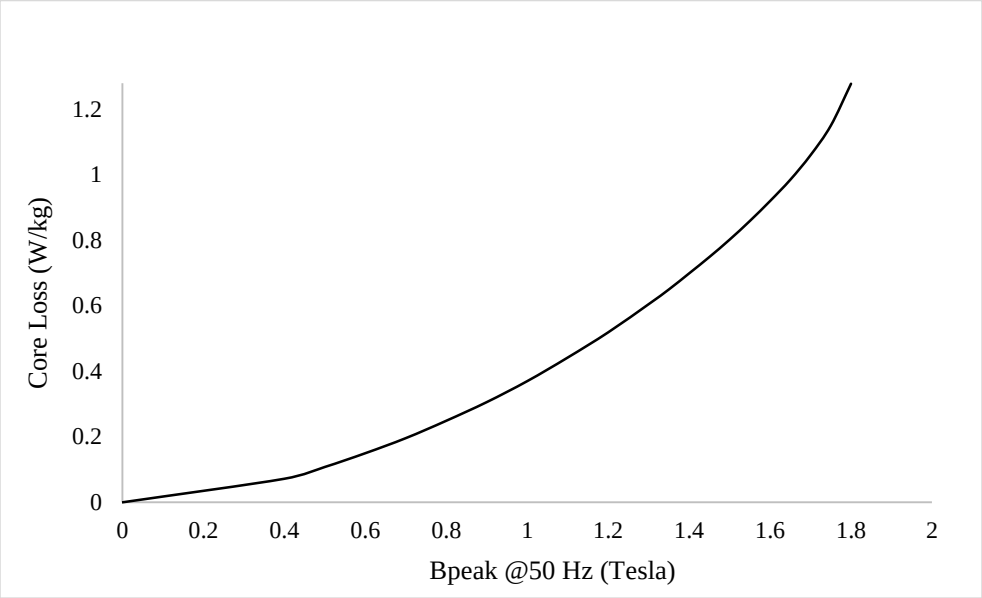

Figure 43: Core loss profile of core steel at 50 Hz

The core loss *P* is calculated using the Steinmetz equation at any B_{peak} value from the profile in Figure 43, and it can be expressed as:

$$P = K_h f^{\alpha} B^{\beta} + K_e (sfB)^2 \tag{7.1}$$

where the hysteresis and anomalous loss are represented in the first term (Pry & Bean, 1958, Bertotti, 1988, Cheng & Pillay, 2002, Ionel *et al*., 2007), and the eddy current loss is represented in the second term (MIT Press, 1944). The lamination thickness ratio is *s*, and the coefficients K_h and K_e and exponents α and β are obtained from a curve fitting algorithm which imposes the theoretical square-law dependence of the eddy current loss on the lamination thickness, as a function of frequency *f* and B_{peak}.

Table IX: Transformer 'as-built' data available for the FEM models

Lamination grade	PowerCore® H111-30
Lamination thickness	0.3 mm
Core loss at 1.7 T at 50 Hz	1.06 W/kg
150 turn winding thickness	19.568 mm
80 turn winding thickness	11.568 mm
150 turn winding height	350 mm
80 turn winding height	280 mm
Conductivity of copper	$5.77 * 10^7$ Siemens/m
Core steel sass sensity	7650 kg/m^3
Core thickness	81 mm
Number of laminations	270
Core steel conductivity	Modelled as 0 in the FEM for 2D and 3D solid cores. The perfect electric insulator (PEI) boundary condition is applied for explicitly modelled very thin interposing laminations.

7.1.2 Core construction

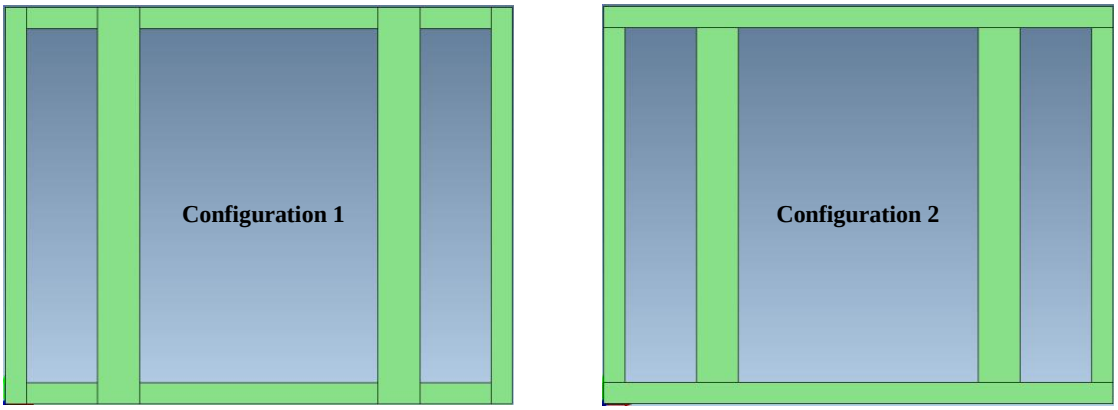

Figure 44: The two stacking patterns used for the 1p4L transformers

The actual 1p4L laboratory transformers had singular laminations stacked with non-step lap butt joints with alternating successive layers of two configurations, illustrated in Figure 44.

The transformer manufacturer used these butt joints because of the small dimensions of the limbs, and the yokes that could not be mitred by the large machines used for much bigger transformers. This configuration, with one lamination per configuration in stacking, called N=1 in literature, comes with the disadvantage of core material reduction at the joints due to air gaps resulting from joint dimension errors during the stacking process (Nakata & Kawase, 1986). Another by-product is that there are higher magnetizing currents than there are with mitred configurations, and the magnetic characteristics are very sensitive to the effect of the air gaps at the joints (Nakata *et al.*, 1982).

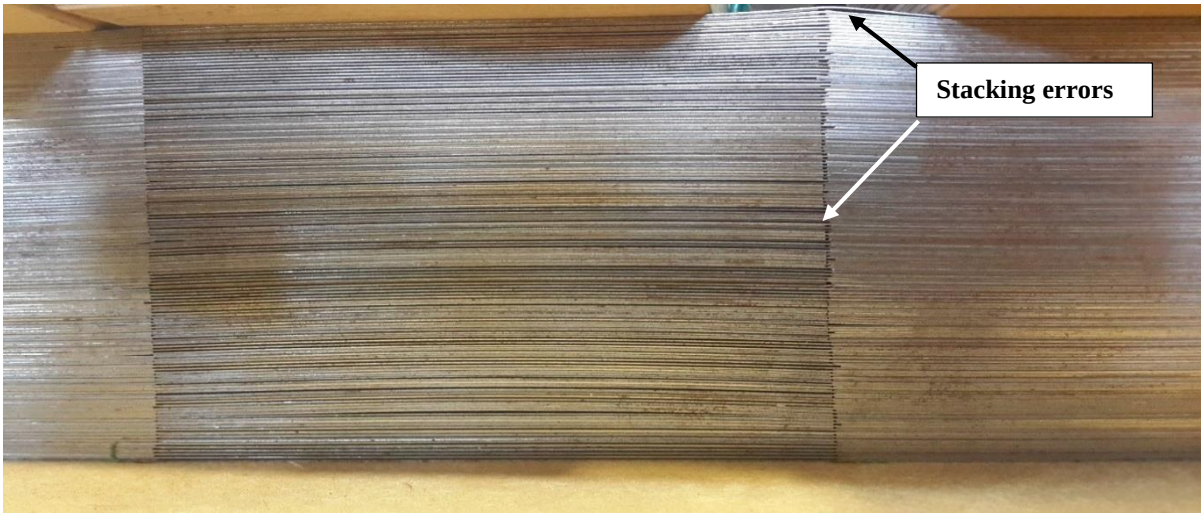

Figure 45: A T-joint of one laboratory 1p4L transformer (T2) showing small air gaps at the joints

7.2 FEM Modelling – 2D

Using the transformer parameters and the material properties, three separate 2D transformer simulation models were prepared. Model S had solid core joints, as is widely practiced in industry for quick 2D simulation. It is not possible to model explicitly in 2D the air gap detail due to stacking errors at the joints explained in the previous section. In an attempt to address this limitation, two other models incorporating 'equivalent air gaps' at the core joints were also considered, termed B1 and B2. The main difference between these two models is that model-B1 assumes that all the equivalent air gaps at the butt joints are equal, whereas model-B2 was calibrated according to variations in air gap sizes at the butt joints of a laboratory transformer T2 (chosen arbitrarily). A combination of uniform and adaptive meshing was applied to these models.

First, simulations were run with ac only at the inception of saturation i.e. knee point voltage (120 V RMS applied to the 80 turn windings). The measured flux distribution in the laboratory (from Figure 35) was compared with the flux distribution calculated by the FEM. The equivalent air gaps at the joints of the 2D models were determined iteratively, using a sensitivity analysis by altering the air gap size using scripting. Model B1 was tested first until a result corresponding to the measured no load current was reached. This equivalent air gap was 0.00875 mm. B2 differed from B1 in that the iterative

process was carried out until the FEM measurements of the leakage flux at each joint agreed as closely as possible with the search coil measurements in the laboratory on Transformer 2 (T2), and so the equivalent air gap varied around +/- 0.00875 mm.

After this, ac and dc were applied to models S, B1 and B2. Based on the experience gained from the laboratory measurements, three conditions were considered at the nominal applied voltage in linear (110 V RMS): 0 A dc – linear core operation, 1 A dc – partial core saturation, and 7 A dc – deep core saturation. Post-processing involved voltage and current RMS calculations, reactive power calculations, flux analysis, and search coil output voltage calculations.

7.3 FEM Modelling – 3D

A good understanding of the core joint detail considerations during ac excitation and simultaneous ac and dc excitation was achieved from the approximate 2D models. More detail was then added to the models by extending the analysis to 3D FEM, where the joint dimension error properties mentioned in 7.1.2 could be explicitly considered. It was necessary to determine the response of explicitly modelling each lamination or a reduced number of them close to the core surface to reduce the calculation time. Since the simulations are done in the transient domain which is computationally intensive, requiring long calculation times, reduction of the entire transformer by symmetry became essential. The possibility of reducing the full model to a 1/8 3D symmetry was tested and validated by adapting the approach to symmetry described and verified in section 5.1.6.

For the 1p4L 1/8 symmetric model the current density J_{sym} is the same as the one for the full model J. The symmetric circular sweep distance of the windings is

$$l_{sym} = \frac{l}{2} \tag{7.2}$$

and their cross-sectional area as a function the winding height is

$$A_{sym} = \frac{A}{2}. \tag{7.3}$$

The number of turns in the symmetric model is halved

$$N_{sym} = \frac{N}{2} \tag{7.4}$$

and now the resistances can be determined by substituting the symmetric parameters in Equation 5.5.

$$R_{sym} = \frac{\left(\frac{l}{2} \cdot \frac{N^2}{4}\right)}{s \cdot \frac{A}{2}} = \frac{R}{4}.$$

(7.5)

Applying Ohm's law, the symmetric applied voltage should be

$$V_{sym} = \frac{V}{4}.$$

(7.6)

and this is also verified by applying the symmetric parameters derived from Equations 7.3 - 7.5 back into Equation 5.4.

$$V_{sym} = \frac{\left(J \cdot \frac{N}{2} \cdot \frac{R}{4}\right)}{\frac{A}{2}} = \frac{JNR}{4A} = \frac{V}{4}.$$

(7.7)

The 3D symmetric model was then prepared. Figure 46 displays the application of symmetry showing the core, windings and search coil placement.

The reduced transformer parameters for this symmetric model, which differ from those in Table IX due to symmetry, are:

- 150 turn winding height – 175 mm
- 80 turn winding height – 140 mm
- Core thickness – 40.5 mm
- Number of laminations – 135

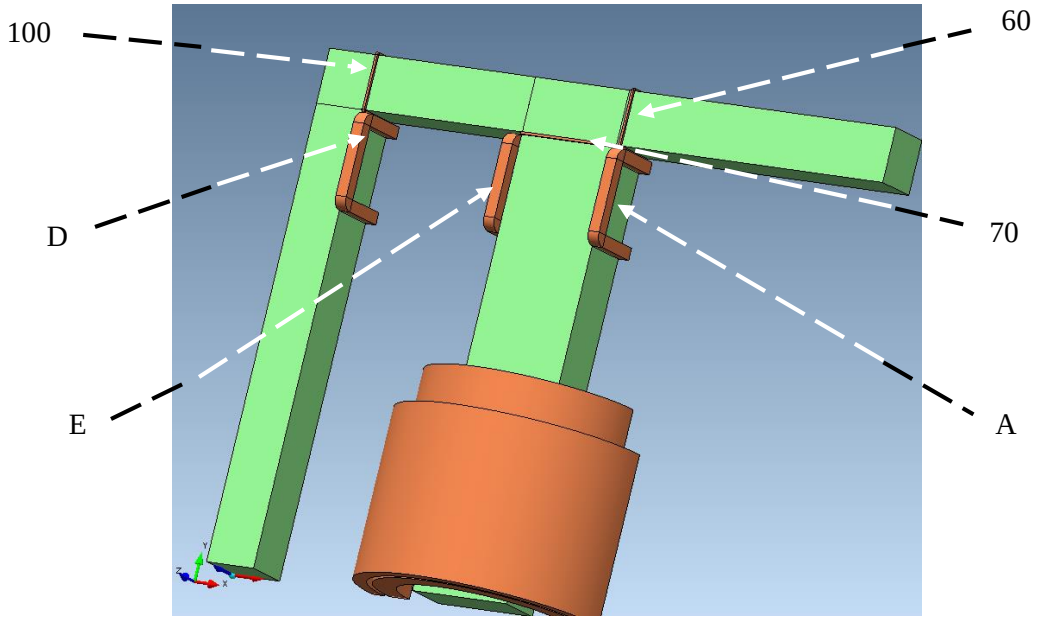

Figure 46: 1/8th symmetric 3D FEM model of 1p4L transformer with search coils wound on the limb at locations 60, 70, 100, and clamped against inside faces of the core at locations A, D and E to measure stray flux

Three types of boundary conditions were used on the 1/8th symmetric FEM models: 'Field Normal' at the bottom of the windings for the flux entering and exiting the model there, another 'Field Normal' on the right hand side of the model, and a 'Flux Tangential' boundary at the back of the model for the flux which is tangential to the surface of the core. A uniform mesh was used for the core and windings, with a less dense mesh in the general airspace. A dense isotropic mesh was given to some parts of the airspace in order to capture the leakage flux around the joints adequately. For the 3D models involving parts of the core with individually modelled laminations, an additional boundary condition called the 'Perfect Electric Insulator' (PEI) was applied. The PEI electrically insulated the laminations which are touching each other, thereby modelling the very thin interlaminar insulation in a real laminated core. Mathematically, the PEI enforced the condition $\boldsymbol{J} \cdot \boldsymbol{n} = 0$ when applied to a lamination surface.

Four cases defined in Table X were to be investigated:

Table X: 1/8 3D symmetric models to be investigated

3D-0	3D-1	3D-2	3D-3
Core with all laminations modelled explicitly	Solid core parts with equivalent air gaps at the joints	20 laminations modelled on the surface of the core – rest of the core solid with equivalent air gaps at the joints	50 laminations modelled on the surface of the core – rest of the core solid with equivalent air gaps at the joints

Simulations were then performed to investigate the response for:

- nominal voltage excitation and resulting magnetising current and core loss
- search coil outputs at the inception of core saturation with ac only
- simultaneous ac-dc excitation calculations for search coil outputs and reactive power
- flux analysis with ac only, and with both ac and dc.

For the symmetric models, care was taken to reduce the voltage and current excitations accordingly and recalculations were performed post-process to revert to the full model solution.

7.4 FEM saturation inductance

This part of the study reports attempted to identify the extent to which the measured $L_{terminal}$ (*vide supra* section 6.3) was consistent with L_{air} measurements of the windings and simulation in FEM. In this thesis, the term "saturation inductance" L_{sat} is used to refer to either $L_{terminal}$ or L_{air}, unless or otherwise specified. Several FEM analyses were performed using 3D FEM models. From the FEM solution, L_{sat} is determined from the magnetic stored energy *W* when a current *i* is flowing in the windings, and is expressed by the following relationship:

$$L_{sat} = \frac{2W}{i^2}.$$

(7.8)

W is the integral over the whole volume of the problem of magnetic energy density derived from Poynting's theorem given in Equation 2.1 (section 2.2), which can now be expressed as

$$W = \int_V w\, dV$$

(7.9)

where *w* is the corresponding magnetic energy volume density from Equation 2.1 relating to the area under B-H curve (MIT Press, 1944; Cheng, 1989). When the magnetic flux density is B_1 the magnetic energy volume is given by

$$w = \int_{B_0}^{B_1} H(B) \cdot dB$$

(8.0)

where *H(B)* is the magnetic field intensity corresponding to a given *B* for non-linear materials.

7.4.1 Air core inductance

The FEM geometry for the windings was based on the actual "air core" transformer in Figure 40. Because excluding the core avoided long calculations of the non-linearities and core joint details, the problem became linear and could be solved in the magnetostatic domain with dc only. Solving for the stored magnetic energy W in the presence of a current using only dc meant that a dense enough mesh could be used without overly lengthening the simulation time. Figure 47 shows the winding assembly modelled in the FEM. Excitations were made on the LV and HV windings separately, with the other side open circuited. For each pair of windings (which were connected in parallel with opposing polarity in the actual laboratory transformers), a dc current of $0.5x$ A injected into Winding Assembly A, and a reverse dc current of $-0.5x$ A was simultaneously injected in the Winding Assembly B to support the flux direction shown in Figure 30. This means that if $x = 1$, then the total current flowing in the windings for substitution into Equation 7.8 is 1 A. Since there was no core, the linear problem meant that the calculated L_{air} was independent of the magnitude of the current. This approach was also repeated with ac in a Time-harmonic problem to check for consistency in the global solutions.

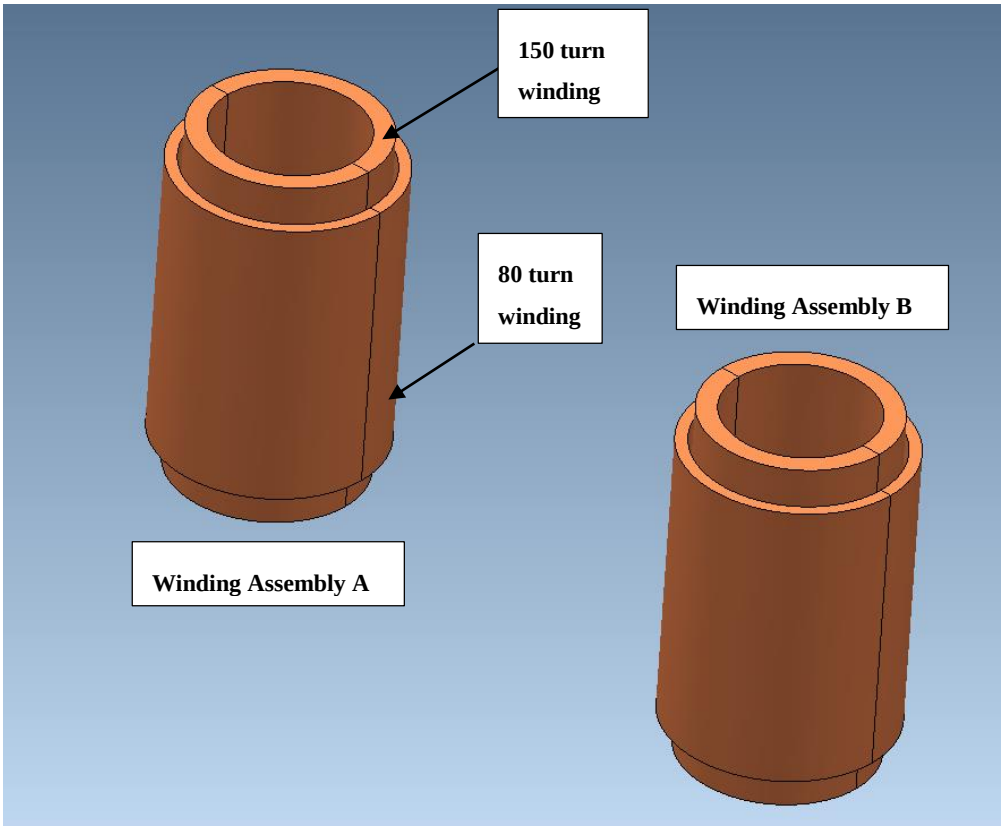

Figure 47: Core-less windings modelled as stranded cylinders

To confirm the linearity of an "air core", different values of dc were used that yielded different magnitudes of w but still maintained the same L_{air}. A coarse mesh with a maximum edge extent of 350 mm (10% of the tallest winding height) was first applied and then halved successively until convergence (no further improvement in accuracy with denser meshes) was reached with a mesh edge length of 50 mm in the surrounding air and windings. The flux distribution around the windings was

also analysed to ensure the correct flow, and then the final solutions for L_{air} were recorded. The effect of mutual inductance L_m between the 80 turn and 150 turn windings was then checked by removing each pair of windings from the entire geometry while the remaining pair was energized, the L_{air} calculated, and then the simulation repeated for the other pair.

7.4.2 Terminal saturation inductance

This part of the simulation protocol simulated the laboratory tests performed in 6.3.1. The winding excitations were performed using a field-circuit coupled approach with an external circuit adapted from the schematic in Figure 39. Unlike the laboratory prodcedure in Chapter 6 which relied on the dominant saturating harmonics to determine a final value for $L_{terminal}$, post-processing of the global quantities in multiple FEM solutions measured the change of $L_{terminal}$ with current It had been observed from the preliminary FEM protocol in Chapter 5 (sub-section 5.1.2.1) that simulations with very high dc solved much more quickly than those with low dc. However, because the core with the necessary joint detail implemented in 7.3 required longer calculations, one-eighth symmetry had to be used to shorten simulation time (this was necessary for multiple runs of parametric analyses) and maintain accuracy.

Initially, there was a concern that one-eighth symmetry could not be applied because the mutual coupling between winding assemblies A and B had to be considered, and so both might need to be modelled further increasing the time to compile in a 3D calculation. A preliminary 2D flux analysis was, therefore, done to verify the applicability of one one-eighth symmetry before the 3D symmetric model could be investigated.

7.4.2.1 Verification of symmetry for terminal saturation inductance

The actual values of the computed inductances were not important here, because it was known that the 2D calculation is more of a qualitative analysis as a proof-of-concept of the expected distribution. However, it was important to verify that the symmetric models yielded the same results as the full model after symmetry correction.

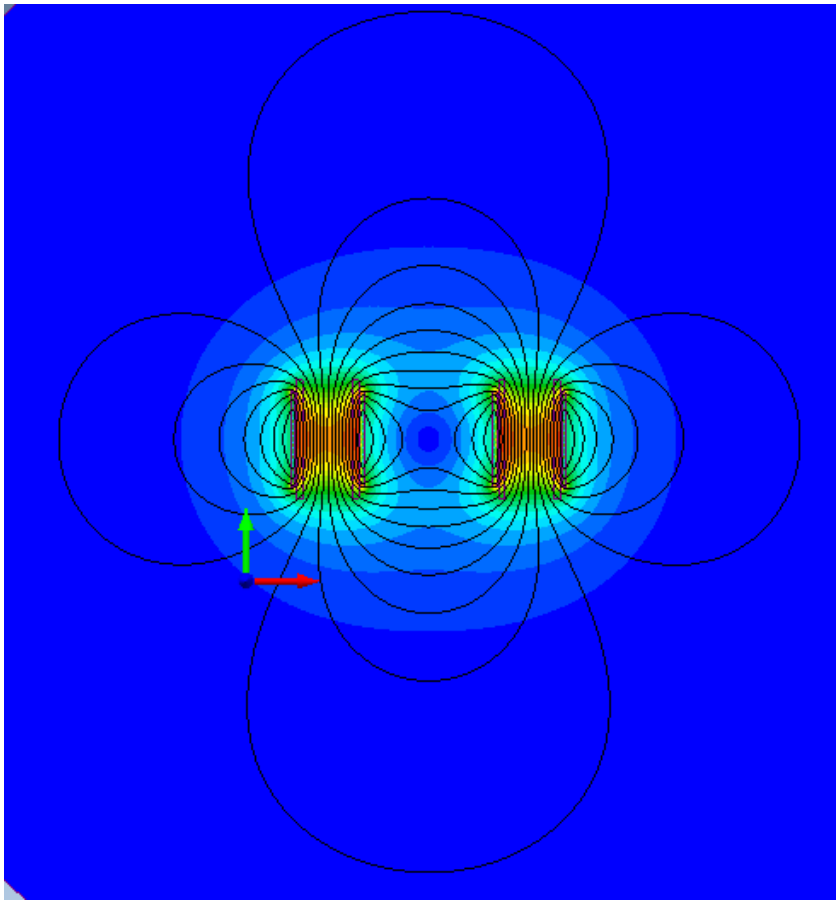

Figure 48: Flux distribution of full model

Figure 48 shows the 2D flux distribution with a total line current of 1 A split between the two windings, consistent with what was expected. Figure 49 is the 2D ½ symmetry showing how the flux is handled by the cutting plane of symmetry.

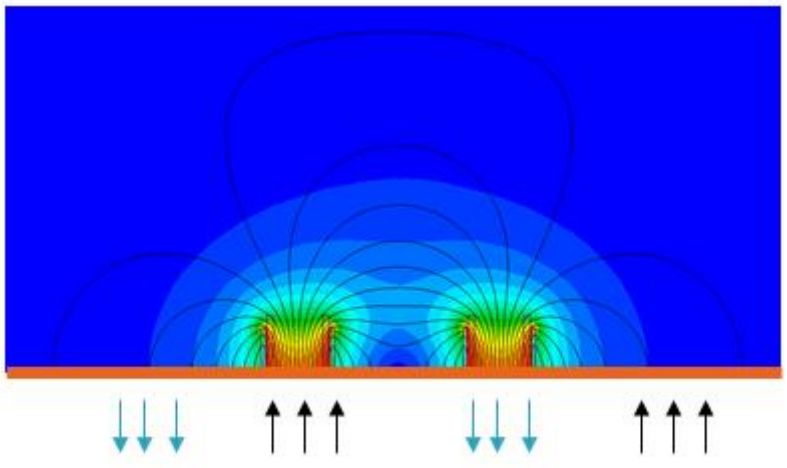

Figure 49: Flux distribution of ½ symmetry model showing leaving and re-entering the model orthogonal to the cutting plane of symmetry

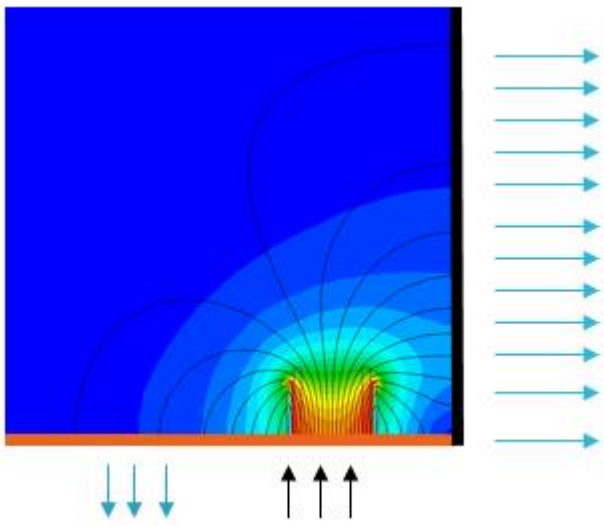

Figure 50: Flux distribution of ¼ symmetry model showing moving in and out of the model orthogonal to the cutting plane of symmetry at the bottom and leaving the model orthogonal to the cutting plane of symmetry on the right-hand side

Figure 50 showing ¼ symmetry is maximum reduction possible for the 2D model which is equivalent to the 3D 1/8 model. Having gained confidence that it was possible and fairly accurate to reduce the full model all the way down to 1/8 symmetry in the FEM domain for the terminal saturation inductance simulation, the next step was to model the 3D symmetric model.

7.4.2.1 Symmetric 3D terminal saturation inductance modelling

Model 3D-2 from Table X was used to investigate the response for $L_{terminal}$ for comparison with measurements. Replicating the laboratory approach, which uses saturating harmonics from a rectified input to achieve deep saturation was not possible in the FEM. Instead, to simulate the small ripple at the output of the rectifier in the laboratory procedure, a voltage excitation of about a quarter of the nominal voltage was applied in series with varying levels of very high dc (compared to the actual dc components used in the physical tests). This field-circuit coupled FEM approach achieved a comparable level of saturation as the measurements at $L_{terminal}$. The external circuit that was employed shown in Figure 51.

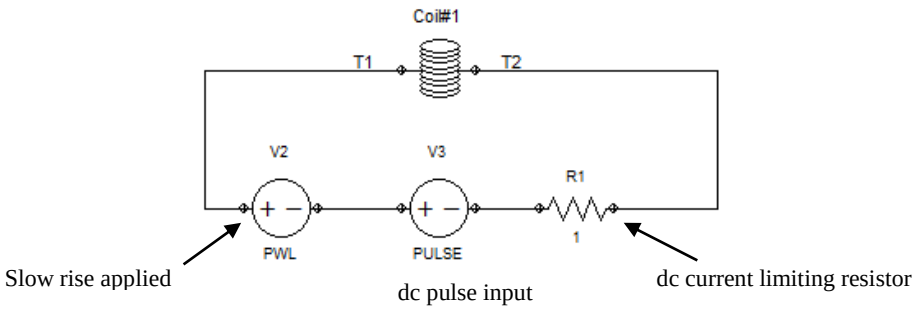

Figure 51: External circuit controlling the excitations on the test winding (with the other winding open circuited)

The method for achieving a value for the inductance L is given in the flow diagram in Figure 52.

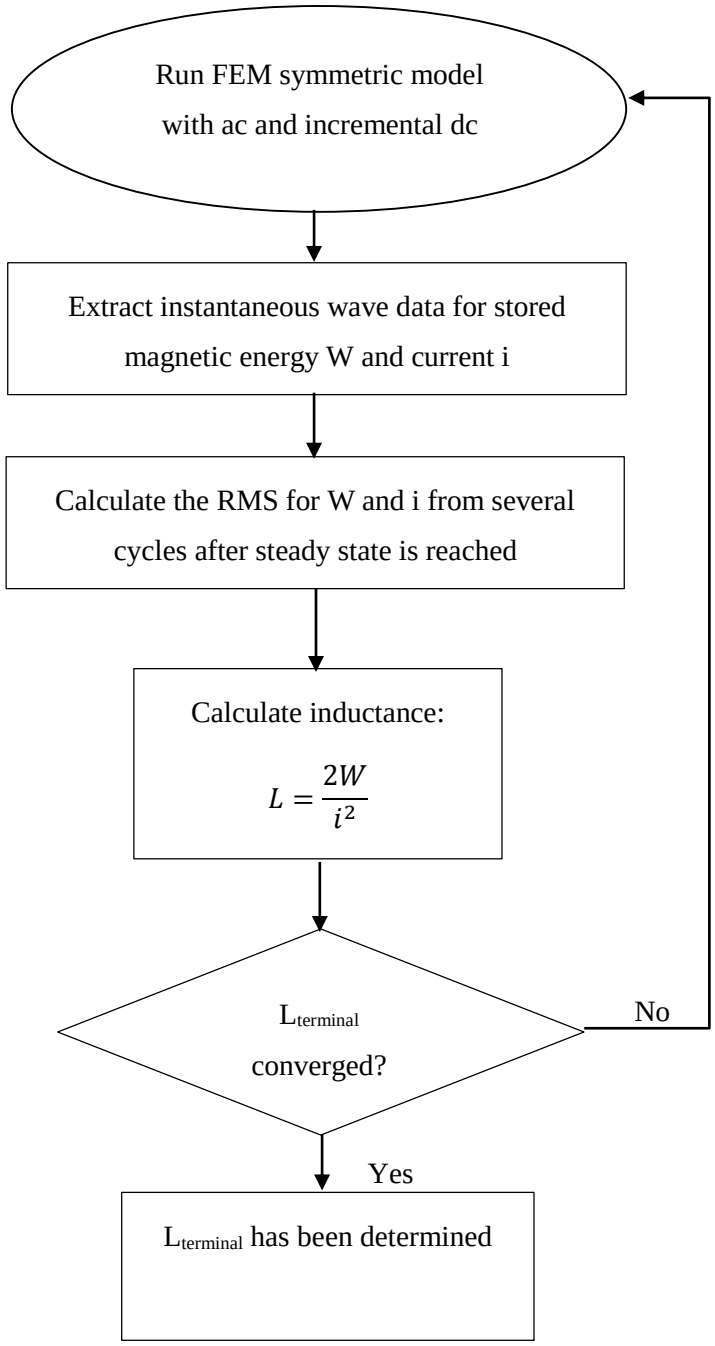

Figure 52: Method for determining $L_{terminal}$

The simulation started off with a relatively low value of dc in the presence of an ac excitation of 60 V RMS. Under the same ac excitation, the level of dc was increased for each simulation until the value of L became comparable with the laboratory measured saturation inductance (also indicating a comparable level of deep saturation).

Further simulations in a parametric analysis were done to test the effect of different parameters involving the tests outlined below:

- Swopping position of the windings to see the effect of differences in the diameters with $L_{terminal}$. See Appendix D.4 depicting the difference.
- Using a small ac excitation (5 V) to simulate a small ripple and investigate the effect on $L_{terminal}$
- Removing a winding from the model (e.g. the 80 turn winding) and leaving the other winding in the model (the 150 turn winding), and vice versa to investigate the effect of mutual inductance L_m between the primary and secondary winding assemblies.

7.5 Summary

This chapter has presented the requirements for the FEM modelling of the 1p4L transformers by first discussing the parameterization and creation of the geometries. The 3Dmodelling of the applied mirror symmetry to reduce simulation time while maintaining accuracy was also given in detail. The simultaneous ac and dc simulation protocol was then developed based on the laboratory measurement protocols. Finally, the FEM protocol to investigate $L_{terminal}$ and L_{air} was derived.

The next chapter presents and contrasts the results from the measurement and simulation protocols in Chapters 6 and 7.

8 MEASURED AND SIMULATED RESULTS

The 1p4L acceptance tests were performed separately from the main laboratory protocol for simultaneous ac-dc and the results were presented in 6.1.1. Therefore, they will not be discussed in this chapter. The main purpose of this chapter is to discuss the measured and simulated results. Close attention is given to the process which led to an improved FEM simulation that was developed using a rigorous experimental protocol.

8.1 Measured ac excitation only and 2D FEM

This section presents measured results with ac excitation only. The magnetization curves of the three 1p4L test transformers are discussed pointing out the key parameters needed for later parts of the procedure. The O.C. and S.C. test results are then presented at a chosen nominal voltage. This is then followed by the laboratory measured search coil outputs used to determine the flux distribution. Some 2 D FEM analyses are then given and compared with the measurement data.

8.1.1 Measured magnetization characteristics

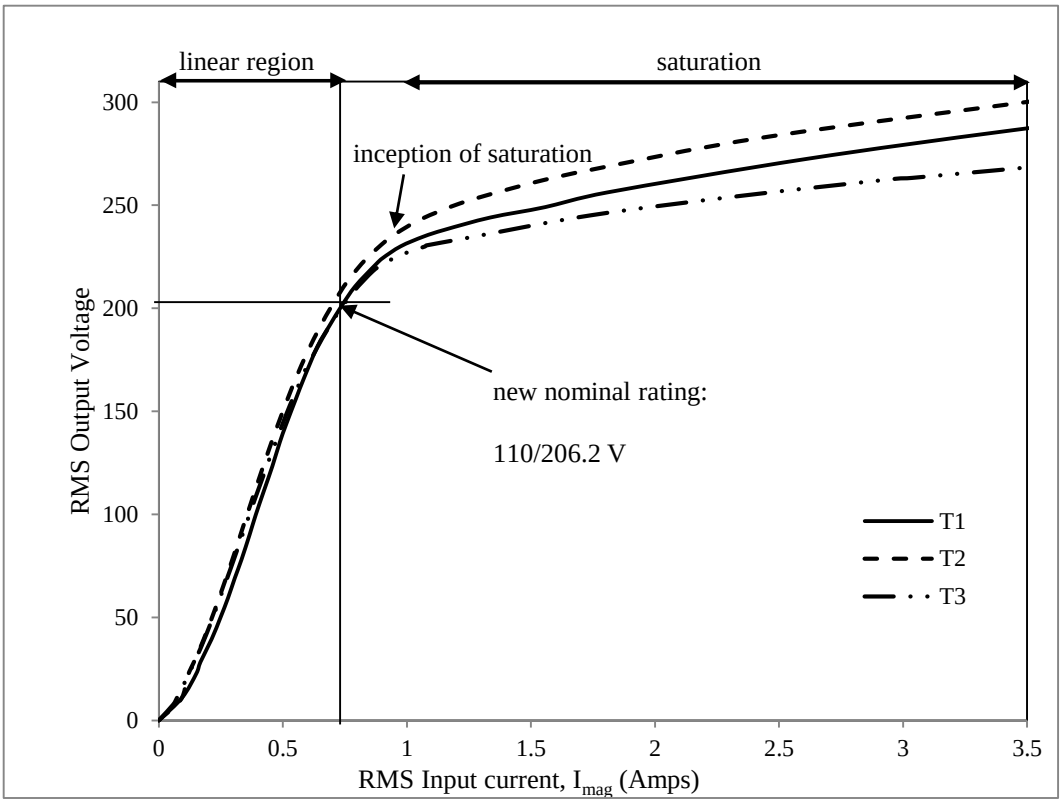

Figure 53: Magnetization curves of the 1p4L test transformers with the 80 turn winding energized

The nameplate ratings of the transformers are 209/390 V, 8.3 kVA, and it is clear from Figure 53 that these voltages represented deep saturation outside of the bounds of the linear regions of the magnetization (v-i) curves. The behaviour of each transformer differed slightly in the saturation region with T3 reaching saturation first, followed by T1, and T2 reached saturation at a slightly higher excitation. Their behaviour in the linear region was fairly consistent, and so it was decided to de-rate

the nameplate voltage ratings to a new nominal value of 110/206.2 V (the capacity was also reduced, to 2.2 kVA resulting in full load currents of 20/10.7 A). This adaption ensured that under normal ac excitation the transformers operated in the linear region without any distortion, making it possible to analyse the distortion which arose from simultaneous ac-dc excitation in later tests. In contrast to real power transformers whose nameplate ratings typically operate a flux density of 1.7 T, the derated 1p4L's had to energized at nominal flux density lower than this to avoid the early saturation caused by the but joints.

Further ac tests involved energizing the secondary 150 turn windings and recording the v-i data. This was done to demonstrate consistent performance of the transformer design. The shapes of the v-i characteristics were found to be consistent on a per unit basis, as expected (see Figure 54).

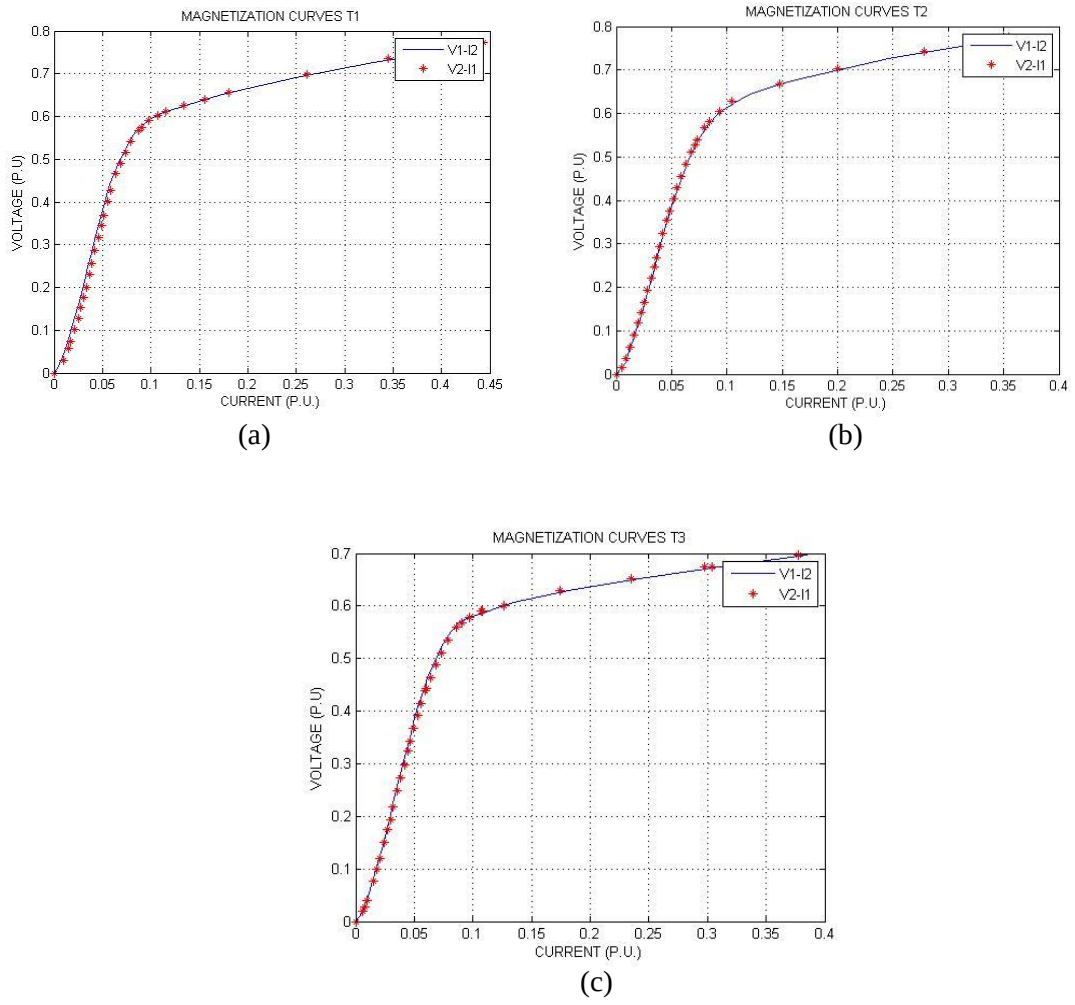

Figure 54: Per unit graphs of T1 (a), T2 (b) and T3 (c) showing reversibility of applied voltage on a base of the design nameplate ratings. V1and I1 are on the primary sides, and V2 and I2 are on the secondary sides

8.1.2 O.C. and S.C tests

Table XI and

Table XII present the results of the open circuit tests performed using the methods used in the literature (Sen, 1997), but at the new nominal voltages.

Table XI: Open circuit test results for all three test transformers energized separately from both sides

Energizing from 150t windings (206.2 V)						
Tut. No.	**Applied voltage (V RMS)**	**Line current (A RMS)**	**Power (Watts)**	**Reactive power (var)**	**R_m (Ω)**	**L_m (H)**
T1@ $T_{ambient}$ = 29,5^{0}C.	206.4	0.398	60,6	55.4	702,7	2.449
T2@ $T_{ambient}$ = 29,5^{0}C.	206.2	0.376	58,0	51.6	733,6	2,619
T3@ $T_{ambient}$ = 29,5^{0}C.	206.2	0.399	60.4	55.8	704,5	2,425
Energizing from 80t windings (110 V)						
Tut. No.	**Applied voltage (V)**	**Line current (A)**	**Power (Watts)**	**Reactive power (var)**	**R_m (Ω)**	**L_m (H)**
T1@ $T_{ambient}$ = 29,2^{0}C.	110.0	0.729	59.6	53.7	203.0	0,7166
T2@ $T_{ambient}$ = 26^{0}C.	110.0	0.709	58.2	52.0	208.2	0,7406
T3@ $T_{ambient}$ = 29,5^{0}C.	110.0	0.747	60.2	55.9	200.9	0,6891

Table XII: Short test results for all three test transformers energized separately from both sides

Energizing from 150t windins (206.2 V RMS)						
Tut. No.	**Applied voltage (V RMS)**	**Line current (A RMS)**	**Power (Watts)**	**Reactive power (var)**	**R_m (Ω)**	**L_m (H)**
T1@ $T_{ambient}$ = 29,5^{0}C.	1.87	20.01	34.2	15.8	0.085	0.126
T2@ $T_{ambient}$ = 29,5^{0}C.	1.85	19.92	33.0	16.0	0.083	0.128
T3@ $T_{ambient}$ = 29,5^{0}C.	1.88	20.21	34.5	16.1	0.084	0.125
Energizing from 80t windings (110 V RMS)						
Tut. No.	**Applied voltage (V)**	**Line current (A)**	**Power (Watts)**	**Reactive power (var)**	**R_m (Ω)**	**L_m (H)**
T1@ $T_{ambient}$ = 29,2^{0}C.	3.53	10.6	34.2	15.3	0.304	0.434
T2@ $T_{ambient}$ = 26^{0}C.	3.54	10.7	34.4	15.9	0.300	0.442
T3@ $T_{ambient}$ = 29,5^{0}C.	3.39	10.1	31.0	13.9	0.310	0.442

The R and L elements from these tests were not necessary for direct input into the FEM as they can be inherently calculated or derived from global quantities in the solutions. The results here are more useful in topologically derived models as inputs into EMT software. These O.C and S.C. parameters were used in the PSCAD proof-of-concept protocol described in 6.3.1 to test the proposed saturation inductance circuit.

8.1.3 Search coil outputs and flux distribution

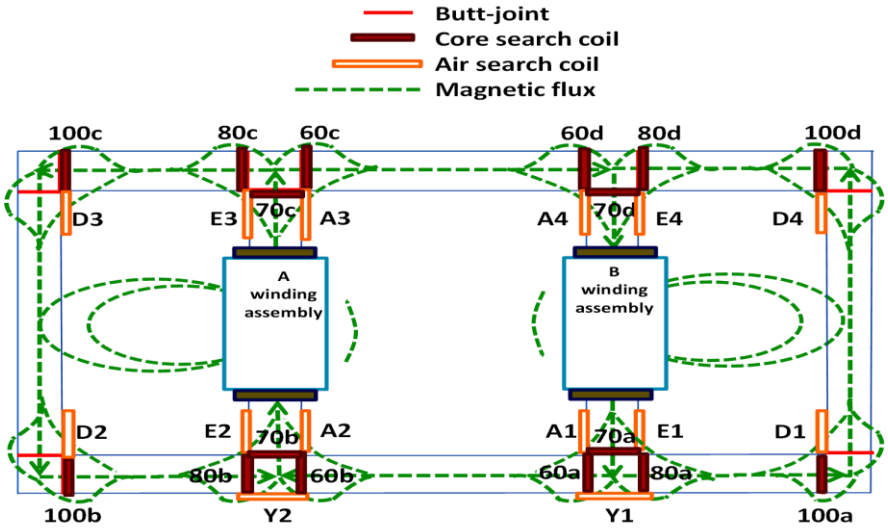

Figure 55: The placement of search coils on 1p4L test transformers and leakage flux derived from the laboratory experiments

Figure 55 shows the placement of search coils and derived leakage flux on the 1p4L test transformers. SCs 70 (a-d) detected the amount of flux in the main (wound) limbs. SCs 60 (a-d), 80 (a-d) and 100 (a-d) indicated the partitioning of the flux between the inner (main) yokes and return yokes and limbs. SCs A (1-4) and E (1-4) detected the magnitude and patterns of any leakage flux in the inner windows of the transformer's T-joints and SCs D (1-4) measured leakage flux at the 90° joints. SCs Y1 and Y2 were expected to be the same, as observed in a preliminary FEM analysis, but in reality their output voltages differed by a very small margin.

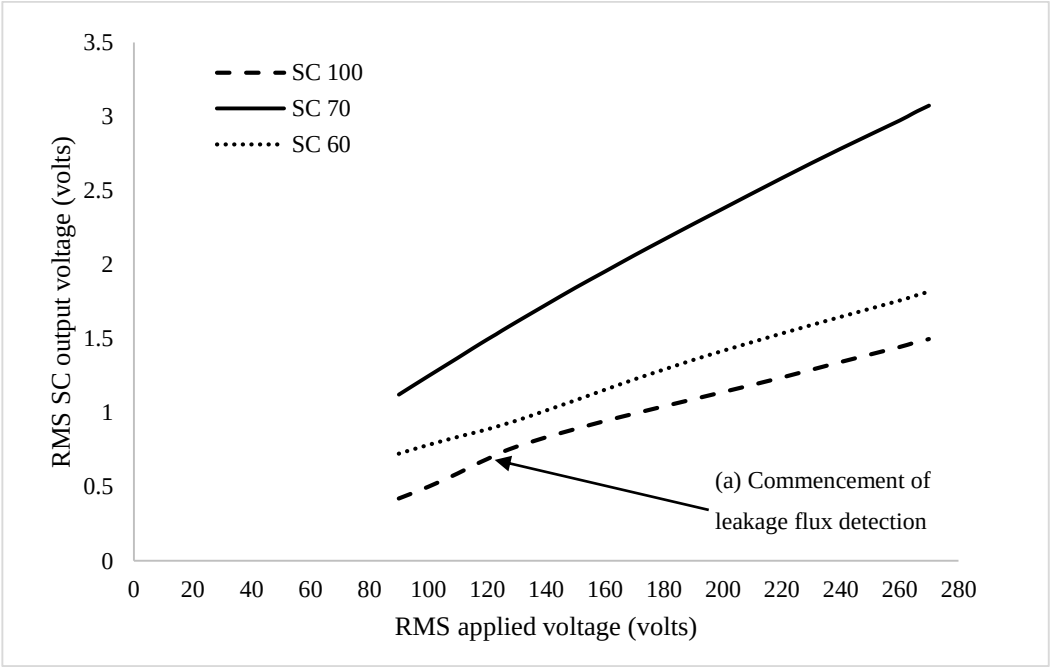

Figure 56: Measured SC outputs with increasing applied voltage at the T-joints (60 and 70) and 90° joint (100)

All three test transformers were subjected to the same protocol, and they yielded similar (but not exact) results. Only one of the test transformers, T3, will be considered in this section. Figure 56 provides some measurement data which were necessary to derive the flux distributions in Figure 55. The test transformer was energized from its primary 80 turn windings while the secondary 150 turn side was open circuited. Leakage flux was first detected by the air search coils at point (a) in Figure 56 where saturation occurring at the joints caused the flux to seek alternative paths back to the core through the air. This level of excitation was designated as 120/225 V, and this was tested against McLyman's formula (McLyman, 2004) which states that (for a single-phase transformer with only self-inductance) when the peak current exceeds twice the mean current then saturation has commenced. Table XIII shows the calculations for T3 where V_{sat} is the voltage at which the transformer starts to saturate, V_{in} is the applied voltage, I_{peak} is the peak current and I_{mean} is the average current taken in one half-cycle. The air search coils A, E, D, Y1, and Y2 were used in conjunction with the readings from Figure 56 to trace the leakage flux patterns shown in Figure 55.

Table XIII: Verification of commencement of saturation using McLyman's formula

McLyman formula test for V_{sat}				
V_{in}	**I_{peak}**	**I_{mean}**	**2 * I_{mean}**	**Saturated?**
115.65	1.4282	0.8095	1.619	**No**
117.76	1.5794	0.8446	1.6892	**No**
119.65	1.6932	0.8833	1.7666	**No**
120.06	1.7165	0.8916	1.7832	**No**
120.17	1.7811	0.8996	1.7992	**No**
120.24	1.8199	0.9079	1.8158	**Yes**
120.556	1.826	0.9075	1.815	**Yes**

The FEM was explored in 2D to test the accuracy of the determination of no-load currents, core loss and voltage transformation under ac excitation only. The flux distributions, too, were analysed. Table XIV shows that the laboratory test transformers do not give exactly the same results at the same level of applied voltage, this discrepancy is due to small errors in the manufacturing process. The FEM model S which assumes solid joints significantly under-estimates the no load magnetizing currents (I_{mag}'s) as was initially observed in the preliminary FEM analyses with models that also assume solid joints, as reported in Chapter 4. The two FEM models which incorporate equivalent air gaps at the joints, models B1 and B2, show a significant improvement in correlation with the measured I_{mag}'s. The FEM core loss calculation closely matches the measured values and appears to be independent of the core joint detail.

Table XIV: ac only open circuit parameters at applied voltage of 120 V on the primary 80 turn windings

Description	Abbreviation	RMS I_{mag} [A]	Core Loss [W]	RMS V_{out} [V]
Test transformer 1	T1	0.902	74	224
Test transformer 2	T2	0.836	70	224
Test transformer 3	T3	0.968	76	225
FEM solid jointed Model S	Model S	0.334	75.8	225
FEM uniform equivalent air-gapped Model B1	Model B1	0.909	76	225
FEM with equivalent air gaps calibrated to T2 Model B2	Model B2	0.891	76	225

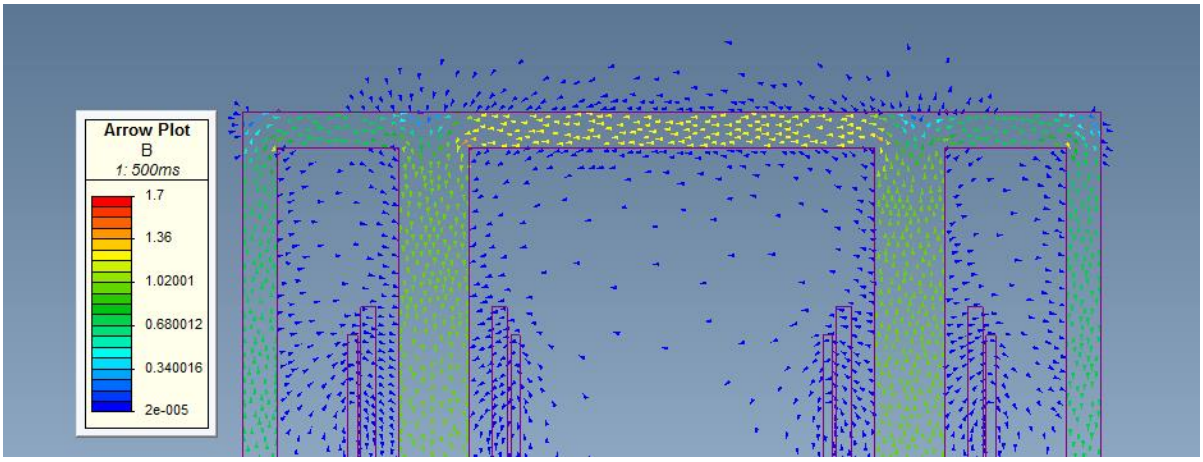

Figure 57: FEM simulation of the flux distribution at the inception of saturation for Model S

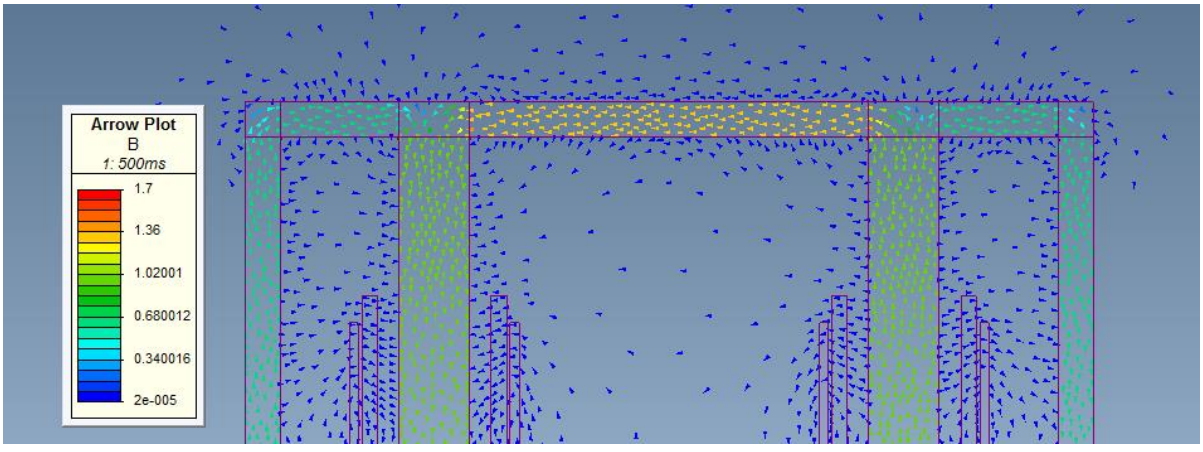

Figure 58: FEM simulation of the flux distribution at the inception of saturation for Model B1

Figure 57 shows the flux patterns of the 2D modelling (energized at 120 V, open circuit) of the transformer with joints simplified as solid, Model S, while Figure 58 shows the transformer with "equivalent air gaps" at the joints, Model B1. Comparing the two FEM plots indicates that the solid joints produce significantly less flux outside the transformer at the joints than when "equivalent air gaps" are introduced. The distribution of extra leakage flux driven outside the core in Model B1 (Figure 58) is consistent with the measurements carried out on the physical transformers in Figure 55.

Table XV presents some search coil data with ac only, at the commencement of core joint saturation (the point where some leakage flux was first detected by the air search coils). The measured SC outputs are taken as averages i.e. measured SC 70 represents the average of SC 70a – SC 70d, SC A is the average of SC A1 – SCA4, and so on The most important results in this table are those for Model S, where the zero value outputs for air SCs A, E and D mean that there is no leakage flux detected. A clear difference is seen from the air search coil response of Model B1 and Model B2 showing comparable leakage fluxes against the measured data for T1, T2 and T3.

Table XV: Table showing RMS SC coil output voltages at applied V_{knee} (120 V RMS) for the laboratory transformers and 2D FEM models

Transformer	70	60	80	100	A	E	D
T1	1.493	0.906	0.662	0.662	0.016	0	0
T2	1.498	0.914	0.642	0.642	0.014	0	0
T3	1.495	1.039	0.890	0.668	0.018	0.011	0
Model S	1.466	0.955	0.515	0.515	0	0	0
Model B1	1.460	1.039	0.424	0.424	0.011	0.007	0.006
Model B2	1.460	1.004	0.458	0.458	0.011	0.007	0.006

8.2 Measured ac excitation only and 3D FEM

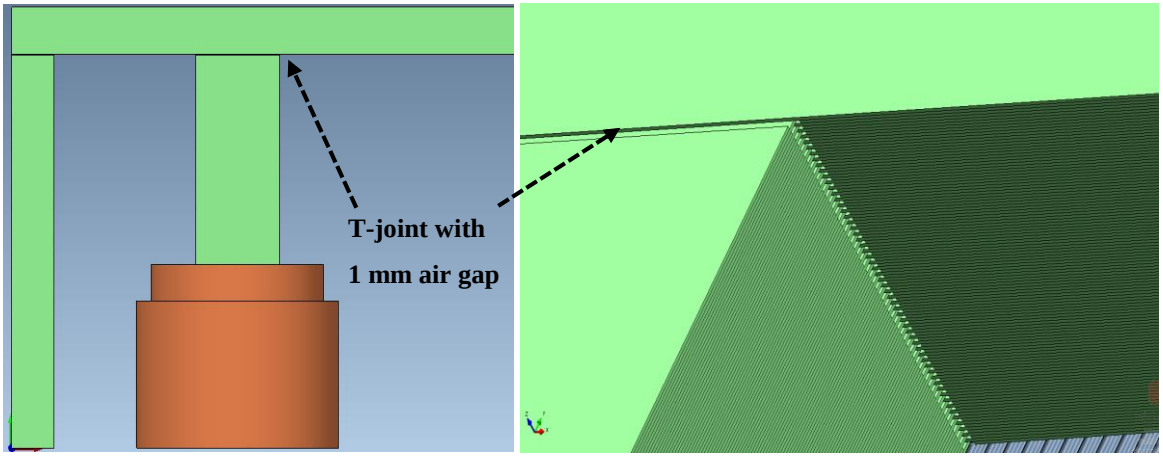

Figure 59: One quarter of 3D model (left). Close up view of the lamination stacking at the inner window's T-joint (right)

To test the limits of the FEM at first, all the laminations were explicitly modelled using the alternating lamination layouts described in section 7.1.2 (see Figure 44 and Figure 45). A 1 mm air gap was assumed at the T-joints and 90° joints based on visual examination of the transformers, confirmation

from partners in the transformer manufacturing industry, and also according to the literature (Nakata & Kawase, 1986). A Visual Basic® (VB) script was used to stack the individual laminations repetitively, alternating between Configuration 1 and Configuration 2 from Figure 44. Some ac only simulations were run, but solutions were never reached because of the complexity of the enormous mesh elements generated and a failure to converge for the 3D problem. This is similar to encounters reported in other studies which have unsuccessfully attempted to mesh individual laminations (Hihat *et al*., 2011). This model was called 3D-0 (see Table X: *1/8 3D symmetric models to be investigated*) and it had all the laminations explicitly modelled, with the incorporation of the Perfect Insulator Boundary (PEI) boundary conditions between laminations, to resemble the actual laboratory test transformers.

After much consideration, it was decided to make some parts of the 3D model's core solid and other parts deliberately laminated at the core surface. This approach resulted in models which arrived at solutions during the ac only testing phase and gave the desired results. Laboratory transformer T2 was chosen for comparison and with simulations. See Table XVI. Model 3D-1 is the model with "equivalent air gaps" at the joints calibrated according to T2 using a solid core, model 3D-2 is the model with 20 laminations (15% of the core thickness) modelled on the core surface with the rest of the core being solid with "equivalent air gaps" at the joints, and model 3D-3 is the model with 50 laminations (37% of the core) with the rest of the core solid with "equivalent air gaps" at the joints.

Table XVI: Simulated I_{mag} and core loss for 3D models defined in Table X compared with actual measurement

	T2	**3D-1**	**3D-2**	**3D-3**
I_{mag}	0.836 A	0.840 A	0.829 A	0.771 A
Difference % against measured I_{mag}	-	0.48%	-0.84%	7.78%
Core loss	70	74	72	65
Difference % against measured core loss	-	-5.7%	-2.8%	7.14%

The results show that there is close agreement between the measured results and those of the simulated I_{mag} and core loss for all the 3D models. A sensitivity analysis was done by increasing the number of laminations close to the core surface and comparing against measurement data. It was found that explicitly modelling more than 20 laminations (model 3D-2) decreased the accuracy of the model (see the results of model 3D-3 with 50 laminations Table XVI). To achieve the response closest to the actual transformer with a good level of accuracy, model 3D-2 was chosen for the rest of ac-dc tests. Even though model 3D-1 has a slightly closer I_{mag} to the one in T2, 3D-2 with explicitly modelled laminations at the core surface was preferred not only because it had a better core loss prediction, but also series of analyses revealed that resultant flux lines matched measured ones better. (See also the differences between models 3D-1 and 3D-2 given in Appendix D: Figures D.3 and D.4, respectively clearly showing that 3D-2 has a more detailed flux distribution at the joints and core surfaces.) Figure 60 shows the simulated flux lines on the core surface at an instant in time when this model was over-excited with

ac at open circuit, and they are in good agreement with the measured flux distributions presented earlier in this chapter. (Flux lines generated at different instances in time on different core surface parts also match the measured flux patterns.) The 3D vector plots corresponding to Figure 60 can be found Appendix D: Figure D.6.

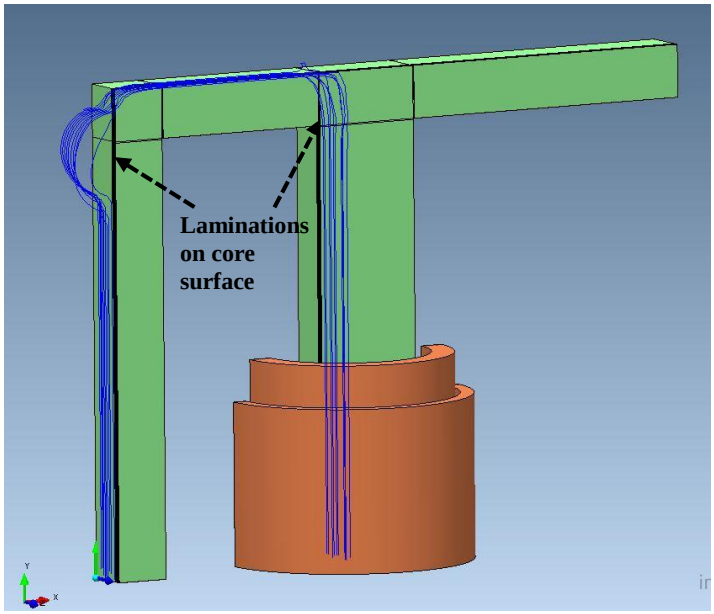

Figure 60: Core surface simulated flux lines with model 3D-2 energized at 120 V RMS at open circuit

8.3 Simultaneous ac-dc excitation

This section presents several measurement data and some comparisons with simulation. Single turn search coil outputs, harmonics and reactive power are presented first. This is followed by an air search coil analysis. Finally, the results for the saturation inductance are discussed. The test transformer used for comparison with the simulation is the arbitrarily selected T2.

8.3.1 SC outputs and electrical parameters

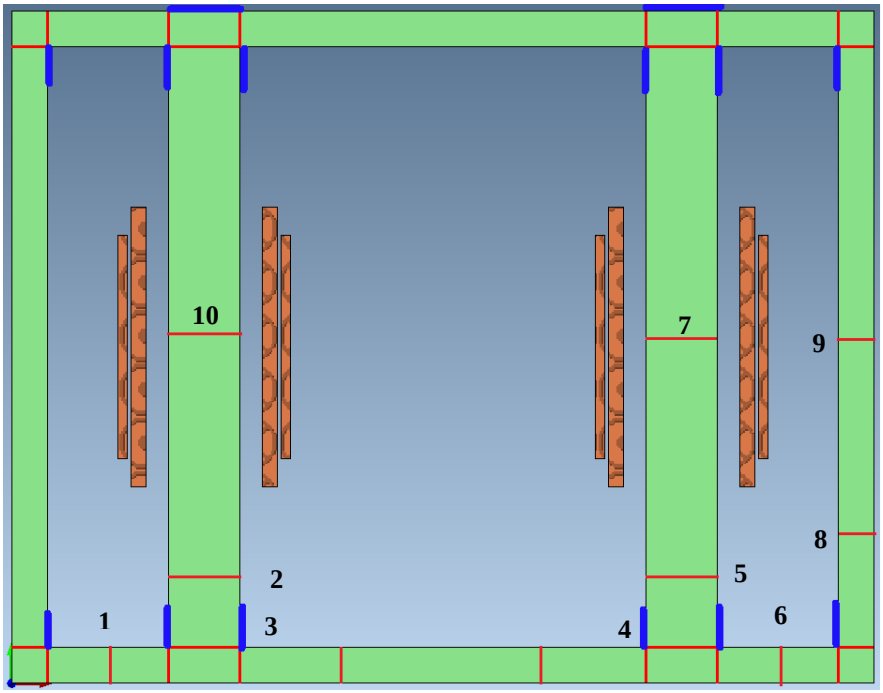

Figure 61: Placement of search coils of interest labelled (1 - 10) wound around laboratory test transformer T2

Figure 61 shows FEM equivalent of the placement of single turn search coils (red) tightly wound around the core and the 20 turn search coils (blue) placed against the joints. At 110 V RMS, the dc was injected incrementally and various responses were recorded.

8.3.1.1 SC outputs

Figure 62 is a presentation of the measured corresponding SC output voltages with increasing dc. Only results from the right-hand side of Figure 61 are presented due to assumed symmetry. It can be seen from SC7 that the part of the core at the midpoint of the windings sees the greatest flux density, which is constant with increasing dc up to 7 A. As the dc is increased with small steps up to 1 A, the flux tends to flow through the interconnecting (main) yokes, with comparably less flux flowing in the outer yokes and return limbs, until the first points of saturation are reached at the T-joints. This can be seen from SC4's curve at 1 A dc. Beyond 1 A, SC5 shows that there is deep saturation at the T-joint, because the flux starts to flow along other air paths on its way back to the core. This increases the flux in the outer yokes and the return limbs (SC6 and 8). The flux in the side limbs (SC9) is slightly higher than the flux in the outer yokes because of magnetic coupling with stray flux from the windings.

The response of model-B2 with 1 and 7 A dc and is shown in Figure 63 and Figure 64, in order to analyse how closely the FEM matched the SC measured data in Figure 62.

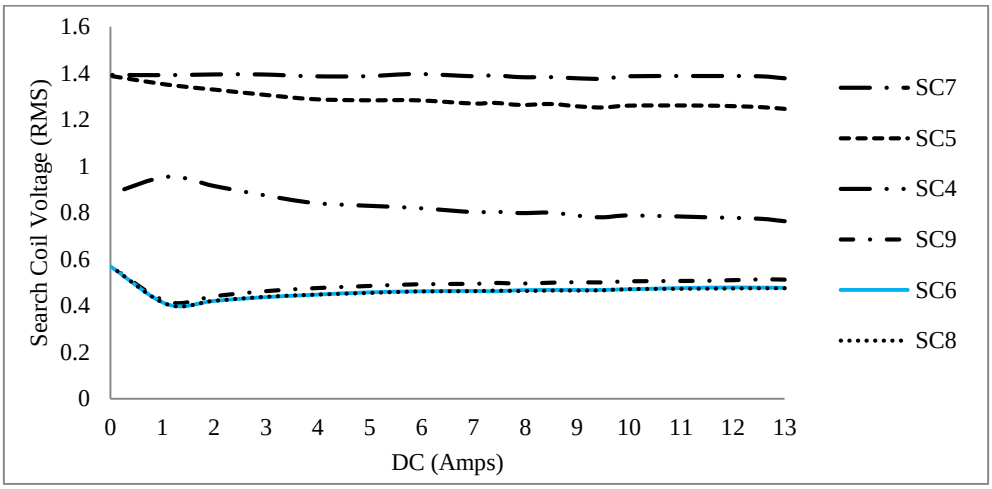

Figure 62: Measured SC output voltages with increasing dc under nominal ac excitation

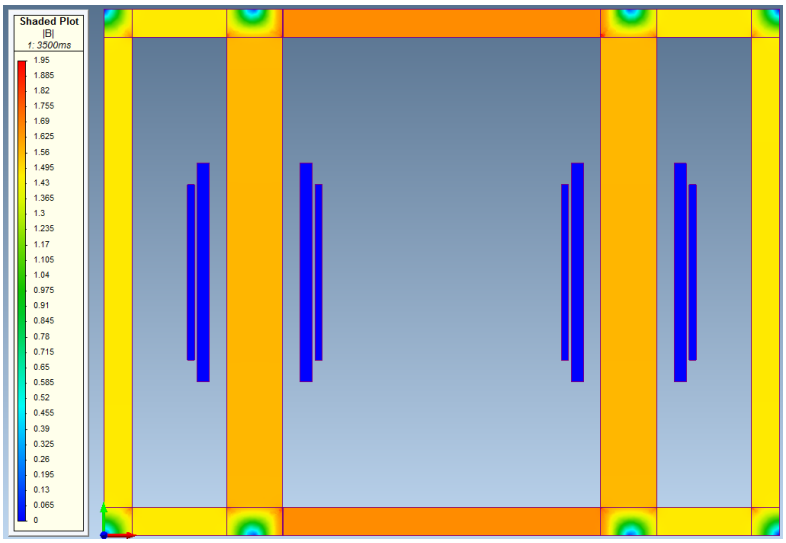

Figure 63: 2D FEM model-B2 with 1.25 A dc at nominal voltage

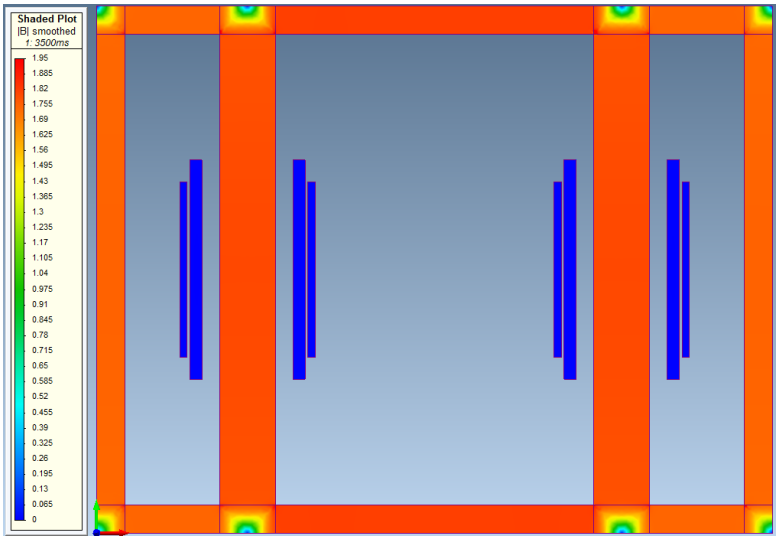

Figure 64: 2D FEM model-B2 with 7.3 A dc at nominal voltage

Similarly, the FEM analysis confirms how the flux is distributed at the start of core joint saturation due to dc (1 A dc) and in deep saturation (7 A), following very closely what was derived from the physical SC measurement data. Some flux vector plots with ac and dc are given in Appendix D.1.

8.3.1.1 Effect of dc bias on the magnetizing current

THD was used to analyse the different levels of core saturation with increasing dc. It can be seen from Figure 65 that in region 1 with dc levels less than 1 A, the transformer is operating linearly with a rapidly increasing current THD. Non-linear operation commences in region 2 where partial saturation at the T-joints causes a drop in THD. Other parts of the core start to saturate, including most of the wound inner limbs, interconnecting yokes, and side return limbs. (This is the shift in core operation moving from the level of saturation in Figure 63 to much deeper saturation in Figure 64.) Region 3 represents bulk core saturation where most of the core is saturated. This region of operation in 4 and beyond has often been considered in the literature (Hock-chuian & Swift, 1984, Picher *et al.*, 1997) to be an "air core" operation. These results confirm the analysis of the SC-dc curves in Figure 62. They are also in agreement with previous studies by Chisepo (2014) on 1p3L bench-scale responses, and by Masoum and Moses (2008) on a 3p3L model, which reported a decline in current THD under "air core" operation arising from very high dc. (At this stage of the study, the questions regarding saturation inductance had not yet been answered as they would only be addressed in detail in section 8.4.)

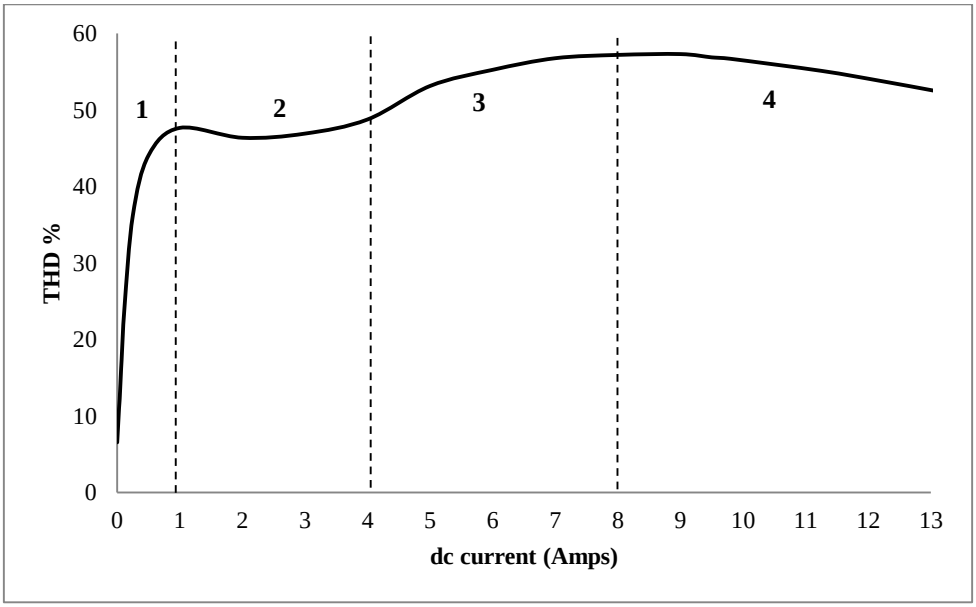

Figure 65: Measured input current THD with increasing dc under nominal ac excitation

The bar graphs indicating the individual magnitudes of both voltage and current harmonics are given in Appendix D.2, showing how the voltage is significantly resilient to distortion due to dc when compared with the magnetizing current. In the same appendix, a graph shows that with increasing dc under nominal ac there is an increase in the 2^{nd}, 3^{rd} and 4^{th} current harmonics. Beyond 4 A dc, the 5^{th} and 6^{th} harmonics start to decline.

Figure 66 depicts the corresponding measured no-load magnetizing current waveforms for test transformer 1 with increasing dc at nominal voltage. The inception of half-cycle saturation from 1 A dc bias at applied nominal voltage results in the distortion of the current waveform with a dominant peak in the positive cycle, as expected. The slight phase shifts in the current waveforms are attributed to the use of resistors in the dc injection scheme connected to series with the 150 turn winding to control the dc. The effect of dc bias on the voltage wave was mostly notable at the higher levels of dc, as seen in Figure 67.

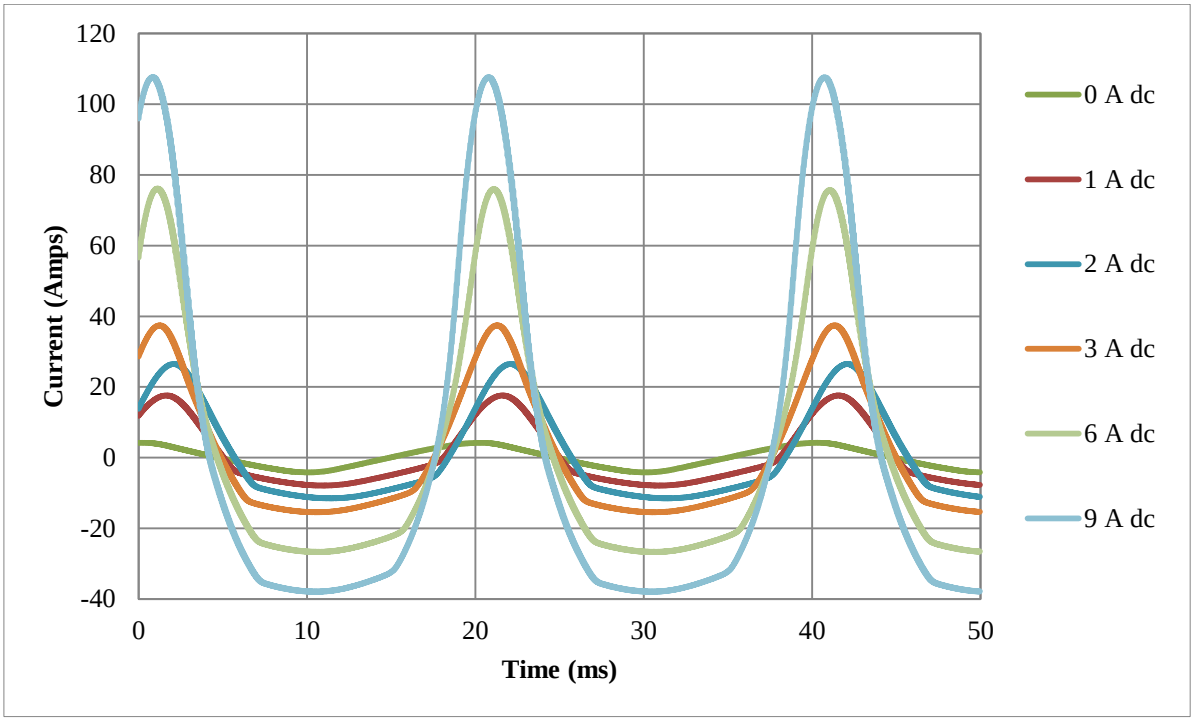

Figure 66: The effect of increasing levels of dc bias up to 9 A dc on the no load magnetizing current signifying half-cycle saturation

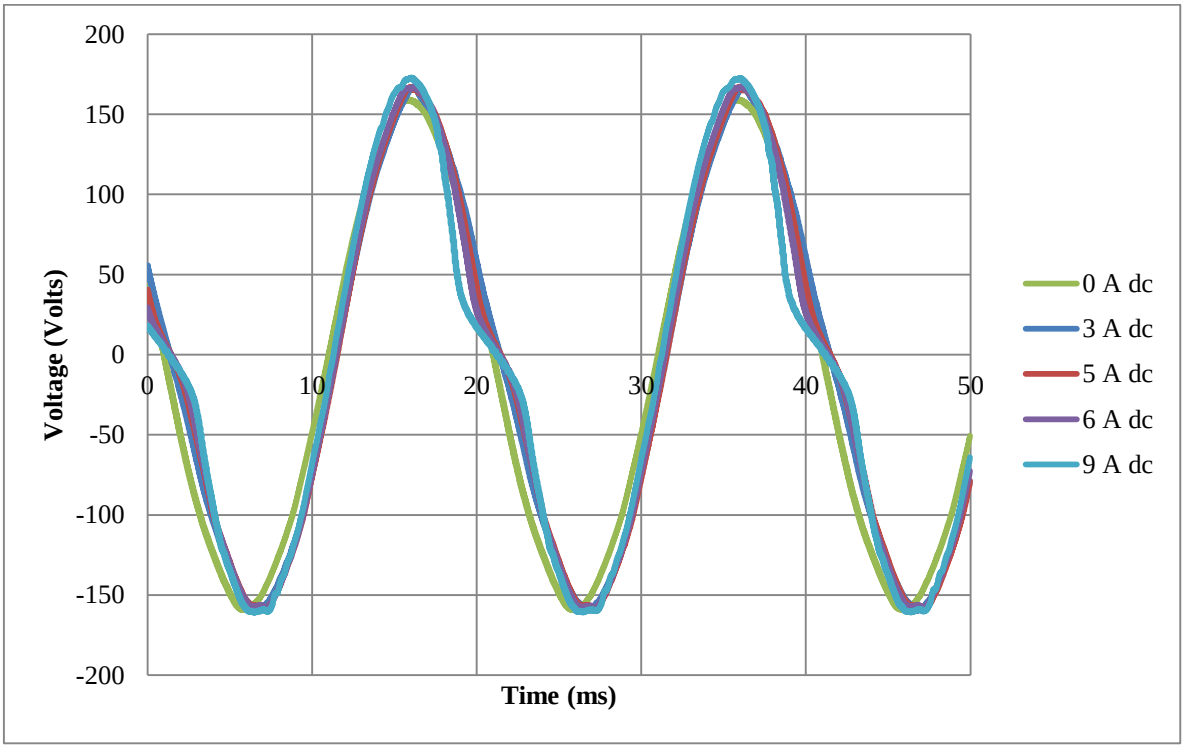

Figure 67: Effect of dc bias on the applied voltage

8.3.1.2 Reactive Power consumption

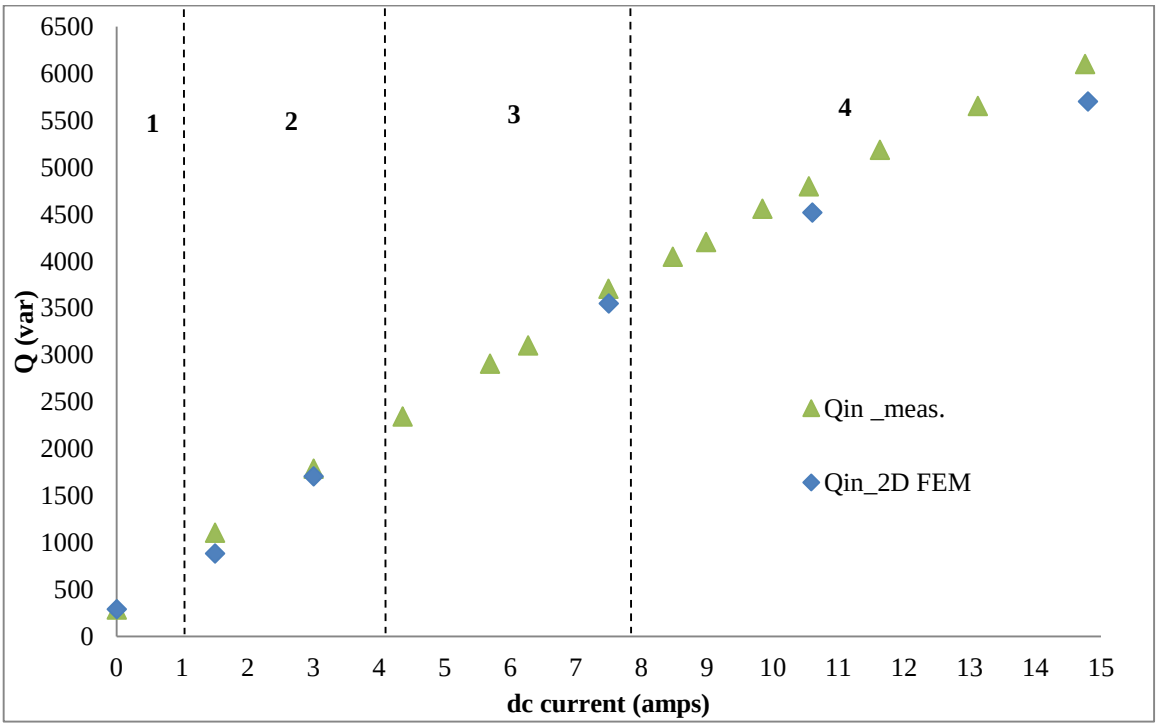

Figure 68: Input reactive power measured at the 80t windings in the presence of dc

The recorded Q-dc measurements in Figure 68 show a roughly linear relationship characteristic. In measurements performed on T1, the term 'weak supply' was used to mean that when the nominal voltage of 110 V RMS was applied, the resulting volt drop due to the dc was not compensated for by restoring it back to the nominal. This experiment simulates a power system which does not have sufficient (or properly operational) static var compensation for reactive power support, and this lack ultimately results in a voltage collapse which was the reason behind the Hydro-Quebec blackout (Kappenman *et al*., 1991).

Another Q-dc experiment was done with a 'stiff' voltage supply which simulates a sufficiently Q supported power system which is impervious to voltage dips due to dc. This was emulated by restoring the applied voltage back to 110 V RMS after each dc injection. Appendix D.3 contrasts the differences between the measured stiff and weak supplies. Because the 'stiff supply' model was not considered in the FEM, the 'weak supply' experiment was chosen for comparison. The 2D FEM model that was used is model B1 with uniform "equivalent air gaps" at the joints because its no load characteristics were close enough to T1's response. Model B1, with an accurate I_{mag} representation for T1 at no load (see Table XIV), yields a very good correlation with the measured data between regions 1, 2, and 3, as can be seen in Figure 68. Further into deep saturation in region 4, however, with higher levels of dc injection the voltage collapse calculated by the FEM is overestimated, resulting in slightly lower Q levels than the measurements. The FEM 3D symmetric (not presented here) yielded a similar Q-dc

response as 2D. These results show an improvement when compared with the preliminary FEM simulation whose models significantly underestimated I_{mag} at no load resulting in discrepancies in the Q-dc response.

8.3.2 Air SC outputs

The 2D model was given very dense isotropic mesh throughout the model for maximum accuracy. The 3D mesh elements were initially restricted to be not more than 10% of the largest extent of the model i.e. 54.2 mm. Refinement of the uniform mesh involved halving the size until convergence was met between two successive solutions. This resulted in a maximum element size of 13.6 mm for the transformer model, this is 2.6% of the largest extent of the model. The air box was given a comparably sparser mesh, while an isotropic (localized) denser mesh of 10 mm (1.9% of the largest extent of the model) was allocated around the joints, shown in Figure 69. The air search coils were allocated an even smaller mesh corresponding to their very small dimensions.

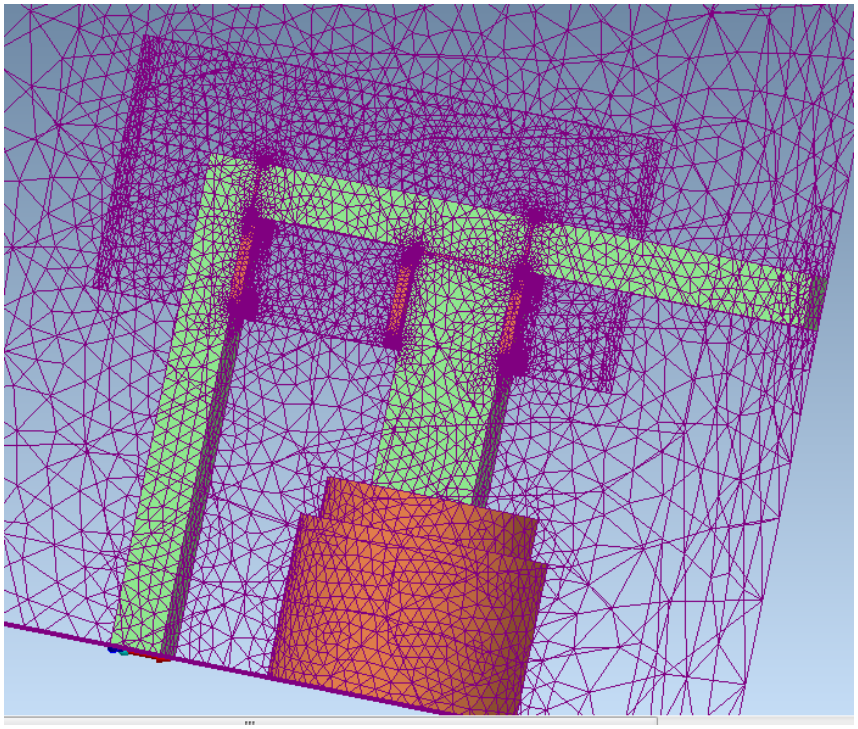

Figure 69: Mesh allocations of 3D model with 251 887 tetrahedra and 44 902 nodes. The tetrahedra are the discrete elements forming the geometry of each component of the model. The nodes are the (four) vertices of each tetrahedron, and they co-join one element to another forming the mesh

Figure 70 shows leakage flux increments resulting from dc injection for the 2D and 3D FEM simulation compared with the actual measurements using the search coils. Both simulations incorporate the equivalent gap factors. Although the simulated air SC output voltages are consistently lower than the measured ones, they follow similar trends during half wave saturation. The results of the 3D simulation are closer to the measurements than achieved with the 2D.

The measurements at SC D, not shown in Figure 70 to avoid over-loading the graph, were consistent with the results from SC A and SC E. (See Figure 46 or Figure 55 for the placement of the air SCs.)

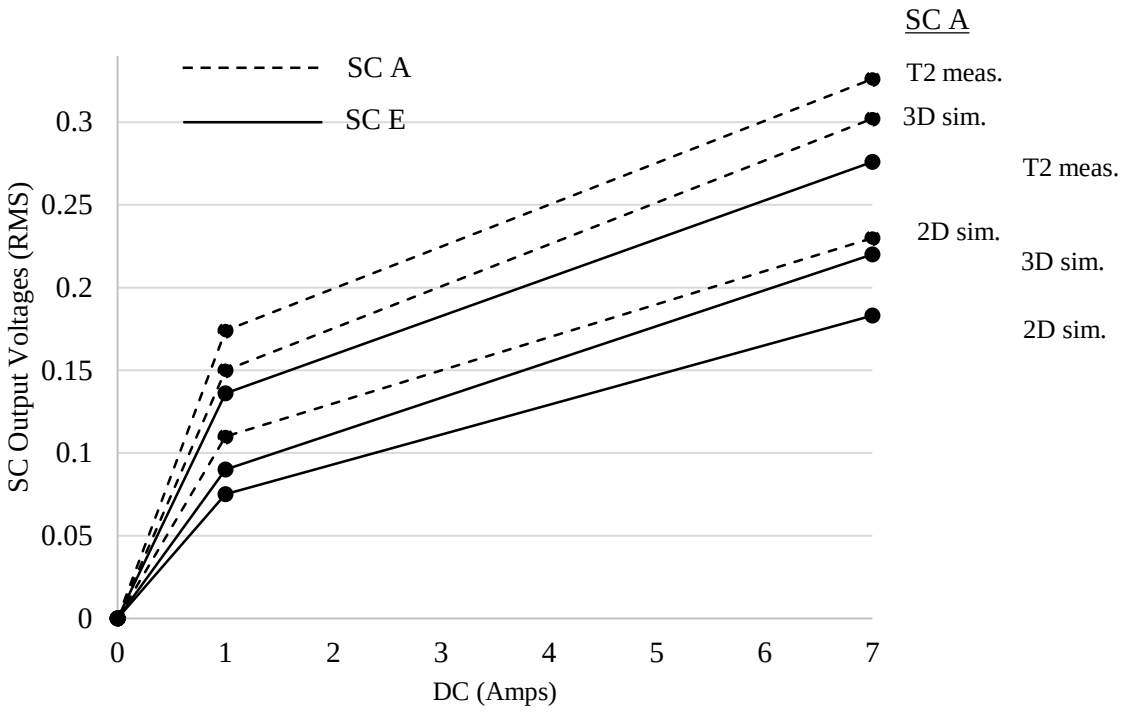

Figure 70: A comparison of simulated and measured results taken from: 2D – the model with equivalent air gaps at the joint calibrated to T2, 3D – the model with 20 explicitly modelled laminations on the surface of solid core parts and with equivalent air gaps at the joints calibrated to T2, and laboratory transformer T2 – the measured values. The locations of search coils A (dashed) and E (solid), are depicted in Figure 46

8.4 Saturation inductance

This section attempts to identify the extent to which the laboratory measurement for "terminal saturation inductance" L_{termin} al is consistent with or differs from other measurements of the windings' "air core inductance" L_{air} simulation in FEM and analytical calculation L_{air_calc}.

The abbreviations that will be used are given below:

Meas. L_{air}	Measured air core tests with GOES core stripped from the transformer energized with ac only
FEM L_{air}	3D FEM full model air core simulation
T1 $L_{terminal}$	Terminal saturation inductance measurement final values for actual 1p4L transformer one T1
FEM $L_{termianl}$	Terminal saturation inductance values for 3D FEM symmetric models
80t outer	The 80 turn outer winding in the FEM modelled in its original position as in the actual 1p4L transformer T1

150t inner	The 150 turn inner winding in the FEM modelled in its original position as in the actual 1p4L transformer T1
80t inner	The 80 turn winding in the FEM modelled in the original position of the 150 turn inner winding of the actual 1p4L transformer
150t outer	The 150 turn winding in the FEM modelled in the original position of the 80 turn outer winding of the actual 1p4L transformer

See Appendix D.4 for some diagrams representing some of the abbreviations given above.

8.4.1 Summary of $L_{terminal}$ and L_{air} results

Table XVII: Table showing comparisons or measurements and simulations with original winding configurations

Windings	Meas. L_{air}	FEM L_{air}	%diff with meas. L_{air}	T1 $L_{terminal}$	%diff with meas. L_{air}	FEM $L_{terminal}$	%diff with meas. L_{air}	%diff with meas. $L_{terminal}$
150t	694	654	5.7	798	-15.0	722	-4.0	9.6
80t	355	340	4.2	275	22.5	380	-7.1	52.3

As Table XVII shows, FEM L_{air} correlates well with laboratory measured L_{air} test for "air core inductance". The laboratory measurements for $L_{terminal}$ shown for T1 differ from those of the measured L_{air} with a higher value for the 150t winding (expected) and a lower value for the 80t winding (unexpected). Performing $L_{terminal}$ simulations in the FEM at the same level of saturation reached in the laboratory resulted in solutions for both the 150t and 80t windings closer to but higher than the measured L_{air}, as expected. Figure 71 shows the FEM $L_{terminal}$ plots for each winding energized separately while the other is open circuited.

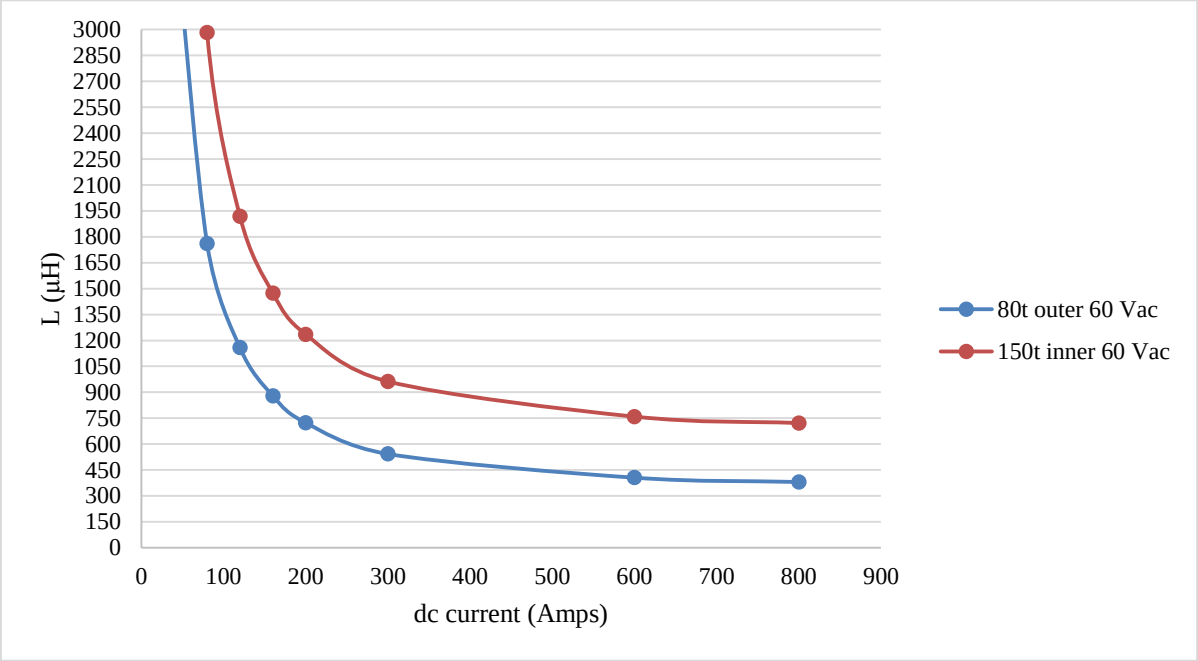

Figure 71: FEM $L_{terminal}$ values for each pair of windings at the same level of saturation reached with the laboratory protocol starting to level at 722 µH for the 150t inner windings and 380 µH for the 80t outer windings

8.4.2 Multiple parameter simulations for $L_{terminal}$

In order to further investigate why the measured 80t $L_{terminal}$ was lower than measured and simulated L_{air}, further simulations were performed with variations in different parameters. The FEM curves with corresponding L-dc profiles are given in Appendix D.4.

Table XVIII: Table of different FEM experiments run to calculate $L_{terminal}$

FEM exp. no.	Description of FEM exp.	FEM $L_{terminal}$ (µH)	Meas. $L_{terminal}$ (µH)
1	80t outer energized with 60 Vac + dc in the presence of the 150t inner winding open circuited	380	275
2	80t outer energized with 60 Vac + dc without the 150t inner winding	396	-
3	80t inner energized with 60 Vac + dc in the presence of an 150t outer winding open circuited	270	-
4	150t inner energized with 60 Vac + dc in the presence of the 80t outer winding open circuited	722	798

5	150t inner energized with 60 Vac + dc without the 80t outer winding	702	-
6	150t inner energized with 5 Vac + dc in the presence of the 80t outer winding open circuited	720	-
7	150t outer energized with 60 Vac + dc in the presence of an 80t inner winding open circuited	1133	

From Table XVIII, FEM exp. no. 1 and 4 are the results already presented in the preceding subsection 8.4.1. FEM exp. no. 2 and 5 were done to see the extent to which mutual inductances L_m between the windings affected the simulated the $L_{terminal}$. This was done by removing the winding not under investigation from the simulation. FEM exp. no. 3 and 7 represent the effect of swopping the positions of the 80 turn and 150 turn windings while keeping the winding not under investigation open circuited. The effect of drastically reducing the applied ac (to approximately 5 V) in the presence of the same high dc did not have any effect of the value of the $L_{terminal}$ (FEM exp. no. 6).

FEM exp. no. 1 and 2 show the effect of mutual inductance L_m between the 80t and 150t windings (an increase of 16 μH when the 150t winding is removed) at $L_{terminal}$. The actual measurement performed on test transformer gave a value for $L_{terminal}$ of 275 μH which is much lower than the FEM calculated and measured L_{air} and this was unexpected. FEM Exp. 3 which moved the 80t closer to the core, swopped with the 150t winding resulted in a smaller diameter for the 80t winding yielded a value of 270 μH, which was expected. Looking at FEM exp. 4, it can be seen that the150t FEM and measured $L_{terminal}$ are comparable (%4 difference). This provides confidence in the accuracy of the $L_{terminal}$ laboratory measurement for the 150t winding because it is consistent with the FEM. FEM Exp. no. 4 and 5 show that the effect of removing the outer 80t winding reduces the 150t $L_{terminal}$ by 20 μH, also revealing the effect of L_m at terminal saturation inductance. When the 150t winding is moved to the outer position (FEM exp. no. 7) giving it a bigger diameter, the $L_{terminal}$ increases to 1133 μH, as expected.

8.4.3 Air core inductance (core-less windings)

Table XIX: Table showing measured, FEM, and calculated values for L_{air}

FEM exp. no.	FEM exp. description	FEM L_{air} (µH)	Meas. L_{air} (µH)	%difference with L_{air}	Calc. L_{air} (µH)	%difference with L_{air}
1	80t energized both windings present	340	355	4.2%	353	0.6%
2	150t energized both windings present	654	694	5.7%	664	4.2%
3	80t energized no 150t	340	-	-	-	-
4	150t energized no 80t	652	-	-	-	-

FEM experiments 1 and 2 in Table XIX modelled a "core-less" transformer with all the windings assemblies present in the domain to simulate the windings shown earlier in Figure 47. A very dense adaptive isotropic (uniform) mesh is used in the air surrounding the windings to ensure that the most accurate 3D solution is achieved (see Figure 72 overleaf). Excitations for dc-magnetostatic only are presented in this section (simulations with ac with the Time-harmonic solver at 50 Hz were also carried out giving virtually the same solutions as those with dc). In order also to investigate the effect of L_m, further simulations were done with one pair of windings removed (experiments 3 and 4). It can be seen in the same table that the FEM L_{air} solution for the outer 80t winding is unaffected by the presence (or absence) of the 150t winding. The 150t winding, however, yields a slightly lower L_{air} value when the 80t is taken out, showing a very small L_m of 2 µH between the two windings.

The analytical hand calculation for air core inductance L_{air} used the following expression

$$L_{air\_calc} = \frac{\mu N^2 A}{l}$$

where $\mu = \mu_0\mu_r$ (with $\mu_r = 1$ for air), N is the number of turns, A is the cross-sectional area of the windings, and l is the winding height. The results showed an even closer correlation with the measured L_{air} values and also had a good agreement with the FEM L_{air} solutions.

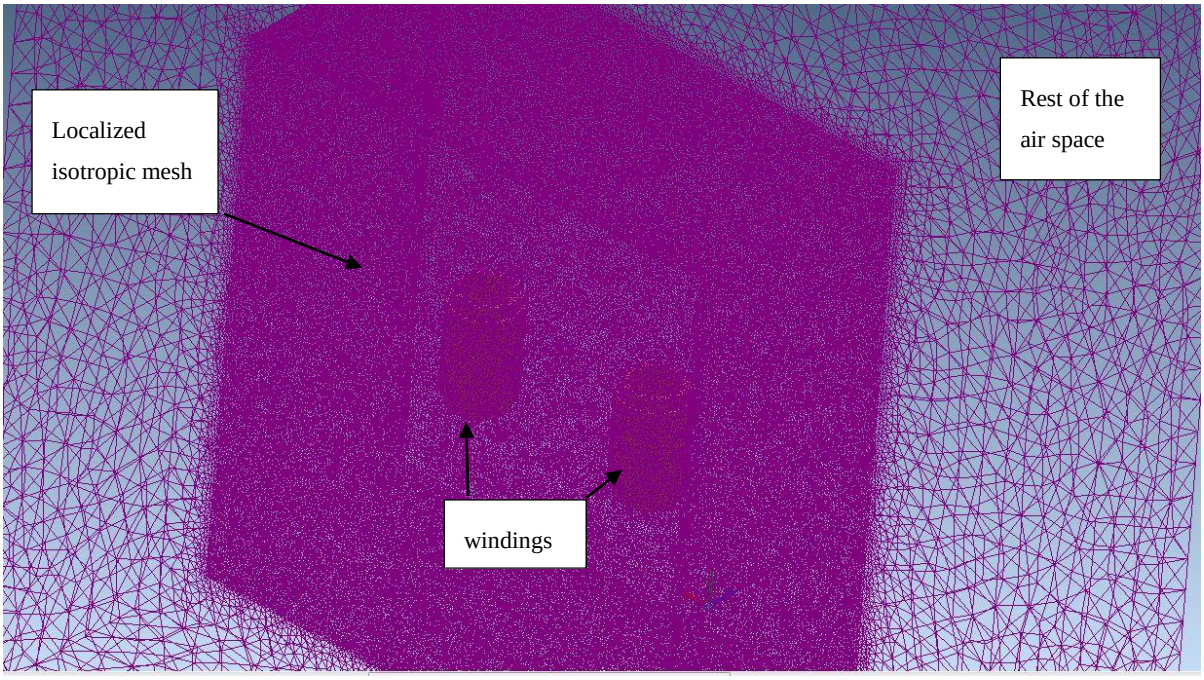

Figure 72: Mesh allocations for accurate air core magnetostatic solution. Windings' maximum mesh extent is 13.6 mm, localized isotropic mesh maximum mesh extent is 50 mm and rest of the air space has a maximum mesh extent of 100 mm. Resulting tetrahedra is 4 735 280 and number of nodes is 831 182. Simulation time - 9 hours and 44 minutes

8.4.4 Discussion

The measured and simulated L_{air} were in good agreement. A comparison between the calculated L_{air} showed an even closer correlation with the measured. The measured $L_{terminal}$ values differed from the measured L_{air} in the sense that the 150t winding had a higher value, as expected, since the core does not reach 100% saturation (see Figure 73). The 80t winding had a lower value than the measured L_{air} which was counterintuitive because μ_r theoretically tends to 1 in deep saturation but never reaches it in reality (see Figure 74). Simulating the $L_{terminal}$ in the FEM with up to 800 A dc resulted in L converging to values which were higher than the measured and simulated L_{air}, for both 80t and 150t windings. From the FEM results, when the dc is large enough, the size of the ac ripple is independent of the final $L_{terminal}$ value. Analysing the all the measurement and simulation data, it is possible that there was a measurement error with the 80t windings. The L_m picked up in the FEM was more noticeable when the150t inner winding was energized with the 80t outer winding open circuited, and it was bigger at $L_{terminal}$. The L_m when the outer 80t winding was energized while the 150t inner winding was open circuited was negligible.

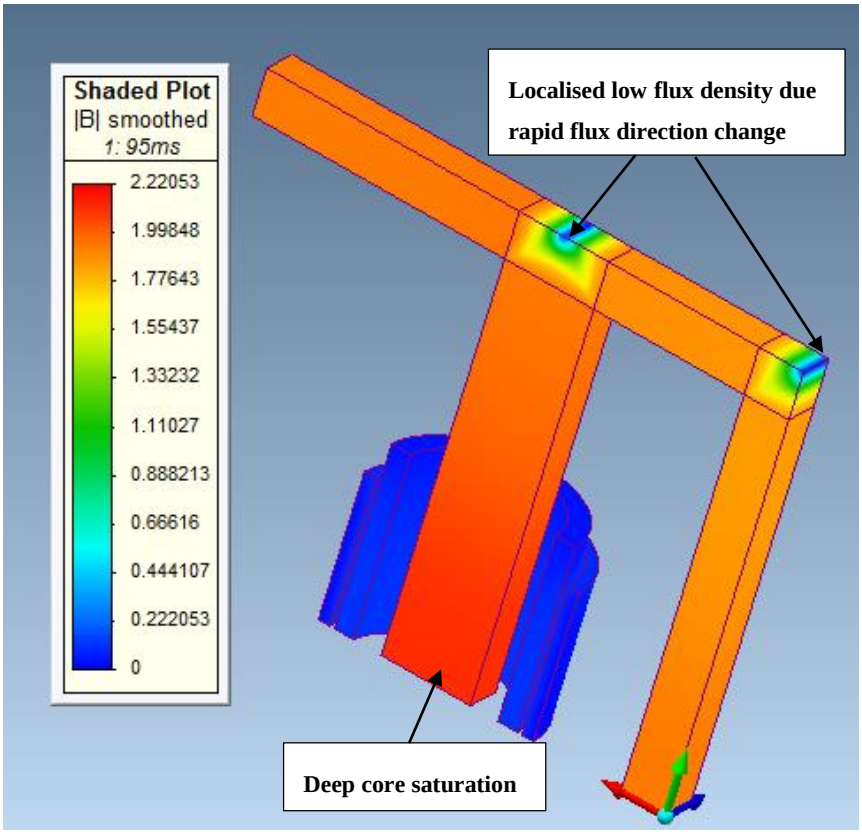

Figure 73: Deep core saturation with 60 V ac and 800 A dc energising the 150t inner in the presence of the 80t outer

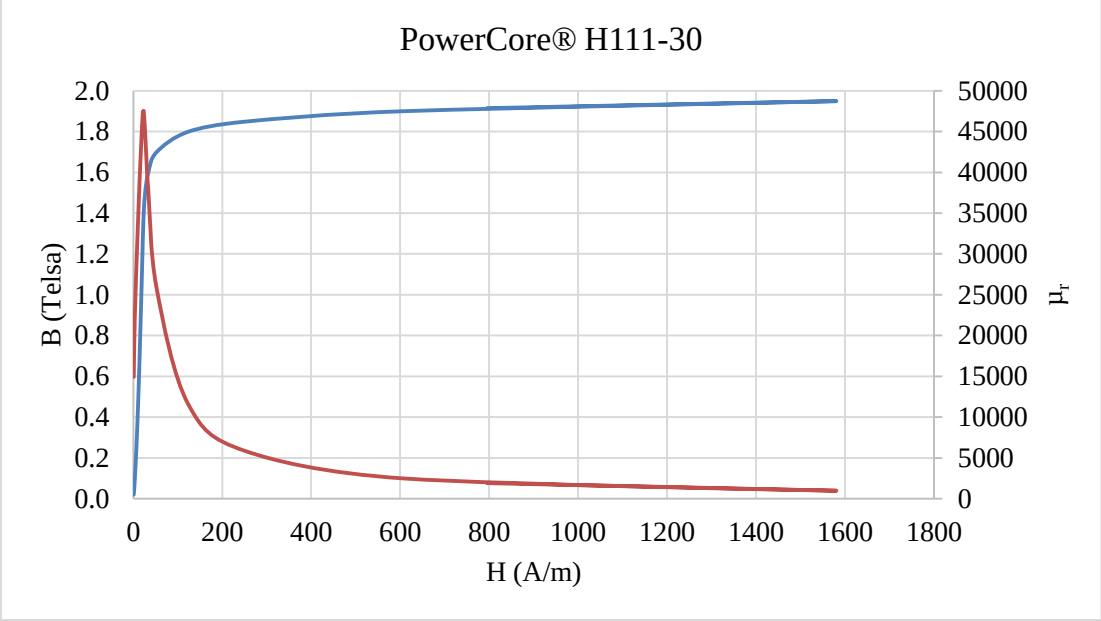

Figure 74: BH curve for test transformer electrical core steel with relative amplitude permeability on secondary axis

In order to test the limits and accuracy of the FEM, further simulations were run to calculate $L_{terminal}$ with up to 10 kA dc in the presence of a 60 V excitation. The results converged at 341 μH and 657 μH for the 80t and 150t windings, respectively, as shown in Figure 75.

These values are a few μH higher than the FEM L_{air} solutions (340 μH and 654 μH, respectively), and they suggest that the FEM model's core is very close to complete "air core" saturation

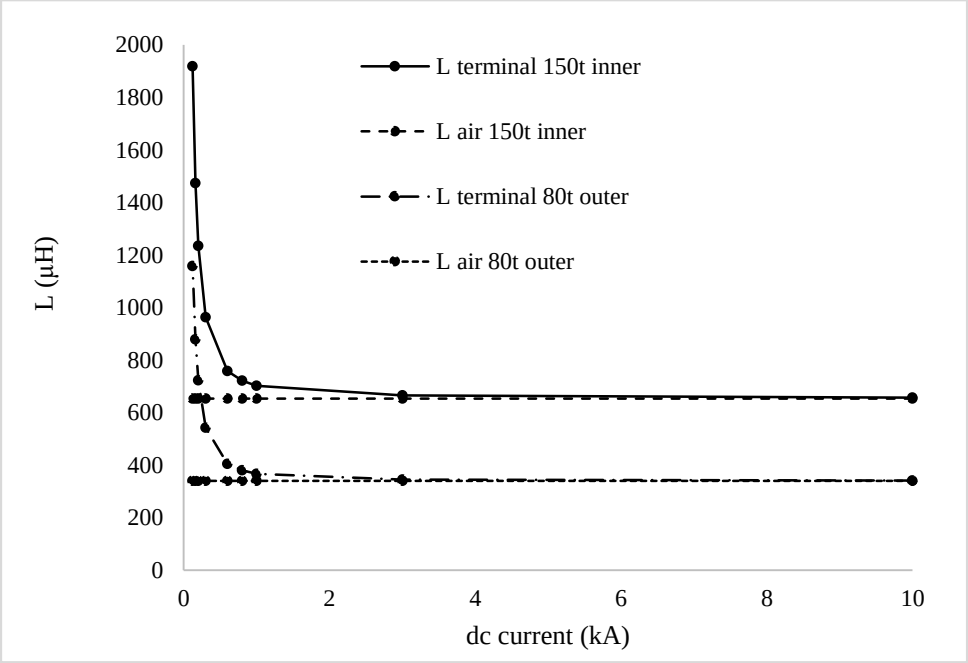

Figure 75: Further simulations with extremely high dc

8.4.5 Summary

The method used to determine $L_{terminal}$ in the FEM differed from the laboratory protocol which made the use of a rectifier with saturating harmonics and much lower levels of dc to achieve deep saturation. As shown in Figure 52, the FEM calculation was based on the stored magnetic energy and input current in the presence of a 50 Hz sinusoidal voltage excitation and very high levels of dc to achieve deep saturation.

The measured $L_{terminal}$ value for the 150t winding seems to be plausible because it is comparable with the FEM simulation with 800 A dc and is higher than the L_{air} measurement, simulation, and analytical calculation. It was unclear why the adapted de León method to calculate $L_{terminal}$ was erroneous for the 80t outer windings. Possibly, the discrepancy is due to erroneous readings being captured by the WT1800 Yokogawa Power Meter with a current limit of 60 A RMS (and a corresponding peak current of 85 A). In order to reach the same level of core saturation from the 80t windings as the one reached by the 150t windings (with a maximum dc input of 76 A dc), much more dc was needed to compensate for the dc Amp-turns (about 140 A dc). Therefore, that the $L_{terminal}$ value measured by the power meter for the 150t windings within its current limits is correct and is supported by the FEM and L_{air} measurement. The measured $L_{terminal}$ value for the 80t windings pushed the limits of the power meter, resulting in its current clamps being saturated and thus affecting the readings. However, with the

augmentation of all the known results and the FEM analyses, it is possible to estimate a more appropriate $L_{terminal}$ value for the 80t windings as 380 μH.

Extending the simulation to unrealistic levels of dc resulted in an $L_{terminal}$ value which was very close to the FEM $L_{air,}$ but it was higher. The FEM simulation picked up mutual inductances between the windings. The implication is that L_m needs to be considered in detailed transformer topological models used in electromagnetic transients' simulation.

From these findings, it is clear that for these model 1p4L transformers there is a difference between the L_{air} and $L_{terminal}$. In other words, a 1p4L transformer energised at nominal ac value(s) while experiencing an achievable dc bias will never get to an "air core "operation state. These results confirm that the de León method is correct in determining the $L_{terminal}$ value by measurement, and it has been shown that an air core state is not achievable in reality. In the context of GIC, therefore the $L_{terminal}$ value is, more applicable to practical experiences with GIC (75 - 110 A/phase being considered to be very high levels (Czech *et al*., 1992, Wik *et al*., 2009)) flowing in the transformer HV windings with a high number of turns. Also, with the tank enclosure and other structural metallic parts (clamps, tie rods, etc.) which all have much higher μ_r's than air, it is highly unlikely that the transformer windings' L_{air} will never be reached during a significant geomagnetic disturbance with high GIC.

9 DISCUSSION

9.1 FEM modelling: lessons learnt

9.1.1 40 MVA Power transformer model

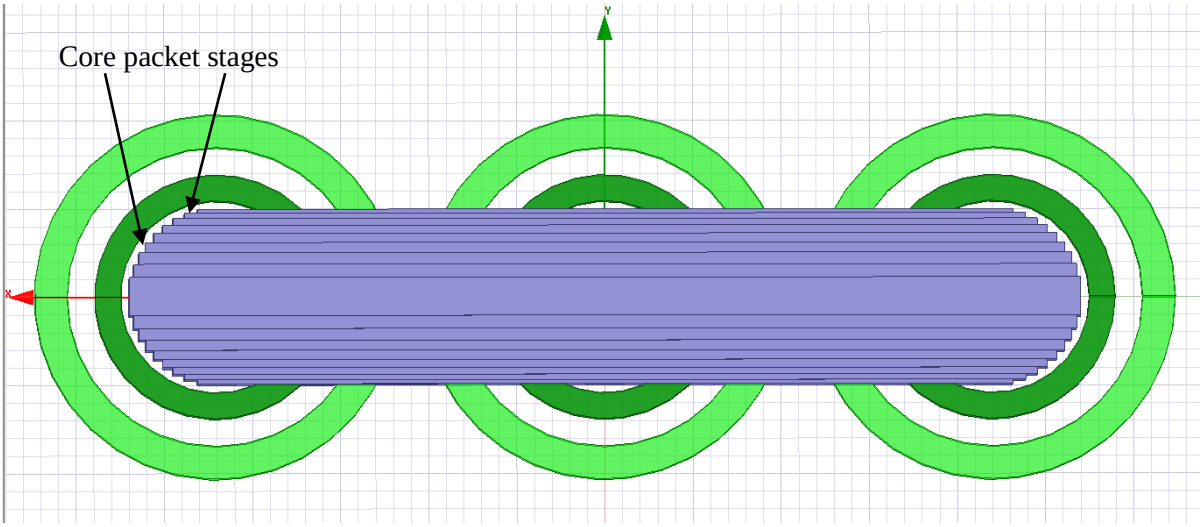

Figure 76: Top view of core and windings of 40 MVA power transformer model with 18 packet stages

Early in this thesis, a preliminary FEM simulation was undertaken to investigate the response using ANSYS. A rigorously modelled 40 MVA 3p3L power transformer with only FAT measurement and design data for comparison was tested in the FEM, and it was found that the magnetizing currents and core loss calculations for both the 2D and 3D models were not sufficiently accurate, even though the 3D model was an improvement on the 2D model. The 2D model had a solid core, while the 3D model was modelled according to the stacking configuration provided by the manufacturer design data (18 packet stages). See Figure 76 for the top view of the core showing the different packet stages.

In order to test the sensitivity of the lamination detail, two further investigations were done at nameplate ac only excitation, involving a) 0.3 mm explicitly laminated core packet stages, and b) half the number of solid packet stages i.e. 9 stages.

Model a) did not successfully run to the end of the specified simulation time, but steady state was reached halfway through the simulation before various errors were encountered. The stored solutions yielded very high no load magnetizing currents in the order of 100 times the FAT data. The core loss calculation, however, was comparable with the measured value.

Model b) with 9 solid packet stages resulted in magnetizing currents that were 3 times more than the FAT data and a comparable core loss.

The findings show that when modelling a 3p3L mitred transformer in the FEM without the incorporation of equivalent air gaps at the joints, explicit modelling of all the laminations gives erroneous results and a solution may never be obtained. This necessitates the reversion to the manufacturer specified number of packets (18 in this case presented in Chapter 4) for the optimal solution. Hihat *et al.* (2011) reported serious challenges in arriving at a 3D FEM solution when attempting to explicitly model the laminations of a transformer core, which is consistent with the response of Model a).

9.2 Measurement and simulation complement

Characterizing the individual 1p4L test transformers by generating magnetization curves was used to analyse the core performance at different levels of ac excitation. Due to the butt joint configuration of these test transformers, it was necessary to de-rate their nameplate ratings, so as not to represent over-excitation, to a newly specified nominal induction representing linear operation. The difference in the shapes of the magnetization curves also revealed that, though these transformers were industrially manufactured with the same design data, their responses to ac excitation differed from one another due to unavoidable manufacturing errors. Further to this, the search coil outputs at the same level of excitation varied slightly, not only at the individual joints where symmetry might be assumed, but also between the transformers. Although this difference was unexpected at first, it is consistent with Nakata & Kawase's study (1986) who associate (unavoidable) joint dimension error in laminated cores due to the stacking process with variations in core losses and overall magnetic performance.

Whenever a FEM approach is proposed, especially in the industry or research (and development), the question often left unanswered is if the model has been validated. If it has been validated, then for which parameters? However, to validate the model, a prototype is needed to test its accuracy, and for the prototype to be fabricated (especially for specialized electromagnetic devices), a preliminary prediction of the response is needed to generate some parameters. In this research, the preliminary FEM simulation guided the acceptance tests to ensure the correct polarity and expected flux distributions in the core and the air around for the 1p4L transformers. The magnetization curves were then used to identify the nominal voltage, commencement of saturation (and hence leakage flux) for testing in the FEM. Knowledge from the literature regarding losses at the core joints and leakage flux due to air gaps at the joints, coupled with the laboratory derived magnetization characteristics, led to the calibration of more accurate FEM models. These models overcame the discrepancies yielded by the earlier FEM models in a preliminary study (chapters 4 and 5). The calibrated models were tested for their response with simultaneous ac and dc excitation, achieving results which correlated with the measured data in most aspects of the investigation. Finally, the validated FEM models and some measurements (of items previously reported to have been too hard to measure) were investigated in parallel.

Despite the apparently erroneous/unsuccessful 80t $L_{terminal}$ measurement owing to limitations in the laboratory equipment, the FEM provided insights on some key differences in the magnetization characteristics needed for topologically derived transformer models. Table XX shows how the simulation complemented the measurement and *vice versa*.

Table XX: A summary of how measurements and the FEM worked in together in the study

Parameter	**Measurements**	**FEM**
Winding polarity		✓
Search coil placement		✓
Magnetization curves	✓	
Calibration of FEM joints	✓	
Confirming the differences between $L_{terminal}$ and L_{air}	✓	✓

9.2.1 1p4L FEM models

Later in this thesis project, the problem of FEM mesh structures being too large to solve for a fully laminated model was addressed by laminating only the core plates closest to the surface through a sensitivity analysis and the application of appropriate boundary conditions which cause a discontinuity between interfaced laminations. This drastically reduces the computational expense for the mesh generator. Keeping the rest of the core solid with equivalent air gaps further simplifies the 3D calculation without sacrificing accuracy. This approach allowed a solution within a reasonable simulation time (25 hours).

It appears in the literature that most researchers give few details of the transformer joints or, like Jazebi *et al.* (2013), provide illustrations of laboratory transformers with butt joints, like those of the 1p4L test transformers in this research. In practice, FEM simulations of power transformers appear to use solid joints despite the limitations in accuracy for slow transients/GIC studies.

As shown in Table XIV and Table XV, application of the "equivalent air gap" approach to 2D FEM modelling of the laboratory transformers improved the estimation of the magnetizing currents and no load losses, compared with FEM models with solid joints, and closely matched the laboratory measurements.

This resulted in better estimations of the reactive power estimation in the presence of differing dc levels (see Figure 68).

Extending the FEM to 3D gave even better responses of the leakage flux (see Figure 70) even though the values still did not exactly match the actual measured values. These discrepancies have been attributed to modelling a 'weak supply' in the FEM and possible differences between the dimensions of the SCs in the lab and the ones modelled in the FEM.

9.3 Confirmation and extension of existing reports

9.3.1 Core joint details

A study on transformer core joints (Tang *et al*., 2015) also identified the challenges faced by Hihat *et al.* (2011) in arriving at a 3D FEM solution when the transformer core laminations are modelled explicitly. Using an approach similar to the one described in this thesis, Tang *et al.* (2015) successfully analysed the flux distribution at the core joints of 3D FEM models by using boundary conditions between 10 lamination layers which created "thin low permeability gaps" between the laminations of a mitred model. In comparison, this project explicitly modelled the 1p4L test transformers' laminations with a Perfect Electric Insulator (PEI) boundary condition (described in section 7.3) between interposed laminations. The PEI effectively simulated the very thin non-conductive layer on actual electrical core steel laminations. It was found that for the butt joints in the 1p4L test transformers, the individual laminations only need to be modelled close to the core surface. Further to this, the rest of the core was modelled using the 2D FEM derived "equivalent air gaps" at the joints. Through a sensitivity analysis which varied the number of laminations close to the core (between 10 and 50 laminations), it was then possible to optimally achieve a no load I_{mag} with less than 1% difference compared with the laboratory measurement. Having achieved a 3D model with satisfactory ac excitation only results, further simulation was done for simultaneous ac-dc excitation for comparison with measurement data in a way that is applicable for transformer-GIC/dc studies.

The qualitative analysis of SSL joints reported by Tang *et al.* (2015) did not have measurement data for comparison, which highlighted the difficulty in using air search coils to measure leakage flux. It is therefore difficult to assess how realistic the modelling results are, since they pointed out only similarities in the flux distributions by comparing their results with an early experimental study by Jones *et al.* (1973). The research project for this thesis made use of numerous search coils wound on the test transformers' cores and air spaces at the joints, resulting in measured leakage flux traces that can be used to calibrate and validate the FEM flux analysis. Another study (Elleuch & Poloujadoff, 1998) made use of dynamic air gaps at the joints in a 3p3L topologically transformer model and then extended the study to test 2D FEM using fixed air gaps around several parts of the core (Khelil & Elleuch, 2009).

Both these studies do not appear to be directly applicable to transformer-GIC studies, because they lack experimental transformer-dc or inrush data and, in addition, do not extend the analysis to detailed 3D.

9.3.2 Analytical Definitions for GIC magnitudes

The literature generally summarizes GIC magnitudes in two stages i.e. base stage – low to moderate levels lasting from several minutes to several hours, and peak GIC impulse stage lasting several seconds to several minutes (Girgis *et al.*, 2016). This thesis has emphasized the need for quantifying GIC/dc as a function of the transformer I_{mag}. This is necessary to establish the *detectability* of GIC through the commencement of half-cycle saturation accompanied by both even and odd harmonics. This principle was demonstrated in the THD results compiled in Figure 65 at 1 A dc. The average I_{mag} across all three 1p4L laboratory test transformers at the chosen knee point voltage was 0.9 A. The bench-scale laboratory protocol (Chisepo, 2014) also reported the inception of saturation in the test transformers to commence around 1 pu dc (per unitized on the base of I_{mag}). This GIC parameter related the detectability of partial saturation and, as a function of the I_{mag}, can now be referred to as the "detection level GIC". For power transformers (assuming an I_{mag} of 2–5 A and a GIC of 10 A/phase) the "detection level GIC" is approximately 2-5 pu.

The next important GIC parameter concerns relatively high levels as a function of the networks' capability to withstand it and maintain stability during the generation of high magnitude harmonics and large draw of reactive power. This GIC parameter can be referred to as "high GIC".

The last possible level, "very high GIC" is the one most likely to cause an outage or transformer failures and it is based on very limited statistics (Czech *et al.*, 1992, Wik *et al.*, 2009) ranging from 75-110 A/phase.

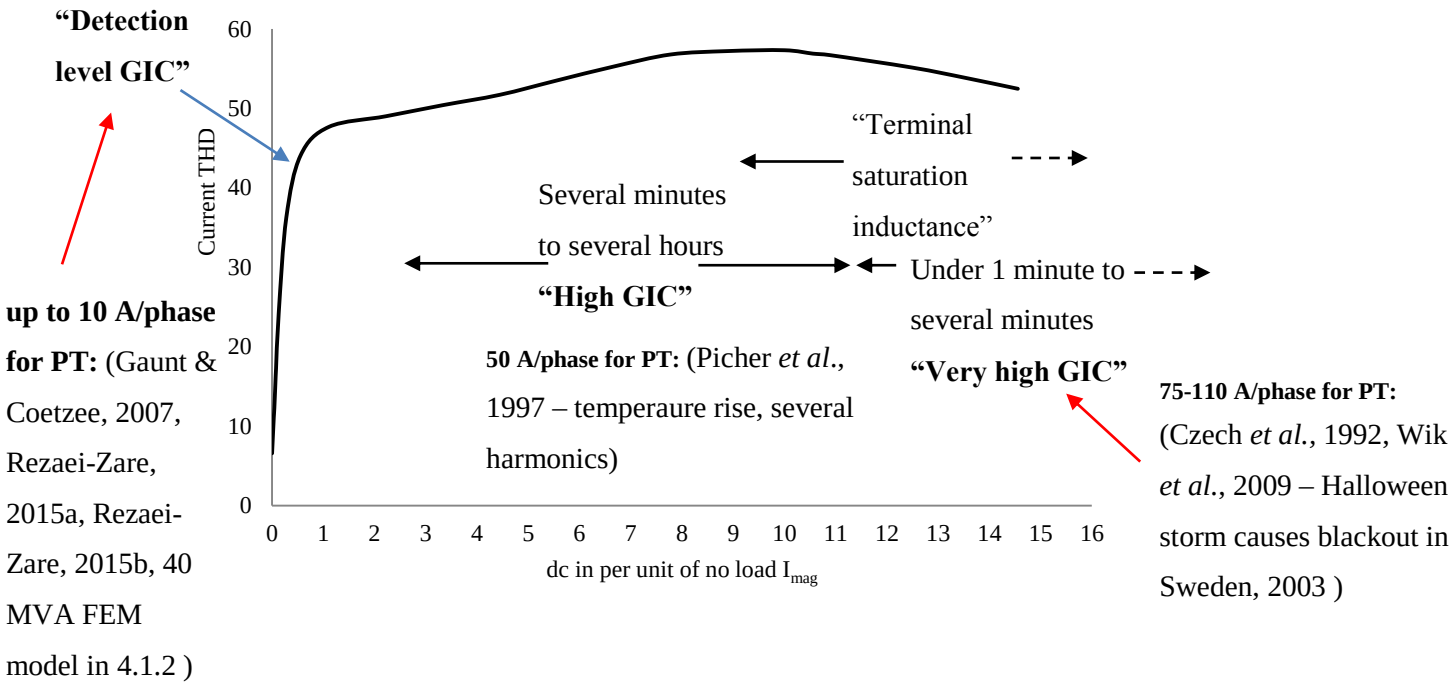

Figure 77: Generalized GIC magnitudes based on measured current THD adapted from Figure 65 and the equivalent power transformer thresholds. "Air core inductance" is not in this diagram because in the context of GIC, it can never be reached.

Figure 77 is a compilation of the characterization of GIC magnitudes for power transformers supported by laboratory measurements and corresponding cases in the literature. Based on these analytical definitions of GIC levels, the recommended threshold for periodical thermal assessment of power transformers that have experienced a GIC of 75 A/phase (FERC, 2015) is too high and may need to be revised to adequately verify the health of a transformer, even at relatively low GIC.

The reliability of transmission and voltages ought to be within 5% of nominal voltage (0.95<v<1.05 pu) in the South African power MV, HV and EHV networks (NRS 048-2:2003, 2003). Figure 78 illustrates how the different levels of GIC could affect the integrity of the voltage profiles in a power system using T2's measured voltage drop profile with increasing dc. The diagram in Figure 78 qualitatively supports previously categorized levels of GIC in Figure 77.

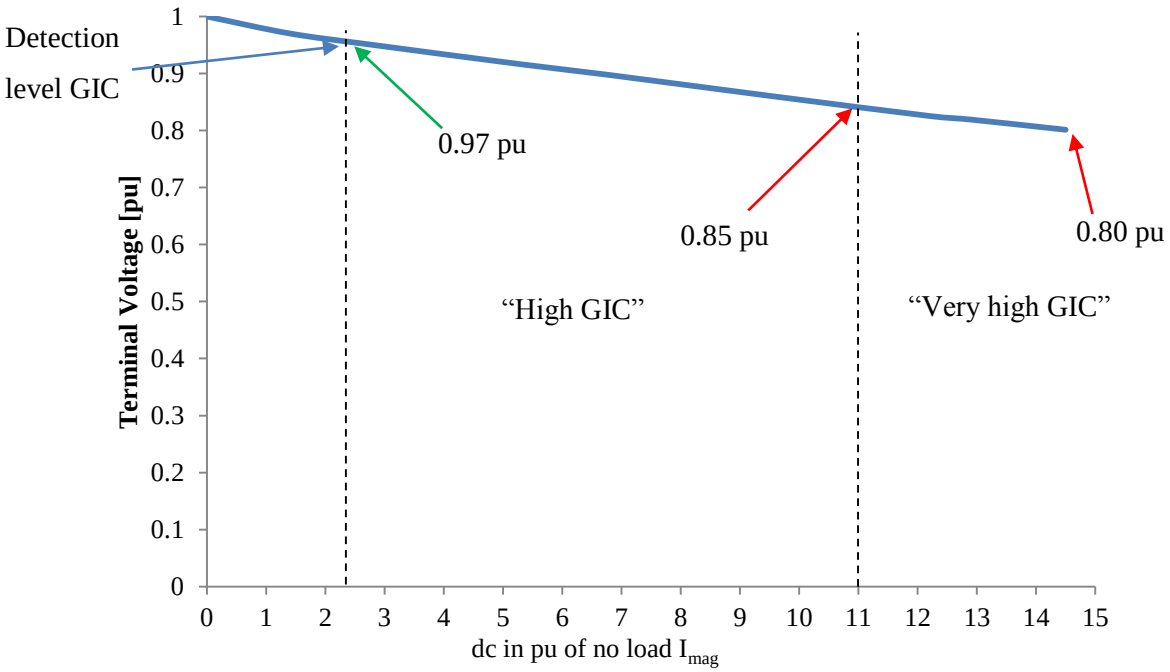

Figure 78: Measured terminal voltage drop at no load with increasing dc at applied nominal voltage for 1p4L T2 showing equivalent approximate definitions of GIC

9.3.3 Extending relationships in half-cycle saturation (Chisepo *et al*, 2019)

Section 2.4 provided the various studies in the literature which illustrate half-cycle saturation with a commonly used diagram (see Figure 79). In the simple illustration of the interaction of the magnetization parameters given in Figure 79, a significant question in transformer modelling (de León *et al.*, 2014) is 'what is the inductance between 'a' and 'b'?'

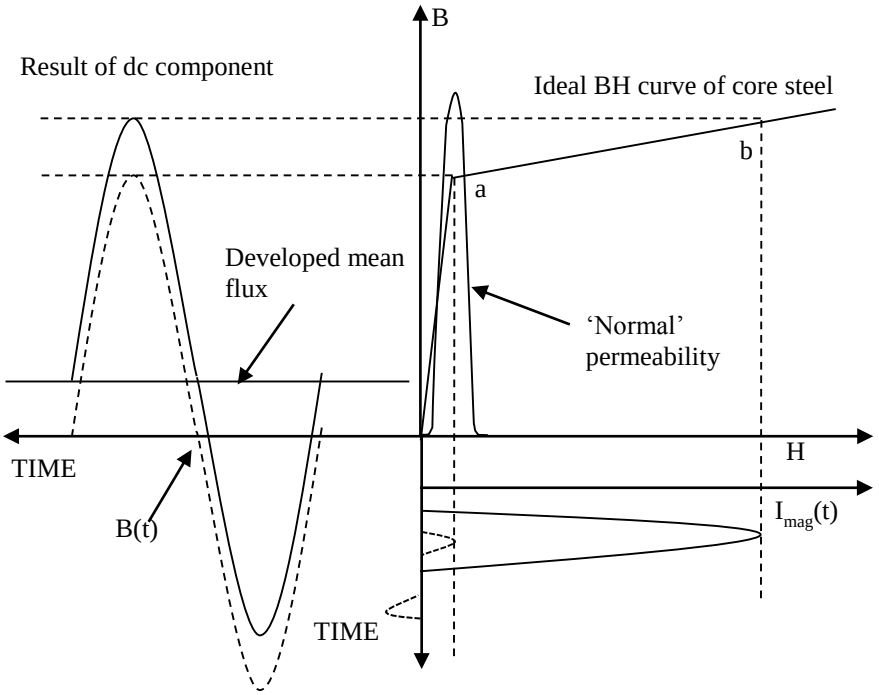

Figure 79: Widely used illustration of transformer core half-cycle saturation due to GIC/dc. Adapted from various reports (Boteler *et al.*, 1989; Tousignant *et al*., 1996; Bolduc *et al*., 2000; Lahtinen & Jarmo, 2002; Girgis & Vedante, 2012; McLyman, 2004)

The results from this thesis allow the depiction of half-cycle saturation to be extended to a consistent multi-parameter illustration. Figure 80 represents some of the relationships under steady state GIC or dc offset of the ac.

The widely used half-cycle saturation depiction (Figure 79) of the parameters related to the BH curve is adapted. The ac flux B(t) and dc component interaction is represented by the black waveform on the left side of Figure 80. When the transformer is driven beyond the knee of the BH curve, the relatively small (exciting) magnetizing current, shown by a green curve in the bottom right part of Figure 80, changes with dc offset to the I_{mag} (solid red) curve for a single-phase transformer. The dc offset creates a 'displaced zero' axis corresponding to a point on the linear part of the BH curve.

A simplified piecewise inductance model, as used in EMTP software (EMTDC/PSCAD, 2005), defines the knee point at the flux density B_n at rated voltage, with two linearized portions at $1.15B_n$ and $1.25B_n$ between the linear ideal operating BH curve and the air core characteristic, but such models often lack accuracy in saturation studies.

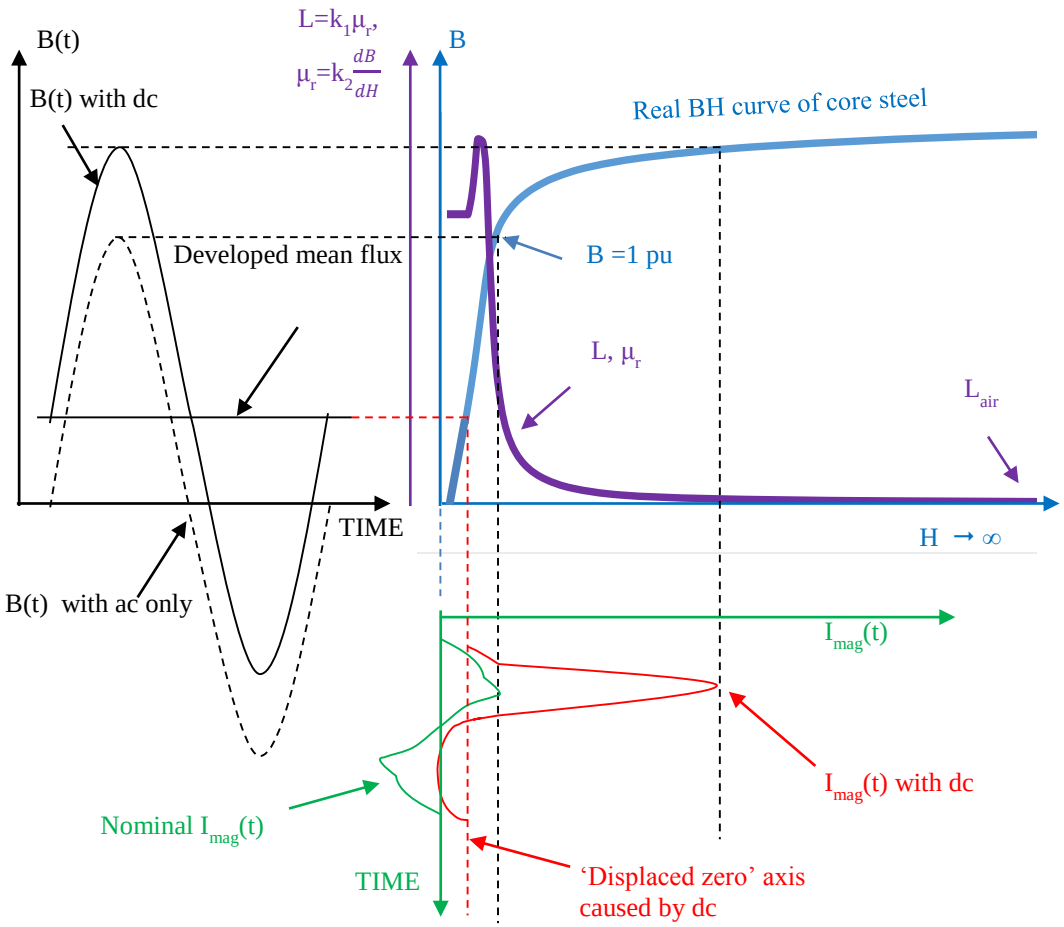

Figure 80: Parametric interplay during half -cycle saturation using a real BH curve and showing instantaneous transformer inductance

According to McLyman (2004) the knee point of the BH curve is where the tangent from the origin identifies the maximum 'normal' permeability ($\propto$ B/H), also called amplitude permeability (Thyssenkrupp, 2014). It should be noted that though the chosen knee point used in the experimental and simulation protocols was according to McLyman as a first approximation, a more accurate representation of the 'knee' is not a 'point' but rather a transition from linearity to saturation as shown from the real BH curve in Figure 80.

The permeability μ and relative permeability μ_r as defined by the local gradient (dB/dH) at any 'point' on the BH curve have a different maximum magnitude and location from that identified by the amplitude permeability.

The instantaneous inductance $L \propto d\varphi/di$ is directly proportional to μ and μ_r. Therefore, L, μ and μ_r follow the same shape with different scaling constants. μ_r tends to 1 and L tends to L_{air} as H tends to infinity, but these values are not reached even with high practical values of dc or GIC.

The shape and slope of μ_r and L were verified using several grades of power transformer electrical core steel. As a result, Figure 80 represents a real BH curve showing the saturation transition beyond the knee in the region of a-b of Figure 79.

Further, the instantaneous inductance and 'point' permeability before the knee are shown without the simplification of the BH curve usually depicted as two intersecting straight lines. This part of the profile is also consistent with the results of FEM simulations for $L_{terminal}$ and L_{aur} presented in Figure 75. (The derived curves in Figure 80 also applies to the partial saturation caused by ac over-excitation.)

10 CONCLUSIONS

This thesis started with the objective of gaining a better understanding of the response of transformers to GICs and stray dc and improving the modelling with simultaneous ac and dc excitation and identified that the spatial distribution of the flux is crucial for transformer engineers in the design for GIC resilience. The conclusions in this chapter represent significant advancements in achieving the answers regarding modelling transformers with simultaneous ac and dc excitation at power frequency.

10.1 Summary of the scope of the work

Two important aspects were identified in Chapter 2, the literature review. They are that most studies of transformer-GIC response used only simulation and modelling or practical testing and few reconciled both approaches; and most FEM model studies simplified the core joint details as being solid. Therefore, this thesis develops a rigorous modelling approach using extensive modelling with measurement data from exhaustive laboratory testing.

Chapter 3 expanded the theory on the computation of electromagnetic fields and the possibility of using of finite element matrix (FEM) models with simultaneously ac and dc components in the transient domain. It was decided that commercially available FEM software used in the transformer industry could be used for the research but needed to be tested.

Chapter 4 describes an opportunity taken to investigate a practical problem in industry. A customer-specified assessment of the GIC response of a large power transformer with a 3p3L core structure could not be made by practical testing because of the reactive power limitations at test facilities and anticipated damage to the generator (overheating due to large harmonics components of current). FEM modelling offered a first approximation of the transformer's half-cycle saturation response. The FEM analysis with ac and dc excitation revealed stray flux in the sides of the tank even with very small GIC in the HV windings. This was consistent with findings of some other researchers of saturation in 3p3L power transformers. However, small differences were seen between the FEM modelling results and some parameters of the factory acceptance tests.

Chapter 5 compared FEM analysis with practical laboratory measurements on three bench-scale transformers (with different core structures) energized with ac and dc. Using a FEM model representing the transformer joints as solid, the magnetizing currents are consistently under-estimated, leading to inaccurate Q-dc responses at relatively low levels of dc.

The research then focused on the analysis of 1p4L transformers. This transformer structure was chosen because banks of 1p4L transformers had recently been installed at a South African power station, representative 1p4L models are not available for power system analysis, and model transformers with the same core steel could procured for physical testing. Laboratory tests and 2D and 3D FEM modelling, with results and discussion are described in Chapters 6 to 9.

10.2 Answering the research questions

In Chapter 1, five research questions were posed to guide the testing of the hypothesis that "Test results from model transformers can augment the data from testing large power transformers in calibrating simulation models, particularly FEM models, to characterize the responses to quasi-dc currents of large power transformers energised at power frequency."

In the following paragraphs, the results of the research are applied to each research question.

What existing models of power transformers are useful in the modelling of their response to dc and power frequency ac voltages?

The literature review revealed that the following topological models exist and are useful for modelling transformers:

- 1p2L, 1p3L, 3p3L and 3p5L

These core structures above have also been research in the FEM domain, often being simplified to 2D even though some 3D simulations have been reported.

Very little has been reported regarding the 1p4L response with GIC/dc and this thesis presents some important findings in the modelling details in the FEM and magnetization parameters for input in the topological models.

How does the GIC phenomenon influence power systems, such that its effects, including overheating and reactive/non-active power absorption during ac-dc excitation, can be studied?

The mechanisms behind the influence of GIC were identified in Chapter 2.

The problems start in the transformer response to the GIC or leakage dc, with half-wave saturation, stray flux, noise, generation of harmonics, increased Q, power system stability and voltage depressions.

Stray flux contributes to possible overheating of windings, core, tank, and other metallic structural parts with possibility of degradation of the winding insulation and transformer oil.

Harmonics contribute to SVC, protection, overheating, and eddy currents.

The overheating leads to incipient transformer damage, and in severe cases transformer failure.

The increased Q contributes to potential loss of voltage stability and higher network losses.

Considering the above factors, various GIC studies can be undertaken through power system analysis using EMTP software (limited to the accuracy of the transformer models), developing topological models where needed, FEM analysis, and measurements on model transformers fabricated to resemble power transformers as closely as possible (as was done in this research).

Which transformer core structures have not been sufficiently studied in the context of GIC?

The most common core structures that have been investigated for GIC response in are the 1p3L, 3p5L, and 3p3L, resulting in the conclusions that their responses are dependent on their differing core structures. While there are other transformer core structures exist, the least understood core structure in the context of simultaneous ac-dc excitation is the 1p4L core structure. This observation was supported by the lack of a 1p4L topological model in EMTP/EMS software. Having identified this need, the main focus in experimentation and FEM modelling was the 1p4L core structure.

How can a previous bench-scale protocol (Chisepo et al., 2013) be adapted to investigate the testing in a laboratory or factory environment of larger test transformers, representative of power transformers?

When testing bigger model transformers (kVA range), the first and most important consideration is the capacity of the supply, relative to the ratings of the test transformers. The protocols regarding the verification of quality of supply, preliminary tests and main test protocol, and conducting experiments safely with high dc levels has been outlined in Chapter 6.

Chapter 6 outlined the various aspects of testing with dc. This is summarized below:

- Verification of quality of supply
- Preliminary tests
- Main test protocol and conducting the experiments safely with high levels of dc
- The nec installation of flux search coils

Experience from testing the model transformers in this research leads to the conclusion that it is not possible to test large transformers (MVA range) in a laboratory or factory environment. Very few field tests, however, have been reported, one of which has led to the testing of 3p3L and 3p5L transformer topological models (Zirka *et al*., 2018) but most utilities do not make the power transformers available for such testing.

In the absence of practical tests on power transformers, tests on model transformers can be used to validate and calibrate other models, such as FEM analysis.

What are the minimum modelling details needed to carry out FEM and related modelling of transformers subjected to GIC (and how does simplification affect the accuracy)?

It still remains a real challenge to actually perform GIC/dc tests on large power transformers. What is needed to overcome this barrier is a good FEM model and the minimum requirements are:

- Power transformer physical construction data
- FAT data
- modelling of the core joint details
- verification of accurate magnetizing currents
- incorporation of core nonlinearity and hysteresis

Meeting these requirements forms the basis for deriving the response of power transformers with a great degree of confidence in the accuracy and this can be extended to more specific investigations depending on the availability of computing resources and input data.

10.3 Assessing the hypothesis

Having assessed all the answers to the research questions, the finding is that the hypothesis is not strictly valid. It is still not possible to test large power transformers in a factory and there is a paucity in field tests' data, therefore, reliance must be placed on 3D FEM models calibrated with selected parameters from FATs on large power transformers and physical tests on smaller, model transformers. It is necessary that the model transformers replicate key characteristics of the power transformer including joint details.

10.4 Limitations

The model transformers used in this study had butt joints. This resulted from limitations in the manufacturer's factory whereby the stacking beds for mitred laminations were designed for large power transformers used in transmission networks. Due to the much smaller size of these model transformers, the only alternative was to resort to butt joint stacking. A good finding from this limitation, one that the manufacturer did not appear to be aware of, was that the calculated (design) nameplate ratings will most certainly require de-rating should a model transformer be needed in experiments involving linear ac operation.

The practical testing and FEM simulation confirmed that the non-step lap butt joints in the laboratory model transformers significantly influence the performance of the transformers. Therefore, appropriate step-lap mitred joint structures should be provided in any laboratory-scale transformers used to investigate the ac-dc performance of large power transformers in future investigations.

The arrangement of the dc injection circuit employed in the measurements as shown in Figure 38 has the limitation of giving magnetizing currents that have a mean current I_0 of approximately zero (at any level of dc injection). This can be seen from inspection of the corresponding measured current waveforms in Figure 66. I_0 carries characteristic information of the GIC and can be used to derive electrical equivalent topological models. The validated FEM 1p4L model, however, can be used to acquire the correct I_0 values should they be needed in other topological modelling studies outside the scope of this thesis. Placing the ac and dc on the same side to emulate the equivalent of the test method by Lahtinen and Elovaara (2002) results in the FEM calculated waveform in Figure 81. It can be seen that a dc of 9 A results in an I_0 of 10.07A ($\neq$0).

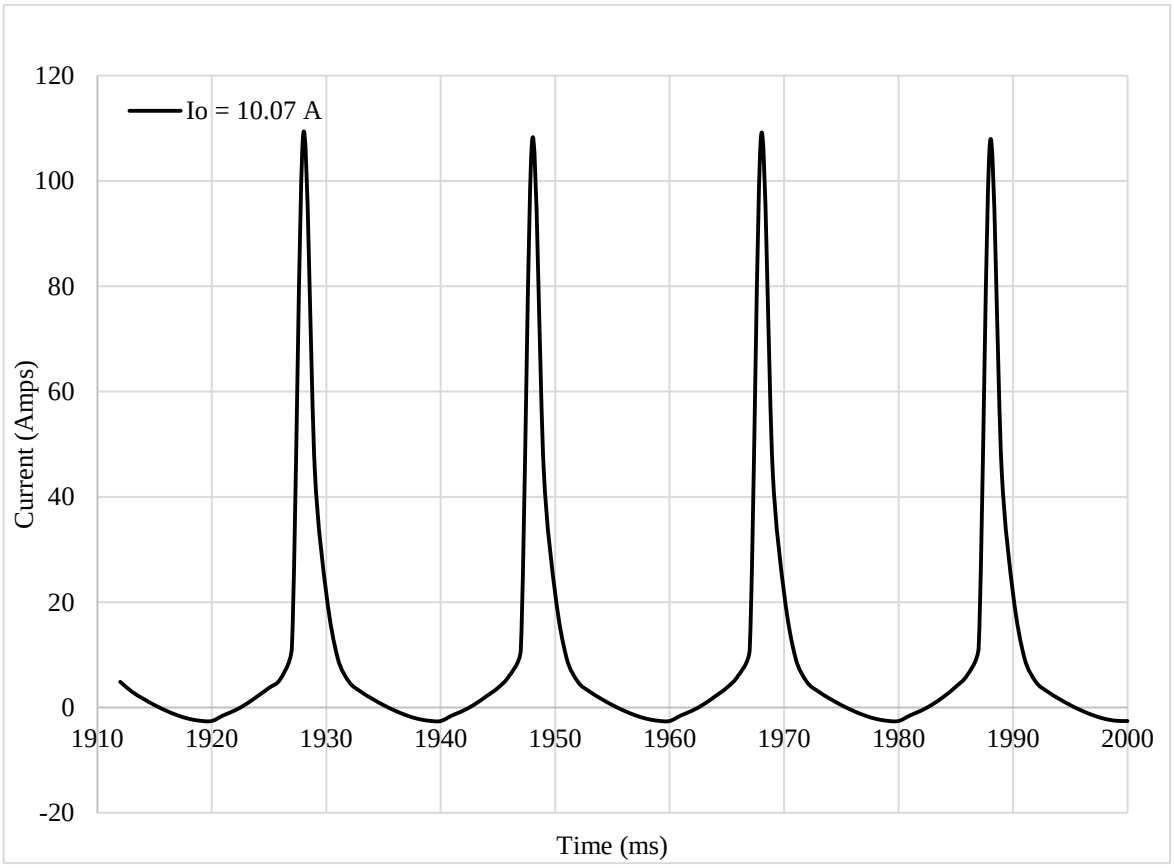

Figure 81: The effect of simulating with ac and dc on the same side in the FEM to derive I_0 for topological modelling studies

Though the FEM can facilitate magnetic anisotropy in the calculations, the actual data was not available from the manufacturer at the time of the study and might be investigated when laboratory models with mitred joints become available for testing and modelling.

The modelling of effects of other metallic parts in the preliminary investigation of a 40 MVA power transformer in Chapter 4 is outside the scope of this thesis due to the lack of data and a perceived need to focus on the primary effect of the core. This research focuses on the untanked 1p4L units which were manufactured deliberately without any metallic structural parts.

Finally, the FEM modelling technique derived in this thesis (incorporating iterative calibration with equivalent air gaps, as sufficiently demonstrated for the 1p4L models) cannot be applied to the 40 MVA because of the lack of required data from the manufacturer. Further studies on scaled down model three-phase units with the required mitred joint configuration information and ac-dc tests are, therefore, reserved for future work to exemplify the applicability of the developed techniques in this research.

10.5 Contributions

This work contributes to better understanding of the effects of dc excitation and the influence of GICs in transformers. It is particularly relevant to the transformer industry and research efforts. The findings of. large international groups such as the IEEE TASS Task Force for GIC/Slow Transients that have published several recent transformer-GIC papers (Jazebi *et al*., 2016) are now supported by measurement and simulation from this thesis regarding saturation inductance. A foundation has been provided for the further modelling and testing of model transformers in ways that are not yet possible with large power transformers.

The contribution is based on two approaches of physical measurement and FEM modelling that achieve coherent results under complex conditions of ac and dc. An extension from the FEM modelling aids in magnetization characteristics parameterization for topologically derived transformer models for GIC.

Three particular contributions of this study are identified below.

10.5.1 Transformer-GIC core joint modelling

It is essential to model the magnetizing current and core loss accurately under no load at nominal ac excitation. This can be achieved for the 2D case by replacing solid core joints with "equivalent air gaps" at the joints calibrated using physical transformer no load data readily provided by manufacturers. The 3D simulation is necessary for more accurate ac-dc responses, and explicit lamination detail is only necessary close to the core surface, while the rest of the core can be modelled with "equivalent air gaps" at the joints, as was observed for the 1p4L transformers.

10.5.2 $L_{terminal}$ and L_{air} and the composite parametric depiction of half

The measurements and FEM simulations have provided further insight to the clear difference between $L_{terminal}$ and L_{air}. In the context of GIC, the more suitable parameter for input into any single-phase topological model is $L_{terminal}$. This is further clarified by relating the statistically achievable GIC magnitudes to the level of saturation in a transformer being far from "air core" operation, even at "very high GIC." The implications are better accuracy in power systems modelling with GIC and instability.

10.5.3 The composite parametric half-cycle saturation depiction

The relationship in the time domain between the input voltage and magnetizing current through the B-H curve, illustrated in Figure 80, provides information about the shape and slope of a transformer's inductance and relative permeability. The instantaneous inductance L falls sharply as the gradient of the BH curve changes and tends to L_{air} but L_{air} is not reached in practice.

It is seldom reported that the transformer Q-GIC characteristic is not strictly linear moving from partial to deep saturation (Rezaei-Zare, 2015b). Figure 75 and Figure 80 from this thesis can be used to explain the non-linearity of L, its effect on Q-GIC, and implications for power system stability studies.

10.6 Summary

In summary, this work achieved the objective of improving the understanding of transformer response to the GIC phenomenon. It added to the theoretical knowledge of the leakage flux distribution with simultaneous ac and dc, and refined the already available information on the topic. It points to areas for future research in extending investigations of the characteristics of large power transformers.

11 REFERENCES

Adhikari, S., Mueller, D., Walling, R. & 0'Laughlin, A. J., 2017. *A comprehensive study of geomagnetic disturbance (GMD) system impact.* Chicago, IL, 2017 IEEE Power & Energy Society General Meeting.

AK Steel Corporation, 2007. *Selection of electrical steels for magnetic cores,* Ohio: AK Steel.

Albertson, V. D. Bozoki, B, Feero, W. E., Kappenman, J. G., Larsen, E. V., Nordell, D. E., Ponder, J., Prabhakara, F. S., Thompson, K. & Walling, R., 1993. Geomagnetic Disturbance Effects on Power Systems. *IEEE Transactions on Power Delivery,* July, 8(3), pp. 1206-1216.

Babaeiyazdi, I., Rezaei-Zare, M. & Rezaei-Zare, A., 2019. Wind Farm Operating Conditions under Geomagnetic Disturbance. *Transactions on Power Delivery,* in press, pp. 1-1.

Berge, J., 2011. *Impact of Geomagnetically Induced Currents on Power Transformers,* Ontario: PhD Thesis, University of Western Ontario.

Berge, J., Marti, L. & Varma, R. K., 2011. *Modelling mitigation of geomagnetically induced currents on a realistic power system.* Winnipeg, MB. Canada. IEEE Electrical Power and Energy Conference (EPEC).

Berge, J., Varma, R. K. & Marti, L., 2011. *Laboratory validation of the relationship between Geomagnetically Induced Current (GIC) and transformer absorbed reactive power.* Winnipeg,MB. Canada. IEEE Electrical Power and Energy Conference (EPEC).

Bergsåker, C., 2014. *Impact of transformer core size on the reactive power requirement of power transformers due to GIC,* Stockholm: KTH.

Bertotti, G., 1988. General properties of power losses in soft ferromagnetic materials. *IEEE Transactions on Magnetics,* 24(1), pp. 621-630.

Bíró, O., 1999. Edge element formulations of eddy current problems. *Computational Methods in Applied Mechanics and Engineering,* 169(3-4), pp. 391-405.

Bíró, O., Außerhofer, S., Buchgraber, G., Preis, K. & Seitlinger, W, 2007. Prediction of magnetising current waveform in a single-phase power transformer under DC bias. *IET Science, Measurement & Technology,* 1(1), pp. 2-5.

Bíró, O., Buchgraber, G., Leber, G. & Preis, K., 2008. Prediction of Magnetizing Current Wave-Forms in a Three-Phase Transformer Under DC Bias. *IEEE Transaction on Magnetics,* June, 44(6), pp. 1554-1557.

Bíró, O., Kockza, G., Leber, G., Preis, K. & Wagner, B., 2014. Finite Element Analysis of Three-Phase Three Limb Power Transformers under DC Bias. *IEEE Transaction on Magnetics,* February, 50(2), pp. 565-568.

Blooming, T. M. & Carnovale, D. J., 2006. *Application of IEEE STD 519-1992 Harmonic Limits.* Appelton,WI. In Pulp and Paper Industry Technical Conference.

Bolduc, L., Gaudreau, A. & Dutil, A., 2000. Saturation time of transformers under dc excitation. *Electric Power Systems Research,* Volume 56, pp. 95-102.

Borrill, L. D., Chisepo, H. K. & Gaunt, C. T., 2016. *Flux measurements with AC and DC components of current present show transformer equivalent circuit models need core joint details.* Wollongong, NSW. IEEE International Conference on Power System Technology (POWERCON).

Boteler , D. H., Shier, R. M., Watanabe, T. & Horita, R. E., 1989. Effects of geomagnetically induced currents in the B.C. Hydro 500 kV system. *IEEE Transactions on Power Delivery,* 4(1), pp. 818-823.

Boteler, D. H. & Pirjola, R. J., 1997. *Nature of the Geoelectric Field associated with GIC in Long Conductors such as Power Systems, Pipeline sand Phone Cables.* Beijing, International Symposium.

Brailsford, F. & Fogg, R., 1964. Anomalous iron losses in cold reduced grain-oriented. *Proceedings of IEEE,* 111(8), pp. 1463-1467.

Brebbia, C. A., Telles, J. C. F. & Wrobel, L. C., 1984. *Boundary Element Techniques: Theory and application in engineering.* 1st ed. Berlin: Springer-Verlag.

Calabrò, S., Coppadoro, F. & Crepaz, S., 1986. The Measurement of the Magnetization Characteristics of Large Power Transformers and Reactors. *IEEE Transactions on Power Delivery,* PWRD-1(4), pp. 224-234.

Campbell, C. F. & Weber, R. J., 1992. *Two dimensional finite difference method for the analysis of piezoelectric devices.* Tucson, AZ. IEEE Ultrasonics Symposium.

CENTRA Techonology Inc., 2011. *Future Global Shocks: Geomagnetic Storms,* Paris: Organisation for Economic Co-operation and Development.

Chen, C., 1986. *Magnetism and metallurgy of soft magnetic materials.* 2nd ed. New York: Dover Publications.

Cheng, D. K., 1989. *Field and Wave Electromagnetics.* 2nd ed. Boston: Addison-Wesley.

Cheng, Y. & Pillay, P., 2002. *An Improved Formula for Lamination Core Loss Calculations in Machines operating with high frequency and high flux density excitation.* Pittsburgh, Industry Applications Conference 37th IAS Annual Meeting.

Chen, Z., Bai, B., Chen, D. & Chai, W., 2018. Direct-current and Alternate-decay-current Hybrid Integrative Power Supplies Design Applied to DC Bias Treatment. *IEEE Transactions on Power Electronics (Early Access),* In Press (1), pp. 1-1.

Cherry, E. C., 1948. The duality between interlinked electric and magnetic circuits and the formation of transformer equivalent circuits. *Proceedings of the Physical Society,* 62(2), pp. 101-11.

Chien, J. & Chung, H., 2018. Rapid beverage cooling analysis. *Engineering Edge: Accelerate Design Innovation,* 7(1), pp. 82-83.

Chisepo, H., 2014. *The response of transformers to geomagneticaly induced-like currents,* Cape Town: MSc(Eng) Dissertation, University of Cape Town.

Chisepo, H. K., 2015. *Finite element model of a three-phase three limb power transformer with GIC-like current.* Stellenbosch, ANSYS® Convergence 2015 Regional Conferences.

Chisepo, H. K., Borrill, L. D. & Gaunt, C. T., 2016. *Measurements and finite element model of transformer core joints with dc and ac excitation.* La Toja Island, Spain. Advanced Research Workshop on Transformers (ARWtr2016).

Chisepo, H. K., Borrill, L. D. & Gaunt, C. T., 2017. *An evaluation of learning through research: the journey of two doctoral students in the same field of interest.* Stellenbosch, SAUPEC.

Chisepo, H. K., Borrill, L. D. & Gaunt, C. T., 2018. Measurements show need for transformer core joint details in finite element modelling of GIC and dc effects. *The International Journal for Computation and Mathematics in Electrical and Electronic Engineering,* 37(3), https://doi.org/10.1108/COMPEL-11-2016-0511), pp. 1011-1028.

Chisepo, H. K., Borrill, L. D. & Gaunt, C. T., 2019, *Measurements and FEM analysis on DC/GIC effects on transformer magnetization parameters*. Milan, IEEE PowerTech Conference.

Chisepo, H. K., Gaunt, C. T. & Oyedokun, D. T. O., 2013. *Testing the response of laboratory bench-scale transformers to geomagnetically induced-like transformers.* Potchefstroom, Southern African Power Universities' Engineering Conference .

Corea-Araujo, J. A., Martinez-Velasco, J. A., Gonzàlez-Molina, F., Barrado-Rodrigo, J. A., Guasch-Pesquer, L. & Castro-Arand, F., 2017. Validation of a single-phase transformer model for ferroresonance. *Springer: Electrical Engineering.*

Costabel, M., 1986. *Principles of Boundary Element Methods,* Darmstadt: Technische Universität Darmstadt.

Cullity, B. D. & Graham, C. D., 2009. *Introduction to Magnetic Materials.* 2nd ed. New Jersey: John Wiley & Sons.

Croegeart, M., 2017. Rocket science and FloMaster. *Engineering Edge: Accelerate Innovation with CFD & Thermal Characterization,* 6(2), pp. 38-41.

Czech, P., Chano, S., Huynh, H. & Dutil, A., 1992. *The Hydro-Québec System Blackout of March 1989: System Response to Geomagnetic Disturbance.* Carlifornia, s.n., pp. 19-1 - 19-21.

de León, F., Farazmand, A. & Joseph, P., 2012. Comparing the T and π equivalent circuits for the calculation of transformer inrush currents. *IEEE Transactions on Power Delivery,* 27(4), pp. 2390-2398.

de León, F., Jazebi, S. & Farazmand, A., 2014. Accurate measurement of the Air-Core Inductance of Iron-Core Transformers with a Non-ideal Low Power Rectifier. *IEEE Transactions on Power Delivery,* 29(1), pp. 294-296.

Dong, X., Liu, Y. & Kappenman, J., 2001. *Comparative analysis of exciting current harmonics and reactive power consumption from GIC saturated transformers.* Columbus, OH. IEEE Power Engineering Society Winter Meeting.

Dowell, P. L., 1966. Effects of eddy currents in transformer windings. *Proceedings of the Institution of Electrical Engineers* , 113(8), pp. 1387-1394.

Dupont, 2017. *Nomex Paper.* [Online]
Available at: http://www.dupont.co.za/products-and-services/personal-protective-equipment/thermal-protective-apparel-accessories/brands/nomex/products/dupont-nomex-paper.html
[Accessed 11 08 2017].

Elleuch, M. & Poloujadoff, M., 1998. New Transformer Model Including Joint Air Gaps and Lamination Anisotropy. *IEEE Transactions on Magnetics,* 5(5), pp. 3701-3711.

EMTDC/PSCAD, 2005. *Classical Approach, Saturation Characteristic,* Manitoba, Canada: HVDC Research Centre.

Etemadi, A. H. & Rezaei-Zare, A., 2014. Optimal Placement of GIC Blocking Devices for Geomagnetic Disturbance Mitigation. *IEEE Transactions on Power Systems,* 29(6), pp. 2753-2762.

FERC, 2015. *Reliability Standard for Transmission System Planned Performance for Geomagnetic Disturbance Events,* USA: Federal Energy Regulation Commission Docket No. RM15-11-00.

Ferreira, J. A., 1994. Improved Analytical Modeling of Conductive Losses in Magnetic Components. *IEEE Transactions on Power Electronics,* 9(1), pp. 127-131.

Gaunt, C. T., 2014. Reducing uncertainty - responses for electricity utilities. *Journal of Space Weather and Space Climate,* 4(A01), pp. 1-7.

Gaunt, C. T. & Coetzee, G., 2007. *Transformer failures in regions incorrectly considered to have low.* Lausanne, Switzerland, IEEE PowerTech.

Gaunt, C. T. & Malengret, M., 2012. *Why we use the term non-active power.* Johannesburg, Power Engineering Society Conference and Exposition in Africa (PowerAfrica).

Girgis, R. & Vedante, K., 2012. *Effects of Geomagnetically Induced Currents on Power Transformers and Power Systems.* Orlando, FL. IEEE PES Transmission and distribution conference and exposition.

Girgis, R., Verner, J. & Hoffman, G., 2016. *Establishing Power Transformers Capability while under Geomagnetic Disturbances.* Paris, A2-202 Cigré.

Gong, R., Ruan, J., Chen, J., Quan, Y., Wang, J. & Jin, S., 2017. A 3-D Coupled Magneto-Fluid-Thermal Analysis of a 220 kV Three-Phase Three-Limb Transformer under DC bias. *Energies,* 23 March, 10(4), pp. 422-431.

Goss, N. P., 1934. *Electrical sheet and method and apparatus for its manufacture and test.* USA, Patent No. 1,965,559.

Griffiths, D. J., 1999. *Introduction to Electrodynamics.* 3rd ed. New Jersey: Prentice Hall International.

Guillaume, L. & Leconte, V., 2016. *Use of Specific Finite Element Methods to Compute Load and no Load Losses in a Power Transformer.* La Toja Island, Spain. Advanced Research Workshop on Transformers.

Hastenrath, M., 2014. *Production, properties and new developments in the manufacturing of GO Electrical Steel.* Pretoria, ThyssenKrupp Electrical Steel.

Heindl, M., Beltle, M., Reuter, M., Schneider, D. & Tenbohlen, S., 2011. *Investigation of GIC related effects on power transformers using modern diagnostic methods.* Hannover, XVII International Symposium on High Voltage Engineering.

Hihat, N., Napieralska-Juszczak, E., Lecointe, J., Sykulski, J. & Komeza, K., 2011. Equivalent Permeability of Step-Lap Joints of Transformer Cores: Computational and Experimental Considerations. *IEEE Transactions on Magnetics,* 47(1), pp. 244-251.

Hock-chuian, T. & Swift, G. W., 1984. A Novel Method of Detecting Asymmetrical Transformer Core Saturation due to GIC. *IEEE Transactions of Power Apparatus and Systems,* Jan, PAS-103(1), pp. 183-189.

Hofstadter, R., 1994. *Felix Bloch 1905-1983.* 1st ed. Washington D.C.: National Academy of Sciences.

Holling, G., 2018. Simulation is Key to Design of High-efficiency Low-cost Synchronous Reluctance Motor. *Engineering Edge: Accelerate Design Innovation,* 7(1), pp. 88-90.

Hutchins, T. R. & Overbye, T. J., 2011. *The effect of geomagnetic disturbances on the electric grid and appropriate mitigation strategies.* Boston, North American Power Symposium (NAPS).

IEEE Std ™ C57.163, 2015. *IEEE Guide for Establishing Power Transformer Capability while under Geomagnetic Disturbances.* USA: IEEE.

Infolytica Corporation, 2015. *Symmetric Coils.* [Online]
Available at: http://www.infolytica.com/secured/customer/elite/livedocs/MagNet/#06-Coils/USC-SpecializedTopics/SymmetricCoils.htm?Highlight=Symmetric coil
[Accessed 7 October 2015].

Infolytica Corporation, 2017a. *Transient solver, Formulation, three-dimensional case.* [Online]
Available at: https://www.infolytica.com/secured/customer/elite/livedocs/MagNet/#10-Solving/BSO-Transient/Formulation.htm%3FTocPath%3DSolving%7CTransient%2520solvers%7C_____7
[Accessed 22 May 2017].

Infolytica Corporation, 2017b. *Energy Calculation.* [Online]
Available at: https://www.infolytica.com/secured/customer/elite/livedocs/MagNet/#11-Results/03-GlobalResults/02-Energy/01-Calculation.htm%3FTocPath%3DResults%7CGlobal%2520results%7CEnergy%7C_____1
[Accessed 11 October 2017].

Ionel, D. M., Popescu, M., McGlip, M. I., Miller, T. J. E., Dellinger, S. J. & Heidman, R. J., 2007. Computation of Core Losses in Electrical Machines Using Improved Models for Laminated Steel. *IEEE Transactions on Industry Applications,* 43(6), pp. 1554-1563.

Jazebi, S., de León, F. & Farazmand, D. D., 2013. Dual Reversible Transformer Model for the Calculation of Low-Frequency Transients. *IEEE Transactions on Power Delivery,* 28(4), pp. 2509-2517.

Jazebi, S., Zirka, S. E., Lambert, M., Rezaei-Zare, A., Chiesa, N., Moroz, Y., Chen, X., Martinez-Duro, M., Arturi, C. M., Dick, E. P., Narang, A., Walling, R. A., Mahseredjian, J., Martinez, J. A. & de León, F., 2016. Duality-Derived Transformer Models for Low-Frequency Electromagnetic Transients - Part II: Complementary Modeling Guidelines. *IEEE Transactions on Power Delivery,* 31(5), pp. 2420-2430.

Jensen, B. B., Guest, E. D. & Mecrow, B. C., 2015. Modeling Overlapping Laminations in Magnetic Core. *IEEE Transactions on Magnetics,* 51(6), pp. 1-6.

Jin, J., 2002. Maxwell's Equations. In: *The Finite Element Method in Electromagnetics.* New York: John Wiley and Sons, pp. 5-6.

Jones, M. A. & Moses, A. J., 1974. Comparison of localized power loss and flux distribution in butt and lap mitred overlap corner configurations. *IEEE Transactions on Magnetics,* MAG-10(2), pp. 321-326.

Jones, M. A., Moses, A. J. & Thompson, J. E., 1973. Flux distribution and power loss in the mitered overlap join in power transfomer cores. *IEEE Transactions on Mangetics,* MAG-9(2), pp. 114-122.

Judd, M. D., 2000. *Using Finite Difference Time Domain Techniques to Model Electrical Discharge Phenomena.* Victoria, Annual Report Conference on Electrical Insulation and Dielectric Phenomena.

Kappenman, J. G. & Albertson, V. D., 1990. Bracing for the geomagnetic storms. *IEEE Spectrum*, March, 27(3), pp. 27-33.

Kappenman, J. G., Norr, S. R., Sweezy, G. A., Carlson, D. L., Albertson, V. D., Harder, J. E. & Damsky, B L., 1991. GIC mitigation: a neutral blocking/bypass device to prevent flow of GIC in power systems. *IEEE Transactions on Power Delivery*, 6(3), pp. 1271-1281.

Khelil, M. & Elleuch, M., 2009. *Modeling of the Air-Gaps of Overlapped Joints in Three-Phase Transformer Iron core for using by FEM.* Djerba, Tunisia, 6th International Multi-Conference on Systems, Signals and Devices.

Koen, J. & Gaunt, C. T., 2002. *Disturbances in the Southern African Power Network due to Geomagnetically Induced Currents.* Paris, Cigré Session.

Kohli, S., Mahajan, S. B., Sanjeevikumar, P., Fedák, V. & Oleshuk, V., 2018a. *Imact of DC Bias on the Magnetic Loading of Three Phase Three Limb Transformer Based on Finite Element Method.* 1st ed. Singapore: Springer.

Kohli, S., Mahajan, S. B., Badave, S. M., Sanjeevikumar, P. & Iqbal, A., 2018b. *Determination of Magnetic Loading of Three-Phase Five-Limb Transformer with Impact of DC Offset.* 1st ed. Singapore: Springer.

Kulkarni, S. V. & Khaparde, S. A., 2013. *Transformer Engineering: Design, Technology and Diagnostics.* 2nd ed. Boca Raton, FL. CRC Press Taylor & Francis Group.

Lahtinen, M. & Elovaara, J., 2002. GIC Occurrences and GIC Test for 400 kV System Transformer. *IEEE Transactions on Power Delivery,* 17(2), pp. 555-561.

Liu, Y., Leng, D., Tian, Z. & Cheng , W., 2013. DC Bias Simulation of 750 kV Autotransformer Based on ANSYS Maxwell. *High Voltage Engineering,* 39(1), pp. 218-225.

Lu, S. & Liu, Y., 1993a. FEM Analysis of dc saturation to assess transformer susceptibility. *IEEE Transactions on Power Delivery,* 8(3), pp. 1367-1376.

Lu, S. & Liu, Y., 1993b. *Study of power transformer excitation under GIC.* Detroit, IEEE Proceedings of the 36th Midwest Symposium on Circuits and Systems, pp. 725-731.

Malengret, M. & Gaunt, C. T., 2011. General theory of instantaneous power for multi-phase systems with distortion, unbalance and direct current systems with distortion, unbalance and direct current components. *Electric Power Systems Research,* 81(10), pp. 1898-1904.

Malengret, M. & Gaunt, C. T., 2012. General theory of average power for multi-phase systems with distortion, unbalance and direct current components. *Electric Power Systems Research,* 84(1), pp. 224-230.

Malik, N. H., 1989. A Review of the Charge Simulation Method. *IEEE Transactions on Electrical Insulation,* 24(1), pp. 3-20.

Marti, L., Berge, J. & Varma, R. K., 2013. Determination of geomagnetically induced current flow in a transformer from reactive power absorption. *IEEE Transcactions on Power Delivery* , 28(3), pp. 1208-1288.

Martindale, C. F., Verrinder, R. A. & Gaunt, C. T., 2014. *Proof-of-concept data logger for non-active power.* Romania, IEEE 49th International Universities Power Engineering Conference (UPEC).

Maruvada, P. S. & Drogi, S., 1988. Field and ion interaction of hybrid ac/dc transmission lines. *IEEE Transactions on power delivery,* 3(3), pp. 1165-1172.

Masoum, M. A. S. & Moses, P. S., 2008. *Influence of Geomagnetically Induced currents on Three-Phase Power Transformers.* Sydney, Australasian Universities' Power Engineering Conference, pp. 1-5.

Masoum, M. A. S. & Moses, P. S., 2010. Impact of balanced and unbalanced direct current bias on harmonic distortion generated by asymmetric three-phase three-leg transformers. *IET Electric Power Applications,* August, 4(7), pp. 507-515.

McLyman, C. W., 2004. *Transformer and Inductor Design Handbook.* 3rd ed. New York: Marcel Dekker.

Mechler, G. D. & Girgis, R. S., 2000. Magnetic Flux Distributions in Transformer Core Joints. *IEEE Transactions on Power Delivery* , 15(1), pp. 198-203.

MIT Press, 1944. *Magnetic circuits and transformers.* 2nd ed. New York: John Wiley & Sons.

Mohammed, O. A., Abed, N. Y. & Liu, S., 2006. Investigation of the Harmonic Behaviour Under Nonsinusoidal Operation Using Finite Element and Wavelet Packets. *IEEE Transactions on Magnetics* , 42(4), pp. 967-970.

Molinski, T. S., 2002. Why utilities respect geomagnetically induced currents. *Journal of Atmospheric and Solar-Terrestrial Physics,* 64(16), pp. 1765-1778.

Moodley, N., 2013. *Power Transformer Health Assesment Derived From Low Energy and Dissolved Parameters.* PhD(Eng) Thesis.

Moodley, N. & Gaunt, C. T., 2017. Low Energy Degradation Triangle for power transformer health assessment. *IEEE Transactions on Dielectrics,* 24(1), pp. 639-646.

Mousavi, S. A., 2012. *Electromagnetic modelling of power transformers with dc magnetization,* Stockholm: KTH Licentiate Thesis.

Mousavi, S. A., Engdahl, G. & Agheb, E., 2011. Investigation of GIC effects on core losses in single phase power transformers. *Archives of Electrical Engineering* , 60(1), pp. 35-47.

Mulasalihović, E., Pfützner, H., Traxler, S. & Yamaguchi, H., 2008. Effects of geomagnetically induced currents on the magnetic performance of transformer cores. *Journal of Magnetism and Magnetic Materials,* 320(20), pp. 920-924.

Nakata, T. & Kawase, Y., 1986. Analysis of Magnetic Characteristics of Laminated Cores for Establishing and Accuracy Standard of Joint Dimension. *Electrical Engineering in Japan,* 106(1), pp. 48-56.

Nakata, T., Takashi, N. & Kawase, Y., 1982. Magnetic performance of step-lap joints in distribution transformer cores. *IEEE Transactions on Magnetics* , 6(6), pp. 1055-1057.

Ney, M. M., 1985. Method of Moments as Applied to Electromagnetic Problems. *IEEE Transactions on Microwave Theory and Techniques,* MTT-33(10), pp. 972-980.

NERC, 2012. *Special reliability assessment interim report: Effects of detailed calculation of geomagnetically induced currents in transmission networks,* Atlanta, GA: North American Electric Reliability Corporation.

NERC Standard, 2017. *TPL-007-2 - Transmission system planned performance for geomagnetic events,* Atlanta, GA: North American Electric Reliability Corporation.

NRS 048-2:2003, 2003. *Electricity Supply - Quality of Supply.* Johannesburg: NERSA.

Olivares-Galván, J. C., Georgilakis, P. S. & Ocon-Valdez, R., 2009. A Review of Transformer Losses. *Electric Power Components and Systems,* 37(9), pp. 1046-1062.

Oyedokun, D. T. O., 2015. *Geomagnetically Induced Currents (GIC) in large power systems including transformer time response,* South Africa: PhD(Eng) Thesis Univerisity of Cape Town.

Picher, P., Bolduc, L., Dutil, A. & Pham, V. Q., 1997. Study of the acceptable dc current limit in core-form power transformers. *IEEE Transactions on Power Delivery ,* 12(1), pp. 257-265.

Pinto, L. M. V. G., Szczupak, J., Drummond, L. H. & Barreto, L. M., 2005. *Geomagnetically induced currents: The ultimate threat to system security.* Russia, IEEE PowerTech .

Polycarpou, A. C., 2006. *Introduction to the Finite Element Method in Electromagnetics.* 1st ed. San Rafael, CA: Morgan & Claypool.

Price, P. R., 2002. Geomagnetically induced current effect on transformers. *IEEE Transactions on Power Delivery,* October, 8(3), pp. 1002-1008.

Pry, R. H. & Bean, C. P., 1958. Calculations of energy loss in magnetic sheet material using a domain model. *Journal of Applied Physics,* Volume 29, pp. 532-533.

Raith, J. & Ausserhofer, S., 2014. *GIC Strength verification of power transformers in a high voltage laboratory.* Cape Town, UCT GIC Workshop.

Ramírez-Niño, J., Haro-Hernàndez, C., Rodriguez-Rodriguez, J. H. & Mijarez, R., 2016. Core saturation effects of geomagnetic induced currents in power transformers. *Journal of Applied Research and Technology,* 14(2), pp. 87-92.

Razaei-Zare, A., 2014. Behavior of Single-Phase Transformers Under Geomagnetically Induced Current Conditions. *IEEE Transactions on Power Delivery,* 29(2), pp. 916-925.

Rezaei-Zare, A., 2015a. Enhanced transformer model for low- and mid-frequency transients - Part I: Model Development. *IEEE Transaction on Power Delivery,* January, 30(1), pp. 307-315.

Rezaei-Zare, A., 2015b. Enhanced transformer model for low- and mid-frequency transients - Part II: Validation and simulation results. *IEEE Transaction on Power Delivery,* January, 30(1), pp. 316-325.

Schrijver, C. J. & Mitchell, S. D., 2013. Disturbances in the U.S. electric grid associated with geomagnetic activity. *Journal of Space Weather and Space Climate,* 3(A19), pp. 1-7.

Sen, P. C., 1997. *Principles of Electric Machines and Power Electronics.* 2nd ed. Ontario: John Wiley & Sons.

Simon, M., 2013. *Estimation of Geomagnetically Induced Currents (GICS) in the Namibian transmission network,* South Africa: MSc(Eng) Dissertation, University of Cape Town.

Sod, A., 1978. A survey of several finite difference methods for systems of nonlinear hyperbolic conservation laws. *Computational Physics,* 27(1), pp. 1-31.

Taguchi, S., Yamamoto, T. & Sakakura, A., 1974. New Grain Silicon Stell with High Permeability. *IEEE Transactions on Magnetics*, 10(2), pp. 123-127.

Takasu, N., Oshi, T., Miyawaki, F., Saito, S. & Fujiwara, Y., 1994. An experimental analysis of dc excitation of transformers by geomagnetically induced currents. *IEEE Transactions on Power Delivery,* April, 9(2), pp. 1173-1182.

Tang, Q., Guo, S. & Zhongdong, W., 2015. Magnetic flux distribution in power transformer core with mitred joints. *Journal of Applied Physics,* 117(17), pp. 17D522-1:17D522-4.

Tenbohlen, M., Betle, M. & Gnädig, M., 2013. *Influence of dc on transformers,* University of Stuttgart: Research Presentation.

Thomson, A., Gaunt., C. T., Cilliers, P., Wild, J. A., Opperman, B., McKinell, L. A., Kotze, P. & Ngwira, C. M,. 2010. Present Challenges in understanding the geomagnetic hazard to national power grids. *Advances in Space Research,* 45(9), pp. 1182-1190.

Thyssenkrupp, 2014. *PowerCore® C 110-23 grain oriented electrical core steel data sheet,* Duisburg, Germany.

Tousignant, D., Bolduc, L. & Dutil, A., 1996. A method for the indication of power transformer saturation. *Electric Power Systems Research,* 37(2), pp. 115-120.

Wang, S., Li, L., Zhao, X. & Xie, Y., 2017. Fixed-point time periodic FEM taking into account hysteresis characteristics of laminated core under dc bias. *International Journal of Applied Electromagnetics and Mechanics ,* 55(2), pp. 289-300.

Webb, J. P. & Forghani, B., 1995. T-Ω method using hierarchal edge elements. *IEEE Proceedings - Science, Measurement and Technology,* 142(2), pp. 133-141.

Wik, M., Pirjola, R., Lundstedt, H., Viljanen, A., Wintoft, P. & Pulkkinen, A., 2009. Space weather events in July 1982 and October 2003 and the effects of geomagnetically induced currents on Swedish technical systems. *Annales Geophysicae,* 27(4), pp. 1775-1787.

Yao , Y., Koh, C. S., Ni, G. & Xie, D., 2005. 3-D Nonlinear Transient Eddy Current Calculation of Online Power Transformer Under DC Bias. *IEEE Transcations on Magnetics,* 41(5), pp. 1840-1843.

Yee, K., 1966. Numerical solution of initial boundary value problems involving maxwell's equations in isotropic media. *IEEE Transactions on Antennas and Propagation,* 14(3), pp. 302-307.

Zhang, B. Liu, Y., Liu, L., McVey, M., Garderner, R. M., & Xiao, X., 2011. Effect of load current on leakage flux of transformer with geomagentically induced current. *European Transactions on Electrical Power ,* 21(1), pp. 165-173.

Zirka, S. E., Moroz, Y. I., Elovaara, J., Lahtinen, M., Walling, R. A., Høidalen, H. Kr., Bonmann, D., Arturi, C. M. & Chiesa, N., 2018. Simplified models of three-phase, five-limb transformer for studying GIC effects. *Internation Journal of Electrical Power & Energy Systems*, 103(2018), pp. 168-175.

Zirka, S. E., Moroz, Y. I., Hødalen, H. K., Lotfi, A., Chiesa N., &
Arturi C. M., 2017. Practical Experience in using topological model of a core-type three-phase transformer - No-load and inrush conditions. *IEEE Transactions on Power Delivery*,32(4), pp. 2081-2091.

APPENDICES

APPENDIX A: 40 MVA Power transformer

A.1 Core, tank and winding parameterization

Table A.1: Core steel data provided by the manufacturer

B in Tesla	H in A/m	P_{loss} in W/kg
0	0	0
0.40	9.85	0.067
0.50	11.56	0.101
0.60	13.17	0.141
0.70	14.66	0.186
0.80	15.97	0.237
0.90	17.26	0.293
1.00	18.43	0.356
1.10	19.55	0.424
1.20	20.63	0.500
1.30	21.66	0.583
1.35	22.17	0.627
1.40	22.73	0.673
1.45	23.39	0.722
1.50	24.64	0.772
1.55	26.57	0.826
1.60	29.39	0.883
1.65	33.68	0.947
1.70	40.64	1.019
1.75	52.99	1.110
1.80	79.96	1.236
1.91	800	
1.92	1000	

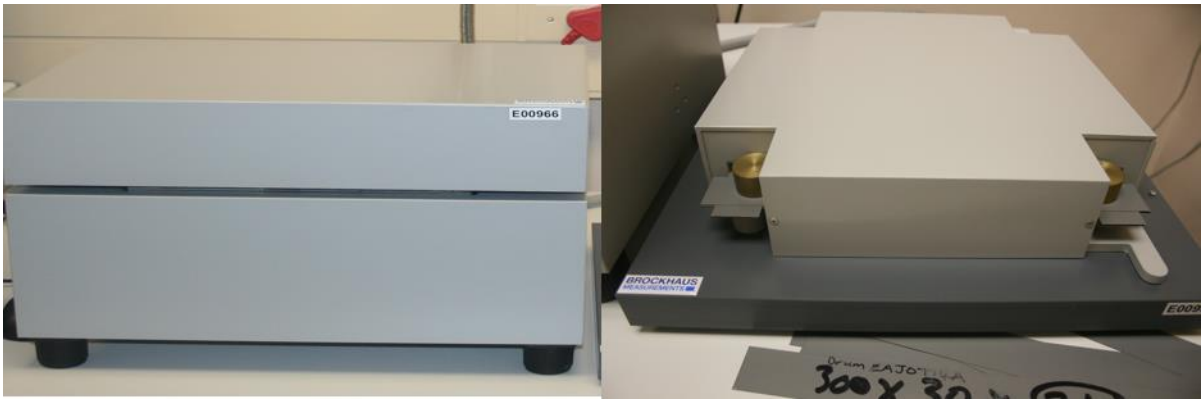

Figure A.1: Single sheet tester (left) and Epstein frame used for verification of magnetic properties of core steel in the laboratory

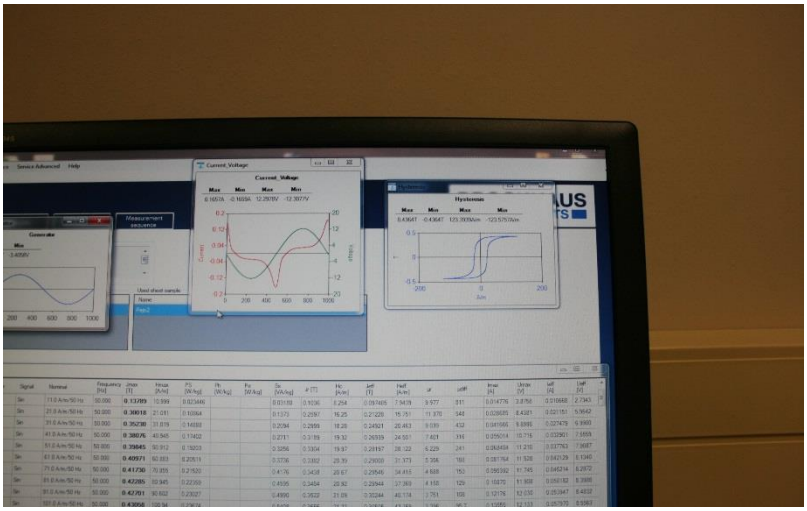

Figure A.2: Typical output from core steel testers

Testing protocol and IEC standards that were applied to very core magnetic properties:

- Epstein frame for core steel characterization
    - IEC 60404-2: Epstein Test
    - 16 samples core steel used
    - Stacked two by two to form D-Type core
    - At least 30 mm * 700 mm
- Single Sheet Tester (SST) similar function
    - IEC 60404-3: SST Method
    - A single sheet of core steel
    - Typically 250 mm * 250 mm

Table A.2: Modelling of the core properties

Name in ANSYS	**Value/ Type**
Relativ Permeability	B-H curve in Figure 11
Bulk Conductivity	0 Siemens/m
Conductivity	2083333.333 Siemens/m
Mass Density	7650 kg/m^3
Composition	Solid
Frequency	50 Hz
Lamination thickness	0.3 mm

Table A.3: Modelling of the LV windings

Name in ANSYS	**Value/Type**	**Description**
DistLeg	1102 mm	Limb pitch or centre-to-centre distance
CoilType	1	1: Solenoid coil, 2: Pancake coil
WidthIn	545 mm	Coil width between two inner sides
DepthIn	545 mm	Coil depth between two inner sides
RadiusIn	272.5 mm	Coil inner fillet radius
ThickCoil	73 mm	Coil thickness of one side
HighCoil	1602 mm	Coil Height
Layers	1	Type of winding is helical (only one layer)
GapLayer	0 mm	Gap between two layers
InfoCore	0	0: all coils, 1: one coil only

Table A.4: Modelling of the HV windings

Name in ANSYS	Value/Type	Description
DistLeg	1102 mm	Limb pitch or centre-to-centre distance
CoilType	1	1: Solenoid coil, 2: Pancake coil
WidthIn	847 mm	Coil width between two inner sides
DepthIn	847 mm	Coil depth between two inner sides
RadiusIn	428.5 mm	Coil inner fillet radius
ThickCoil	93 mm	Coil thickness of one side
HighCoil	1520 mm	Coil height
Layers	1	Type of winding is disk (only one layer)
GapLayer	0 mm	Gap between two layers
InfoCore	0	0: all coils, 1: one coil only

Table A.5: Additional winding data

Name in ANSYS	Value	Description
Copper coils	58000000	Electrical conductivity of copper
Total Resistance (LV)	0.01946 ohm	
Total Resistance (HV)	1.06175 ohm	
Duct inside shell (LV)	16 mm	Distance between core and inner part of LV winding
Duct inside shell (HV)	40 mm	Distance between outer LV winding and inner HV winding
Number of turns (LV)	163	
Number of turns (HV)	1128	

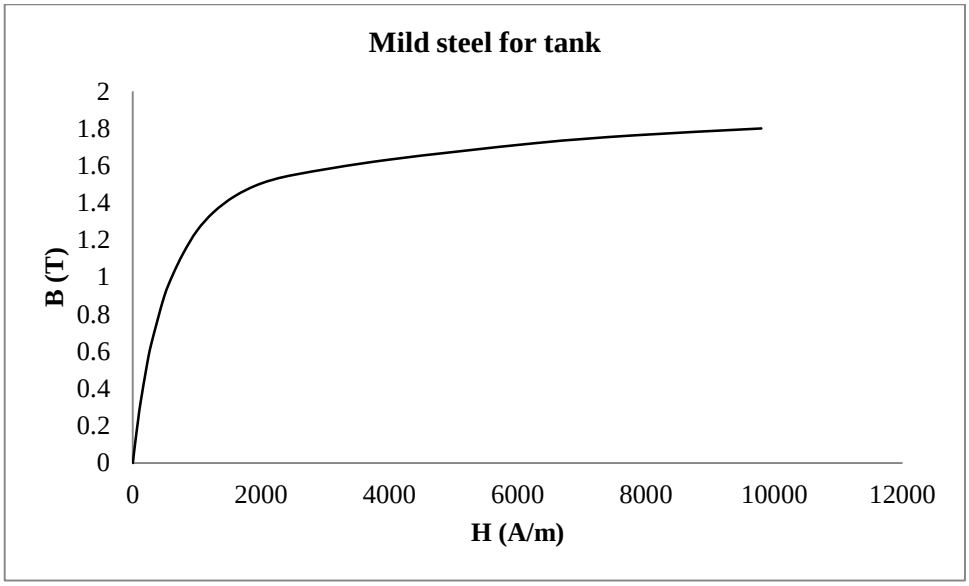

Figure A.3: BH curve for tank steel

A.2 Power transformer FEM waveforms

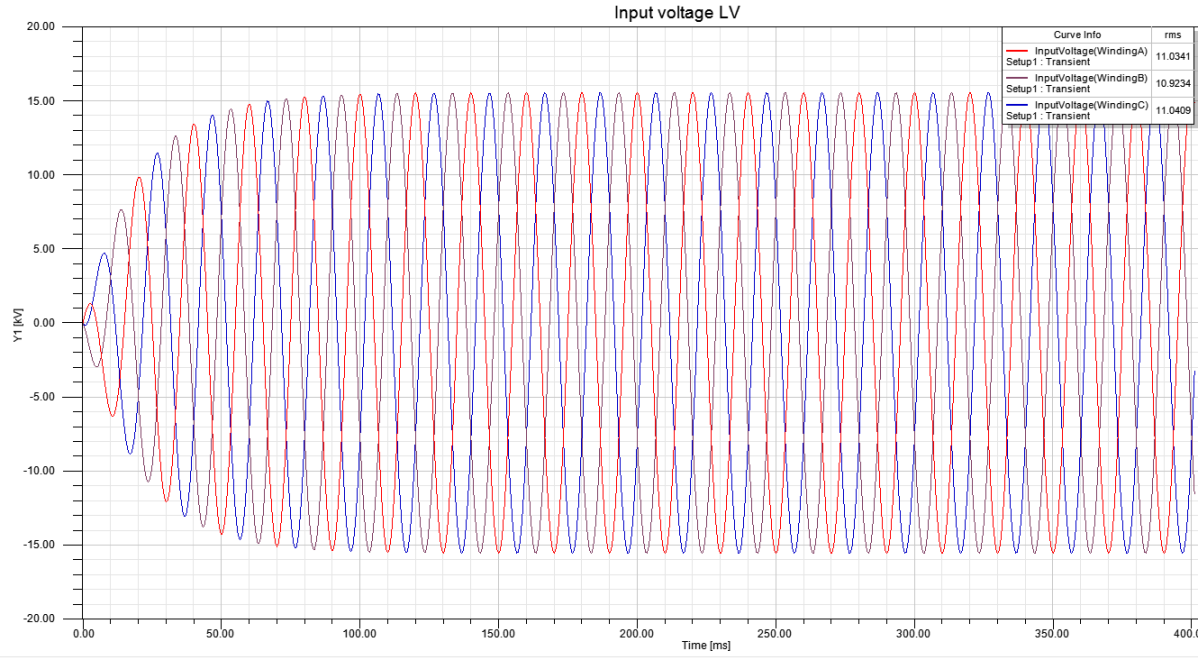

Figure A.4: Slow rise input voltage on the delta side at no load

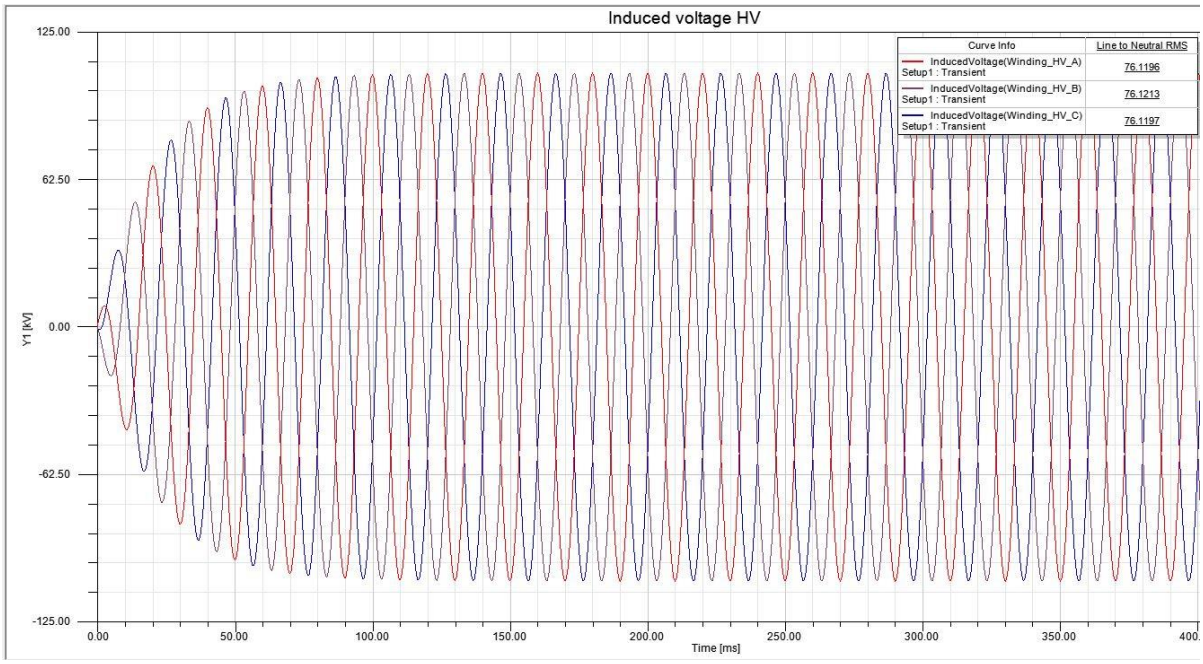

Figure A.5: Slow rise induced output voltage at no load (measurement is line to neutral)

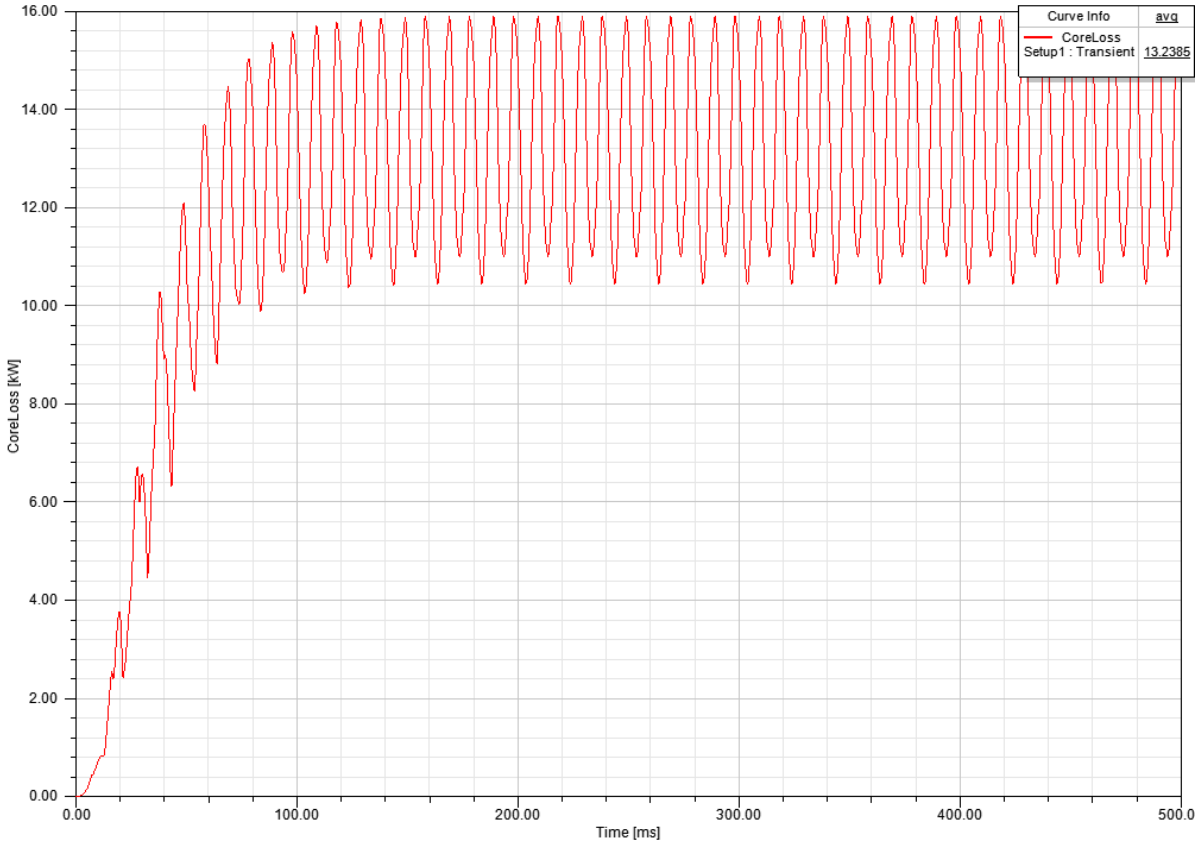

Figure A.6: FEM calculated time average core loss for 2D between 200 ms and 500 ms

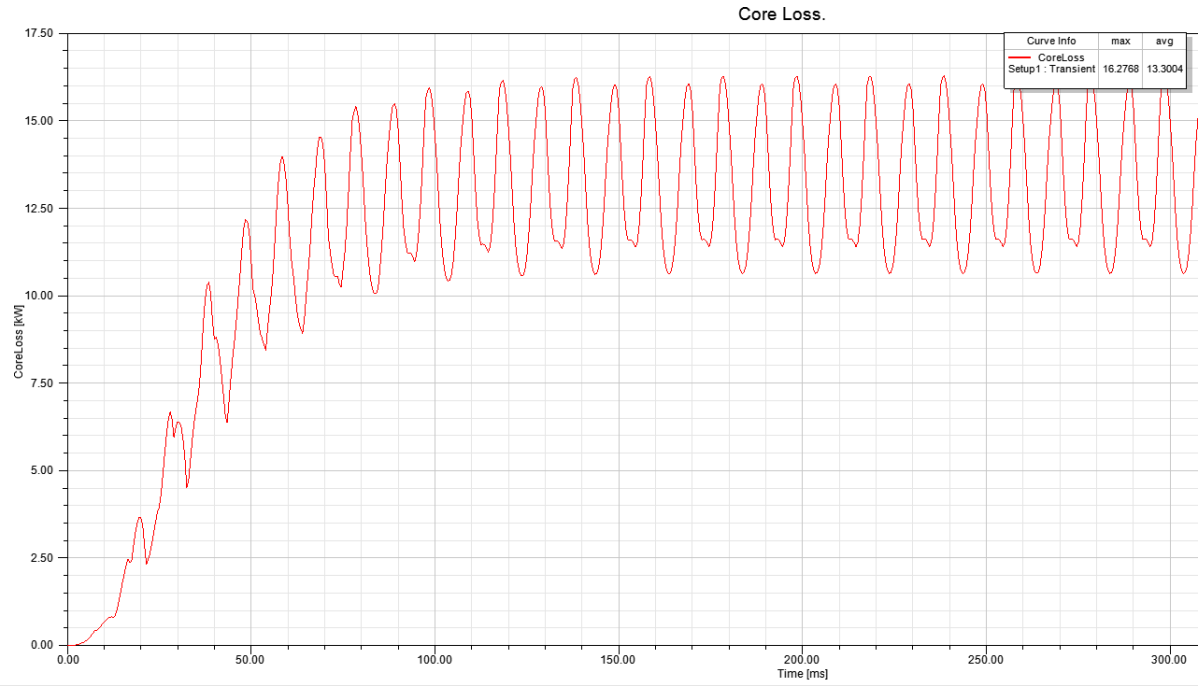

Figure A.7: FEM calculated time average core loss for 3D model between 200 ms and 500 ms

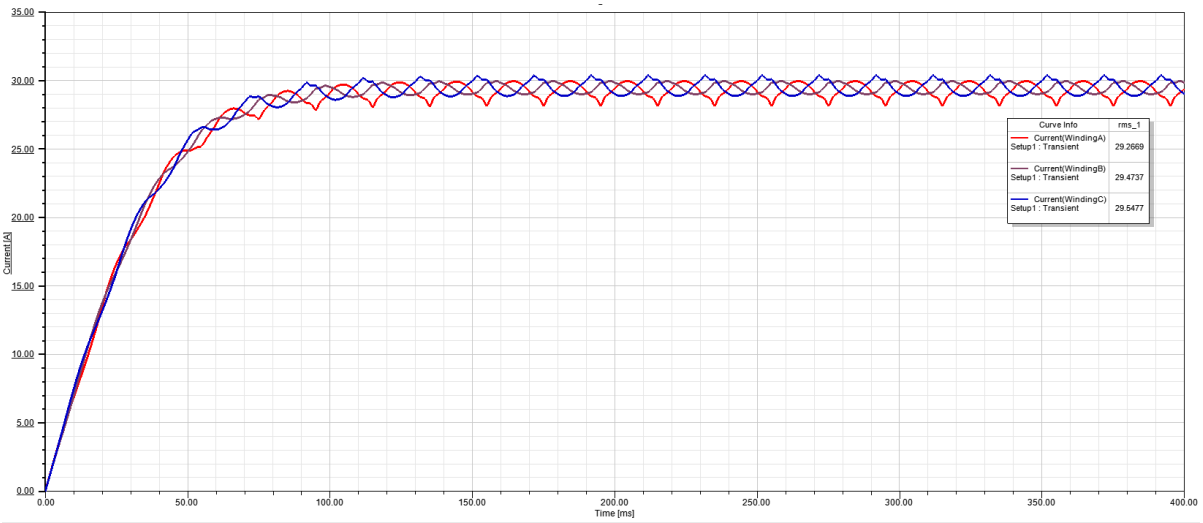

Figure A.8: Effect of 30 A GIC on magnetizing currents

APPENDIX B: Bench-scale FEM Investigation

B.1 Bench-scale Parameters

Table B.1: Bench-scale parameters. The nominal voltage is represent linear operation around the knee point, and it is significantly lower than the nameplate ratings. The load currents are calculated from the original nameplate ratings

	Nominal line-to-neutral Voltage (V RMS)	**VA base (VA)**	**I_{mag} (A)**	**Load current (A)**	**Primary turns**	**Secondary turns**	**Core thickness (mm)**	**Core height (mm)**	**Core length (mm)**
1p3L	80/153	200	0.055	0.84	444	865	30	80	96
3p3L	44/85	200	0.073	1.45	256	496	30	132	152
3p5L	80/153	200	0.070	0.84	153	298	47.5	95	229

B.2 Applied Voltage Soft Start VB Script

The following algorithm (modified by Infolytica Corporation Support) was used to generate a progressive start-up voltage of any amplitude in order to avoid an inrush current phenomenon caused by a sudden switching on of the supply.

```
' This script allows one to add a progressive start-up to a coil or a voltage source which has a sinusoidal waveform of the form:
'           For t < Td : Vo + Va*sin(phi*pi/180)
'           For t > Td : Vo + Va*sin(2*pi*F*(t-Td) + phi*pi/180)
'
' With the progressive envelope, the waveform becomes:
'           For t < Td : Vo
'           For t > Td : Vo + Va*sin(2*pi*F*(t-Td) + phi*pi/180) * 1/(1+A/(t-Td)^2)   where A = (N/F)^2, N being the number of cycles needed for the envelope function to reach 50%
' which is implemented as a PWL waveform.
'
' The coil or source has to be selected in the object tree before running the script. The script can handle multiple problems with different waveforms or transient settings.
```

```
CALL ProgressiveStartUp()


SUB ProgressiveStartUp()


      Dim sSourceName, dStartTime, dEndTime, dTimeStep,
iNumberOfTimeInstant, numberofobjects, dT, iTimeIndex, waveform,
newwaveform, NumberOfProblems, n, m, dA, sourceType, dV0, dVa, dPhase,
dF,waveformtype, prob, TimeSteps, dampingfactor, delay, Path


      'Ask which damping factor to use for the envelope
      dampingfactor = CDbl(InputBox("Enter the number of cycles for the
waveform's envelope to reach 50% of the final amplitude.","Progressive
Start-Up","1"))
      numberofobjects =
getDocument().getView().getSelection().getNumberOfObjects()


      For k = 0 To numberofobjects-1 Step 1
      'Get the path to the object
      Path = getDocument().getView().getSelection().getObjectId(k)


      If getDocument().getProblem(1).isCoil(Path) Then
            CALL getDocument().getParameter(Path, "CoilSourceType",
sourceType)
            If sourceType <> "VoltageDriven" Then
                  msgbox("The selection must be a voltage driven coil or a
voltage source.")
                  Exit Sub
            End If
      ElseIf getDocument().getProblem(1).isCircuitComponent(Path) Then
            If getDocument().getCircuit().getComponentType(Path) <>
infoVoltageSource Then
                  msgbox("The selection must be a voltage driven coil or a
voltage source.")
                  Exit Sub
            End If
      Else
            msgbox("The selection must be a voltage driven coil or a
voltage source.")
            Exit Sub
      End If


      'Get the number of problems
      NumberOfProblems=getDocument().getNumberOfproblems()


      newwaveform = ""


      'Make sure the waveform is sinusoidal
      CALL getDocument().getParameter(Path, "WaveFormType", waveformtype)
```

```
	If waveformtype <> "SIN" Then
		msgbox("The source type must be sinusoidal.")
		Exit sub
	End If


	'Define how many waveforms (problems) to generate for the
coil/voltage source
	prob = 1
	If NumberOfProblems > 1 Then
		If (MsgBox("Does the waveform of " & Path & " or the transient
settings (Start, Stop and Step times) vary from one problem to the
other?", vbYesNo) = VbYes) Then
			prob = NumberOfProblems
		End If
	End If


	'For each problem with a different waveform...
	For n=1 To prob


		'Get the transient settings
		CALL getDocument().getProblem(n).getParameter("", "TimeSteps",
TimeSteps)
		If isEmpty(TimeSteps) Then
			MsgBox "No transient data specified in the model."
			Exit Sub
		End If
		dStartTime = TimeSteps(0)
		dTimeStep = TimeSteps(1)-TimeSteps(0)
		dEndTime = TimeSteps(2)
		If dTimeStep = 0 Then
			msgbox("The step time must be different from zero.")
			Exit Sub
		End If


		'Get the waveform parameters
		CALL getDocument().getProblem(n).getParameter(Path,
"WaveFormValues", waveform)
		dV0 = waveform(0)
		dVa = waveform(1)
		If Ubound(waveform) >= 2 Then
			dF = waveform(2)
		Else
			dF = 1/dEndTime
		End If
		If Ubound(waveform) >= 3 Then
```

```
                  delay = waveform(3)
            Else
                  delay = 0
            End If
            If Ubound(waveform) >= 5 Then
                  dPhase = waveform(5)
            Else
                  dPhase = 0
            End If
            If Ubound(waveform) >= 4 Then
                  If waveform(4) <> 0 Then
                        msgbox("The waveform's exponential damping factor
(theta) will not be taken into account.")
                  End If
            End If


            'Build the array for the PWL waveform (including time and
voltage values)
            iNumberOfTimeInstant = CInt((dEndTime-dStartTime)/dTimeStep) +
1
            REDIM ArrayOfValues(2*iNumberOfTimeInstant - 1)
            dT = dStartTime
            For iTimeIndex = 0 To 2*(iNumberOfTimeInstant - 1) Step 2
                  ArrayOfValues(iTimeIndex) = dT
                  ArrayOfValues(iTimeIndex + 1) = dV0 +
OriginalWaveForm(dT, dVa, dF, delay, dPhase) *
ProgressiveStartUpWaveForm(dampingfactor,dF,dT,delay) 'calculates the
progressive waveform
                  dT = dT + dTimeStep
            Next
            newwaveform = newwaveform & ", [" & Join(ArrayOfValues, ",") &
"]" 'concatenates the arrays for all the problems


      Next 'n


      'Change the waveform to PWL with the calculated progressive waveform
      CALL getDocument().setParameter(Path, "WaveFormType", "PWL",
infoStringParameter)
      CALL getDocument().setParameter(Path, "WaveFormValues",
Right(newwaveform,Len(newwaveform)-1), infoArrayParameter)


    Next 'k


End SUB
Function OriginalWaveForm(dT, dVa, dF, delay, dPhase)
      Const dPI=
3.14159265358979323846264338327950288419716939937510582097494459
```

```
	If dT <= delay Then
		OriginalWaveForm = 0
	Else
		OriginalWaveForm = dVa*SIN(2*dPI*dF*(dT-delay)+dPhase*dPI/180)
	End If
End Function

Function ProgressiveStartUpWaveForm(dampingfactor,dF,dT,delay)
	Dim dA
	dA = (dampingfactor/dF)^2

	If dT > delay Then
		ProgressiveStartUpWaveForm = 1/(1+dA/(dT-delay)^2)
	Else
		ProgressiveStartUpWaveForm = 0
	End If
End Function
```

APPENDIX C: 1p4L Physical Test Set Up

C.1 1p4L Acceptance test

Table C.1: Winding resistance measurements indicated at individual winding temperatures T_{wind}

Winding dc resistance measurements				
Determined and Verified Polarity: Subtractive				
Tut no.	**$R_{150t\ inner}$, (Ω) Phase A**	**$R_{80t\ outer}$, (Ω) Phase A**	**$R_{150t\ inner}$, (Ω) Phase B**	**$R_{80t\ inner}$, (Ω Phase B**
T1	T_{wind} =25,9^{0}C V =0,152 V I =1.02 A $R_{150t\ inner}$ =0,149 Ω	T_{wind} =25,6^{0}C V =0,1063 V I =1,03 A $R_{80t\ outer}$ = 0,103Ω	T_{wind} =26^{0}C V =0,1525 V I =1,03 A $R_{150t\ inner}$ = 0,148Ω	T_{wind} = 26^{0}C V =0,1062 V I =1,03 A $R_{80t\ outer}$ = 0,103Ω
T2	T_{wind} =25,8^{0}C V =0,1497V I =1,01A $R_{150t\ inner}$ = 0,148Ω	T_{wind} =25,6^{0}C V =0,1053 I =1,02A $R_{80t\ outer}$ = 0,103Ω	T_{wind} =25,4^{0}C V =0,1519V I =1.02A $R_{150t\ inner}$ = 0,149Ω	T_{wind} =25,5^{0}C V =0,1068V I =1,03A $R_{80t\ outer}$ = 0,104Ω
T3	T_{wind} =25,5^{0}C V =0,152V I =1,02A $R_{DCinner}$ = 0,149 Ω	T_{wind} =25,5^{0}C V =0,1068V I =1,03A $R_{DCouter}$ = 0,104 Ω	T_{wind} =25,8^{0}C V =0,1504V I =1,01A $R_{DCinner}$ = 0,149Ω	T_{wind} =25,4^{0}C V =0,1052V I =1,02A $R_{DCouter}$ = 0,103 Ω

Table C.2: Winding dc resistance corrected to 20°C

Tut. no.	**$R_{150t\ inner}$, (Ω) Phase A**	**$R_{80t\ outer}$, (Ω) Phase A**	**$R_{150t\ inner}$, (Ω) Phase B**	**$R_{80t\ inner}$, (Ω Phase B**
T1	0,146 Ω	0,101 Ω	0,145 Ω	0,101 Ω
T2	0.145 Ω	0,101 Ω	0,146 Ω	0,102 Ω
T3	0,146 Ω	0,102 Ω	0,146 Ω	0,101 Ω

Table C.3: Transformation ratio check

Tut. No.	Transformer turns ratio Phase A	%difference Phase A	Transformer turns ratio Phase B	%difference Phase B
1	1,8757	0,22%	1,8757	0,22%
2	1,8756	0,22%	1,8757	0,22%
3	1,8757	0,22%	1,8755	0,23%

C.2 500 kVA Nameplate Ratings

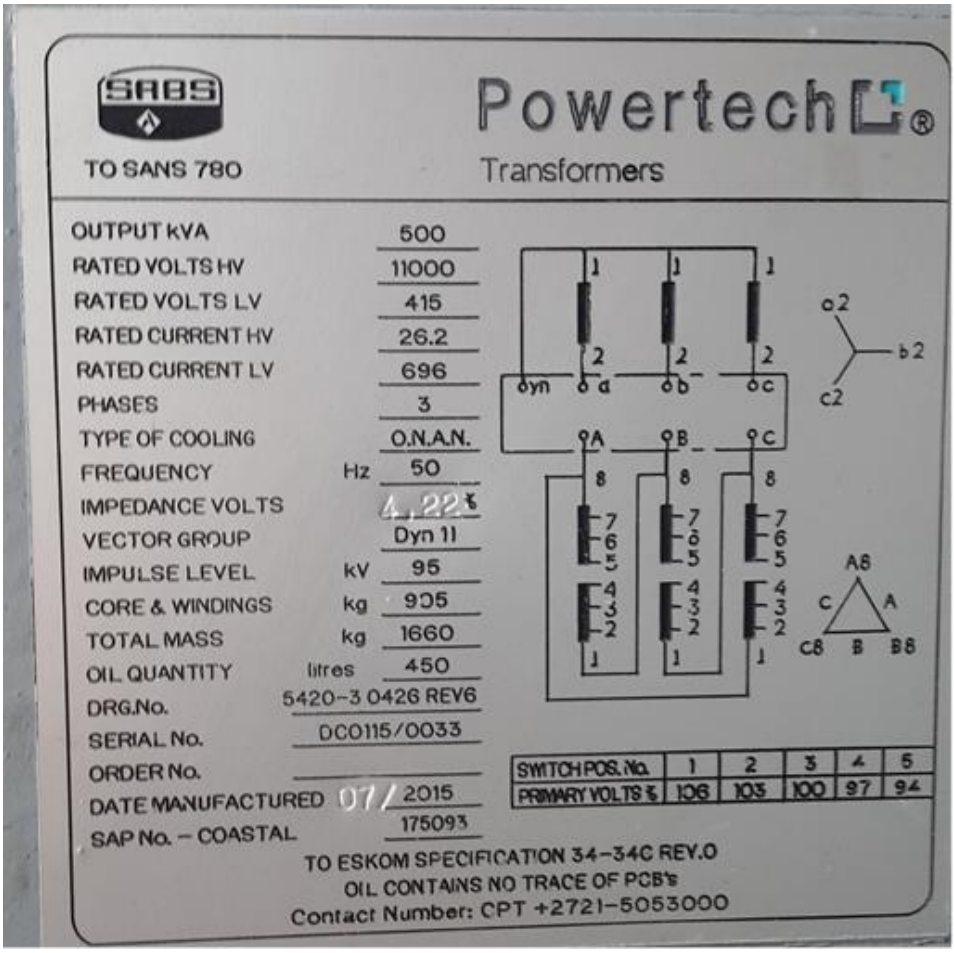

Figure C.2: Nameplate ratings of Powertech distribution transformers connected back-to-back in laboratory set up

APPENDIX D: Measured Results and FEM models

The construction of real power transformers typically has windings that cover the majority of the limbs. The model 1p4L used in this thesis have relatively small winding heights (see Figures D.1 and D.2). This was done deliberately to allow for the installation of air search coils at the T-joints. The small winding height, however, does not invalidate the research the flux distribution is a function of the core-joint configuration and characteristic of the excitation inside the windings and is not significantly influenced by the winding height.

D.1 FEM Vector Plots with ac and dc

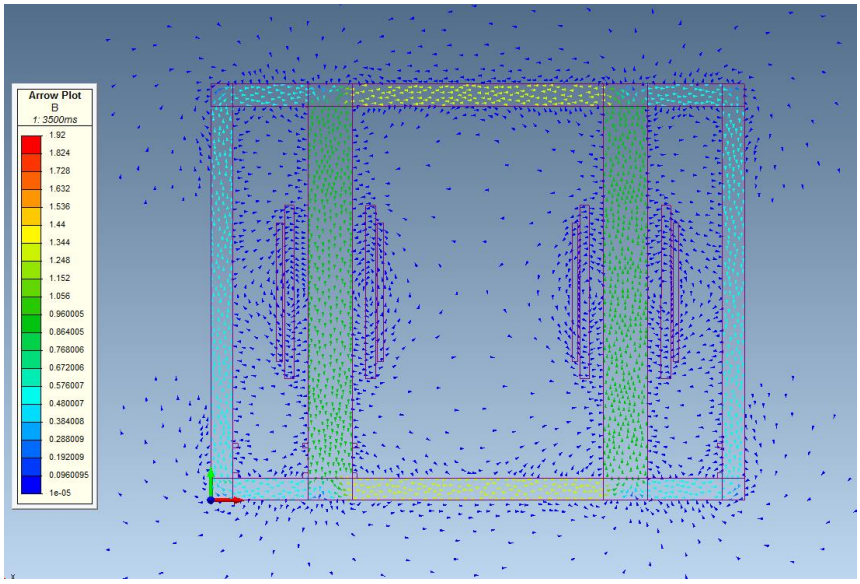

Figure D.1: Effect of 1.25 A dc at nominal voltage visualized as a vector plot for model-B2 with equivalent air gaps at the joints at time *t* = 3.5 s

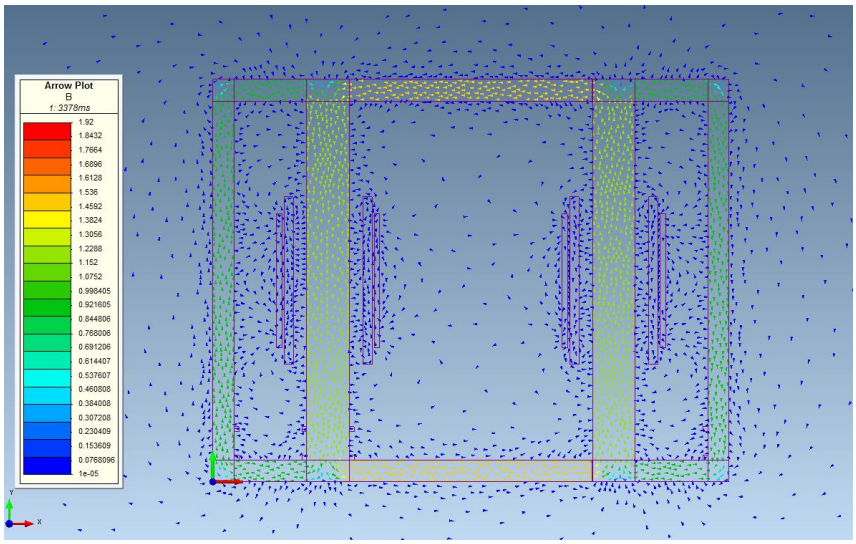

Figure D.2: Effect of 7.3 A dc at nominal voltage visualized as a vector plot for model-B2 with equivalent air gaps at the joints at time *t* = 3.378 s

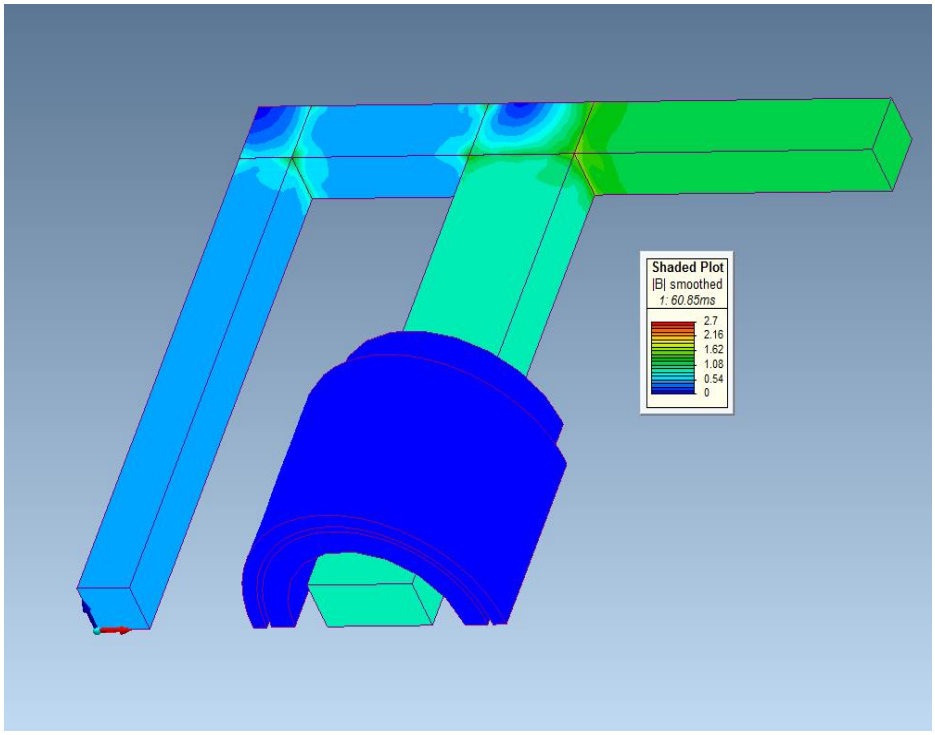

Figure D.3: Model 3D-1 Solid core parts with equivalent air gaps at the joints

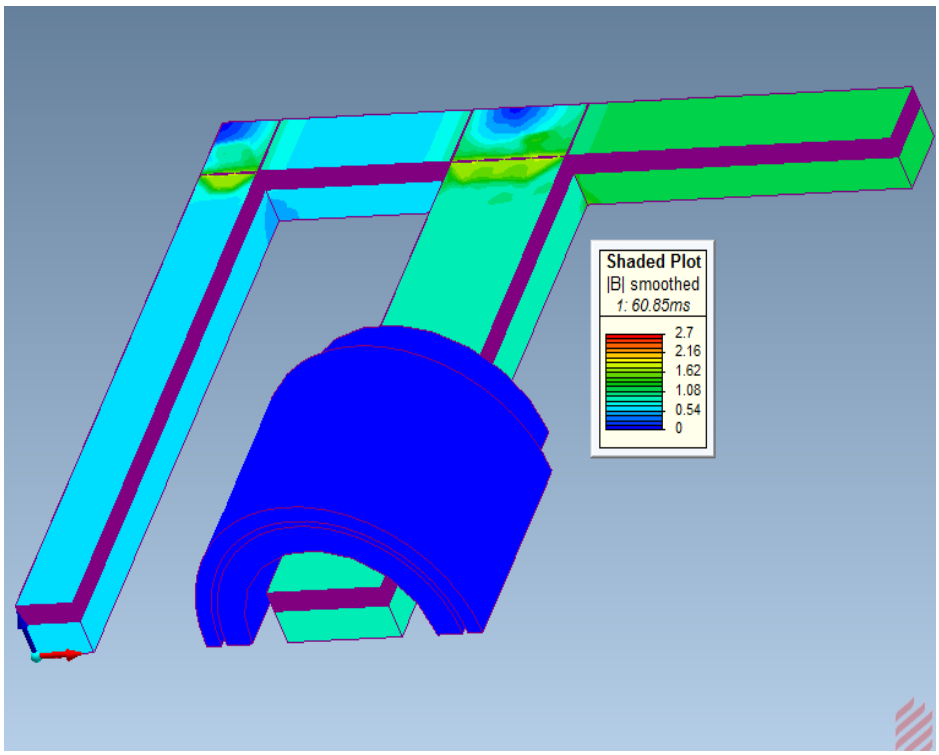

Figure D.4: Model 3D-2 laminations modelled on the surface of the core – rest of the core solid with equivalent air gaps at the joints

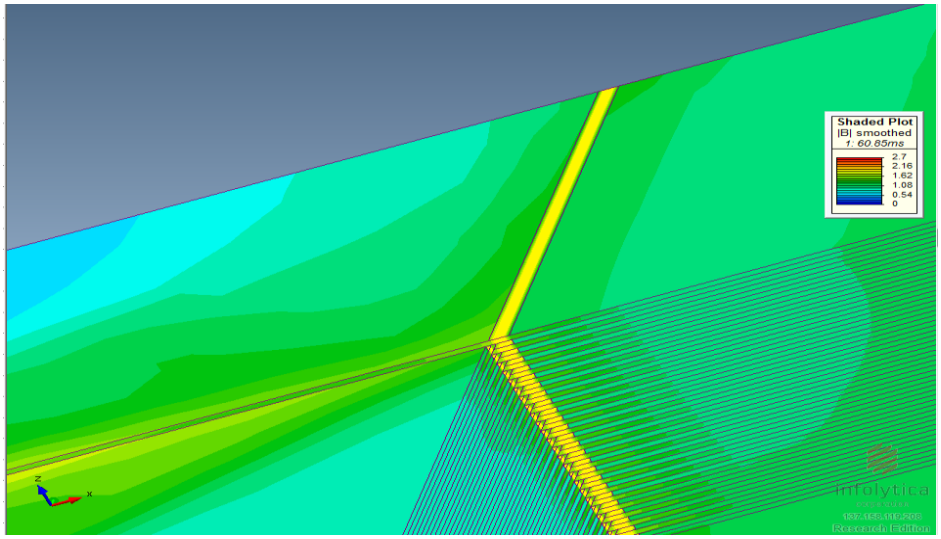

Figure D.5: Model 3D-2 close up of laminations explicitly modelled only at the surface of the core while the rest of the core is modelled as solid with equivalent air gaps at the joints.

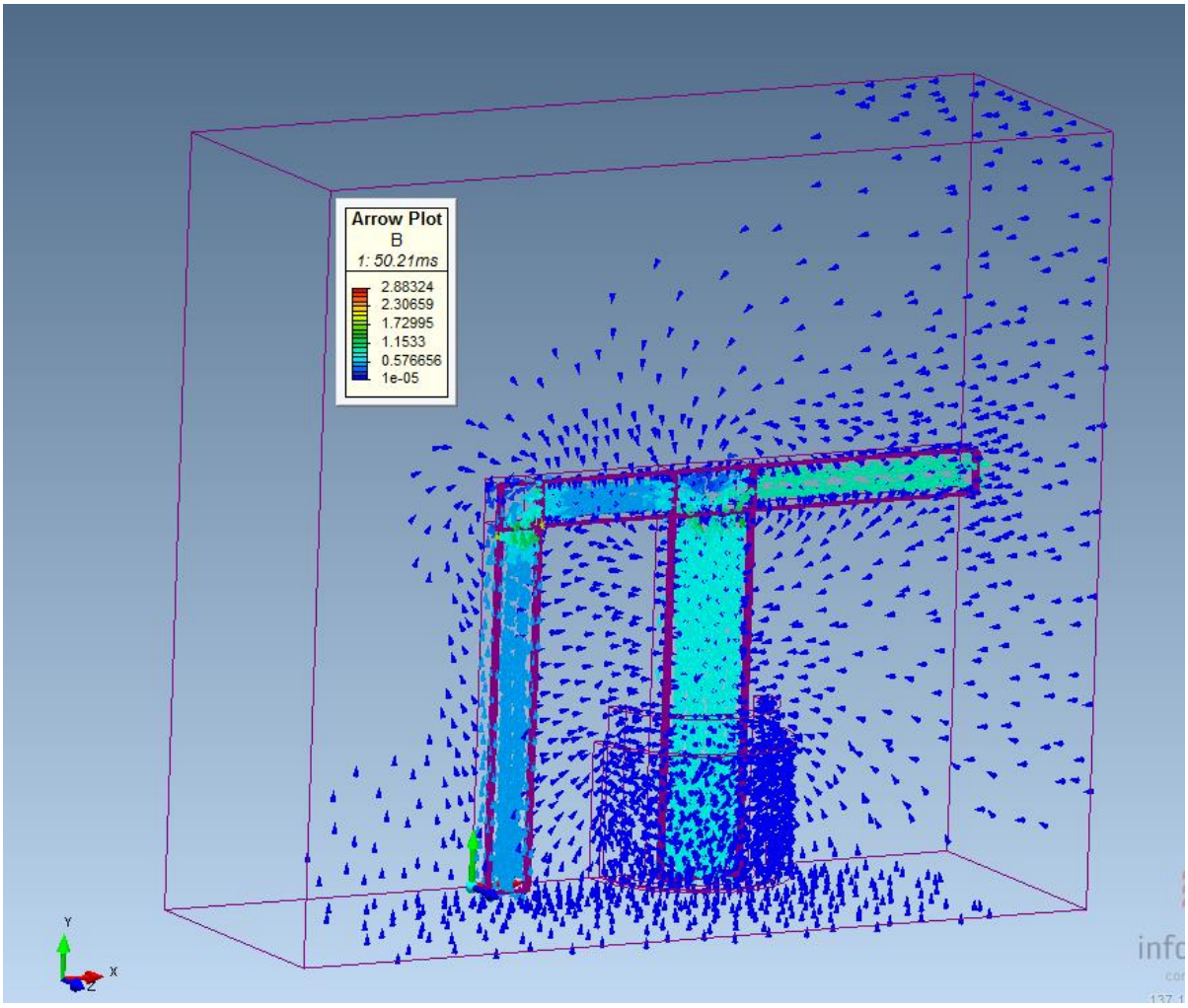

Figure D.6: Model 3D-2 At the commencement of saturation to analyse the distributions of the flux for comparison with measured flux.

D.3 Q-dc Input current and voltage harmonics with dc

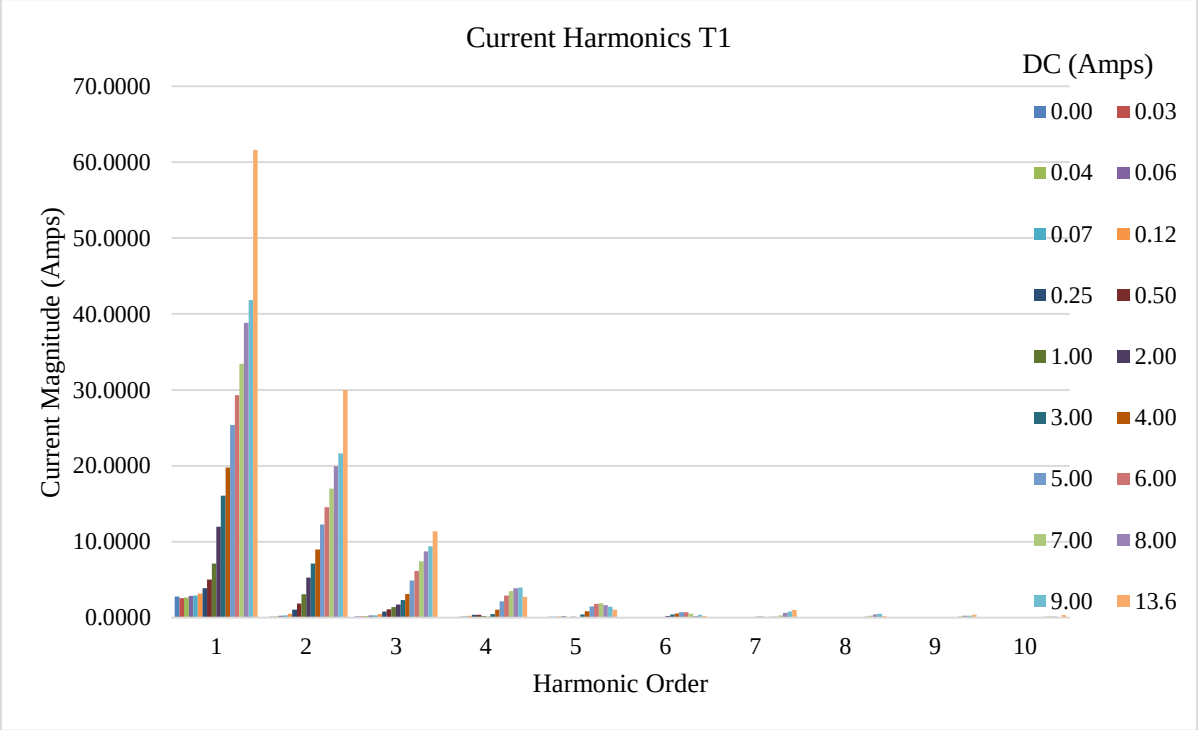

Figure D.7: Laboratory T2 current harmonic profile with incremental dc at nominal voltage

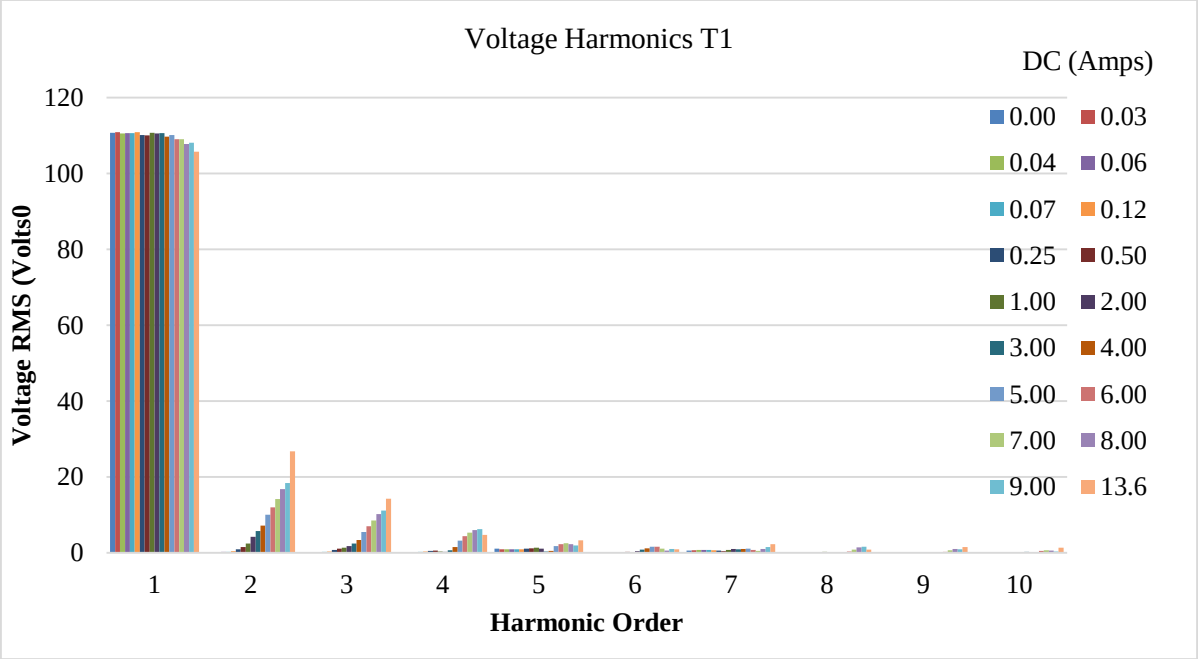

Figure D.8: Laboratory T2 voltage harmonic profile with incremental dc at nominal voltage

D.3 Q-dc laboratory measurements on test transformer T2

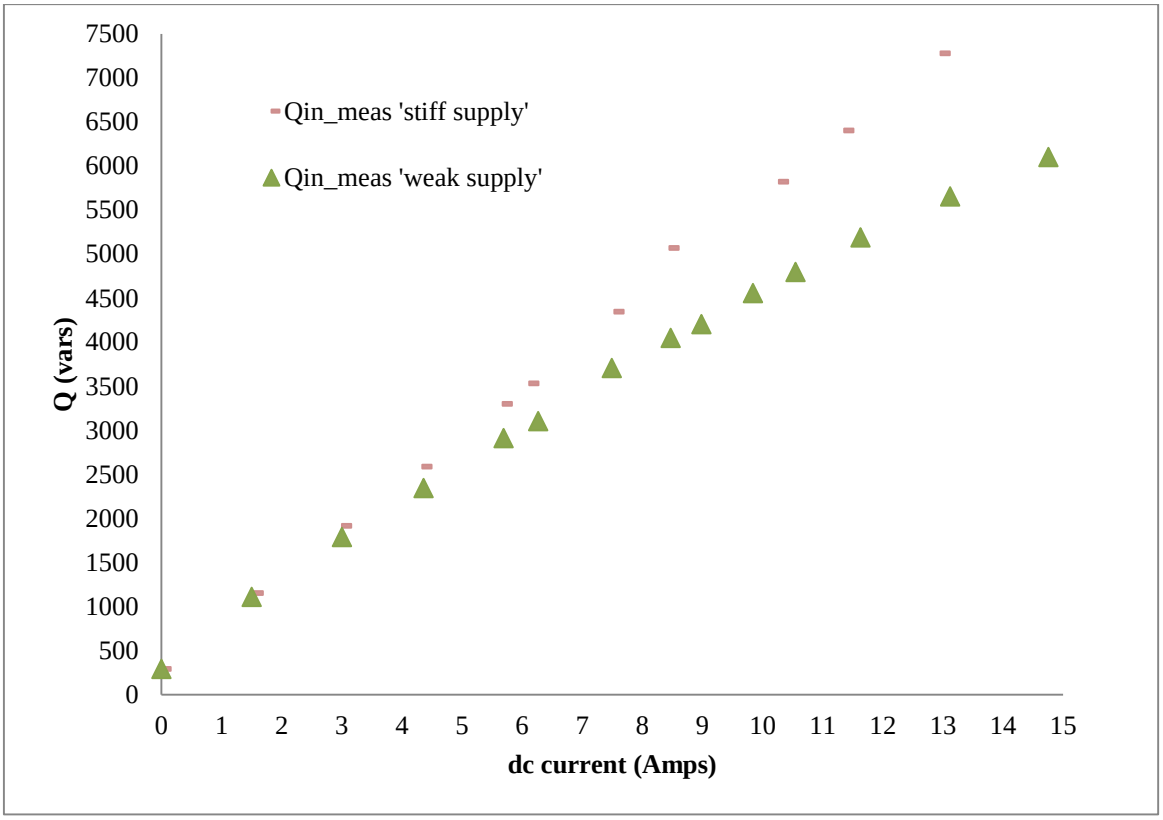

Figure D.9: Q-dc response laboratory measurements with 'weak supply' and 'stiff supply'

D.4 Saturation inductance investigation

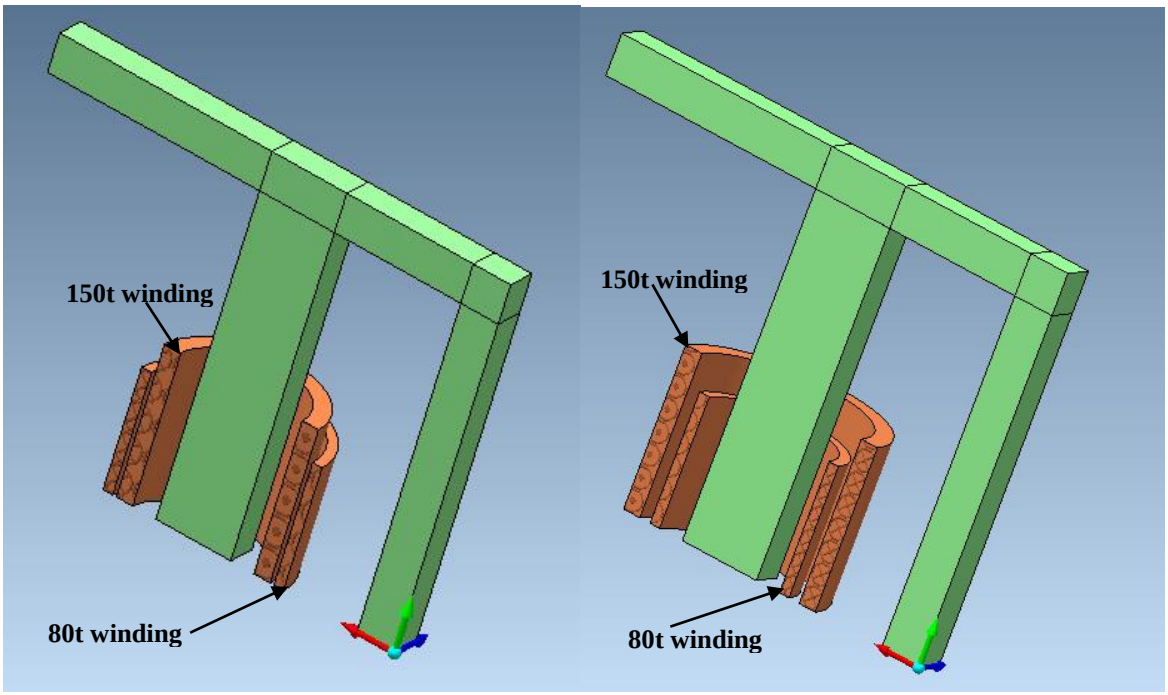

Figure D.10: Original winding configuration (left). Swopped winding positions (right)

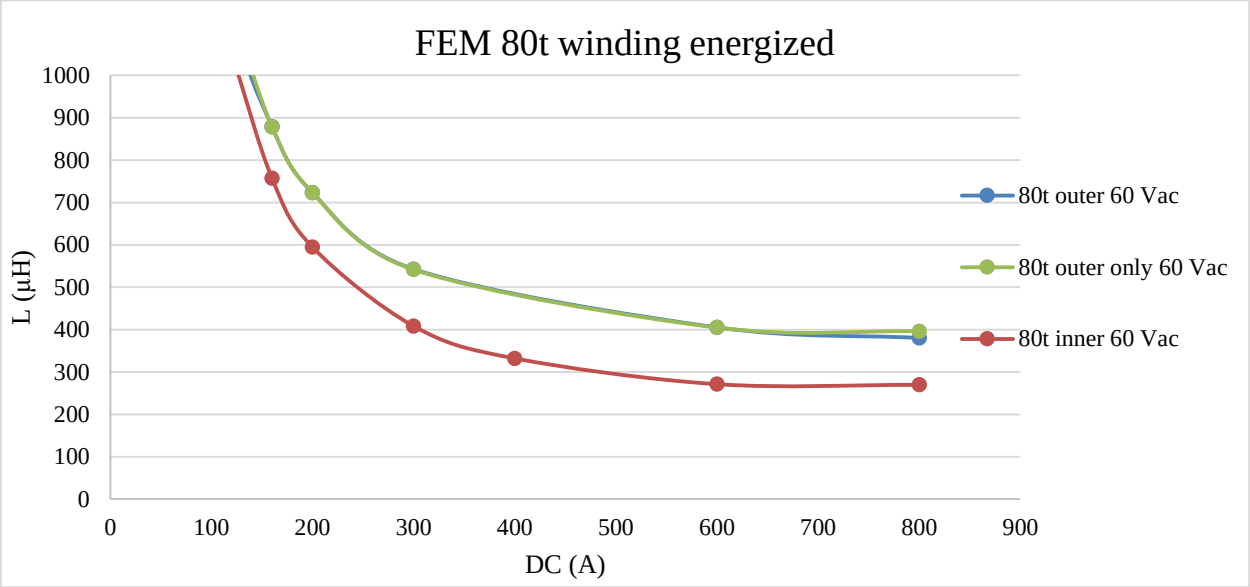

Figure D.11 Different FEM models used to calculate $L_{terminal}$ seen from the 80t winding

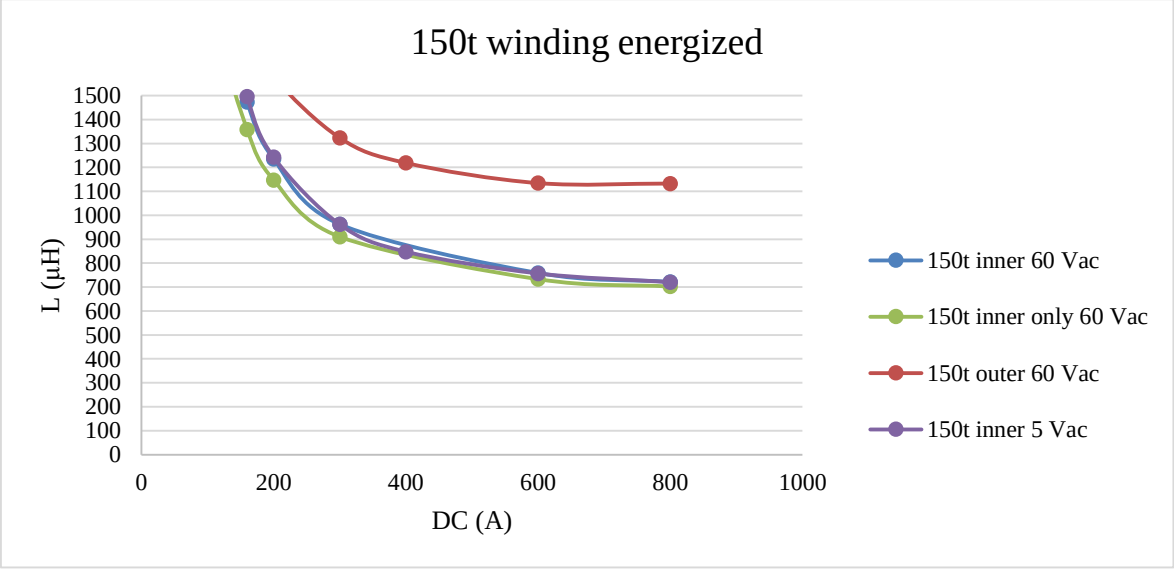

Figure D.12: Different FEM models used to calculate $L_{terminal}$ seen from the 150t winding